Alma Mater Studiorum – Università di Bologna

DOTTORATO DI RICERCA IN

Ingegneria Civile, Chimica, Ambientale e dei Materiali

Ciclo XXIX

Settore Concorsuale di afferenza: 08/B3

Settore Scientifico disciplinare: ICAR/09

TITOLO TESI

On the Seismic Behavior of Ground-Supported Circular Silos Containing Grain-like Material

Presentata da: **Luca Pieraccini**

Coordinatore Dottorato

Prof. Luca Vittuari

Relatore

Prof. Ing. Tomaso Trombetti

Correlatore

Prof. Ing. Stefano Silvestri

Esame finale anno 2017

Abstract

This thesis is focused on the analysis of the seismic response of flat-bottom cylindrical grain-silos. Part A constitutes an updated state-of-the-art on the structural seismic design of flat-bottom cylindrical grain-silos, Part B critically analysis the theoretical framework developed in the last decade at the University of Bologna by the research work coordinated by Prof. Trombetti and the experimental tests conducted in 2012-2013 for its experimental verification, whilst Part C provides some refinement on the theoretical framework and some further insight into the dynamic behavior of flat-bottom cylindrical grain-silos, representing the main scientific contribution of the work.

Part A begins with a comprehensive review of the main analytical, numerical and experimental researches devoted to the study of the static and dynamic behavior of flat-bottom cylindrical grain-silos, together with a review of the current design code provisions for the seismic design of grain-silo structures. A comparison between the current code provisions on the seismic behavior of flat-bottom grain-silo structures and the actual body of knowledge is provided.

Part B is focused on the previous research works conducted by Prof. Trombetti and co-workers in the year 2012-2013. First, the theoretical study on the horizontal forces produced by grain-like material inside silos during earthquakes is presented. Then, the experimental investigation conducted via shaking-table tests at the EQUALS laboratory of the University of Bristol (ASESGRAM project) are reported. Finally, the analytical-experimental correlation study for the verification of the original analytical formulation is illustrated.

Part C presents some refinements of the original analytical formulation for the estimation of the maximum lateral actions developed during an earthquake as well as an analytical formulation for the estimation of the fundamental period of vibration of flat-bottom circular grain-silos. Finally, the results of a preliminary on-field experimental campaign on a real silo structure are illustrated.

Acknowledgements

I am very grateful to my supervisors Prof. Tomaso Trombetti and Prof. Stefano Silvestri for the opportunity to undertake this Ph.D. course, which represents a tremendous experience of personal growth, and for their continuous technical guidance during the entire period of my research work in Bologna.

I am thankful to all my Department colleagues (Giada, Simonetta, Roberta, Michele, Antoine) for sharing ideas and providing a congenial and friendly working atmosphere.

I also want to thank my parents, my brothers and my sister for their constant support. A special thank goes to my wife, Andrea, for her constant support and lovely encouragement during all these last three years.

Alla famiglia di ieri,

di oggi,

e di domani

Table of contents

List of Figures

List of Table

1. Introduction

1.1 Background and motivations

Silos are widely used in many different industries for storing a huge range of different granular materials and powders, such as wheat, maize, cement, flour and play an integral and essential role in industrial plants and processing industries. The typologies of silos may be different: flat-bottom ground-supported silos are generally used for long-term storage of significant amounts of agricultural products; above-ground hopper silos are typically supported by slender steel frames when the complete unloading of the bins is needed without the usage of mechanical devices or operators' intervention. The sizes of engineered silos may vary from capacities less than 10 tons to the largest containing as much as 100,000 tons. In particular, due to their versatility and great structural efficiency, their cost and simplicity of implementation, cylindrical grain-silos are widespread all around the world as storage solutions, even in high seismic areas.

During the last century, various earthquakes strongly stroke grain-silos (Dogangun et al. 2009, Fierro et al. 2011 and Uckan et al. 2015), provoking catastrophic collapses, significant and extensive economic losses, collateral damages on adjacent buildings as consequence of a domino effect and, in some circumstances, even causalities. After the 1999 Chi-Chi (Taiwan) earthquake when almost all the silos located in Taichung Port, 70 *km* far from the epicenter, collapsed, the EQE report (1999) stated that "*the seismic design of practice that is used for the design and construction of such facilities clearly requires a major revision*", thus clearly indicating that actual design procedures have limits and therefore significant advancements in the knowledge of the structural behavior of silo structures are necessary.

Despite the scientific efforts devoted to the investigation of the dynamic response of grain-silos subjected to seismic excitation made during the last century, the seismic behavior of flat-bottom cylindrical silos containing grain-like material still presents strong uncertainties. From a theoretical point of view, only few attempts have been made in order to analytically predict the dynamic behavior of grain-silos, thus the general issue of the assessment of the actions exerted by the ensiled content on the silo-wall under dynamic conditions still represents a challenging task. For these reasons, current design codes tend to provide too conservative formulations for the estimation of the seismic actions, giving little guidance or without explicitly covering some important issues related to the actual seismic behavior of grain-silos. Thus, advancements in the actual knowledge on the

dynamic behavior of grain-silos could promote the development of rational methods for their seismic design, making possible to safely design silos in seismic areas without waste of material and excessive redundancy.

1.2 The objectives of the research work

Based on the introductory discussion, it appears that the assessment of the seismic response of flat-bottom cylindrical grain-silos still represents a challenging task from a theoretical point of view, especially regarding the prediction of the horizontal actions exerted by the ensiled granular content on the wall and the understanding of the complex dynamic interaction between wall and ensiled grain-like material.

The main objectives are to get a further insight into the actions exerted by the ensiled granular content on the wall of flat-bottom circular grain-silos and to better understand the overall response of grain-silo systems subjected to base excitation. This interest is based on the possibility/ambition of providing more appropriate design rules closer to the effective seismic behavior of grain-silos. Starting from the theoretical formulation developed at the University of Bologna in 2012 and the interpretation of the experimental results obtained via shaking-table tests carried out on scaled silo specimens at the EQUALS laboratory of the University of Bristol in August 2012 and January 2013, novel original analytical formulations for the assessment of the actions exerted by the ensiled content on the silo wall under static and dynamic conditions and for the estimation of the fundamental period of vibration of flat-bottom circular grain-silo systems are developed. The novel original analytical predictions are compared with (i) the classical theories for the estimation of the horizontal grain-wall pressure under static, accelerated and seismic conditions, (ii) the recent code provisions and (iii) the shaking-table tests available in the scientific literature.

1.3 Text organization

The thesis is organized in three parts: part A, part B and part C. Part A provides an updated state-of-the-art of the structural seismic design of flat-bottom cylindrical grain-silos, presents a comprehensive review of the main analytical, numerical and experimental researches devoted to the study of the static and dynamic behavior of flat-bottom cylindrical grain-silos, together with a review of the current design code provisions for the

seismic design of silo structures, and it is composed of four chapters (from chapter 2 to chapter 5). Part B presents the previous research work coordinated by Prof. Trombetti at the University of Bologna and reports (i) the theoretical study on the horizontal forces produced by grain-like material inside silos during earthquakes and (ii) the experimental investigation conducted via shaking-table tests at the EQUALS laboratory of the University of Bristol and it is composed of three chapters (from chapter 6 to chapter 8). Part C presents the research developed and reports (i) some refinements of the original analytical formulation, (ii) a novel analytical formulation for the estimation of the fundamental period of vibration of flat-bottom circular grain-silos and (iii) the results of a preliminary on-field experimental campaign on a real silo structure and it is composed by three chapters (from chapter 9 to chapter 11).

Chapter 2 provides a comprehensive review of the main analytical and numerical researches devoted to the assessment of the static and the dynamic behavior of flat-bottom circular grain-silos. First, the main analytical studies assessing the static response and the dynamic behavior of grain-silos are discussed; then, the main numerical studies assessing the static response and the dynamic behavior of grain-silos are discussed.

Chapter 3 provides a comprehensive review of the main scientific experimental works on the dynamic behavior of ground-supported circular grain-silos under base excitation and a collection of on-field reconnaissance data on the effects of strong earth motions on real silo structures. First, an insight into the complex behavior of granular material subjected to horizontal shaking is presented before focusing on the behavior of granular material poured inside cylindrical containers in order to better understand the global structural response of grain-silo systems. Then, a review of various experimental tests aimed at investigating the dynamic behavior of ground-supported circular grain-silos performed during the last century is presented. Finally, a review of the most significant cases of structural collapses related to the failures of grain-silo structures due to strong earth motion is chronologically presented.

Chapter 4 collects the main international current code provisions dealing with the structural seismic design of grain-silo structures and draws the actual state-of-the art established in practical and code literature. First, the most salient aspects related to the evaluation of the seismic actions exerted by ensiled bulk content on the silo wall, and the analytical and/or numerical tools applicable to the seismic design of grain-silo structures

are summarized. Then, the main common aspects and the most critical shortcomings individuated among the considered international current code provisions are discussed.

Chapter 5 provides a comparison between the current code provisions and the actual scientific body of knowledge on the static and the seismic behavior of grain-silo structures is presented and the most significant research challenges in the field are summarized

Chapter 6 presents the analytical formulation proposed by Prof. Trombetti and co-workers in 2012 for the evaluation of the horizontal forces produced by grain-like material on the silo wall during earthquake. The problem formulation, the analytical developments and the limits of validity of the proposed analytical formulation are reported. Then, the analytical formulation for the prediction of the shear forces and the bending moments acting on the silo wall are presented. Finally, a comparison of the main analytical findings, in terms of pressures and actions exerted on the silo wall, with those predicted by the classical theories and code provisions is presented.

Chapter 7 presents the shaking-table experimental campaign carried out on silo specimens filled with Ballottini glass carried out at the EQUALS laboratory of the University of Bristol (ASESGRAM project). A full description of the experimental tests is beyond the scope of the present work and has been the objective of a previous Master Thesis (Di Chiacchio 2013). Therefore, only the information necessary for a better understanding of the interpretation of the test results are recalled.

Chapter 8 reports the main experimental results acquired via shaking-table tests and the comparison with the analytical predictions given by the proposed analytical formulation. First, the procedure adopted to reconstruct the experimental bending moment is presented. Then, the influence of the grain-wall friction coefficients on the magnitude of the reconstructed wall base bending moment is presented. Finally, the comparison between the experimental values of the reconstructed wall bending moment and those predicted according to the proposed analytical formulation is performed.

Chapter 9 presents some refinements to the original analytical formulation in 2012. The refinements yield to a significant extension of the theoretical limits of validity and to a new set of analytical formulas for the wall pressures and for the wall shear and bending moment actions. A comparison of the refined analytical formulation with the classical

theories for the static design of grain-silos, the actual code provisions for seismic design of silos and the experimental results described in chapter 8 is also presented.

Chapter 10 presents a novel original analytical formulation for the estimation of the fundamental period of vibration of ground-supported grain-silo systems, starting from the analytical frameworks proposed in chapter 6 and 9. First, the theoretical framework adopted, the basic assumptions and the closed-form expressions for the analytical evaluation of the fundamental period of vibration are presented. Then, the theoretical estimation is compared with the experimental data gathered via shaking-table tests performed within the ASESGRAM project and those available in the scientific literature. Finally, a simple code-like formula and a procedure for the analysis of the dynamic behavior of circular on-ground grain-silos via simplified FE model is also proposed.

Chapter 11 reports the main results of an on-field experimental campaign carried out in the year 2014 on a real operational, horizontally corrugated, vertically stiffened cylindrical steel silo under progressive symmetric filling. Even if beyond the scope of the present thesis, the main aim of such experimental activity is to investigate the structural behavior under static loading of such typology of complex silo structures. This represents a preliminary, first, essential step to be performed in order to get confidence on the peculiar structural response of horizontally corrugated vertically stiffened silos and to develop future experimental investigations focused on the assessment of their dynamic behavior.

Finally, Chapter 12 summarizes the main findings of the previous chapters. Recommendations for future research topics are then provided.

Reference

Di Chiacchio, L. (2013). Interpretation of shaking-table tests of flat-bottom silos containing grain-like material. Master Thesis Dissertation, University of Bologna. http://amslaurea.unibo.it/5756/

Dogangun, A., Karaca, Z., Durmus, A., & Sezen, H. (2009). Cause of damage and failures in silo structures. Journal of performance of constructed facilities, 23(2), 65-71.

EQE. 1999. "Chichi, Taiwan earthquake of September 21, 1999 M7.6." An EQE Briefing, http://www.absconsulting.com/resources/ Catastrophe_Reports/Chichi-Taiwan-1999.pdf Jan. 29, 2008.

Fierro, E. A., Miranda, E., Perry, C. L., Lynn, A. C., & Reitherman, R. (2011). Behavior of nonstructural components in recent earthquakes. In Proc. 2011 Architectural Engineering National Conference, Oakland, CA.

Uckan, E., Akbas, B., Shen, J., Wen, R., Turandar, K., & Erdik, M. (2015). Seismic performance of elevated steel silos during Van earthquake, October 23, 2011. Natural Hazards, 75(1), 265-287.

PART A: Updated state of the art

Part A presents a comprehensive review of the main analytical, numerical and experimental researches devoted to the study of the static and dynamic behavior of flat-bottom cylindrical grain-silos, together with a review of the current design code provisions for the seismic design of grain-silo structures. A comparison between the current code provisions on the seismic behavior of flat-bottom grain-silo structures and the actual body of knowledge is provided.

2. Literature review of the analytical and the numerical studies on the dynamics of flat-bottom silos containing grain-like material

In the present chapter, a review of the main analytical and numerical works on the static and the dynamic behavior of ground-supported circular grain-silos proposed in the scientific literature is presented. The main aims of this review activity are to (i) collect and trace the time-evolution of the analytical and numerical studies on the static and the dynamic behavior of grain-silos and (ii) organize, condense, compare and critically discuss the main aspects related to the analytical and numerical works on the static and the dynamic behavior of grain-silos. First, the main analytical studies assessing the static response and the dynamic behavior of grain-silos are discussed. Then, the main numerical studies assessing the static response and the dynamic behavior of grain-silos are discussed.

2.1 Analytical studies

In this section, a review of the analytical formulations on the static and the dynamic behavior of grain-silos is reported. Various analytical models have been proposed in the scientific literature for: (i) the assessment of the actions exerted by the grain on the silo wall under static conditions or under accelerated conditions; (ii) the prediction of the dynamic response of vibration of ground-supported circular grain-silo systems under base excitation. First, among the many analytical formulations proposed in the scientific literature for the prediction of the grain-wall pressures after filling (static conditions), the most significant theoretical studies are presented; then, the theoretical formulations on the dynamic behavior of grain-silo systems under base excitation reported in the scientific literature are presented.

2.1.1. Janssen (1895) (static)

The first analytical model aimed at estimating the actual distribution of the vertical and horizontal pressures on the wall of circular silos containing grain-like material is dated back to the end of the 19^{th} century and was proposed by Janssen (1895).

By means of a continuum approach, the grain-like material is treated as a set of overlapped layers of infinitesimal height *dz*, where *z* represents the distance of a single horizontal layer of grain from the free surface. With the purpose of evaluating the *effective*

mass of grain that leans against the wall and providing conservative design indications for the static case, the vertical grain-grain pressure at a generic distance *z* from the grain free surface, referred to as $p_v(z)$, is assumed to be equally distributed over the whole cross-section surface *A* and independent on the radial coordinate *x*. This assumption leads to an axial-symmetric distribution of the horizontal and vertical forces on the wall. The frictional vertical forces along the grain-wall contact surface are conservatively assumed to be fully exploited following the Coulomb yield criterion:

$$p_0(z) = \lambda \cdot p_v(z) \tag{1}$$

$$\tau_0(z) = \mu_{GW} \cdot p_0(z) \tag{2}$$

where $p_0(z)$ is the normal horizontal pressure, λ is the pressure ratio (between horizontal and vertical pressures, invariant with the depth), $\tau_0(z)$ is the vertical frictional stress and μ_{GW} is the grain-wall friction coefficient. Numerical values of μ_{GW} and λ need to be evaluated and punctually defined case by case trough specific laboratory tests.

Assuming a horizontal top surface for the grain and considering the vertical forces equilibrium of an elementary grain layer (differential equation of the first order) gives the following exponential form of the normal horizontal pressure $p_0(z)$ that insists on the silo wall at a generic height z:

$$p_0(z) = \frac{\gamma_b \cdot R}{2\mu_{GW}} \left[1 - e^{-2\frac{z \cdot \mu_{GW} \cdot \lambda}{R}} \right] \tag{3}$$

Where γ_b is the specific weight of the ensiled material and *R* is the radius of the silo.

Figure 2.1 shows the pressures distribution acting on the grain and on the wall in static conditions according to the physical idealized model proposed by Janssen (1895).

Later on, Koenen (1986) suggested that the active lateral earth pressure ratio by Rankine (1857) should be used for the prediction of the numerical value of the pressure ratio λ and most of the other theories for silo pressure attempted to find better means of predicting this single quantity (Jaky, 1948; Pieper and Wenzel, 1963; Walker, 1966; Homes, 1972; Walters, 1973; Jenike *et al.*, 1973). Thus, all these Authors adopted the Janssen pressure distribution as basis.

The Janssen's formula is well consolidated in both the scientific and the practical literature. Experimental evidences reported from tests on small scale models or full scale silos such as those by Prante (1986), Toltz (1903), Jamieson (1903), Lufft (1904), Bovey (1904), Pleissner (1906), Phillips (1910), Ketchum (1919), Amundson (1945), Negi and Norris (1977), Schwab et al. (1994), Vanel et al. (2000), Ovarlez et al. (2003), Tatko and Kobielak (2008) and numerical discrete-particle simulation as those by Rotter et al. (1998), Landry et al. (2003) seem to validate such expression. It usually represents the starting point of any analytical and numerical work concerning grain-silo behavior and widely adopted for the numerical validation of finite element and discrete element models. It is incorporated in most, if not all, silo codes and standards. The adoption of the Janssen formula is suggested for the class of slender silos, where the effect on the grain-wall pressure distribution of the conical pile at the silo top is negligible. The model proposed by Janssen is not straightforward applicable in dynamic (e.g. accelerated) conditions due to the lack of axial-symmetry of the problem.

A translation of the original article by Janssen (1895) is given by Sperl (2006).

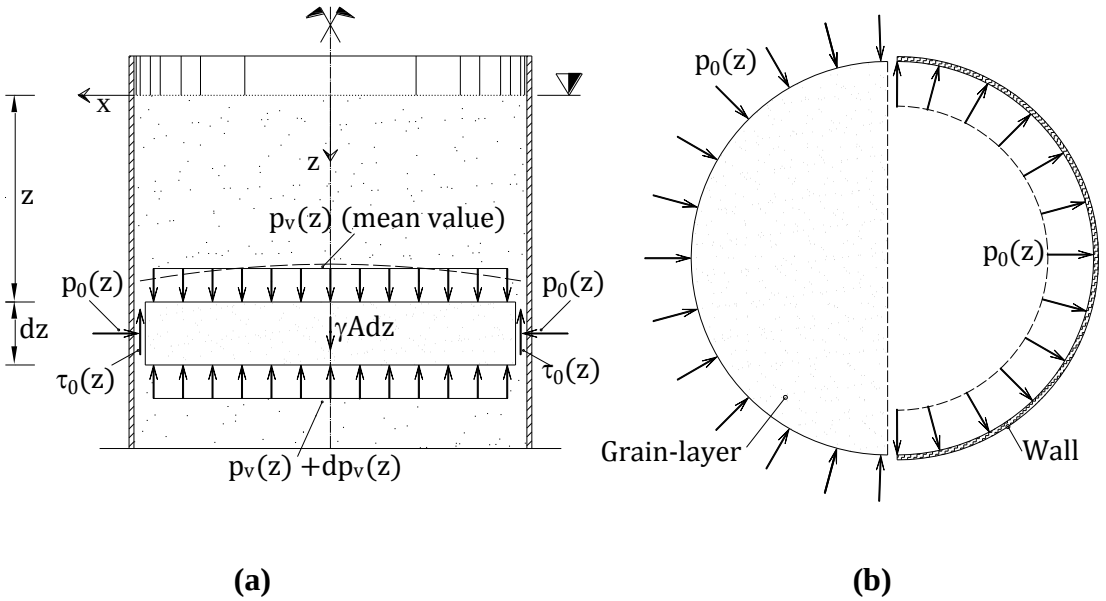

Figure 2.1 - Physical idealized model of Janssen theory (1895) for static conditions. (a) Vertical cross-section. The forces are referred to the grain. (b) Horizontal cross-section. On the left the forces are referred to the grain, on the right to the wall

2.1.2. Reimbert and Reimbert (1943, 1976) (static)

Reimbert and Reimbert (1943, 1976), starting from the classical Janssen (1895) equation, proposed an alternative semi-empirical solution, which effectively allows to

consider the variation of the value of the parameter λ (pressure ratio) along the height of the ensiled granular material. In detail, the formulation considers, via a hyperbolic function, that λ varies between zero at the grain free surface and the value of Rankine active pressure ratio at a great depth. The semi-empirical solution was obtained by curve fitting the experimental results of several tests (conducted on full-scale silos) within the two surface boundaries (free grain surface and silo bottom).

The semi-empirical formulation for the assessment of the normal horizontal pressure $p_0(z)$ that insists on the silo wall at a generic height *z* results:

$$p_0(z) = \frac{\gamma_b \cdot R}{2 \cdot \mu_{GW}} \cdot \left[1 - \left(\frac{z}{z_0} + 1 \right)^{-2} \right] \tag{4}$$

where $z_0 = \frac{R}{2 \cdot \mu_{GW} \cdot \lambda} - \frac{h_s}{3}$, h_s is the height of the superposed conical portion, starting from the highest grain-wall contact, which value could be calculated as $h_s = R \cdot tg(\varphi_r)$, where φ_r is the angle of repose of the ensiled granular material.

Such formulation allows to account for the effect (not directly accounted by the Janssen formulation) of the upper conical portion on the vertical profile and magnitude of the horizontal grain-wall pressure under filling conditions close to the grain free surface. Some comparisons of this solution with Janssen's formula have been made (Briassoulis 1986, 1987, 1991 and Reimbert and Reimbert 1987), demonstrating the effectiveness of the formulation in case of squat-silos. The formula proposed by Reimbert and Reimbert is currently adopted in its modified version by few standards to determine the static loads during filling for squat and intermediate-slender circular grain-silos, where the effect of the upper conical portion on the vertical distribution of the horizontal grain-wall pressure may be significant.

Many different theories were developed for predicting the static pressures in silos after initial filling and during storage (Airy, 1897; Pieper and Wenzel, 1963; Walker, 1966; Homes, 1972; Walters, 1973; Jenike et al., 1973; Abdel-Sayed et al., 1985), which cannot be exhaustively discussed here. Discussions of these theories and fuller descriptions may be found elsewhere (Arnold et al., 1980; Gaylord and Gaylord, 1984; Abdel Sayed et al., 1985; Bishara, 1985; Ooi and Rotter, 1990; Roberts 1998).

2.1.3. Yang (1976) (dynamic)

Yang (1976) studied the dynamic behavior of cylindrical shell filled with liquid. Even if focused on fluid-liquid storage tanks, this research work provides an analytical framework for the evaluation of dynamic properties (such as fundamental period of vibration and modal shapes) of such cylindrical shell structures. The shell structure is modeled as a cantilever beam. The entire mass of the liquid is considered as a uniformly distributed on the cylindrical shell wall.

2.1.4. Lee (1981) (dynamic)

Lee (1981) proposed an analytical model for the estimation of the mass of the ensiled grain participating with the wall of cylindrical ground-supported silos subjected to harmonic base excitation. In detail, by analyzing the variation of the fundamental frequency of vibration *f* of grain-silo systems between the empty and the filled condition, the fraction of grain mass participating with the silo wall to the motion (i.e. the *effective mass*) is identified. The analytical framework grounds on the following assumptions:

- The cylindrical shell deforms only in flexure;
- The ensiled granular material does not contribute to the stiffness of the silo wall;
- The mass of the system (under different filling conditions) participating to the motion is composed by the wall mass (M_{wall}) plus the mass added by the portion of the grain interacting with the silo under dynamic excitation (M_{added});
- The silo is assumed to behave as a cantilever beam characterized by a uniform distribution of mass, uniform cross-section properties and material, over the whole height of the silo wall;
- The vibration mode shape of the grain-silo under dynamic excitation is approximated by the vertical profile of the deformed configuration of the grain-silo system under uniform lateral load.

Starting from the analytical definition of the fundamental frequency of vibration *f* of a uniform flexural cantilever beam with uniform distributed mass $\overline{m}$ (using Rayleigh-Ritz method) and considering two different filling configurations, referred to as c_1 and c_2

(characterized by a corresponding fundamental frequency of vibration f_{c1} and f_{c2}), the ratio between the value of the uniform distributed masses $\overline{m}_{c1}$ and $\overline{m}_{c2}$ results:

$$\frac{\overline{m}_{c1}}{\overline{m}_{c2}} = \frac{f_{c2}^2}{f_{c1}^2} \tag{5}$$

For any filling configuration, the uniform distributed mass $\overline{m}$ results as the sum of the wall mass (M_{wall}) and the mass added by grain participating with the silo wall to the motion (M_{added}), divided by the height of the silo wall *L*, i.e. $\overline{m} = \left(M_{wall} + M_{added}\right)/L = \overline{m}_{wall} + \overline{m}_{added}$. Thus, considering the first filling configuration c_1 coincident to the filled configuration, whilst the second filling configuration c_2 coincident with the empty configuration, it simply results that $\overline{m}_{added} = \overline{m}_{c1} - \overline{m}_{c2} = \overline{m}_{filled} - \overline{m}_{empty}$. Taking into account Eq. (5), after some calculations, the value of the *effective mass* m_{eff}, i.e. the ratio between the uniform added mass per unit length $\overline{m}_{added}$ and the uniform mass per unit length corresponding to the whole mass of ensiled grain-like material $\overline{m}_{grain}$, results:

$$m_{eff} = \frac{\overline{m}_{added}}{\overline{m}_{grain}} = \frac{\left(\frac{f_{empty}^2}{f_{filled}^2} - 1\right) \cdot \overline{m}_{wall}}{\overline{m}_{grain}} \tag{6}$$

The values of fundamental frequency of vibration in empty condition f_{empty} and filled condition f_{filled} have to be experimentally evaluated, and it should be observed that the analytical framework by Lee (1981) retraces that proposed by Chandrasekaran and Saini (1968) and Chandrasekaran and Jain (1968). Although it could be applicable to various filling configurations, because of the assumption of uniform mass distribution along the whole silo wall height *L*, the application of such analytical model should be applied with reference to such filling configurations that match the aforementioned assumption, i.e. those referred as the empty and the full-filled configurations.

2.1.5. Trahair et al. (1983) (dynamic)

The analytical formulation proposed by Trahair et al. (1983) represents the earliest closed-form prediction of the additional grain-pressure distributions acting on the silo wall

under accelerated conditions. It is developed considering a continuum approach. This formulation grounds on the simplest assumption that each horizontal layer of the ensiled grain applies a load directly to the wall uniformly around the wall circumference. This load is the result of a rigid body motion of the whole ensiled content. This formulation does not consider the load transfer to the base through horizontal grain-grain frictional stresses and ignores the vertical grain-wall frictional stresses (Rotter and Hull, 1989).

These assumptions lead to very simple, conservative, expressions of the radial and circumferential additional pressures (as referred to as $\Delta p_{n,GW}(\vartheta)$ and $\Delta p_{\vartheta,GW}(\vartheta)$, respectively) acting on the silo wall in order to balance the inertial forces:

$$\Delta p_{n,GW}(\vartheta) = \frac{\alpha_g \cdot \gamma_b \cdot R \cdot \cos(\vartheta)}{2} \cdot \phi \tag{7}$$

$$\Delta p_{\vartheta,GW}(\vartheta) = \frac{\alpha_g \cdot \gamma_b \cdot R \cdot \sin(\vartheta)}{2} \cdot \phi \tag{8}$$

where α_g is the ratio of the constant horizontal acceleration to the gravity acceleration g, ϑ is the latitude with respect to the direction of the horizontal acceleration and ϕ depends on the slenderness ratio of the silo: 1 if $H/R \geq 1$, (H/R) for shallower silos.

The influence of the grain properties on the overpressure distributions acting on the silo wall is not considered (except for the unit weight, γ_b). Considering that the whole ensiled content experiences a rigid body motion, the *effective mass* equals the unity.

2.1.6. Younan and Veletsos (1998) (dynamic)

Younan and Veletsos (1998*a*) and Veletsos and Younan (1998*b*) analyzed the dynamic response of vertical, rigid and flexible circular cylindrical tanks filled with a homogeneous, linear viscous-elastic solid medium (Figure 2.2*a*) under the following basic assumptions: (i) the contained material behaves as a continuous unconstrained cantilever shear-beam (with fundamental circular frequency ω_1); (ii) the ensiled content with its whole mass dynamically interacts with the circular wall; (iii) no sliding between the contained material and the basement may occur; (iv) two different limit wall-grain interface conditions (ideally rough and ideally smooth) are considered for the circumferential motion in the horizontal plane. The dynamic response of the grain-silo system is characterized by vertical modes (subscript *n*) and radial modes (subscript *m*). The

frequency of vibration corresponding to the *n-th* vertical mode and *m-th* radial mode is referred to as ω_{mn}. Within this framework, the dynamic response of the grain-silo system is governed by the natural mode corresponding to the first fundamental vertical mode and several horizontal modes (ω_{m1}). The fundamental circular frequency of the system, referred to as ω_{11}, depends on the viscous-elastic properties of the solid medium, on the medium-wall interface limit conditions (ideally smooth or ideally rough) and on the slenderness ratio of the silo, only. In other words, the mechanical properties of the silo wall do not affect the natural frequencies of the system. Starting from the equation of motion for the medium under harmonic response, the dynamic stresses acting on the silo wall, whose integral along the circumference at the base is equal to the base wall shear, are identified. By using these fundamental results, the base wall shear is then evaluated for various dynamic input such as constant acceleration, harmonic excitation, and earthquake-induced ground motion at the silo base. Accordingly, the *effective mass* is evaluated as the ratio of the base wall static shear (i.e. the base shear evaluated for a harmonic input with frequency far from the fundamental frequency) and the horizontal inertia force associated to the entire ensiled mass. For slenderness ratios larger than 0.5 (encompassing almost all realistic cases) it assumes an almost constant value which is around 0.8 for the case of rough interface and 0.7 for the case of smooth interface. Current EN 1998-3:2006 (Eurocode 8) provisions ground on this analytical formulation.

2.1.7. Durmuş and Livaoglu (2015) (dynamic)

Durmuş and Livaoglu (2015) proposed an analytical model to assess the magnitude and the vertical profile of the dynamic pressures exerted on the silo wall, the value of the wall base shear action and to estimate the fundamental frequency of vibration f_1^* of circular flat-bottom silos containing elastic material. The formulation is based on the following assumptions: (i) the system is modeled as an equivalent Single Degree Of Freedom (SDOF) flexural cantilever beam with a top lumped mass; (ii) the granular ensiled content is modeled as a homogeneous linear-elastic continuum (Figure 2.2*b*). For the evaluation of the fundamental frequency of vibration, the total mass of the equivalent SDOF system is equal to the silo wall mass plus the 100% of the ensiled mass. The resulting total mass is further reduced by a factor equal to 2/3 according to ACI 317R-98

prescriptions. The equivalent lateral stiffness of the SDOF system results as the sum of the flexural lateral stiffness of the silo wall and ensiled content.

The fundamental frequency of vibration f_1^* of the equivalent SDOF results:

$$f_1^* = \frac{1}{2\pi} \cdot \sqrt{\frac{\frac{3\pi \cdot E_w \cdot \left(r_2^4 - r_1^4\right)}{4 \cdot H_w^3} + \frac{3\pi \cdot E_m \cdot r_1^4}{4 \cdot H^3}}{\left(2/3\right) \cdot \left(m + m_w\right)}} \tag{9}$$

where E_w, E_m and H_w, H are the wall and the bulk materials' modules of elasticity and the heights, respectively; r_1 and r_2 are the internal and external radius of the silo, respectively; m_w and m are the silo wall mass and the total mass of the ensiled bulk solid, respectively.

The reaction of the SDOF exposed to ground motion, such as the wall base shear and bending moment, may be obtained by solving the equation of motion in general terms. The vertical profile and magnitude of the dynamic overpressure exerted by the ensiled material against the silo wall is correlated to the vertical profile of the horizontal acceleration along the silo wall, which is expressed by means of a pre-defined shape function.

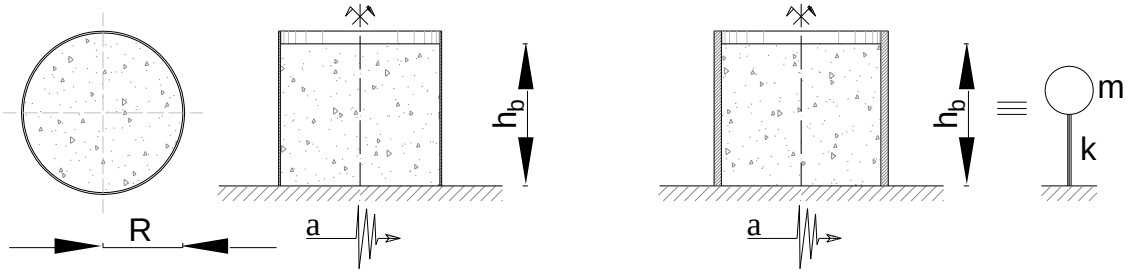

Figure 2.2 - Analytical model by Younan and Veletsos (1988) and (b) Durmuş and Livaoglu (2015) (Figure adapted by Younan and Veletsos 1988 and Durmuş and Livaoglu 2015)

2.1.8. Critical considerations

In the scientific literature, different analytical formulations have been proposed since the end of the 19th century to predict the static behavior or the dynamic response of

grain-silos. The former aims to evaluate the pressures distributions exerted on the silo wall after filling, whilst the latter aims to assess the distributions and the magnitude of the pressures exerted by the ensiled grain on the silo wall and to evaluate the overall response of the grain-silo system subjected to base excitation.

Among the many analytical formulations proposed for the prediction of the grain-wall pressure under filling (which have been not all reported here for sake of conciseness), the most consolidated are the Janssen (1895) and the Reimbert and Reimbert (1976) formulations, which have been widely experimentally verified and thus represent mile stones in both the scientific and the practical literatures (and generally are referred to as classical theories). According to such theories, under static conditions, only a fraction of the whole ensiled granular content pushes on the silo wall (referred to as *effective mass*), depending on the slenderness ratio, the pressure ratio and the grain-wall friction coefficient. In particular, for slender silos, the *effective mass* approaches roughly the 80%, with a marginal effect of the pressure ratio and the grain-wall friction coefficient. On the contrary, for squat silos, the *effective mass* approaches lower values, the effect of the pressure ratio and the grain-wall friction coefficient may result significant and the influence of the upper conical pile at the silo top on the pressure distributions may be significant.

Only few are the analytical formulations proposed in scientific literature for the prediction of the dynamic behavior of grain-silo systems and generally they are of relatively recent formulation. In general, it appears that the amount of mass pushing on the silo wall and participating in the motion (*effective mass*) is significantly dependent on the slenderness ratio and the grain-wall interface conditions. In particular, for slender silos, the *effective mass* approaches the 100%, regardless on the grain-wall interface conditions. On the contrary, for squat silos, a reduction of the *effective mass* should be accounted and its value may approach roughly the 80%; the effect of the grain-wall interface conditions may result significant and tends to increase the value of the *effective mass*. In addition, under lateral loading (such as horizontal inertial actions), the overall stiffness of the grain-silo system can be adequately captured by a cantilever model which accounts for both flexural and shear contributions. In this respect, the stiffness contribution provided by the ensiled materials, for common dry granular materials, results to be negligible. In general, those proposed analytical models are focused in assessing a specific issue (such as evaluation of the grain-wall overpressures, determination of the *effective mass*, prediction of the grain-

silo dynamic response under base excitation) and restricted to dynamic conditions only. Thus, a general and comprehensive analytical formulation able to encompass both static and dynamic conditions has not yet formulated.

2.2 Numerical studies

In this section, a review of the main numerical studies on the static and the dynamic behavior of grain-silos is reported. Various modeling techniques have been proposed in the scientific literature in order to predict specific aspects of the problem, such as the grain-wall pressures and the wall actions (both under static and seismic conditions), or the dynamic response of vibration of grain-silo systems under base excitation. The most of such specific modeling techniques implement continuum Finite Element (FE) models and are validated by means of some experimental results (which are reported in chapter 3). Among the many numerical works performed for the prediction of the grain-wall pressure under filling conditions, a non-exhaustive number of works is reported, together with the numerical works carried out for the prediction of the dynamic behavior of grain-silo systems under base-excitation available in the scientific literature.

2.2.1 Yokota et al. (1983) (dynamic)

Yokota et al. (1983) developed a linear FE model of a cylindrical shell and the ensiled coal made of 253 axisymmetric finite elements of triangular cross-section in order to compare numerical results and experimental findings relative to their tested coal-silo. Perfect grain-wall compatibility is assured. The coal is divided in layers characterized by increasing values of grain Young's modulus going from the top to the bottom in order to account for the dependence of the coal physical properties with the confining pressure. The numerical natural frequencies, the modal shapes and the wall stress-distributions were compared with the experimental ones. The first and the second numerical natural frequencies are around 30-40% larger than the experimental ones. The numerical modal shapes and wall stress-distributions correspondent to the first and the second natural mode are qualitatively well captured.

2.2.2 Shimamoto et al. (1984) (dynamic)

Shimamoto et al. (1984) simulated their tested silo specimens with conical shell elements, while the ensiled coal is simulated with nonlinear axisymmetric solid elements. Material properties adopted in the model (shear modulus and equivalent damping ratio of the coal) are based on cyclic triaxial tests. Numerical results of the dynamic response are obtained by means of an equivalent linear analysis (developed by Lysmer et al. 1972), which account for the dependency of the dynamic properties of the coal on the strain experienced during motion. The comparison between experimental and numerical results is carried out in terms of resonance curves of the grain and of the silo wall for two level of base acceleration a (0.03 and 0.10, in units of g). For a= 0.03, the resonance frequency as well as the amplification at the resonance is well captured; for a= 0.10 the tendency of the shift of the resonance amplification was captured, whilst the dynamic amplifications are not well captured due to grain sliding.

2.2.3 Sakai et al. (1985) (dynamic)

Sakai et al. (1985) modeled their tested silo specimens with shell elements and solid elements for the cylindrical wall and the ensiled content (coal and air granulated slag), respectively. Two values of the equivalent Young's modulus are used for the grain in the central part of the silo and for the grain in contact to the wall, the latter being smaller than the former. The equivalent damping ratios of the coal and air granulated slag was assumed equal to 40% and 23%, respectively. The resonance curves were obtained by using a dynamic analysis program ("SPHESRAN"). Considering a base input a of 0.05-0.10, the numerical results in terms of resonance curves are in good agreement with those detected under harmonic signal. Note that experimental equivalent damping ratios obtained for the coal and air granulated slag are equal to 20% and 12%, respectively.

2.2.4 Naito (1988) (dynamic)

Naito (1988) performed numerical investigations focused on the nonlinear dynamic behavior of silos by implementing an equivalent linear technique accounting for granular material plasticization. The ensiled content and the cylindrical shell are modeled by solid axisymmetric elements. The equivalent elastic properties of the ensiled coal (Young's modulus and Poisson's coefficient) are related to the confining pressure. The initial rigidity

of the coal is obtained from elastic wave velocity tests. The numerical results were represented in terms of resonance curves of the ensiled content under harmonic signal with various input magnitude (0.02 – 0.20), which are compared with the corresponding experimental results. The FE model reproduces: (i) the decreasing of the first resonance frequency and of the dynamic amplification for increasing magnitude of the input; (ii) the progressive reduction of the dynamic amplifications for frequency progressively higher than the first resonance frequency.

2.2.5 Rotter and Hull (1989) (dynamic)

Rotter and Hull (1989) studied the earthquake response of squat ground-supported circular grain-silos by means of an elastic finite element analysis. The silo wall and the ensiled content are assumed to respond elastically to seismic loading and modeled as an axisymmetric elastic body using FE method, with the ensiled content subjected to a uniform horizontal acceleration. It is assumed that vertical slip between grain and silo wall does not occur during the earthquake (although such assumption is almost certainly not valid). The roof is ignored, since it provides negligible effects in terms of restrain the displacement of the upper portion of the silo wall. The silo wall is clamped at the base and the grain-wall interface is ideally rough. A parametric study is conducted by varying the radius-to-wall thickness ratio, the slenderness ratio and the modular ratio between silo wall and ensiled content in order to explore the dependence of the stress distributions. Results indicate that the membrane wall stresses tend to increase with the slenderness ratio and with the radius-to-thickness ratio. The modulus of the stored solid has only a minor effect on the amplitude of the wall stresses. These findings are explicitly mentioned in EN 1998-4:2006 provisions.

2.2.6 Ooi and Rotter (1990) (static)

Ooi and Rotter (1990) developed a simple FE analysis in order to study the horizontal pressure exerted by ensiled bulk solids on the wall of squat steel silos during the initial filling conditions. The study is undertaken to explore the stress states which occur in a homogeneous linear elastic mass of material without initial strains, subjected to the self-weight, and stored in a flat-bottom circular silo with frictional sliding contact on the wall. The finite element predictions are compared with existing classical theories and with

experimental results. The finite element model consists of three component: (i) the silo wall; (ii) the grain-wall interface; (iii) the ensiled granular material. The silo wall and the stored solid are modelled as axisymmetric bodies by using 12-noded cubic elements, whilst the grain-wall interface is modelled via contact elements which implements the Coulomb friction law. The finite element predictions of the vertical profile of the horizontal pressures exerted by the grain on the silo wall after filling result in good agreement with those given by experimental results by Mahmoud and Abdel-Sayed (1981) and other performed by the University of Sydney (1983). The Authors state that complex non-linear material characterization is not necessarily needed to produce satisfactory predictions of wall pressures during the initial filling conditions.

2.2.7 Sasaki and Yoshimura (1992) (dynamic)

Sasaki and Yoshimura (1992) developed a numerical model in order to reproduce the seismic response of the tested 1/8-scale ($\Delta = 1.95$) stave-silo model (Sasaki and Yoshimura 1984, 1986, 1988), i.e. the specimen characterized by structural discontinuities, filled with rice (Figure 2.3*a*). The silo wall is modeled with a so called "stave silo element", with a fictitious mass density in order to account for the contribution of the ensiled grain mass participating to the motion leading to an *effective mass* of 0.7. The equivalent spring stiffness to the cylindrical shell is calculated based on the shell theory. The effect of the grain in avoiding any ovalization of the circular cross-section is neglected. The suggested value of the *effective mass* is the one that best fit the experimental resonance curves.

2.2.8 Yoshida (1993) (static)

Yoshida (1993) developed a two-dimensional model using Discrete Element Method (DEM) in order to study the distribution of the horizontal pressure exerted by ensiled bulk solid on the silo wall after filling. The influence of many parameters such as the grain-wall friction coefficient, the arrangement of particles, the diameter of the particles are investigated and the numerical predictions are compared with existing classical theories. The numerical model consists in a 40 *cm* width and 50 *cm* height two-dimensional silo, filled with 5000 particles of 6 *mm* diameter. First, the particles are arbitrarily arranged inside the silo with small spaces between them; then, gravity force is

applied at each particle. The calculation is continued until the motion of the particles is sufficiently converged. Once the total calculation is performed (usually 10000 steps were necessary), the distributions of grain-wall pressures are obtained by integrating the contact forces at each 4 to 5 *cm* interval. It observed that: (i) the vertical profiles of the grain-wall pressure is similar to those given by the classical theories; (ii) the numerical results are significantly influenced by the particles arrangement (random or regular); (iii) the numerical results are influenced by the particle size and for smaller diameters the pressure distributions become smoother; (iv) the pressure distribution over an horizontal section tends to decrease near to the wall.

2.2.9 Hardin et al. (1996) (dynamic)

Hardin et al. (1996) developed a numerical model with the main aim of evaluating the seismic response of a real metal flat-bottom on-ground circular grain-silos filled with wheat ($\Delta = 0.9$). It is assumed that the silo wall presents linear-elastic behavior, whilst the ensiled content presents a strongly nonlinear shear stress-strain relationship (tests on the bulk solid are required in order to characterize the material properties to be inserted in the numerical model). The grain-silo system is modelled by means of a composite shear-beam model. The variation of thickness of the silo wall and the variation in the shear modulus and the damping of the ensiled content are taken into account by dividing the shear-beam into several sublayers, where the material properties are considered uniform. Considering a horizontal sublayer of the grain-silo system, the composite shear stiffness, the composite hysteretic damping ratio and the composite mass density, which account for the grain and wall contributions, are assigned to the equivalent shear-beam at each level. The response of the grain-silo system is estimated via an iterative equivalent linear analysis in the frequency domain. The composite shear-beam is then subjected to a real earthquake record (N21°E horizontal Castaice earthquake) scaled to a maximum acceleration of 0.1 *g*. The frequency contents of the grain-silo response, the top amplification of the horizontal acceleration, the acceleration history and the stress-strain distributions are obtained. In particular, a natural frequency of 4 *Hz* is obtained and a maximum amplification factor of 2.9 is calculated.

2.2.10 Rotter et al. (1998) (static)

Rotter et al. (1998) reported the main results of an international collaborative study into the predictive capacity of current Discrete Element Method (DEM) and Finite Element Method (FEM) in calculating the order of magnitude and profile of the pressure distributions exerted by stored materials against the silo wall under filling and discharging conditions. Simplified silo problems were taken as case studies and well-documented real sand was chosen as ensiled granular material. The study was restricted to a two-dimensional (2D) planar problem. The numerical results were also compared with theoretical formulations and empirically derived design rules. With specific regards to the filling predictions, Rotter et al. (1998) showed that different FE and DE programs and modelling assumptions gave surprisingly different predictions in terms of vertical distribution of the horizontal grain-wall pressure. The differences between FE models appear to be mainly related to the modelling of the progressive filling process and the value of the effective pressure ratio to be accounted by means of a well-defined constitutive model for the ensiled granular material. The differences between DE models appear to be related with the algorithms and contact models adopted. By comparing the numerical outputs given by the FE and the DE analyses, a very large difference was observed in the profiles of the wall pressures, mainly related to the different character of the two methods. It is concluded that DEM can give acceptable qualitative predictions of several dynamic phenomena that occur in silos; however, due to the huge numbers of particles needed for quantitative and meaningful predictions of silo calculations (where around 10^7-10^{15} particles are typically involved), the adoption of DE models is still not feasible for practical use. FEM can give credible quantitative predictions of silo pressures, despite the simplifications performed and the assumption of rather simple material behavior; however, the scatter between FE analyses performed by different Authors shows that the requirements for a reliable finite-element analysis of filling have not yet been adequately studied.

2.2.11 Ayuga et al. (2001) (static)

Ayuga et al. (2001) developed several finite element models in order to analyze the behavior of cylindrical grain-silos under filling and discharging conditions. The influence of the type of wall (steel or r.c.) and the geometrical characteristics of the silo structure (flat-bottomed or with conical hopper), the influence of different parameters of the stored

granular material and the mesh sizes were analyzed with regard to their effect on pressures. The FE models are axisymmetric and consist of three component: (i) the silo wall; (ii) the ensiled granular material; (iii) the grain-wall interface. The silo wall is modelled by means of shell elements. The granular material (Camacho wheat) is modelled via four-node elements accounting for Drucker-Prager (1952) criterion of plasticity. The grain-wall interface is modeled via two-nodes contact elements, having the possibility of taking into account friction and loss of contact. The numerical distributions and the values of the grain-wall pressures are validated by comparing them with those predicted by the classical theories and code provisions of EN 1991-4:1995 and DIN 1055 (1987). Regarding with the numerical modeling of the filling condition, it is shown that: (i) the variation of the Poisson's ratio between 0.2 and 0.4 may produce up to a 90% in the pressures magnitude and may have a notable effect on the way the ensiled material behaves; (ii) the greater the grain-wall friction coefficient, greater the horizontal pressure, with a 30% increase when moving from a coefficient of 0.25 to that of 0.5; (iii) large mesh size (of about 1 *m*) provides good results and produces little difference compare to finer mesh sizes.

2.2.12 Wagner et al. (2002) (dynamic)

Wagner et al. (2002) developed two FE models in order to: (i) reproduce the time-evolution of the experimental dynamic grain-wall pressure acting on a steel silo under seismic excitation; (ii) predict the damage occurring on a r.c. grain-silo subjected to a base triangular impulse load. The numerical model includes three components: (i) the granular material; (ii) the contact area between the granular material and the silo wall; (iii) the silo wall. The granular material is modeled by means of solid elements. Intergranular strain approach is adopted for describing the non-linear time dependent behavior of the ensiled granular material. The contact area between the material and the silo wall is modeled by means of an interface to simulate the interaction between the silo shell and the granular material. In detail, the interface is modelled using an 8-node volume element consisting of two layers of nodes. Such element links the adjacent nodes of the shell element with the nodes of the solid element representing the granular material, thus permitting an eventual local decoupling of the granular material from the shell. The Mohr-Coulomb friction law is adopted. The silo walls are modeled by means of shell finite elements, both for the steel and r.c. silo. For the steel silo, linear-elastic behavior of the material is consider. For the r.c. silo, physical nonlinearity of the wall material is implemented by means of multi-

layered shell model and the concrete model proposed by Darwin and Pecknold (1977) is adopted to account the mechanical nonlinearity of concrete. The steel silo has 20 *m* height and 10 *m* diameter, with a uniform 0.03 *m* wall thickness. The r.c. silo has an height of 40 *m* and 16 *m* diameter, with a uniform 0.30 *m* wall thickness. The bottom section of the silos is considered as rigidly fixed. The silos are full-filled with "Hochstetten sand" (whose main parameters are described in Wolffersdorff, 1996); a grain-wall friction coefficient $\mu_{GW} = 0.5$ is considered.

The r.c. silo model is first checked computing the static loads only, i.e. the dead load of the silo wall and the granular material, then comparing the numerical output expressed in terms of vertical distribution of the horizontal grain-wall pressure with that predicted by Janssen (1895) (Wagner and Meskouris, 2001). Under static loads, cracks in the lower part and medium part of the silo wall are detected, due to the effect of bending and radial tension acting on the wall, respectively. Subsequently, the silo is subjected to a triangular impulse base load with a peak acceleration of approximatively 0.1 *g* and a 2 *s* duration. It is observed that: (i) the cracks in the lower part of the shell increases; (ii) the concrete layers on the side under tension due to the lateral inertial loading completely crack; (iii) such crack state does not heal after complete unloading.

The steel silo FE model is subjected to a synthetically generated strong earth motions (compatible with the prEN 1998-1, CEN 2003*a*). Under shaking, the time-dependent behavior of the dynamic horizontal pressure exerted on the silo wall on two opposite nodes appears anti-symmetric, however the maximum horizontal dynamic pressures during excitation on both sides do not reach the same value. After shaking, an increase of the static pressures is observed. The numerical results appear to qualitatively reproduce the experimental findings observed on silo models and later reported by Holler and Meskouris (2006).

2.2.13 Holler and Meskouris (2006) (dynamic)

Holler and Meskouris (2006) developed a numerical model accounting for five components: silo wall, ensiled content, grain-wall interface, silo foundation and subsoil, in order to simulate the dynamic behavior of ground supported flat-bottom circular grain-silos (Figure 2.3*b*). The silo wall is modeled by shell elements with linear-elastic behavior, the ensiled content is modeled by solid elements with hypoplastic behavior, grain-wall

interface is modeled by contact elements in order to ensure geometrical compatibility between silo wall and ensiled material (if contact is present shear stresses according to Coulomb friction law are exchanged by grain and wall, otherwise local separation occurs). Soil-structure interaction effects are also taken into account. Harmonic signal with low frequency and synthetically generated strong earth motions (compatible with the prEN 1998-1, CEN 2003*a*) are applied to the model (including the vertical ground motion). Comparisons between the numerical results and experimental measurements in terms of time-history dynamic overpressures acting on the silo wall (see section 3.2) indicate that the model is able to reasonably capture the overpressure profiles. The validated modeling technique is also used to model two realistic steel silos, one squat and one slender, in order to compared the model response in terms of circumferential and meridional wall stresses with those obtained following prEN 1998-4 prescriptions (CEN 2003*b*). In detail, the numerical model is used to obtain the silo fundamental period (assuming linear elastic behavior and grain-wall compatibility) in order to get the design loads to be used according to prEN 1998-4. The stresses are evaluated with and without soil-structure induced effects. For the particular example, the value on the code design spectrum corresponding to the situation in which soil-structure interaction is included increases with respect to the situation when no soil-structure interaction is considered, thus leading to an increase in both circumferential and meridional wall stresses. Such an increase is obtained for both the squat and slender silos given that the *effective mass* prescribed by prEN 1998-4 did not account for the slenderness ratio (entire mass of the content). The numerical simulation reveals that for the squat silo a substantially fraction of the ensiled weight is transferred directly to the ground by friction, thus not participating in the horizontal motion.

2.2.14 González-Montellano et al. (2012) (static)

González-Montellano et al. (2012) developed numerical analyses by means of three-dimensional DE models in order to simulate the filling and the discharge of a silo for two different granular materials: glass beads and maize grains. The research work was aimed to assess the capacity of the numerical models to predict the behavior of the studied ensiled materials. The numerical results included the vertical distributions of the normal pressure, frictional pressure and mobilized friction and the horizontal distribution of normal pressure. All these results are compared with the expected behavior during silo filling and emptying. The particles represented as reliably as possible the materials to be

simulated (glass beads and maize grains). The values for the variables associated with the glass beads and maize grains, i.e. those necessary for the models to function, were obtained experimentally. The virtual silo was filled progressively by the particles progressively generated and fell under gravity into the silo until reaching a static position. In all simulations non-linear contact model was employed for the simulation of particle–particle and particle–wall contacts. The vertical distributions of the normal pressure, frictional pressure and mobilized friction and the horizontal distribution of normal pressure were calculated using different discrete values for the variable under consideration. The calculation of these discrete values requires the use of spatial averaging procedures applied to small areas along the line of interest. In general, most of the results obtained (for the vertical distribution of normal and tangential pressure, the vertical distribution of mobilized friction, velocity profiles, and the surface distribution of the bulk density) were in line with those indicated by classic theories and prior experimentation. This demonstrates the great capacity of DEM for studying the behavior of granular materials in silos. However, the numerical predictions of the horizontal distribution of normal pressure did not agree with those obtained experimentally in the past, due to the contemplation of the silo walls as rigid. Thus, from a scientific point of view, the use of hybrid models that combine DEM and FEM is suggested in order to take into account the discrete nature of the granular material and the flexibility of the walls.

2.2.15 Livaoglu and Durmuş (2016) (dynamic)

Livaoglu and Durmuş (2016) developed a three-dimensional FE models of an intermediate-slender (Δ =1.5) and a slender (Δ =2.5) r.c. silos containing wheat in order to evaluate the effects of grain-wall interaction during of ground shaking. The vertical distribution of the dynamic grain-wall pressures, the horizontal wall displacements and wall base shear force are analyzed. The FE models account for three components: (i) the ensiled granular material; (ii) the grain-wall contact surface; (iii) the silo wall. The ensiled material is modelled via linear-elastic solid elements with material damping ratio equal to 10%. The grain-wall contact surface is modelled via interface elements where the contact mechanism is accounted by means of a surface-to-surface contact mechanism, which implements the Coulomb friction law. It enables load transfer by friction if contact is present; whilst it allows local loss in case of separation, with zero normal pressure. The silo wall of uniform thickness is modelled via linear-elastic solid element with material

damping ratio equal to 5%. Full transient dynamic analysis are develop and Rayleigh damping approximation is chosen in order to take damping into account. The horizontal N-S component of the 1999 Marmara earthquake is applied to the base of the model (the vertical component is neglected).

It results that the maximum dynamic grain-wall pressures occur at around the 60% and the 40% of the silo height (measured from the bottom) for intermediate-slender and slender silo, respectively. The vertical profile is qualitatively similar to those given by Eurocode 8 provisions. The horizontal wall displacements are related to the dominant mode shapes corresponding to intermediate-slender and slender silo. The slender silo tends to behave as a cantilever beam, whilst the intermediate-slender silo does not present a clear flexural mode. The wall base shear force are related to an *effective mass* resulting roughly the 80% of the total mass of the ensiled granular material for both silo models.

2.2.16 Bellos et al. (2015) (dynamic)

Bellos et al. (2015) studied the seismic response of an elevated grain-silo by means of different numerical modeling approaches. A sophisticated numerical model consists in a fiber-based nonlinear model including both material and geometrical nonlinearities for the shell of the silo and the supporting steel frames, whilst the ensiled content is modelled using 3D bricks elements incorporating Dracker-Prager soil constitutive law. The grain-wall interaction is provided by means of connection elements. A simpler numerical model consists in the crude silo-supporting frame structures on which the ensiled material is simply modelled by applying additional non-structural masses on the silo wall. Modal analysis and non-linear transient dynamic analysis (applying El-Centro ground motion record) are carried out on the models in order to define the natural frequencies and the global seismic response. Cross-section ovalizations is observed. However, the complex and simple modelling approaches do not lead to substantially difference in the estimation of the natural frequencies and in the evaluation of the response of the supporting steel frame.

A similar approach has been also considered by Uckan et al. (2015) for the assessment of the seismic response of elevated circular grain-silos subjected to the Van (Turkey) earthquake.

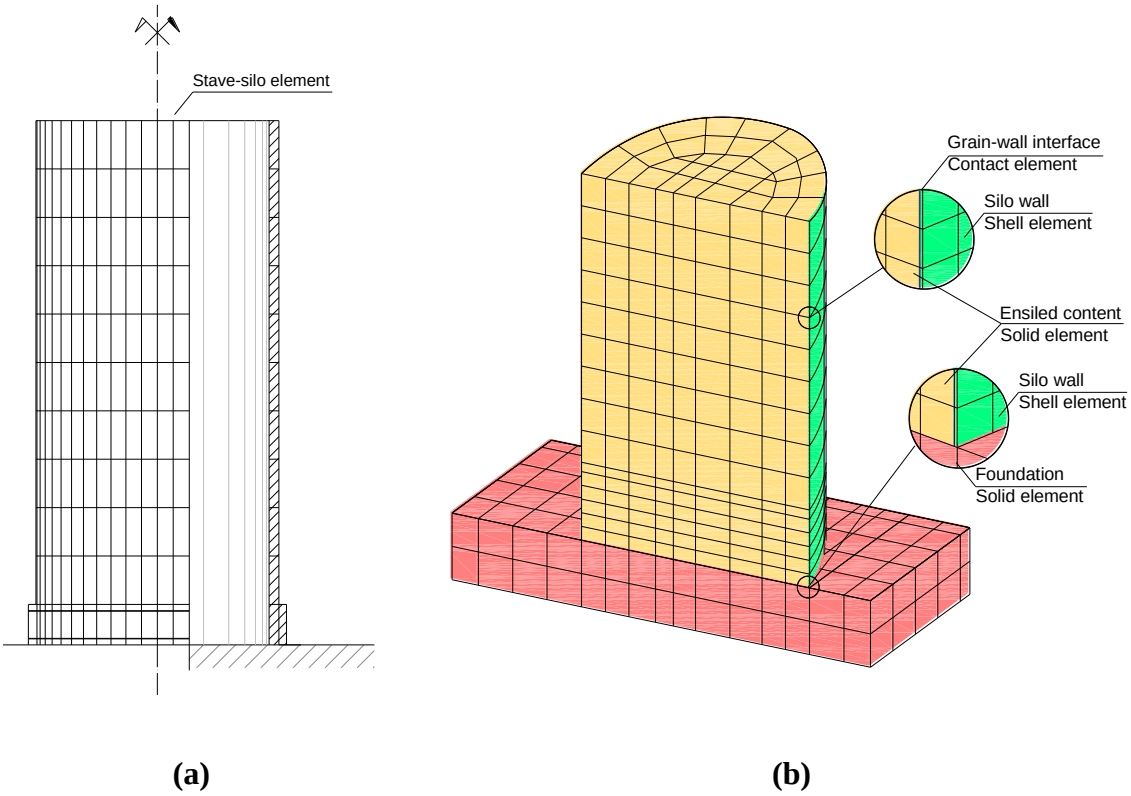

Figure 2.3 - FE models: (a) stave-silo model by Sasaki and Yoshimura (1992) and (b) grain-silo model by Holler and Meskouris (2006)

2.2.17 Critical considerations

From the 1980s, a large number of research teams have worked on the application of numerical models to silo problems. In general, the increasing capacity and speed of computers allowed to turn from simpler two-dimensional models to three-dimensional models.

As far as the numerical modeling techniques under static conditions are concerned, the behavior of grain-silos after filling is treated considering either Finite Element or Discrete Element models, either simple linear-elastic behavior or plasticity/non-linearity of the ensiled content. Hybrid models combining DEM and FEM may be adopted in the future to take into account the discrete nature of the granular material and the flexibility of the silo wall. For simple specific applications, numerical models appear, in general, able to well predict the distribution and magnitude of the grain-wall pressures under static conditions given by classical theories. Thus, due to the broad band of the values of the main parameters to be considered inside numerical models (especially for the ensiled granular content), a reliable numerical modelling cannot disregard from the experimental

estimation of the main physical and mechanical properties of the involved materials. Rotter (2009) recognized that continuum finite element treatment of the ensiled content have rather limited success in capturing actual silo behavior under filling and discharging conditions for more complex and general cases and thus further research is needed is such direction.

As far as numerical modeling techniques under dynamic conditions are concerned, the behavior of grain-silos under dynamic conditions is treated considering exclusively Finite Element models, considering either simple linear-elastic behavior or plasticity/non-linearity of the ensiled content, either taking perfect compatibility between grain and wall or considering frictional contact interface and eventually taking into account soil-structure interaction. Thus, it appears that a quite broad range of different FE numerical models, computational techniques and type of analysis may be applied for simulating grain-silos under dynamic conditions. On the contrary, Discrete Element models appear to be not used in the dynamic analysis of grain-silos.

Table 2.1 provides a summary/comparison of the main features of the numerical studies described in the previous section. In particular, the following information are reported:

- Modeling technique for: silo wall, ensiled material, grain-wall interface and soil-foundation;
- Type of analysis: eigenvalue, equivalent linear, pseudo-static, time-history, modal response, equivalent static;
- General objective of the numerical analysis and eventual experimental verification of the numerical results: evaluation of the fundamental periods, resonance curves, wall stresses, wall pressures and *effective mass*;

Table 2.1 - Summary of the main information from the relevant numerical studies on the dynamic response of grain-silos available in literature

Reference	Modeling techniques				Analysis	Objective	Experimentally validated
	silo wall	ensiled material	grain-wall interface	soil-foundation			
Yokota et al. (1983)	linear-elastic shell	linear-elastic solid	/	/	eigenvalue	natural periods	yes
Shimamoto et al. (1984)	linear-elastic shell	nonlinear-elastic solid	/	/	equivalent linear analysis	resonance curves	yes
Sakai et al. (1985)	linear-elastic shell	nonlinear-elastic solid	/	/	dynamic analysis *	resonance curves	yes
Naito (1988)	linear-elastic shell	nonlinear-elastic solid	/	/	equivalent linear analysis	resonance curves	yes
Rotter and Hull (1989)	linear-elastic shell	linear-elastic solid	/	/	pseudo-static analysis	wall stresses	no
Sasaki and Yoshimura (1992)	linear-elastic shell	/	/	/	time-history	resonance curves / *effective mass*	yes
Hardin et al. (1996)	linear-elastic shell	nonlinear elastic solid	/	/	equivalent linear analysis	Seismic response	no
Wagner et al. (2002)	linear-elastic shell	nonlinear elastic solid	contact element	/	time-history	wall pressures	no
	nonlinear elastic shell	nonlinear elastic solid	contact element	/	time-history	wall damage	no
Holler and Meskouris (2006)	linear-elastic shell	hypoplastic solid	contact element	yes	time-history	wall pressures	yes
	linear-elastic shell	linear-elastic solid	/	yes	modal response	natural periods	no
	linear-elastic shell	/	/	/	equivalent static analysis	wall stresses	no
Durmuş and Livaoglu (2015)	linear-elastic shell	linear-elastic solid	friction-to-friction contact element	/	time-history	wall pressure wall deformation base shear	no
Bellos et al. (2015)	non-linear shell	Drucker-Prager law	connection element	/	modal response and non-linear transient dynamic analysis	time-history of member stresses	no

* dynamic analysis implemented inside "SPHESRAN" program.

The modeling techniques summarize in Table 2.1 may be grouped in two families:

1. Full silo model (approach 1): both the silo wall and the ensiled material are explicitly modelled through finite elements. Typically, shell elements can be used to model the silo wall, while solid elements are necessary to model the ensiled content. The sophistication of the model varies depending on the

objective of the simulations. If the aim is to evaluate the fundamental period, linear elastic elements have to be used and no interface elements are required. If the aim is to evaluate stresses and pressures exerted by the grains to the wall, then more sophisticated non-linear constitutive laws for the solid elements are required and generally contact elements at the grain-wall interface need to be introduced.

2. Equivalent silo wall model (approach 2): only the silo wall are explicitly modelled, while the effect of the ensiled material is accounted by increasing the wall density by adding the effective mass of the grain uniformly on the wall. Nonetheless, special attention should be devoted in inhibiting local modes of the shell.

The use of approach 1 should allow at automatically avoiding any ovalization of the circular cross-section, i.e. additional constraints are not required. On the other hand, depending on the aim of the simulations, additional information on the behavior of the ensiled material and grain-wall interaction are required. If the aim is to evaluate the fundamental period, specific knowledge of the equivalent elastic properties of the particulate solid (at least Young's modulus and Poisson's coefficient) are required. Even though reference values can be found in various works by Hartlen et al. (1984), Thompson and Ross (1984), Roberts and Ooms (1983), wide discrepancies have been recognized by Abdel-Sayed et al. (1985) and Rotter and Hull (1989), thus suggesting on-site measurements (Rombach and Martinez 2009). The dependence of the elastic properties on the confinement pressure should be also accounted for. No direct control of the resulting *effective mass* is possible. If the aim is to evaluate stresses and pressures acting on the silo wall, the additional information needed to describe the nonlinear grain behavior and the grain-wall frictional interaction have to be somehow available. Also significant experience and expertise in numerical modeling, usually above that of practitioners, is suggested given that the numerical response is highly dependent on the adopted constitutive models for the solid elements, remembering that a disaggregated material does not strictly obey to the solid mechanics laws (Ayuga et al. 2005). Such approach allows to carry out various kind of seismic analyses, from more simple equivalent static analysis to more sophisticated non-linear time history analysis.

The use of approach 2 for the assessment of the natural period requires the inclusion of additional constraints (such as rigid diaphragm) in order to ensure that no

ovalizations arise. The *effective mass* has to be explicitly introduced by the user and its amount could be obtained according to: (i) code prescriptions (disregarding from the dependence on slenderness ratio and friction coefficient and pressure ratio); (ii) available analytical formulations; (iii) experimental data. If the aim is to evaluate stresses acting on the silo wall, appropriate pressure patterns have to be directly applied by the users. Such approach is suitable for seismic equivalent static and response spectrum analyses.

2.3 Critical considerations

In this section, a review of the main analytical and numerical works on the static and the dynamic behavior of ground-supported circular grain-silos is presented.

As far as the study of the static behavior of grain-silos is concerned, the theoretical formulations for the prediction of the horizontal and the vertical pressure distributions exerted by the grain on the silo wall by Janssen (1985) and Reimbert and Reimbert (1976) have been extensively verified and thus they are well consolidated in both the scientific and the practical literature. Numerical models (using Finite Element or Discrete Element Method) appear, in general, able to well predict the distribution and magnitude of the grain-wall pressures under static conditions given by classical theories only for simple specific cases, whilst they have rather limited success in capturing actual silo behavior under filling and discharging conditions for more complex and general cases.

As far as the study of the dynamic behavior of grain-silos is concerned, the theoretical formulations are few and generally aimed at assessing a specific issue (such as evaluation of the grain-wall overpressures, determination of the *effective mass*, prediction of the grain-silo dynamic response under base excitation) and restricted to dynamic conditions only. Thus, a general and comprehensive analytical formulation able to encompass both static and dynamic conditions has not yet formulated. Numerical models (using exclusively Finite Element models) are generally performed considering two different approaches (full silo model and equivalent silo model). Such approaches allow to carry out various kind of seismic analyses, from more simple equivalent static analysis to more sophisticated non-linear time history analysis. Numerical models appear, in general, able to well predict specific aspects of the grain-silos dynamics (resonance curve, grain-wall pressure distributions) for simple specific cases. Their application for practical purposes requires specific knowledge of the equivalent elastic properties of the particulate

solid and significant experience and expertise in numerical modeling, usually above that of practitioners, are necessary as well given that the numerical response is highly dependent on the adopted constitutive models for the solid elements.

Reference

Abdel-Sayed, G., Monasa, F. and Siddall,W. (1985) "Cold-Formed Steel Farm Structures Part I: Grain Bins", Journal of Structural Engineering, ASCE, III (STI 0), Oct., 2065-2089.

Airy, W., 1897, The pressure of grain, Proc of Inst of Civil Eng, CXXXI

Amundson LR. Determination of band stresses and lateral wheat pressures for a cylindrical grain bin. Agricultura Engineering 1945; 26:321‑345.

Arnold, ac, McLean, AG. and Roberts, AW. (1980) "Bulk Solids: Storage, Flow and Handling", Tunra Bulk Solids Handling Research Associates, University of Newcastle, Australia, Sept.

Ayuga, F., Aguado, P., Gallego, E., & Ramirez, A. (2005). New steps towards the knowledge of silos behaviour. International Agrophysics, 19(1), 7-17.

Ayuga, F., Guaita, M., & Aguado, P. (2001). SE—Structures and Environment: Static and Dynamic Silo Loads using Finite Element Models. Journal of Agricultural Engineering Research, 78(3), 299-308.

Bellos, J., Kanyilmaz, A., & Castiglioni, C. A. (2015). Simplified Numerical Modeling of Elevated Silos for Nonlinear Dynamic Analysis.

Bishara, A.G. (1985) "Interaction of Bin and Stored Bulk Solids", in Design of Steel Bins for the Storage of Bulk Solids (ed. J.M. Rotter), The University of Sydney, pp 27-33.

Briassoulis D. (1986) "Design Friction Loads for Concrete Silos", ACI Structural Journal, V.83, No.3, 438-445.

Briassoulis D. (1987), "Author's Closure to Discussion of 'Design Friction Loads for Concrete Silos' ", ACI Structural Journal, 84(2),178-179.

Briassoulis D. (1991), "Limitations in the Range of Applicability of the Classical Silo Theories", ACI Structural Journal, 88(4), 437-444.

Bovey, H.T., 1904, Engineering News, LII.

Chandrasekaran, A. R., & Jain, P. C. (1968). Effective live load of storage materials under dynamic conditions. Indian Concrete Journal, 42(9), 364-365.

Chandrasekaran, A. R., & Saini, S. S. (1968). Live load effect on dynamic response of structures. Journal of the Structural Division, 95(4), 649-660.

Darwin, D., & Pecknold, D. A. (1977). Nonlinear biaxial stress-strain law for concrete. Journal of Engineering Mechanics, 103(ASCE 12839 Proceeding).

DIN 1055 Part 6 (1987). Design loads for buildings. Loads in silo bins

Durmuş, A., & Livaoglu, R. (2015). A simplified 3 DOF model of a FEM model for seismic analysis of a silo containing elastic material accounting for soil–structure interaction. Soil Dynamics and Earthquake Engineering, 77, 1-14.

Drucker, D. C., & Prager, W. (1952). Soil mechanics and plastic analysis or limit design. Quarterly of applied mathematics, 10(2), 157-165

EN 1991-4 (2006) Eurocode 1. Actions on structures, Part 4 -Silos, tanks and pipelines, CEN, Brussels.

EN 1998-4 (2006) Eurocode 8. Design of structures for earthquake resistance, Part 4 -Silos, tanks and pipelines, CEN, Brussels.

Eurocode 1, ENV 1991-4. (1995). Basis of design and actions on structures. Part 4: Actions on silos and tanks

Gaylord, E.H. and Gaylord, e.N. (1984) "Design of Steel Bins for Storage of Bulk Solids", Prentice Hall.

González-Montellano, C., Gallego, E., Ramírez-Gómez, Á., & Ayuga, F. (2012). Three dimensional discrete element models for simulating the filling and emptying of silos: analysis of numerical results. Computers & Chemical Engineering, 40, 22-32.

Jaky, J. (1948) "Pressures in Silos", Proc., 2nd Int. Conf on Soil Mechanics and Foundation Engineering, Rotterdam, 21-30 June, I, 103-107.

Jamieson JA. Grain pressures in deep bins. CSCE Transactions 1903; 17:554‑607.

Janssen, H. A. (1895). Versuche über getreidedruck in silozellen. Zeitschr. d. Vereines deutscher Ingenieure, 39(35), 1045-1049.

Jenike A.W., Johnson J.R and Carson 1.w. (1973) "Bin Loads Part: Mass Flow Bins",Jnl. Engng Industry, Trans. ASME, 95 (Ser. B, No.1), 6-12.

Hardin, B. O., Bucklin, R. A., & Ross, I. J. (1996). Shear-beam analysis for seismic response of metal wheat bins. Transactions of the ASAE, 39(2), 677-687.

Hartlen, J., Nielsen, J., Ljunggren, L., Martensson, G. and Wigram S. The wall pressure in Large Grain Silos. Swedish Council for Building Research, Stockholm, 1984

Holler, S., & Meskouris, K. (2006). Granular material silos under dynamic excitation: numerical simulation and experimental validation. Journal of structural Engineering, 132(10), 1573-1579.

Homes A.G. (1972) "Lateral Pressures of Granular Material in Silos", ASME Paper No. 72-MH-30 for Meeting, Sept., 17-20.

Ketchum, M.S., 1919, The Design of Walls, Bins and Grain Elevators, (McGraw Hill. Third Edition (First Published 1907)).

Koenen, M.: Berechnung des Seiten- und Bodendrucks in Silozellen, Centralblatt der Bauverwaltung 16 (1896), pp. 446-449

Landry JW, Grest GS, Silbert LE, Plimpton SJ (2003) Confined granular packings: structure, stress, and forces. Phys Rev E 67(4):041303

Lee, S. J. (1981). Experimental study of cylindrical silos subject to seismic excitation (Doctoral dissertation, The Ohio State University).

Livaoglu, R., & Durmuş, A. (2016). A simplified approximation for seismic analysis of silo–bulk material system. Bulletin of Earthquake Engineering, 14(3), 863-887.

Lufft, E., 1904, Engineering News. LII: 531.

Lysmer, J., Seed, H. B., & Schanable, P. B. (1972). SHAKE: A computer program for earthquake response analysis of horizontally layered sites. Earthquake Engineering Research Center, University of California, Berkeley, Report No. EERC, 72-12.

Mahmoud, A. A., & Abdel-Sayed, G. (1981). Loading on shallow cylindrical flexible grain bins. J. Powder Bulk Solids Tech, 5(3), 12-19.

Naito, Y. Equivalent linear technique in the finite element method applied to deformation with volume change and to an axisymmetric body under an unaxisymmetric load. In Proceedings of the 9th World Conference on Earthquake Engineering, Tokyo-Kyoto, Japan (Vol. 3, pp. 133-138).

Negi SC, Ogilvie JR, Norris ER. Silage pressures in tower silos. Part 3. Experimental model studies and comparison with Canadian Agricultural Engineering 1977; 19(2):107‑110.

Ooi, J. Y., & Rotter, J. M. (1990). Wall pressures in squat steel silos from simple finite element analysis. Computers & Structures, 37(4), 361-374.

Ovarlez G, Fond C, Clément E. Overshoot effect in the Janssen granular column: a crucial test for granular mechanics. Physical Review E 2003; 67(6):060302.

Phillips, C.E.S., 1910, Proc Royal Institution, 19: 742.

Pieper K. and Wenzel F. (1963) "Comments on D1NI055: Design Loads for Buildings Loads in Silos Bins", Beton-und Stahlbetonbau, 6-11.

Pleissner, J., 1906, Versuche zur Ermittlung der Boden und Seitenwanddrucke in Getreidesilos, Zeitschrift des Vereines deutscher Ingenieure, 976

Prante, 1896, Messungen des Getreidedruckes in Silozellen, Zeitschrift des Vereines deutscher Ingenieure, 1192

Rankine, W. M. (1857). On the stability of loose earth. Philos Trans R Soc Lond 147:9–27

Reimbert, M., & Reimbert, A. (1943). Recherches novelles sur les efforts exercés par le matieres pulverulentes ensiles sur les parois des silos. Circulaire Serie I, (11).

Reimbert, M. and A. Reimbert. 1976. Silos—Theories and Practice. Clausthal, Germany, Trans Tech Publishers. 250p.

Reimbert, M. and Reimbert.A, (1987) Discussion of “Design Friction Loads for Concrete Silos”, ACl Structural Journal, 84(2), 178-179.

Roberts, A. W. (1998). Particle technology—Reflections and horizons: An engineering perspective. Chemical Engineering Research and Design, 76(7), 775-796.

Roberts A.W. & Ooms M. (1983). Wall Loads in Large Metal and Concrete Silos and Silos due to Eccentric Draw-Down and other Factors. Proc. 2nd Int. Conf. on Design of Silos for Strength and Flow, 151-170.

Rombach, G. and Martinez, J. (2009), Introduction and scope, Eds. Brown, C.J. and Nielsen, J., Silos: Fundamental of Theory, Behavior and Design, Taylor & Francis, London and New York.

Rotter, J. M., & Hull, T. S. (1989). Wall loads in squat steel silos during earthquakes. Engineering Structures, 11(3), 139-147.

Rotter, J. M., Holst, J. M. F. G., Ooi, J. Y., & Sanad, A. M. (1998). Silo pressure predictions using discrete-element and finite-element analyses. PHILOSOPHICAL TRANSACTIONS-ROYAL SOCIETY OF LONDON SERIES A MATHEMATICAL PHYSICAL AND ENGINEERING SCIENCES, 2685-2712

Sakai, M., Matsumura, H., Sasaki, M., Nakamura, N., Kobayashi, M., & Kitagawa, Y. (1985). Study on the dynamic behavior of coal silos against earthquakes. Bulk Solids Handling, 5(5), 1021.

Sasaki, Y., & Yoshimura, J. (1984). Dynamic behavior of concrete stave silos. In Proceedings of the 8th World Conference on Earthquake Engineering.

Sasaki, Y., & Yoshimura, J. (1988). Seismic Response of Concrete Stave Silos with Structural Discontinuity. Proceedings of the Ninth World Conference on Earthquake Engineering, Tokyo-Kyoto, Japan (Vol. VI).

Sasaki, Y., & Yoshimura, J. (1992). Dynamic discrete modeling and computer simulation of seismic response of concrete stave silos with structural discontinuity. In Earthquake Engineering, Proceedings of the Tenth World Conference, Balkema, Rotterdam (pp. 5065-6070).

School of Civil Engineering, The effect of increasing grain moisture content on the stresses in silo walls. Investigation Report S444, University of Sydney (1983)

Schwab CV, Ross IJ, White GM, Colliver DG.Wheat loads and vertical pressure distribution in a full-scale bin part I−filling. Transactions of the ASAE 1994; 37(5):1613.

Shimamoto, A., Kodama, M., & Yamamura, M. (1984). Vibration tests for scale model of cylindrical coal storing silo. In Proceedings of the 8th World Conference on Earthquake Engineering (Vol. 5, pp. 287-294). San Francisco.

Sperl M. Experiments on corn pressure in silo cells−translation and comment of Janssen's paper from 1895. Granular Matter 2006; 8(2):59‑65.

Tatko R, Kobielak S. Horizontal bulk material pressure in silo subjected to impulsive load. Shock and Vibration 2008; 15:543‑550.

Thompson, S. A., & Ross, I. J. (1984). Thermal stresses in steel grain bins using the tangent modulus of grain. STRAIN, 5, 1.

Toltz, M., 1903, Trans Canad Soc Civil Engineers, XVII

Uckan, E., Akbas, B., Shen, J., Wen, R., Turandar, K., & Erdik, M. (2015). Seismic performance of elevated steel silos during Van earthquake, October 23, 2011. Natural Hazards, 75(1), 265-287.

Vanel L, Clément E. Pressure screening and fluctuations at the bottom of a granular column. The European Physical Journal B—Condensed Matter and Complex Systems 1999; 11(3):525‑533.

Vanel L, Claudin P, Bouchaud JP, Cates ME, Clément E, Wittmer JP. Stresses in silos: comparison between theoretical models and new experiments. Physical Review Letters 2000; 84(7):1439.

Veletsos AS, Younan AH (1998) Dynamics of solid-containing tanks. II: flexible tanks. J Struct Eng ASCE 124(1):62–70

Walters). K. (1973) "A Theoretical Analysis of stresses in silos with vertical Walls.", Chem. Engng. Sci., 28,13-21.

Wagner, R., & Meskouris, K. (2001). Granular Material Behaviour under Dynamic Excitation.

Wagner, R., Noh, S. Y., Butenweg, C., & Meskouris, K. (2002). Seismic excited granular material silos. In Proceedings of Eurodyn (pp. 253-258).

Walker, D.M.(1966)"An Approximate Theory for Pressure and Arching in Hoppers". Chemical Engineering Science, 21, 975-997.

Wolffersdorff P. A. von (1996), A hypoplastic relation for granular materials with a predefined limit state surface, Mechanics of Cohesive-Frictional Materials, 1, 251–271

Yokota, H., Sugita, M., & Mita, I. (1983, November). Vibration tests and analyses of coal-silo model. In Proc., 2nd Int. Conf. on the Design of Silos for Strength and Flow, Stratford-upon-Avon, Powder Advisory Centre (November 1983) (pp. 107-116).

Yoshida, J. (1993). Study of Static Pressures of Granular Materials in a Silo Using the Distinct Element Method [Translated]. KONA Powder and Particle Journal, 11, 215-222.

Younan AH, Veletsos AS (1998) Dynamics of solid-containing tanks I: rigid tanks. J Struct Eng ASCE 124(1):52–61

3. Literature review of the experimental tests on the dynamics flat-bottom silos containing grain-like material and on-field reconnaissance campaigns

In this chapter, a review of the main scientific experimental works on the dynamic behavior of ground-supported circular grain-silos under base excitation and a collection of on-field reconnaissance data on the effects of strong-earth motions on real silo structures are presented. The main purpose of this review activity are to (i) collect and trace the time-evolution of the experimental studies on the dynamic behavior of grain-silos; (ii) organize, condense, compare and then critically discuss the evidences and the studies regarding the dynamic behavior of grain-silos in order to better understand their seismic behavior; (iii) collect the most significant data regarding the actual response of real grain-silo structures subjected to the major past seismic events and recognize the most typical failure modes affecting silos exposed to earthquake loadings. First, an insight into the complex behavior of granular material subjected to horizontal shaking is presented before focusing on the behavior of granular material poured inside cylindrical containers in order to better understand the global structural response of grain-silo systems. Then, a review of various experimental tests aimed at investigating the dynamic behavior of ground-supported circular grain-silos performed during the last century is presented. Finally, a review of the most significant cases of structural collapses related to the failures of grain-silo structures due to strong earth motion is chronologically presented.

3.1 Experimental tests on horizontally shaken granular material

In the present section, the main scientific works related to the dynamic behavior of horizontally shaken granular material is presented in order to provide a first insight into the complex behavior of particulate bulk solids under vibrations.

The experimental tests here reported are generally conducted by imposing, at the base of a rectangular box containing the granular material, a harmonic motion (characterized by a frequency f and a maximum amplitude of the acceleration a, which is usually expressed in unit of g. Figure 3.1 depicts the typical setups adopted for such tests.

3.1.1 Ristow (1997)

Ristow (1997) experimentally studied the behavior of horizontally vibrated thin layers (20 *mm* thick) of Ballottini glass (0.5-0.6 *mm* diameter), sampling the dislocation of grains. At low frequency, particles do not move; for increasing frequency particles start to move; a further increase of the frequency beyond a critical value determines the transition to the fluidized phase.

3.1.2 Liffman et al. (1992)

Liffman et al. (1997) performed computational studies of a horizontally shaken granular bed subjected to increasing acceleration. The analysis of the average grain displacement shows that no motion occurs until *a* reaches a critical value (referred to as a_{cu} , around 0.5); increasing of *a* provokes modest surface agitation (surface sloshing); further increasing of *a* enlarges the surface agitation and bulk convection occurs. Similar findings were presented by Salueña et al. (1999).

3.1.3 Metcalfe et al. (2002)

Metcalfe et al. (2002) performed a series of experiments and three-dimensional molecular dynamics simulations focused on the transition between fluid and solid states of granular materials (glass beads, sand) subjected to horizontal shaking. The evolution of the system is analyzed by slowly increasing *a*, keeping *f* constant. A critical value of a_{cu} (between 0.4 and 0.6, similar to that found by Liffman et al. 1999) leads to strong sloshing motion of the upper part of the granular material when grains overcome frictional and dilatancy effects. The existence of a small number of free grains (so-called "sliders"), sliding on the surface at any value of *a*, is recognized. For frequency within 2-8 *Hz*, fluidization occurs at similar value of a_{cu}. It appears that a_{cu} does depend on the physical properties of the material and increases for rougher grains.

3.1.4 Raihane et al. (2009)

Raihane et al. (2009) performed an experimental work dealing with horizontally shaken granular medium with thickness comparable with the other two dimensions (full 3D

geometry, as schematized in Figure 3.1). Sinusoidal vibration with wide frequency range (20 – 300 *Hz*) and acceleration *a* between 0.1 and 8.0 are imposed to the container base. The grain movement during vibration is captured by means of ultra-fast acquisition video record. For acceleration below a_{cu} (around 0.4, similar to that reported by other Authors), the granular medium state evolves from uniformly jammed to jammed in the lower part and glassy in the upper part (i.e. surface simmering and core densification). For higher *a*, fluidized layer appears above the jammed and glassy zones and convection motions are observed.

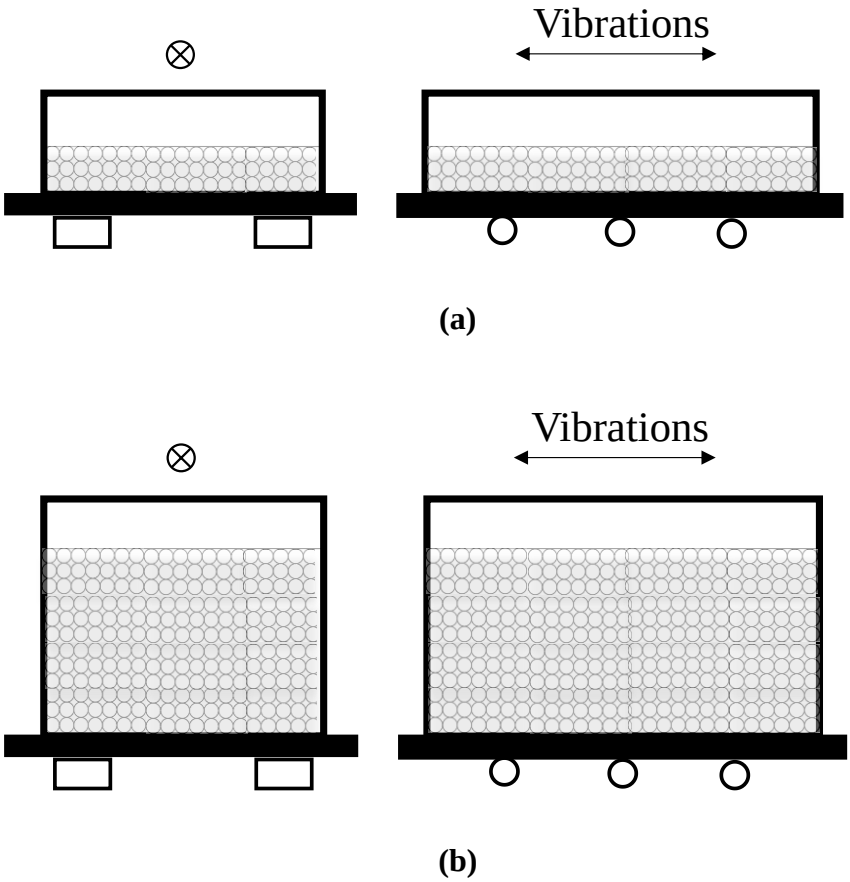

Figure 3.1 - Typical setup for experimental tests on horizontally shaken granular material: (a) thin-layer; (b) full 3D geometry

3.1.5 Critical considerations

The observations collected on the dynamic response of particulate bulk solids by horizontally shaking granular material poured in rectangular boxes, both in two-dimensional and three-dimensional configurations, allows to better identify their behavior under harmonic base excitations. Granular medium may present three different states: (i)

jammed, the granular medium behaves like a rigid solid; (ii) glassy, grains present slight chaotic movement and a densification may occur; (iii) fluid, convection motion may appear and grain medium behaves like a fluid and the grain layers close to the free-surface start to exhibit a back-and-forth sloshing motion. The state changes in relation to the frequency (*f*) and the maximum amplitude of the base acceleration (*a*) of the exciting harmonic input and appears to depend on the physical and frictional properties of the grains as well. The existence of a small number of free grains (so-called "sliders"), sliding on the surface at any value of *a*, is recognized. A threshold amplitude of the base acceleration (a_{cu}, roughly around 0.40) leading to fluidization of the upper part of the granular medium is recognized.

3.2 Dynamic tests on circular flat-bottom ground-supported grain-silos

In the present section, a review of the main scientific experimental works on the dynamic behavior of ground-supported circular grain-silos under dynamic excitation is presented. During the last century, various experimental tests have been performed in order to investigate the dynamic behavior of ground-supported circular grain-silos, to fully understand the complex interaction between cylindrical shell and ensiled content under earthquake excitation and to validate earthquake response analysis programs. Almost all the investigations were performed through shaking-table tests. Few Free-Vibrations tests (FV) are also available in the scientific literature. Usually, four different type of dynamic excitations are imposed: (i) White Noise signal (WN); (ii) Impulsive Load (IL); (iii) stationary Harmonic Signal (HS) with increasing frequency until resonance of the grain-silo occurs; (iv) Earthquake recorded signals (EQK).

3.2.1 Chandrasekaran and Jain (1968)

Chandrasekaran and Jain (1968) performed the first known vibration tests on circular grain-silos. Two silo specimens (made of Perspex and steel) were instrumented with strain gauges and vibration transducers. The silo specimens presented various filling conditions (empty, 2/4, 3/4, 4/4 of the maximum filling height h_b); at full filling the slenderness ratios $\Delta = h_b / d_c$ (where d_c is the diameter) were 9.6 and 10.8 for the Perspex and the steel specimens, respectively. Various granular materials were poured inside the

specimens including wheat, cement and sand. The specimens are excited by imposing an initial lateral displacement and then sudden releasing them, so that free vibrations may develop. It is found that the filling does not modify the lateral stiffness of the empty silo. Also the grain mass participating to the motion, often expressed in term of fraction of the total ensiled mass, referred to as *effective mass*, was determined according to a theoretical relationship developed by Chandrasekaran and Saini (1968). The values of the *effective mass*, for 25 different configurations, remains sensibly lower than unity (values around 0.22 and 0.54). Currently, FEMA P-750 (NEHRP 2009) provisions for seismic design of grain-silos adopts an *effective density factor*, which explicitly refers to these findings.

3.2.2 Lee (1981)

Lee (1981) performed shaking-table tests on a scaled circular silo specimen, conducted at the Ohio State University. The tests were aimed at simulate the seismic response of a cylindrical silos filled with different levels of granular material. The silo specimen was composed by a Lucite cylinder (Young's modulus E_w= 3100 *MPa* and Poisson's ratio ν_w = 0.35) with total height around 1500 *mm*, external diameter 300 *mm* and wall thickness 3 *mm*. The silo model was equipped with a silo base bolted to the base of the shaking-table. The silo wall was instrumented with six accelerometers disposed along the height of the silo wall (at the 15%, 30%, 50%, 65%, 80% and 100% of the height, starting from the silo bottom) along the excitation axis and longitudinal and circumferential strain gauges on the outer surface of the silo wall (at the 4%, 23%, 42%, 62%, 80% and 100% of the height from the bottom). The silo model was tested for five different filling heights (empty, 1/4, 1/2, 3/4 and 1/1) with sand. For each filling height, the silo model was subjected to a sinusoidal input with 15 *Hz* frequency and maximum acceleration of 0.5 *g* of 5 *s* duration. The horizontal acceleration response of the silo wall and the longitudinal and circumferential strains experienced by the wall are detected. The analyses of the acceleration response allows to compute: (i) the equivalent damping ratio ξ; (ii) the vertical profile of the dynamic amplification of the horizontal accelerations measured at different distance *z* with respect to the base acceleration $\zeta_w(z)$; (iii) the fundamental frequency of vibration; (iv) the stresses experienced by the wall. It is observed that:

- The fundamental frequency of vibration reduces for increasing filling heights. In detail, the fundamental frequency of vibration for the half-filled and full filled condition is around 13 *Hz* and 6 *Hz*, resulting roughly 1/2 and 1/5 of that corresponding to the empty configuration, respectively;
- For constant base input frequency and different levels of filling, resonance of the grain-silo specimen occurs for the half-filled condition, characterized by a fundamental frequency of vibration around 13 *Hz*;
- The damping ratio results around 3% for the empty silo, 4% for all configuration with exception of the half-filled configuration where 8% damping ratio is observed;
- The vertical profile of the dynamic amplification of the horizontal acceleration along the silo wall shows a general linear increasing trend, going from the bottom to the top of the silo, with exception for the full filled configuration where the vertical profile of the dynamic amplification of the horizontal acceleration tends to diminish going from the bottom to the top of the silo and a significant local amplification close to the silo top is detected. In particular, values of the dynamic amplification at the top of the silo wall result roughly 15 and 1 for the half-filled and full-filled configuration, respectively.
- The vertical profile of the reconstructed longitudinal and circumferential wall stresses generally increases from the top of the silo to the base of the silo wall. In particular, the highest values of the wall stresses in steady-state response are observed for the half-filled configuration, when resonance of the grain-silo system is observed.

3.2.3 Yokota et al. (1983)

Yokota et al. (1983) performed shaking-table tests on an acrylic resin circular coal-silo specimen with constant slenderness ratio $\Delta = 1.0$. The silo specimen was instrumented with accelerometers at different heights attached to the silo wall and inside the grain along the central line (axis of symmetry), strain gauges and earth pressure gauges. Two geometrical configurations are considered: with and without lid. Two filling conditions are considered: empty and full-filled. The silo specimen was excited by impulsive loads (IL) via hammering, and through shaking table under stationary harmonic signal (HS) and

white noise excitation (WN). The natural frequencies and the modal shapes were determined. For the empty silo without lid, IL and WN were applied and the first mode (characterized by a frequency of 36 *Hz*) presented section ovalization. For the empty silo with lid, IL and WN were applied and the first mode is of a cantilever type (no section ovalization) with a frequency roughly doubled with respect to the previous case (76 *Hz*). For the full-filled silo without lid, HS was applied and the first frequency is around one half (19 *Hz*) of that of the empty silo without lid and section ovalization are inhibited. The damping ratio strongly increases with grain filling (from 2.5% for the empty silo to 10% for the full-filled silo). The vertical and the circumferential variation of the horizontal acceleration on the wall, the vertical profile of the horizontal acceleration inside the grain, the dynamic overpressure exerted by the grain and the vertical and horizontal strains experienced by the wall during the tests are also reported. The dynamic amplification of the horizontal accelerations measured at different distance *z* from the grain free surface is also reported and indicated as $\zeta_g(z)$ for the grain and $\zeta_w(z)$ for the wall. Under HS excitation the maximum amplifications at the top of the silo wall reaches values around 3. When the system is excited by an harmonic signal (HS) with frequency equal to the first and second natural frequencies of the grain-silo: (i) both the grain and wall dynamic amplifications increase along the silo height; (ii) the dynamic amplifications of the ensiled grain are larger than those of the silo wall along the whole height, thus indicating relative movements; (iii) the vertical profile of the horizontal overpressure significantly increases going from the top to the bottom with a peak value at ¼ of the silo height equal to more than 4 times the value at 3/4 of the silo height. The overpressure at the base is around 1/3 of the peak value.

3.2.4 Shimamoto et al. (1984)

Shimamoto et al. (1984) investigated the seismic response of four small-scale (scale factor of 25 and 44) coal-silo specimens ($\Delta \cong 1.0$) through shaking-table tests. Each specimen was intended to simulate a 38 *m* diameter 40 *m* high silo. The specimens are instrumented with accelerometers placed inside the grain along the central line (axis of symmetry) and along two opposite vertical lines close to shell generatrices (along the excitation direction) at various height. Other accelerometers are attached to the silo wall, just above the top stiffening ring. The shaking tests are performed with the following input:

(i) stationary sinusoidal waves (HS) with acceleration amplitudes *a* between 0.01 and 0.2 and wide frequency range between 5 *Hz* and 45 *Hz*; (ii) real earthquake records (EQK), such as El Centro 1940 (NS component) and Hachinohe 1968 (EW component) with peak ground accelerations PGA between 0.20 - 0.30 *g*. Resonance curves, i.e. the curves providing the dynamic amplifications as a function of the frequency *f* for various distance *z* from the grain free surface and amplitude of acceleration *a*, $\zeta(z)$ were constructed from HS test results. In this regard, Figure 3.2 provides a brief example of resonance curve. In detail, $\zeta_g(z)$ and $\zeta_w(z)$ refers to the dynamic amplifications as measured by the accelerometers inside the grain and by the accelerometers attached to the top silo wall, respectively. The peaks of the resonance curves allow at identifying the natural frequencies of the silo specimens under stationary HS waves. For low input magnitude $a \le 0.03$ and frequency substantially lower than the fundamental frequency f_1, both $\zeta_g(z)$ and $\zeta_w(z)$ are close to unit along the whole silo height, thus indicating a rigid body response. At low frequencies the rigid body response seems to be not affected by the acceleration amplitudes, up to *a*= 0.20. For low input magnitude $a \le 0.03$, at the resonance, $\zeta_g(z)$ and $\zeta_w(z)$ achieve similar peak values (even larger than 10) at the level of grain free surface; $\zeta_g(z)$ decreases going from the top to the bottom. As *a* increases, values of $\zeta_g(z)$ tend to decrease and the resonance frequency f_1 tends to shifts toward lower frequencies. Although not quantitatively estimated, this could be related to a progressively higher dissipation of energy due to frictional damping triggered by grain sliding (observed even for the *a*= 0.03 test) which invests the whole grain height (see Figure 4 of Shimamoto et al. 1984). For low input magnitude $a \le 0.03$ and frequencies larger than f_1, values of $\zeta_g(z)$ and $\zeta_w(z)$ are quite different at the level of grain free surface, thus indicating a relative motion. Those findings are in line with the observations reported by Ristow (1997). When exited at frequencies close to the first and second natural frequencies significant differences in the acceleration profiles (amplitude and phase) of the grain portions close to the wall and along the central line were detected. The data recorded by the accelerometers attached to the top stiffening ring also allowed to obtain the circumferential modes. For values of $a = 0.01 \div 0.10$ the circular cross section practically remained un-deformed. This is in accordance with that detected by Yokota et al. (1983) as well. During the seismic tests the time instant of the maximum response acceleration for all measured points (both on the

wall and on inside the grain) is coincident with the time instant corresponding to the peak table acceleration; maximum dynamic amplifications at the top silo wall are around 1-3; the grain amplifications increases going from the bottom to the free surface achieving values around 2-5.

3.2.5 Harris and von Nad (1985)

Harris and von Nad (1985) performed shaking tests on two very slender steel silo specimens (Δ = 6.7 and 7.5) containing wheat and sand. The silo base was welded on the top of an elastic support frame, where the horizontal harmonic excitation (HS) (varying the frequency between 1 *Hz* to 8 *Hz*) is applied by a hydraulic actuator (Figure 3.3*a*). The displacements of the silo top and bottom were measured. The tests are uniquely devoted at determining the *effective mass*, which is analytically evaluated by using the recorded displacements and solving the dynamic equilibrium equations assuming bending flexible silo response and accounting for the effects of the rotational and translation flexibility of the supporting frame. The *effective mass* is highly dependent on the exciting frequency and tends to increase as the frequency decreases with values between 0.58 and 0.90. Moreover, a phase-angle shift between the applied force and the measured displacements indicates some damping (even if not directly measured).

3.2.6 Sakai et al. (1985)

Sakai et al. (1985) performed a large experimental campaign devoted at assessing the dynamic response of an acrylic plastic silo ($\Delta \cong 1.3$) via shaking table tests. The 1/30-scale silo specimen represents a 15.000 *tons* capacity silo prototype. The specimen was instrumented with accelerometers along the height (attached to the wall, inside the grain next to the wall and along the central line), pressure gauges and strain gauges (Figure 3.3*b*). The cylindrical silo-wall and the bottom plate were separated and mounted with a base shear-measuring device in order to separately measure the amount of grain mass leaning against the silo wall and the remaining mass, which lays on the bottom. Around 40 steady-state vibration tests are performed by imposing a harmonic excitation (HS) with increasing frequency (between 1 *Hz* to 60 *Hz*) and magnitude (between 0.05 and 0.30). The silo is filled with different type of ensiled granular material (coal and air granulated slag) and different filling conditions (empty, 1/3, 2/3 and 3/3 of the maximum filling height h_b).

The influence of the roof on the silo response is also investigated. Resonance curves were produced, allowing at identifying the first natural frequencies of the silo under stationary HS waves. For constant *a*, the first natural frequency f_1 decreases for increasing h_b. At the resonance: (i) the damping significantly increases from 3% (empty silo) to about 20% (full silo) for increasing h_b; (ii) the *effective mass* is around 0.75-0.80, independently on the input magnitude; (iii) the vertical profile of the horizontal acceleration of the silo wall varies almost linearly along the height achieving maximum amplifications at the top around 7, which reduces to 4 as the amplitude of the base acceleration increases. A similar trend, even though characterized by larger amplification values, was observed for the horizontal acceleration of the coal, as measured along the central axis of the silo, which achieves maximum amplifications of around 6. At large input acceleration, also a phase shift between the response of the coal along the central line and next to the silo-wall was observed; the vertical distribution of the wall dynamic overpressure along the input direction presents a peak at about two-thirds of the silo height. The resonance frequency is slightly influenced by the amplitude of the base acceleration. The presence of the ensiled material inhibited any eventual deformation of the circular cross section of the silo wall, even in the model without roof. For *a* between 0.05 and 0.2 and frequency less than 20 *Hz* no dynamic amplifications were detected, thus indicating a rigid body response. On the contrary, for values of *a* larger than 0.3 and frequency larger than 10 *Hz* a sudden acceleration amplification of the top grain layers occurs, without significant dynamic amplifications of the wall accelerations.

3.2.7 Sasaki and Yoshimura (1984, 1988)

Sasaki and Yoshimura (1984 and 1988) performed shaking-table tests on two cylindrical concrete stave-silo specimens and one uniform mortar cylindrical silo specimen. In detail, the first work (Sasaki and Yoshimura 1984) relates to one stave-silo specimen (1/6-scale, $\Delta \cong 1.5$) made of mortar blocks and steel hoops filled with different ensiled materials and considering empty and full conditions. Both harmonic (HS) and earthquake (EQK) tests were carried out. The type of the ensiled content (brown rice and saw dust) determines a significant variation in the dynamic interaction between silo wall and ensiled content. In general, the maximum lateral overpressure distribution is almost uniform along the whole height, excluding the base where a peak is observed, and for *a* <

0.3 the values remain lower than the static pressure. For *a* >0.3 a peak in the overpressure distribution arises around 2/3 of the filling height. The second work (Sasaki and Yoshimura 1988) relates to two specimens (1/8 scale, $\Delta \cong 1.9$): one stave silo made of mortar blocks and steel hoops and the corresponding continuous uniform mortar silo in order to evaluate the effect of the structural discontinuity of the concrete stave-silo construction system on the earthquake response. Both specimens are filled with rice (empty and full conditions are considered) and instrumented with accelerometers, strain gauges and lateral pressure gauges. The specimens are tested under both harmonic excitations (HS) (with input magnitude a between 0.1 and 1.1 and frequency between 5 to 60 *Hz*), and recorded earthquakes (EQK) (Tokachu-oki 1968 and Nemurohanto-oki 1973). Under harmonic excitation, filling reduces the first resonance frequency f_1 of the specimens and no sectional deformations are observed up to input frequencies around 50 *Hz*. Maximum dynamic amplifications are around 25 (for the empty conditions) and 10 (for the full-filled conditions). Under seismic excitation, the stave-silo specimen exhibits a slightly reduction (from 4 to 2) of the amplifications of horizontal accelerations ζ_w of the top silo wall for increasing peak table acceleration. On the contrary, the continuous uniform mortar silo presents slight reduced values of ζ_w at the top silo wall (from 3 to 2, as the peak table acceleration increases).

3.2.8 Naito (1988)

Naito (1998) conducted shaking-table tests on one steel coal silo specimen (Δ = 1.0). The specimen is instrumented with accelerometers located along the vertical central line inside the grain and with strain gauges mounted on the silo wall. Cylindrical wall and base plate stand on two separate load cells in order to measure the base shear at each part. Harmonic excitations with increasing amplitudes (*a* between 0.02 and 0.20) and frequency (*f* between 1 *Hz* and 40 *Hz*) were imposed in order to obtain resonance curves of the ensiled content along the central line. For frequency significantly lower than f_1, a rigid body response was observed. At the resonance, for increasing values of *a* the maximum dynamic amplifications significantly decrease (from 25 to 5) and the curves become smoother within a larger frequency range around f_1. For frequency larger than f_1 the base shear exerted on the wall tend to decrease, even though no numerical values are provided.

3.2.9 Holler and Meskouris (2006)

Holler and Meskouris (2006) performed shaking-table tests on a steel silo specimen (Δ = 1.1) filled with sand. The model is instrumented with pressure sensors and accelerometers. The base excitation consisted of both sinusoidal signal (HS) with fixed magnitude (a= 0.3) and frequency (f =1 *Hz*) and two synthetically generated earthquakes in order to match the Type B and Type E Soil according to CEN (2003*a*). The specimen is instrumented with accelerometers and piezoelectric pressure sensors attached to the wall at three height (close to the base, around ½ of the height and close to the top). Both the time-history of static and dynamic overpressures are reported. The aim is the evaluate the effectiveness of Eurocode 8 provisions (EN 1998-4:2006), referred to as EC8, prescriptions in terms of *effective mass* (CEN 2003*b*). While for slender silos, EC8 provisions appear quite good, for squat silos the *effective mass* activated during the shaking appears lower than that prescribed by the code.

3.2.10 Takto and Kobielak (2008)

Takto and Kobielak (2008) applied horizontal impulsive loads (IL) on one steel flat-bottom slender silo specimen (Δ = 3.0) filled with sand. The silo specimen is supported on a system of springs modeling the soil stiffness, since the main aim is the analysis of the dynamic soil-structure interaction. The specimen is instrumented with pressure cells attached to the silo wall along various heights. The dynamic inputs were generated by a ballistic pendulum in the form of a single impulse horizontally applied to the bottom plate. The fundamental frequencies, the horizontal pressure-time variation and the radial overpressure vertical profile were measured. The dynamic overpressures along the silo height are influenced by subsoil stiffness. For soft soil, the values are around 2-3 times less than those prescribed by Eurocode 8 (EN 1998-4:2006) and the profiles are not too far from being uniform. For stiffer soil, dynamic overpressures exhibit larger peaks which can also slightly exceed the value given by EC8.

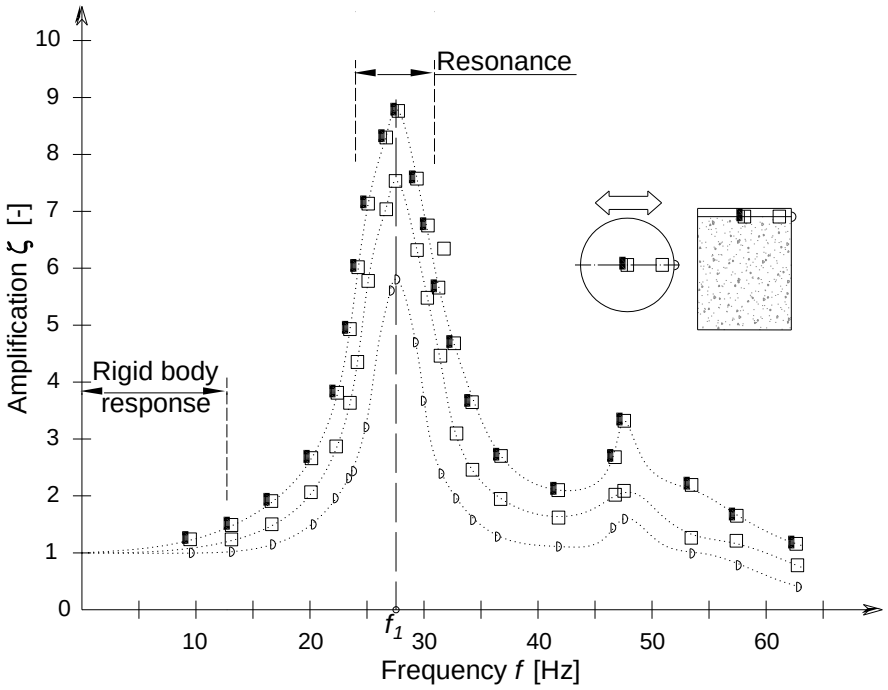

Figure 3.2 - Typical experimental resonance curve

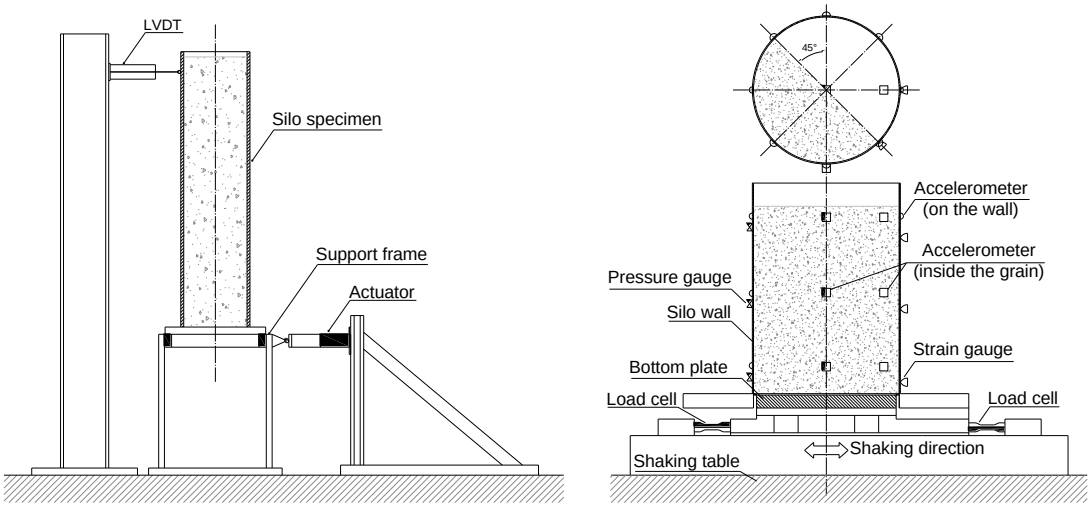

(a) *(b)*

Figure 3.3 – (a) Test setup used by Harris and Von Nad (1985) and (b) test setup and instrumentation used by Sakai et al. (1985) with shaking table

3.2.11 Critical considerations

In this section, a summary/comparison of the main geometrical and physical characteristics and the relevant response quantities of ground-supported circular grain-silos as obtained from the experimental tests described in the previous section is given. In detail, Table 3.1 reports information regarding:

- Specimen properties: slenderness ratio, wall material, ensiled material;
- Input: type of excitation (free vibration, FV, harmonic signal, HS, white noise, WN, earthquake record, EQK, impulsive load, IL), frequency content, f, acceleration range, a;
- Relevant results: effective mass, m_{eff}, natural frequencies, f_1 and f_2, and equivalent damping ratio ξ.

Table 3.1 - Summary of the main experimental results from dynamic tests on grain-silo specimens

Reference	Specimen			Input			Main results			
	Wall material	Δ [-]	Ensiled material	Type	*a* [*g*]	*f* [*Hz*]	m_{eff} [-]	f_1 [*Hz*]	ζ [-]	ξ [%]
Chandrasekaran and Jain (1968)	Perspex	5.3-10.6	Charcoal, wheat, cement, sand, aggregate	FV	-	-	0.22 - 0.48 (**)	-	-	-
	Steel	4.9-9.8		FV	-	-	0.27- 0.54 (**)	-		-
Lee (1981)	Lucite	empty	/	HS/FV	0.5	15	0	26.3	1.6	3
		1.25	Sand				0.04 (**)	22.8	3	4
		2.5					0.18 (**)	13.7	12-16	8
		3.75					0.46 (**)	7.9	2.8	5
		4.9					0.68 (**)	5.8	1	3
Yokota et al. (1983)	Acrylic resin	empty	/	WN /HS/EQK				76 (WN)		4
		1.0	Coal		0.05	-	-	19 (HS)	3 (HS)	10
Shimamoto et al. (1984)	PVC resin	1.01	Coal	HS/EQK	0.30	5 ÷ 45	-	14 (HS)	4-16 (HS) 2-5 (EQK)	-
	PVC resin	1.01		HS/EQK	0.10	5 ÷ 45	-	21 (HS)		-
	PVC resin	1.01		HS/EQK	0.10	5 ÷ 45	-	22 (HS)		-
	Steel	1.01		HS/EQK	0.10	5 ÷ 45	-	23 (HS)		-

Reference	Specimen			Input			Main results			
	Wall material	Δ [-]	Ensiled material	Type	a [g]	f [Hz]	m_{eff} [-]	f_1 [Hz]	ζ [-]	ξ [%]
Harris and Von Nad (1985)	Steel	6.67	Sand, wheat	HS	-	1 ÷ 9	0.60-0.90 (**)	-		-
		7.49		HS	-	1 ÷ 9	0.58-0.85 (**)	-		-
Sakai et al. (1985)	Acrylic plastic	empty	/	HS	0.1	1 ÷ 60	-	85 (HS)		3
		0.44	Coal	HS	0.1	1 ÷ 60	0.67 (*)	81 (HS)	5-7 (HS)	14
		0.89		HS	0.1		0.79 (*)	42 (HS)		20
		1.33		HS	0.05		0.78 (*)	29 (HS)		19
		1.33		HS	0.10		0.76 (*)	31 (HS)		20
		1.33		HS	0.20		0.77 (*)	34 (HS)		17
		1.33		HS	0.30		0.79 (*)	29 (HS)		19
		1.33	Slag	HS	0.1		0.69 (*)	25 (HS)		12
Sasaki and Yoshimura (1988)	Mortar	empty	/	HS/EQK	0.1 ÷ 1.1	5 ÷ 60	-	46 (HS)	25 (HS)	-
		1.9	Rice	HS/EQK	0.1 ÷ 1.1	5 ÷ 60	-	30 (HS)	10 (HS) 2-3 (EQK)	-
Naito (1988)	Steel	1.0	Coal	HS	0.02	1 ÷ 40	-	20 (HS)	25 (HS)	-
				HS	0.05	1 ÷ 40	-	19 (HS)	14 (HS)	-
				HS	0.10	1 ÷ 40	-	16 (HS)	8 (HS)	-
				HS	0.20	1 ÷ 40	-	13 (HS)	5 (HS)	-
Takto and Kobielak (2008)	Steel	3.0	Coarse sand	IL	0.06 ÷ 0.23	-	-	10 ÷ 12		-
Silvestri et al. (2015)	Polycarbonate (smooth)	empty	/	WN	0.1	-	-	30-35	15 (WN)	1-4
		1.0	Ballottini glass	WN/HS/ EQK	0.05 ÷ 0.55	1 ÷ 2	0.32 (**)	14	6-12 (WN) 2-2.5 (EQK)	6-21.0
	Polycarbonate (roughened)	1.0	Ballottini glass	WN/HS	0.05 ÷ 1.20	1 ÷ 2	0.43 (**)	16	8 (WN)	10

(*) direct measured; (**) derived from data using analytical models

First, it can be observed that almost all the shaking-table tests were conducted on squat ($0.4 < \Delta \leq 1.0$) or intermediate slender silos ($1.0 < \Delta < 2.0$), according to EN 1991-

4:2006 provisions. Only the tests performed by Chandrasekaran and Jain (1968) and Harris and von Nad (1985) deal with very slender silos ($\Delta \gg 2.0$), even though they report information on the *effective mass*, only.

Comparisons of the most relevant results allows the following observations.

In general:

- The dynamic response of grain-silos is significantly affected by the nature of the dynamic input. Due to the presence of the ensiled granular material, which may exhibit changes of state in relation to the frequency content and amplitude of the input, the natural frequencies of vibration and the equivalent damping ratios may change as well depending on the input frequency content and magnitude.
- The properties of the ensiled material may affect the dynamic response. In particular, rough material (with large friction coefficients) may lead to both large equivalent damping ratio and large *effective mass*.

As far as the *effective mass* is concerned the following considerations arise:

- In almost all the tests the *effective mass* is measured indirectly, i.e. using data mixed to some analytical models. This means that the so-obtained values are also depending on the reliability of the assumed models.
- The values of the *effective mass* seems to be significantly influenced by the excitation: (i) large values (around 0.8) are obtained when the silo in excited close to its natural frequency by HS stationary waves, (ii) lower values are obtained under with noise, seismic excitation, free-vibration and also under harmonic excitation far from the resonance.
- Far from the resonance, the value of the *effective mass* appears to increase for increasing value of the slenderness ratio; in particularly, squat silos appear to present values lower than the 80%.

As far as the natural frequencies and the equivalent damping ratios are concerned the following considerations arise:

- The natural frequencies are largely influenced by the excitation type (white noise or harmonic signal) and acceleration amplitude (values larger or smaller than the critical acceleration a_{crit}). In particular, under harmonic

excitations a larger amount of grain mass tends to be involved in the motion with respect to the mass typically involved during earthquake excitation. On the contrary, under WN excitation the amount of grain mass involved in the motion is similar to that excited under strong earth motion. Values of a_{crit} are around 0.3 (in unit of g). Those facts suggest that the dynamic identification (natural period and equivalent damping ratio) should be conducted by mean of WN test and varying the amplitude acceleration up to the critical value.

- As expected the frequencies and equivalent damping ratios substantially changes from empty to full filled conditions. In detail, the ratios between the first frequency of the empty and full-filled silos varies between 1.5 and 4.0. Correspondently, the damping ratios increases from 1-4% up to 20%.

As far as the maximum dynamic amplifications are concerned the following considerations arise:

- Again the values are significantly influenced by the excitation type: under harmonic excitation, at the resonance, the maximum dynamic amplifications achieve values around 20-25 for empty conditions or very low acceleration amplitudes (a<0.05) and around 5-10 for full filled conditions. Under white noise and earthquake excitations, the maximum dynamic amplifications are between 2 and 5.
- At the resonance (under harmonic excitations) and for acceleration larger than the critical value (under earthquake) dynamic amplifications of the grain tend to be larger than the dynamic amplifications of the silo wall, thus indicating a relevant horizontal grain sliding.

3.3 On-field reconnaissance data after strong earth motions

For a more comprehensive vision and understanding of the behavior of grain-silos it appears necessary to include, in addition to the main scientific theoretical, numerical and experimental studies presented in the previous section, a brief overview of the lessons learned from silos failures.

During the last centuries, various earthquakes strongly stroke grain-silos even with catastrophic collapses. Surveys of the main seismic events, which caused relevant

damages, and failure of silos are reported by various authors such as Dogangun et al. (2009), Fierro et al. (2011) and Uckan et al. (2015). During the Lima (Peru) 1974 earthquake a secondary structure not properly attached to the silo structure leaded to significant structural damages. In 1984, the 6.9 magnitude earthquake that stroke Spitak (Armenia) caused failure of a concrete storage complex silos (many non-cylindrical silos collapsed, whilst nearby cylindrical silos suffered limited damages). In 1987, the 6.3 magnitude Edgecumbe (New Zealand) earthquake provoked extensive and serious damages at several storage facilities of a local food processing industry at 14 *km* from the epicenter, which were not designed against earthquakes, revealing the need for safer design methods for storage structures and facilities (Dowrick, 1988; Arze, 1992). Again, in 1988 a M7.0 earthquake stroke Spitak (Armenia), provoking disastrous consequence on the industries, mainly related to deficient construction and lack of adequate inspection, as stated after on-field reconnaissance (Griffin et al. 1991; Arze, 1992). In 1989, a wheat silo collapsed during a minor earthquake event in the rather low seismicity area west of Sydney (Australia) due to the impact of the upper part of the ensiled content on the upper silo wall (Jia, 2016). The Kobe earthquake (Japan) occurred in 1995 severely damaged silos (provoking tilting and collapses) next to Rokko Island, according to the EQE (1995) report. In 1999 two large earthquakes hit Kocaeli and Duzce (Turkey) causing the collapse of concrete silos supported by six square non-ductile columns (Rahnama and Morrow, 2000). During the Chi-Chi (Taiwan) 1999 earthquake a concrete factory silo fell to the ground due to anchorage failure, with the upper portion, which did not suffer any apparent damage. In addition, in Taichung port all the full grain silos of a food processing plant collapsed, also causing severe damages to adjacent buildings and equipment. Brace fractures and other damages were observed on steel silos in many aggregate-producing plants (Lee and Loh, 1999). During the 2001 El Salvador earthquake three people lost their lives as a result of a silo failure (Mendez, 2001). In 2003, the 6.8 magnitude Zemmouri (Algeria) earthquake stroke a silo complex. The full silos experienced severe concrete crashing near the bottom, extensive steel buckling and fractures, associated to a large sliding of the external concrete shell. During the 6.3 magnitude L'Aquila (Italy) 2009 earthquake, three tall steel silos collapsed and collided with adjacent buildings, provoking additional damages (Grimaz, 2014). During 2010, the huge Chile earthquake extensive damages and collapses interested grain silos in many areas of the country. Failures to all sizes of grain silos (up to 5000 *tons* capacity) were observed on full silos (Grossi et al. 2011). In 2011, Van earthquake (Turkey) caused the collapse of full loaded elevated cement and wheat silos due to rupture

at the base, local buckling and anchorage failures, whilst the Great East Japan earthquake caused the buckle of many silos at Sendai harbor. During the Emilia (Italy) 2012 earthquakes, few tall steel silos collapsed (Augenti et al. 2013). The collapse of one steel silo was triggered by the formation of a plastic hinge at the base (Gioncu and Mazzolani, 2014).

3.3.1 Critical considerations

In general, most of the failures (not only the ones induced by seismic effects) are sudden and brittle because of lack of structural redundancy and alternative load paths, proper of the structural configuration of silos. Details are key issues in order to ensure the desired structural response. For instance, when designing bolted silos, bolted connections should be sized accounting for (at least four) different failure modes. Moreover, compressive buckling must also be considered, particularly if the bolted silo has corrugated walls. Another important issue is related to the number of undesired-unexpected effects of different nature and complexity, which derive from the particular ensiled material and its storage condition (temperature, production cycle). A quantitative evaluation of all possible effects (thermal effects, fatigue, non-uniform pressure distributions) appears to much complex, practically almost unfeasible and also conceptually not suggested. A more engineering sound approach should be oriented toward the choice of additional safety factors in the design, as suggested by Carson (2000).

Regarding failures under strong earth motion, experiences in the seismic areas of Chile, New Zealand and Russia indicate that more than the 85% of important failures are due to gross errors of construction or design concept (Arze, 1992). In addition, it appears that slender silos are intrinsically more prone to fail with respect to squat silos. The evidence is justified by two concurrent factors: the quite intuitive increase in the moment lever arm and the increases in the effective mass. Those two factors leads to a significant increase in both bending moment and shear induced stresses. At the same time in some cases, severe damages were also observed in the upper portions of the silo, thus indicating large overpressure close to the free surface, especially in slender silos. In light of these a safe silos design (especially in case of slender silos) cannot disregard from a detailed evaluation of the seismic actions and their effects on the structural elements. Unfortunately, straightforward code provisions for a safe, but reasonably economic, seismic design of silos are still not available.

3.4 Critical considerations

In this section, a review of the main scientific experimental works on the dynamic behavior of ground-supported circular grain-silos under base excitation and a collection of on-field reconnaissance data on the effects of strong-earth motions on real silo structures are presented. The analysis of different experimental tests conducted on grain-silos specimens (mainly performed via shaking-table) shows the complexity of the dynamic response of grain-silo systems due to the interaction between cylindrical shell and ensiled content under base excitation. In detail, it appears that the dynamic response of grain-silos, the *effective mass* participating with the silo wall, the natural frequencies, the equivalent damping ratios, and the maximum dynamic amplifications of grain-silo systems are significantly affected by the nature of the dynamic input (frequency content and amplitude) and the properties of the ensiled material.

The *effective mass* reaches values around the 80% when the silo in excited close to its natural frequency by HS stationary waves, whilst lower values are obtained under with noise, seismic excitation, free-vibration and also under harmonic excitation far from the resonance. It has to be noted that, the direct experimental measurement of the *effective mass* presents practical difficulties and thus the estimation of the *effective mass* starting from analytical models depends on the reliability of the assumed models. Far from the resonance, the value of the *effective mass* appears to increase for increasing value of the slenderness ratio: for slender silos it approaches values around the 80-90%, whilst for squat silos there are some indications that suggests values far lower than the 80%.

The natural frequencies and the equivalent damping ratios seem to be largely influenced by the filling level, the excitation type and the acceleration amplitude. As expected the frequencies and the equivalent damping ratios substantially changes from empty to full filled conditions. The ratios between the first frequency of the empty and full-filled silos varies between 1.5 and 4.0; correspondently, the damping ratios increases from 1-4% up to 20%. Under harmonic excitations close to the first natural frequency a larger amount of grain mass tends to be involved in the motion with respect to the mass typically involved during earthquake excitation. On the contrary, under WN excitation the amount of grain mass involved in the motion is similar to that excited under strong earth motion. Values of a_{crit} are around 0.3 (in unit of g). Those facts suggest that the dynamic identification (natural period and equivalent damping ratio) should be conducted by mean of WN test and varying the amplitude acceleration up to the critical value.

The maximum dynamic amplifications achieve, under harmonic excitation, at the resonance, values around 5-10 for full filled conditions, whilst under white noise and earthquake excitations, the maximum dynamic amplifications are between 2 and 5. At the resonance (under harmonic excitations) and for acceleration larger than the critical value (under earthquake) dynamic amplifications of the grain tend to be larger than the dynamic amplifications of the silo wall, thus indicating a relevant horizontal grain sliding.

In general, from an experimental point of view, it appears that further efforts and investigations have to be carried out in order to fully understand the dynamic behavior of ground-supported circular grain-silos.

The analysis of on-field reconnaissance data after strong earth motions ranging over the last thirty years shows that silo structures are particularly prone to fail in case of major seismic events, provoking significant and extensive economic losses and, in some cases, even causalities. Experiences in the seismic areas of Chile, New Zealand and Russia indicate that more than the 85% of important failures are due to gross errors of construction or design concept. In addition, it appears that slender silos are intrinsically more prone to fail with respect to squat silos, due to the increase in the moment lever arm and the increases in the *effective mass*. In some cases, severe damages were also observed in the upper portions of the silo, thus indicating large overpressure close to the grain free surface. In light of these a safe silos design (especially in case of slender silos) cannot disregard from a detailed evaluation of the seismic actions and their effects on the structural elements. Unfortunately, straightforward code provisions for a safe, but reasonably economic, seismic design of silos are still not available.

Reference

Arze L., (1992). Seismic design practices of industries, Tenth World Conference on Earthquake Engineering, 19-24 July, Madrid, Spain.

Augenti, N., Nanni, A., & Parisi, F. (2013). Construction Failures and Innovative Retrofitting Buildings, 3(1), 100-121.

Chandrasekaran, A. R., & Jain, P. C. (1968). Effective live load of storage materials under dynamic conditions. Indian Concrete Journal, 42(9), 364-365.

Chandrasekaran, A. R., & Saini, S. S. (1968). Live load effect on dynamic response of structures. Journal of the Structural Division, 95(4), 649-660.

Dogangun, A., Karaca, Z., Durmus, A., & Sezen, H. (2009). Cause of damage and failures in silo structures. Journal of performance of constructed facilities, 23(2), 65-71.

Dowrick, D. J. (1988). Edgecumbe earthquake-Some notes on its source, ground motions, and damage in relation to safety. Bulletin of the New Zealand National Society for Earthquake Engineering, 21(3), 198-203.

European Committee for Standardization (CEN). (2003a). prEN 1998-1 Draft 6, Brussels, Belgium.

European Committee for Standardization (CEN). (2003b). prEN 1998-4, Brussels, Belgium

EN 1991-4 (2006) Eurocode 1. Actions on structures, Part 4 -Silos, tanks and pipelines, CEN, Brussels.

EN 1998-4 (2006) Eurocode 8. Design of structures for earthquake resistance, Part 4 -Silos, tanks and pipelines, CEN, Brussels.

EQE International. (1995). The January 17, 1995 Kobe earthquake: An EQE summary report. San Francisco: EQE International.

EQE. 1999. "Chichi, Taiwan earthquake of September 21, 1999 M7.6." An EQE Briefing, http://www.absconsulting.com/resources/ Catastrophe_Reports/Chichi-Taiwan-1999.pdf Jan. 29, 2008.

Fierro, E. A., Miranda, E., Perry, C. L., Lynn, A. C., & Reitherman, R. (2011). Behavior of nonstructural components in recent earthquakes. In Proc. 2011 Architectural Engineering National Conference, Oakland, CA.

Gioncu, V., & Mazzolani, F. M. (2014). Seismic design of steel structures. CRC Press.

Griffin, M. J., Bragagnolo, L. J., & Yanev, P. I. (1991). The December 7, 1988, Armenia earthquake: Effects on selected power, industrial, and commercial facilities (No. EPRI-NP-7359-M). Electric Power Research Inst., Palo Alto, CA (United States); EQE, Inc., San Francisco, CA (United States)

Grimaz, S. (2014). Can earthquakes trigger serious industrial accidents in Italy? Some considerations following the experiences of 2009 L'Aquila (Italy) and 2012 Emilia (Italy) earthquakes. Bollettino di Geofisica Teorica e Applicata, 55(1), 227-237.

Grossi P., Williams C., Cabrera C., Tabucchi T., Sarabandi P., Rodriguez A., Aslani H., and Rahnama M., 2011. The 2010 Maule, Chile Earthquake: Lessons and Future Challenges. http://forms2.rms.com/rs/729-DJX-565/images/eq_2010_chile_eq.pdf

Jia, J. (2016). Modern Earthquake Engineering: Offshore and Land-based Structures. Springer

Harris, E. C., & von Nad, J. D. (1985, November). Experimental determination of effective weight of stored material for use in seismic design of silos. In ACI Journal Proceedings (Vol. 82, No. 6). ACI.

Holler, S., & Meskouris, K. (2006). Granular material silos under dynamic excitation: numerical simulation and experimental validation. Journal of structural Engineering, 132(10), 1573-1579.

Lee, S. J. (1981). Experimental study of cylindrical silos subject to seismic excitation (Doctoral dissertation, The Ohio State University).

Lee, G. C., & Loh, C. H. (1999). Preliminary report from MCEER-NCREE workshop on the 921 Taiwan earthquake. Multidisciplinary Center for Earthquake Engineering Research.

Liffman, K., Metcalfe, G., & Cleary, P. (1997). Granular convection and transport due to horizontal shaking. Physical Review Letters, 79(23), 4574.

Mendez, D. 2001. "Stunned Salvador suffers second deadly quake in a month." The BG News, Feb. 14, http://media.www.bgnews.com/media/storage/paper883/news/2001/02/14/World/Stunned.Salvador.uffers.Second.Deadly.Quake.In.A.Month-1283510.shtml Jan. 22, 2008.

Metcalfe, G., Tennakoon, S. G. K., Kondic, L., Schaeffer, D. G., & Behringer, R. P. (2002). Granular friction, Coulomb failure, and the fluid-solid transition for horizontally shaken granular materials. Physical Review E, 65(3), 031302.

Naito, Y. Equivalent linear technique in the finite element method applied to deformation with volume change and to an axisymmetric body under an unaxisymmetric load. In Proceedings of the 9th World Conference on Earthquake Engineering, Tokyo-Kyoto, Japan (Vol. 3, pp. 133-138).

NEHRP (National Earthquake Hazards Reduction Program) (2009). Recommended Seismic Provisions for New Buildings and Other Structures (FEMA P-750).

Rahnama, M., & Morrow, G. (2000). Performance of industrial facilities in the August 17, 1999, Izmit earthquake. Proceedings of the 12WCEE, Paper, (2851).

Raihane, A., Bonnefoy, O., Gelet, J. L., Chaix, J. M., & Thomas, G. (2009). Experimental study of a 3D dry granular medium submitted to horizontal shaking. Powder technology, 190(1), 252-257.

Ristow, G. H., Straßburger, G., & Rehberg, I. (1997). Phase diagram and scaling of granular materials under horizontal vibrations. Physical review letters, 79(5), 833.

Sakai, M., Matsumura, H., Sasaki, M., Nakamura, N., Kobayashi, M., & Kitagawa, Y. (1985). Study on the dynamic behavior of coal silos against earthquakes. Bulk Solids Handling, 5(5), 1021.

Salueña, C., Pöschel, T., & Esipov, S. E. (1999). Dissipative properties of vibrated granular materials. Physical Review E, 59(4), 4422.

Sasaki, Y., & Yoshimura, J. (1984). Dynamic behavior of concrete stave silos. In Proceedings of the 8th World Conference on Earthquake Engineering.

Sasaki, Y., & Yoshimura, J. (1988). Seismic Response of Concrete Stave Silos with Structural Discontinuity. Proceedings of the Ninth World Conference on Earthquake Engineering, Tokyo-Kyoto, Japan (Vol. VI).

Shimamoto, A., Kodama, M., & Yamamura, M. (1984). Vibration tests for scale model of cylindrical coal storing silo. In Proceedings of the 8th World Conference on Earthquake Engineering (Vol. 5, pp. 287-294). San Francisco.

Tatko, R., & Kobielak, S. (2008). Horizontal bulk material pressure in silo subjected to impulsive load. Shock and Vibration, 15(5), 543-550.

Uckan, E., Akbas, B., Shen, J., Wen, R., Turandar, K., & Erdik, M. (2015). Seismic performance of elevated steel silos during Van earthquake, October 23, 2011. Natural Hazards, 75(1), 265-287.

Yokota, H., Sugita, M., & Mita, I. (1983, November). Vibration tests and analyses of coal-silo model. In Proc., 2nd Int. Conf. on the Design of Silos for Strength and Flow, Stratford-upon-Avon, Powder Advisory Centre (November 1983) (pp. 107-116).

4. Current code provisions for the structural seismic design of grain-silos

In this chapter, the main international current code provisions established for the structural seismic design of grain-silo structures are collected and discussed. The main aim is to draw the actual state-of-the art established in practical and code literature. First, the most salient aspects related to (i) the evaluation of the seismic actions exerted by ensiled bulk content on the silo wall, and (ii) the analytical and/or numerical tools applicable for the seismic design of grain-silo structures are summarized. Then, the main common aspects and the most critical shortcomings individuated among the considered international current code provisions are discussed.

4.1 Uniform Building code UBC (1994) provisions

Uniform Building Code (UBC, 1994) provisions suggest that ground-supported silos should be designed using the procedure for rigid structures (i.e. as those characterized by a fundamental period of vibration less than 0.06 *s*) for an equivalent later seismic force *V* equal to:

$$V = 0.5 \cdot Z \cdot I \cdot W \tag{1}$$

where *Z* is the seismic-zone coefficient, *I* is the structure importance factor (equal to 1.25 for essential and hazardous facilities, 1 for other facilitates), *W* is the total weight of the structure plus the weight of content.

Alternatively, such structures may be designed using a response spectrum analysis.

Silos which are not covered by the above procedures (i.e. non-rigid structures) should be designed to resist an equivalent lateral seismic force *V* equal to:

$$V = \frac{Z \cdot I \cdot C \cdot W}{R_w} \tag{2}$$

where $C = \frac{1.25 \cdot S}{T^{2/3}} \leq 2.75$ is a coefficient related to the fundamental period of vibration of the structure *T*, *S* is the site coefficient depending on the soil profiles and R_w is a numerical coefficient equal to 5 for storage silos.

The computed lateral force *V* is assumed to be distributed in proportion to the vertical distribution of *W*.

4.2 ACI 313-97 (1997) provisions

ACI 313-97 (1997) provisions give synthetic indications on the assessment of the seismic forces acting on grain-silos. ACI 313-97 (1997) provisions indicate that the effective weight of the stored material should be taken as the 80% of the actual weight in order to compute the lateral seismic forces related to the inertia of the stored grain mass (see section 4.4.8 of ACI 313-97, 1997). The reduction of lateral force is allowed because of energy loss through inter-granular movement and particle-to-particle friction in the stored material, according to the experimental evidences reported by Chandrasekaran and Jain (1968) and Harris and Von Nad (1985), which are explicitly cited by the code.

In addition, the estimation of the magnitude and the effects of the lateral seismic force on the structure should be assessed by considering the following aspects:

- The fundamental period of vibration of the silo should be estimated by any rational method;
- The centroid of the effective weight should coincide with the centroid of the actual grain volume.

4.3 NCh2369 (2003) provisions

The Chilean NCh2369 (2003) provisions deals exclusively on the earthquake – resistant design of industrial structures and facilities. The NCh2369 (2003) provisions mainly focus on the seismic design of liquid tanks and generally suggest to refer to alternative design provisions published in industry standards (such organizations as API, AWWA). However, proper prescriptions are given regarding the model of analysis to be used and the definition of the design spectrum to be used. In general, the NCh2369 (2003) provisions consider more stringent performance objectives with respect to those adopted in building seismic design philosophy. In particular, for industrial facilities the continuity of operation of facilities under severe earthquakes is required. These performance objectives aim to guarantee the absence of structural damage and continuous operation after moderate and small earthquakes as well. In more details, the performance objectives required for new industrial facilities, the seismic design provisions by NCh2369 (2003) may be summarized as follows:

- **Continuity of operation in industry**:
    - Non-interruption of essential processes and services;
    - Prevention or minimization of the standstill of operations;
    - Guarantee of inspection and the reparation of damaged elements.
- **Protection of life in industry**:
    - Prevention of the collapse of structures in the event of severe over-design earthquakes;
    - Prevention of fire, explosions or emission of toxic gases and liquids;
    - Protection of the environment.

4.4 Eurocode 1998-4 (2006) provisions

EN 1998-4 (2006) provisions give some specific principles and application rules for the seismic design of grain-silos, both for elevated and ground-supported silos. The code provisions mainly provide indication related to:

- The assessment of the additional horizontal pressures exerted on the wall under seismic excitation;
- The method of analysis of silos under seismic excitation;
- The numerical modelling of the grain-silo systems under seismic excitation.

Regarding with the assessment of the additional horizontal pressures exerted on the silo wall under seismic excitation, the stresses induced on the wall (i.e. in the shell) due to the response of the contents is accounted by means of additional normal pressure acting on the wall (see section 3.3 of EN 1998-4:2006). The additional normal pressure acting on the wall $\Delta_{ph,s}$ presents a horizontal distribution around the circumference and the height of the silo wall equal to:

$$\Delta_{ph,s}(z,\theta) = \Delta_{ph,so}(z) \cdot \cos\theta \tag{3}$$

where $\Delta_{ph,so}(z)$ is the reference pressure and θ is the angle ($0° \le \theta < 360°$) between the radial line to the point of interest on the wall and the direction of the

horizontal component of the seismic action. The reference pressure $\Delta_{ph,so}(z)$ may be evaluated as follows:

$$\Delta_{ph,so}(z) = \alpha(z) \cdot \gamma_b \cdot \left[\min\left\{ r_s^*; 3x \right\} \right] \tag{4}$$

where $\alpha(z)$ is an amplification factor representing the vertical profile of the ratio of the horizontal response acceleration of the silo at any *z* to the acceleration of gravity, γ_b is the bulk unit weight of the particulate material in the seismic design situation; $r_s^* = \min\{h_b; d_c/2\}$, h_b is the equivalent height of the ensiled content, d_c is the silo diameter, and *x* is the vertical distance measured from the silo bottom to the generic horizontal layer. The horizontal base acceleration should be evaluated on the basis of a design spectra, whilst the vertical profile of $\alpha(z)$ has to be selected by the designer. In general, the vertical profile of the horizontal pressure $\Delta_{ph,s}(z,\theta)$ results practically constant over the whole height of the silo wall. The resultant of the seismic pressure and the static pressure should not be less than zero; in case of negative value, the additional normal pressures on the wall should be redistributed to ensure that the sum of the dynamic pressure with the static pressure of the particulate material on the wall is everywhere non-negative, while maintaining the same force resultant over the same horizontal plane as the values of $\Delta_{ph,so}(z)$.

Once the spatial distribution of the horizontal overpressure $\Delta_{ph,s}(z,\theta)$ is defined, both the wall shear and the wall bending moment may be computed.

The wall base shear (at the bottom of the silo wall), referred to as T_{EC8}, is given as the integral, on the lateral surface of the silo, of the projection of the overpressures $\Delta_{ph,s}(z,\theta)$ towards the direction of the horizontal acceleration. For a constant vertical profile of $\alpha(z)$ and for $\Delta > 1/2$, the wall base shear T_{EC8} may be computed as follows:

$$T_{EC8} = \alpha \cdot \gamma \cdot \pi \cdot R^2 \cdot H \cdot \left(1 - \frac{R}{6 \cdot H}\right) = \alpha \cdot \gamma \cdot V_b \cdot \left(1 - \frac{1}{12 \cdot \Delta}\right) \tag{5}$$

where V_b is the total volume of the ensiled granular material.

By eliminating the term $\alpha \cdot \gamma \cdot V_b$ corresponding to the horizontal inertial action of the whole ensiled content from Eq. (5), the remaining term $\left(1-\frac{1}{12\cdot\Delta}\right)=m_{eff}$ and represents the *effective mass*, i.e. the fraction of the whole ensiled mass which participate with the silo wall during seismic excitation.

The wall base bending moment (at the bottom of the silo wall), referred to as M_{EC8}, is given as the integral, on the lateral surface of the silo, of the projection of the overpressures $\Delta_{ph,s}(z,\theta)$ towards the direction of the horizontal acceleration multiplied for the corresponding vertical lever arm. For a constant vertical profile of $\alpha(z)$ and for $\Delta > 1/2$, the wall base shear T_{EC8} may be computed as follows

$$M_{EC8}=\alpha\cdot\gamma\cdot\pi\cdot\frac{R^2}{2}\cdot\left(H^2-\frac{R^2}{27}\right)=\alpha\cdot\gamma\cdot V_b\cdot\frac{H}{2}\left(1-\frac{1}{108\cdot\Delta^2}\right) \quad (6)$$

Regarding with the method of analysis, the types of analysis that may be applied according to the EN 1998-4 (2006) provisions are listed below:

- The “lateral force method”;
- The “modal response spectrum” analysis;
- The non-linear static analysis;
- The non-linear time history analysis.

Regarding with the numerical modeling of the grain-silo systems under seismic excitation, the EN 1998-4 (2006) provisions suggest that:

- The model to be used for the determination of the seismic action effects should reproduce accurately the stiffness, the mass and the geometrical properties of the containment structure, should account for the response of the contained particulate material and for the effects of any interaction with the foundation soil;
- Silos should be analyzed by considering elastic behavior of the silo shell;
- Unless more accurate evaluations are undertaken, the global seismic response should be calculated assuming that the particulate contents move together with the silo shell and modelling them with their *effective mass* at

their center of gravity and its rotational inertia with respect to it. Unless a more accurate evaluation is made, the contents of the silo may be taken to have an *effective mass* equal to 80% of their total mass.

- Unless the mechanical properties and the dynamic response of the particulate solid are explicitly and accurately accounted for in the analysis (e.g. by using finite elements to model the mechanical properties and the dynamic response of the particu1ate solid), the effect on the shell of the response of the particulate solid to the horizontal component of the seismic action may be represented through an additiona1 normal pressure on the wall, $\Delta_{ph,s}$.

The EN 1998-4 (2006) provisions are mainly grounded on: (i) the analytical formulation proposed by Younan and Veletsos (1998), just considering the most conservative conditions (rigid silo wall with rough interface) and (ii) the numerical investigation performed by Rotter and Hull (1989).

4.5 FEMA P-750 (2009) provisions

FEMA P-750 provisions (NEHRP, 2009) treat the seismic structural design of seismic design of ground-supported storage silos within Chapter 15 and classify grain-silos as "Nonbuilding Structures not similar to buildings". FEMA P-750 provisions explicitly give indications on the assessment of: (i) the global lateral forces acting on the silo and (ii) the increased lateral pressure distribution acting on the silo wall. FEMA P-750 provisions suggest to refer to alternative design provisions published in industry standards (such organizations as ASCE) to perform proper structural design against earthquake

The global lateral seismic forces are considered of impulsive type only and related to the fundamental period of vibration of the storage structure. The fundamental period of vibration of storage structures is considered as relatively short, so that the design spectral response acceleration could be taken as the highest value of the spectrum, on the plateau region, equal to S_{DS}. The global lateral seismic forces are related to the effective weight of the total ensiled mass $W_{effective}$ plus the weight of the head of the silo. The effective weight of the total ensiled mass $W_{effective}$ is taken proportional to the gross weight of the stored product multiplied by an effective mass factor and an effective density factor. It is

recommended that the product of the effective mass factor and effective density factor be taken as no less than 0.5 (due to the limited test data and the highly variable properties of the stored products). Therefore, the seismic base shear V is calculated as follows:

$$V = \frac{S_{DS}}{\left(\frac{R}{I}\right)} \cdot W_{effective} \tag{7}$$

where R and I are the response modification coefficient and the occupancy importance factor, respectively.

The increased lateral pressure distribution may be computed in accordance with the conservative formulation proposed by Trahair et al. (1983), which considers a rigid body motion of the whole ensiled content under shaking.

The *effective mass* may be estimated in accordance with the formulation by Trahair et al. (1983) and accounting for: (i) the slenderness ratio of the grain-silo; (ii) the load transfer within the grain directly into the foundation via inter-granular shear; (iii) the energy loss through grain movement and grain-grain friction. For slenderness ratios Δ less than 2.0, significant reductions in the *effective mass* should be accounted for; the characteristics of the stored product should be accounted. The effect of internal friction is taken into account by means of an effective density factor, less than the unity and estimated around 0.80. The estimation of such value is performed making references to the experimental evidences by Chandrasekaran and Jain (1968).

4.6 ASCE 7-10 (2010) provisions

ASCE 7-10 (2010) provisions treat the seismic structural design of ground-supported silos within Chapter 15, which focuses on the seismic design requirements for "Nonbuilding structures" (see section 15.7.9 of ASCE 7-10, 2010). The provisions are applicable to steel silos (both welded and bolted ones), whilst r.c. silos (both cast in-place r.c. and pre-stressed r.c. ones) should be designed in accordance with the seismic force requirements of the standard and the requirements of ACI 313-97 (1997).

ASCE 7-10 (2010) provisions give indications on the assessment of: (i) the global lateral forces acting on the silo and (ii) the force distribution acting on the shell and the foundation of the silo.

The lateral forces acting on grain-silos should be determined by the requirements and accelerations for short period structures. It implies that that the design spectral response acceleration to be considered in computing the lateral forces equals to the highest value of the spectrum, i.e. that corresponding to the plateau region of the response spectrum.

The *effective mass* is defined as the portion of the stored granular mass acting on the shell during ground shaking and should be used for the assessment of the shear and overturning moment acting on the silo. The *effective mass* is considered related to: (i) the physical characteristics of the bulk solids; (ii) the slenderness ratio of the silo; (iii) the intensity of the seismic event. For the assessment of the value of *effective mass* the inter-granular behavior (friction) of the ensiled material, which can transfer seismic shear directly to the foundation, has to be taken into account. No explicit formulation for the estimation of the *effective mass* is provided by the standard.

The force distribution to shell and foundation of the silo should be performed taking into account the increased lateral pressure (and the resulting hoop stress) due to loss of the inter-granular friction of the material during the seismic shaking. The increased lateral pressure acting on the silo wall should be added to the static design lateral pressure. No explicit formulation for the estimation of the increased lateral pressure is provided by the standard.

4.7 AIJ (2010) provisions

AIJ (2010) provisions assess the seismic design of grain-silos in a specific section (see section 5.2.3 of AIJ 2010) and refer to both metal and reinforced concrete silos. The AIJ (2010) provisions mainly refer to the evaluation of the effect of the inertial force related to the impulsive mass interacting with the silo wall on the base of structure. The impulsive mass is considered as a fraction of the total ensiled mass. Due to energy loss caused by internal friction between granular particles and friction between particles and silo wall, the impulsive mass results lower than the total ensiled mass; however, it should not be less than the 80% of the total ensiled mass.

The assessment of the design seismic loads for aboveground storage tanks could be performed by adopting two methods: (i) the “modified seismic coefficient method”, and (ii) the modal analysis.

The so-called "modified seismic coefficient analysis "implements the "Equivalent Lateral Force" method. It computes the design lateral seismic force as product of: (i) the design weight imposed on the base of the structure *W* (equal to the sum of dead weight of structure and weight of impulsive mass of the content) and (ii) the value of the horizontal acceleration corresponding to the ordinate of the design acceleration response spectrum corresponding to the first natural period of vibration of the grain-silo system S_{a1}. In case that the first natural period of vibration of the grain-silo system is unknown, it should be taken as 0.6 *s* for the assessment of the design value of the horizontal acceleration. The base shear force *V* is calculated as follows:

$$V = \left(Z_s \cdot I \cdot D_s \cdot \frac{S_{a1}}{g} \right) \cdot W \tag{8}$$

where Z_s is the seismic zone factor, *I* is the importance factor, D_s is the structural characteristic coefficient and *g* is the gravity acceleration.

The modal analysis method evaluates the action exerted on the structure by modelling the grain-silo system as a cantilever beam with different point masses (lumped mass model with *n* point masses). The design lateral seismic force is essentially computed by means of the Square Root of the Square Sum (SRSS) of the base shear related to the significant natural modes of vibration of the lumped mass system.

4.8 Critical considerations

In this section, a summary/comparison of the main provisions and shortcomings related to the current code provisions dealing with the structural seismic design of flat-bottom cylindrical grain-silos is given. In detail, Table 4.1 reports information regarding:

- The amount of *effective mass* to be considered;
- The provision of formulas for the estimation of the horizontal overpressure exerted on the silo wall (Δp);
- The provision of formulas for the estimation of the fundamental period of vibration (*T*) or of suggested values;
- The methods of analysis suggested for the seismic design of silo structures.

Table 4.1 - Summary of the main provisions and shortcomings related to current code provisions

Code	m_{eff} [%]	Δp	T	**Methods of analysis**
UBC (1994)	100	not provided	≤ 0.06 *s*	equivalent lateral force
ACI 313-97 (1997)	80	not provided	To be evaluated by means of any rational method	equivalent lateral force
NCh2369 (2003)	-	not provided	not provided	-
EN 1998-4 (2006)	≥ 80	provided	not provided	equivalent lateral force modal response spectrum analysis non-linear static analysis non-linear time history analysis
FEMA P-750 (2009)	≥ 50	not provided	≤ 0.06 *s*	equivalent lateral force
ASCE 7-10 (2010)	-	not provided	≤ 0.06 *s*	equivalent lateral force
AIJ (2010)	≥ 80	not provided	0.6 *s*	equivalent lateral force modal response spectrum analysis

Very few international standards include explicit requirements for the design of silo against earthquakes. Most standards for silos do not cover the subject at all, or they refer to general building codes, or they just refer to the earthquake loading issue as another loading case to be considered, offering only general suggestions. As a result, in practice silos are designed against earthquakes according to the corresponding codes for buildings and equipment. However, seismic codes developed for buildings are not straight applicable to industrial structures, such as grain-silos (Arze, 1992). Nonetheless, for the consideration of earthquake effects no finally agreed calculation procedures are available (Brown and Nielsen 1998).

Given that silos structural design need to account for unconventional loads, such as the actions transmitted to the structures by the ensiled grain under both static and dynamic loadings, grain-silos are classified and treated as "non-building structures" (FEMA P-750 and ASCE 7-10) or considered as different to many other structures because they may be subjected to the full loads from particulate solids for most of their life. Such actions, due to the fact that that the weight of the silo structure is typically much lower than that of the ensiled mass, in case of strong earth motion, play a fundamental role on the global dynamic response of grain-silos.

Silo design against earthquake is generally treated in dedicated specific sections of such standards. However, even if such provisions face the seismic design of silo structure, generally only little guidance on the main aspects are given. The main shortcomings related to the most of the codes dealing with the seismic design of grain-silos may be summarized as follows:

- No specific formulas are given for the quantitative assessment of the *effective mass*, the estimation of the value of the fundamental period of vibration and the definition of the distribution of the additional horizontal pressure exerted by the grain on the silo wall;
- Even if most earthquake regularization and standards offer the possibility of calculating the seismic effects on the silo structure by means of dynamic analysis, little guidance is given regarding the numerical procedure to be used for the modelling of grain-silo system via finite elements models (such as more sophisticated three-dimensional or simpler two-dimensional finite element models);
- The standards explicitly prescribing the value of the *effective mass* generally refers to the 80% of the whole stored grain mass, independently on the slenderness ratio and the physical characteristic of the stored bulk solid;
- Generally, in the estimation of the design horizontal acceleration, grain-silos are considered to behave as rigid-structures, regardless on their slenderness ratio and typology (r.c., steel). Then, the value of the horizontal spectrum acceleration to be used in the estimation of the base shear resultant V (proportional to the horizontal inertial forces) equals the highest value of the pseudo-acceleration spectrum, on the plateau region;

- Considering the *effective* mass of the ensiled bulk solid as concentrated as a single mass at its centre of gravity may an acceptable approximation for the calculation of the vertical forces within columns or foundation walls of elevated silos. On the contrary, such schematization could lead to a rough estimation of the internal actions exerted on the wall for ground-supported silos, where the pressure variation results in a moment resultant and a shear resultant at the silo base, which has to be resisted through the development of axial stresses and membrane shear stresses within the silo wall, respectively.

Reference

American Concrete Institute (ACI) (1997). Standard practice for design and construction of concrete silos and stacking tubes for storing granular materials and commentary. ACI 313-97/313-R97, Farmington Hills, MI

Architectural Institute Of Japan (AIJ) (2010) Design Recommendation For Storage Tanks And Their Supports With Emphasis On Seismic Design

Arze L., (1992). Seismic design practices of industries, Tenth World Conference on Earthquake Engineering, 19-24 July, Madrid, Spain.

ASCE-7 (2010) - Chapter 15. Seismic Design Requirements for Nonbuilding Structures

Brown, C. J., & Nielsen, J. (Eds.). (1998). Silos: fundamentals of theory, behavior and design. CRC Press.

Chandrasekaran, A. R., & Jain, P. C. (1968). Effective live load of storage materials under dynamic conditions. Indian Concrete Journal, 42(9), 364-365.

EN 1998-4 (2006) Eurocode 8: Design of structures for earthquake resistance – Part 4: Silos, tanks and pipelines

Harris, E. C., & von Nad, J. D. (1985, November). Experimental determination of effective weight of stored material for use in seismic design of silos. In ACI Journal Proceedings (Vol. 82, No. 6). ACI.

NEHRP (National Earthquake Hazards Reduction Program) (2009). Recommended Seismic Provisions for New Buildings and Other Structures (FEMA P-750).

NCh2369, I. N. N. (2003). National Institute of Normalization. Earthquake-resistant design of industrial structures and facilities. National Institute of Normalization: Santiago, Chile.

Rotter, J. M., & Hull, T. S. (1989). Wall loads in squat steel silos during earthquakes. Engineering Structures, 11(3), 139-147.

Rotter, J. M., Pham, L. & Nielsen, J. 1986. On the specification of loads for the structural design of bins and silos. In *Proc. 2nd Int. Conf. on Bulk Materials Storage Handling and Transportation, July*, pp. 241-247. Wollongong, Australia: IEAust.

Trahair NS, Abel A, Ansourian P, Irvine HM, Rotter JM (1983) Structural design of steel bins for bulk solids. Australian Institute of Steel Construction, Sydney, Australia.

UBC (1994). Uniform Building Code. Structural engineering design provisions.

Younan, A. H., & Veletsos, A. S. (1998). Dynamics of solid-containing tanks. I: Rigid tanks. Journal of Structural Engineering, 124(1), 52-61.

5. Current body of knowledge and the challenges

In the present chapter, a comparison between the actual body of knowledge and the current code provisions on the static and the seismic behavior of grain-silo structures is presented and the most significant research challenges in the field are summarized.

Loading due to filling and discharging, i.e. the determination of the static pressures exerted by stored granular or powder materials in silos, has been subject of extensive research efforts, as is apparent from the relevant international scientific literature (Brown and Nielsen, 1998). The analytical formulations developed since the end of the 19th century for the prediction of the pressure distributions acting on the silo wall, so called classical theories, have been widely experimentally investigated for more than a century and today they are well consolidated in both the scientific and technical literature. From the 1970s onwards, a large number of research teams have worked on the application of finite element analysis to silo problem (Ayuga et al. 2001). For simple specific applications, numerical models appear, in general, able to well predict the distribution and magnitude of the grain-wall pressures under static conditions given by classical theories; on the contrary, continuum finite element treatment of the ensiled content have rather limited success in capturing actual silo behavior observed during tests under filling and discharging conditions (Rotter 2009). This reflects in a gap between the international bibliography concerning the use of potent commercial software able to work with complex behavior of the stored content and that of the silo structure (Ayuga et al. 2001).

Loading due to earthquake on silo structures represents a specific loading condition that is not very well covered in both the scientific and the technical literature (Brown and Nielsen, 1998). Despite the scientific efforts on the silo dynamics profuse over the last 50 years, loading due to earthquake on silo structures still represents one of the high priority needs for pre-normative research. In addition, the comprehension of the complex grain-silos dynamics still presents many uncertainties and analytical, numerical, experimental researches in this field are rather limited and fragmented. It is well known that on-ground circular grain-silo systems are characterized by a strong non-linear response, even under static loadings, when no important dynamic effects arise, due to the grain-wall interaction ruled by Coulomb friction law, as demonstrated by numerous analytical, experimental and numerical research works since the late 19th century (Janssen 1895, Vanel et al. 1999, Ovarlez et al. 2003, Qadir et al. 2010 and 2016, Lazarevic et al. 2010, Landry et al. 2003,

Masson and Martinez, 2000). In case of dynamic excitation, such as strong earth motion, the grain-wall friction interaction becomes even more complex and the prediction of the structural response further increases in complexity at the point that no comprehensive analytical theory has been established in the scientific literature (Nielsen, 1998 and Rotter, 2008). On the contrary, a number of more specific studies focused on rather particular aspects are available in the scientific literature. The highly nonlinear nature of the structural response of grain-silos has been first highlighted by Naito (1988). The granular ensiled content could slide with random motions due to its discrete nature and the amount of mass interacting with the silo wall could varies as well, as observed during different experimental tests since 1980s (Yokota et al. 1983, Shimamoto et al. 1984, Sakai et al. 1985, Sasaki and Yoshimura 1988). As far as the analytical formulations assessing the silo dynamics are concerned, no well-established formulations have been proposed. As matter of fact, the agreement between analytical predictions of the *effective* mass participating with the silo wall during dynamic excitation and experimental data is not always satisfactory and recent investigations (Holler and Meskouris 2006, Silvestri et al. 2016) suggest that a sensible reduction in the *effective mass* should be accounted for squat and intermediate-slender silos with respect to the value of 80% adopted by the most of codes. As far as the numerical models assessing the silo dynamics are concerned, continuum approaches have shown limited capabilities in capturing the complex interaction between granular ensiled content and silo wall and their application for practical purposes requires specific knowledge of the equivalent elastic properties of the particulate solid and significant experience and expertise in numerical modeling, usually above that of practitioners, are necessary as well given that the numerical response is highly dependent on the adopted constitutive models for the solid elements.

The analysis of the structural behavior of silo structures under filling and discharge conditions has been subject of extensive research efforts as well, but even after more than one century of research, many uncertainties still exists in various areas of silo structural behavior, and the high rate of failure encountered on grain-silos structures over the last 100 years tends to proof it (Ravenet, 1981, Carson 2001, Ayuga et al. 2001, Rotter 2009). Especially for the case of horizontally corrugated vertically stiffened steel silos, commonly adopted worldwide for long-term storage of agricultural products, their structural response

has not been fully understood and structural failures are commonly induced by discharging and seismic loading.

It is evident that the actual scientific body of knowledge and the code provisions in the case of grain-silos presents a remarkable gap, especially if compared to the case of frame structures, where the scientific body of knowledge and code provisions are reasonably close to their actual dynamic behavior (the gap is relatively small). A significant scientific advancement of knowledge in the field of grain-silo dynamics is desirable as recognized by some of the most eminent researchers (Dowrick 1988, Holler and Meskouris 2006, Ayuga 2008, Rotter 2009) and practitioners (Carson and Craig 2015) in the field. A conceptual schematization that allows to appreciate the mutual relations in terms of complexity in the actual dynamic behavior, advancement in the scientific knowledge and related code provisions for grain-silos as compared to frame structures is provided in Figure 5.1.

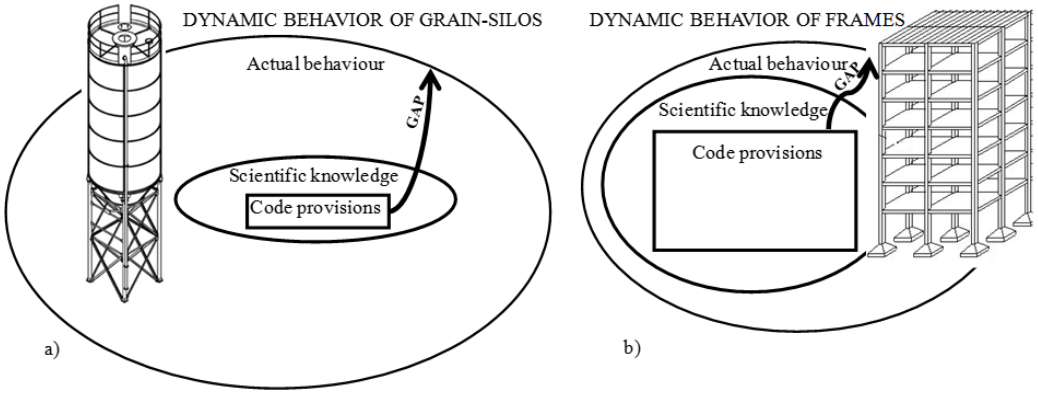

Figure 5.1 - Actual behavior vs scientific knowledge vs code provisions: (a) grain silos; (b) frame structures

The lack of a general and universally accepted theoretical framework for the dynamic behavior of grain-silos reflects in important shortcomings in actual seismic design provisions (Holler and Meskouris 2006, Carson and Craig 2015). In addition, no computational models (both FE and DE models) appear yet able to capture the phenomena seen in tests, let alone to quantify them well enough to give guidance on the development of better rules for design (Rotter 2009). For those reasons, current design codes are based almost exclusively on simplified interpretation of experimental observation in the light of very simple theories (Rotter et al. 1986), or ground on very empirical treatments of test

records (Rotter 2009) and tend to take very conservative provisions for the definition of the seismic actions investing grain-silo structures. From a practical point of view, design of grain-silos is still based on practical trial-and-correction procedure, rational semi-analytical approaches (Abdel-Sayed et al. 1985), engineers experience and/or specification prepared for each project (Arze, 1992, 1993). In this context, design based on experience of previous successes and, most of all, on failures appears more robust and sound with respect to the mere application of code prescriptions. However, according to Brown and Nielsen (1998), for very large silo structures (as they are seen today), it is considered an oversimplification to base on existing rules, especially when taking into account the extensive effects of a collapse of such silos on property and lives.

From a scientific point of view, the main challenges to be faced deal with:

- The definition of specific numerical models and/or computational strategies able to predict the response of grain-silos with sufficient approximation, both under static and dynamic conditions;
- A better understanding of the grain-silos dynamics, the pressures distributions exerted on the silo wall during earthquakes and the *effective mass* participating with the motion of the structure;
- A better comprehension of the complex structural response of real silo structures under discharging and earthquake loading.

In the present work, attention will be paid on the aspects related to the silo dynamics and a first insight into the complex structural response of a real silo structure composed by horizontally corrugated wall and vertical stiffeners will be presented.

Reference

Abdel-Saved, G., Monasa, F., & Siddal, W. (1985). Cold-Formed Steel Farm Structures, Part I: Grain Bins. Journal of Structural Engineering, 111(10), 2065-2089.

Arze L., (1992). Seismic design practices of industries, Tenth World Conference on Earthquake Engineering, 19-24 July, Madrid, Spain.

Arze, E. (1993). Seismic design of industrial facilities. Tectonophysics, 218(1-3), 23-41.

Ayuga, F., Guaita, M., & Aguado, P. (2001). SE—Structures and Environment: Static and Dynamic Silo Loads using Finite Element Models. Journal of Agricultural Engineering Research, 78(3), 299-308

Ayuga, F. (2008, June). Some unresolved problems in the design of steel cylindrical silos. In International conference on structures and granular solids-from scientific principles to engineering applications. The Royal society of Edinburgh, Scotland, UK (pp. 123-133).

Brown, C. J., & Nielsen, J. (Eds.). (1998). Silos: fundamentals of theory, behavior and design. CRC Press.

Carson, J. W. (2001). Silo failures: Case histories and lessons learned. Handbook of Powder Technology, 10, 153-166.

Carson, J., & Craig, D. (2015). Silo Design Codes: Their Limits and Inconsistencies. Procedia Engineering, 102, 647-656.

Dowrick, D. J. (1988). Edgecumbe earthquake-Some notes on its source, ground motions, and damage in relation to safety. Bulletin of the New Zealand National Society for Earthquake Engineering, 21(3), 198-203.

Janssen, H. A. (1895). Versuche über getreidedruck in silozellen. Zeitschr. d. Vereines deutscher Ingenieure, 39(35), 1045-1049.

Holler, S., & Meskouris, K. (2006). Granular material silos under dynamic excitation: numerical simulation and experimental validation. Journal of structural Engineering, 132(10), 1573-1579.

Landry JW, Grest GS, Silbert LE, Plimpton SJ (2003) Confined granular packings: structure, stress, and forces. Phys Rev E 67(4):041303

Lazarević, D., Fresl, K., & Milovanović, B. (2010, January). Some Discrete Properties of the Granular Contents of Silos. In The Seventh International Conference on Engineering Computational Technology.

Masson, S., & Martinez, J. (2000). Effect of particle mechanical properties on silo flow and stresses from distinct element simulations. Powder Technology, 109(1), 164-178.

Naito, Y. Equivalent linear technique in the finite element method applied to deformation with volume change and to an axisymmetric body under an unaxisymmetric load. In Proceedings of the 9th World Conference on Earthquake Engineering, Tokyo-Kyoto, Japan (Vol. 3, pp. 133-138).

Nielsen, J. (1998). Pressures from flowing granular solids in silos. Philosophical Transactions-Royal Society of London Series A Mathematical Physical and Engineering Sciences, 2667-2684.

Ovarlez, G., Fond, C., & Clément, E. (2003). Overshoot effect in the Janssen granular column: a crucial test for granular mechanics. Physical Review E, 67(6), 060302.

Qadir, A., Guo, H., Liang, X., Shi, Q., & Sun, G. (2010). Effect of the ratios of diameter of silo to bead on the pressure screening in granular columns. The European Physical Journal E, 31(3), 311-314.

Qadir, A., Ispalove, N. A., Ali, A., Chand, R., Shah, M. A., Khan, A., & Hussain, K. (2016). Experimental and Numerical Determination of Apparent Mass Variation of Granular Media Confined in Silo Geometry. Acta Physica Polonica, A., 129(3).

Ravenet, J. (1981). Silo problems. Bulk Solids Handling, 1(4), 667-679.

Rotter, J. M., Pham, L., & Neilsen, J. (1986). On the specification of loads for the structural design of bins and silos. In Second International Conference on Bulk Materials Storage, Handling and Transportation: 1986; Preprints of Papers (p. 241). Institution of Engineers, Australia.

Rotter, J. M. (2008). Structures, stability, silos and granular solids: a personal adventure. Structures and Granular Solids: From Scientific Principles to Engineering Application, 1.

Rotter, J. M. (2009, November). Silos and tanks in research and practice: state of the art and current challenges. In Symposium of the International Association for Shell and Spatial Structures (50th. 2009. Valencia). Evolution and Trends in Design, Analysis and Construction of Shell and Spatial Structures: Proceedings. Editorial Universitat Politècnica de València.

Sakai, M., Matsumura, H., Sasaki, M., Nakamura, N., Kobayashi, M., & Kitagawa, Y. (1985). Study on the dynamic behavior of coal silos against earthquakes. Bulk Solids Handling, 5(5), 1021.

Shimamoto, A., Kodama, M., & Yamamura, M. (1984). Vibration tests for scale model of cylindrical coal storing silo. In Proceedings of the 8th World Conference on Earthquake Engineering (Vol. 5, pp. 287-294). San Francisco.

Sasaki, Y., & Yoshimura, J. (1988). Seismic Response of Concrete Stave Silos with Structural Discontinuity. Proceedings of the Ninth World Conference on Earthquake Engineering, Tokyo-Kyoto, Japan (Vol. VI).

Vanel, L., & Clément, E. (1999). Pressure screening and fluctuations at the bottom of a granular column. The European Physical Journal B-Condensed Matter and Complex Systems, 11(3), 525-533.

Yokota, H., Sugita, M., & Mita, I. (1983, November). Vibration tests and analyses of coal-silo model. In Proc., 2nd Int. Conf. on the Design of Silos for Strength and Flow, Stratford-upon-Avon, Powder Advisory Centre (November 1983) (pp. 107-116).

PART B: Previous research work

Part B is focused on the previous research works conducted by Prof. Trombetti and co-workers in the year 2012-2013. First, the theoretical study on the horizontal forces produced by grain-like material inside silos during earthquakes is presented. Then, the experimental investigation conducted via shaking-table tests at the EQUALS laboratory of the University of Bristol (ASESGRAM project) are reported. Finally, the analytical-experimental correlation study for the verification of the original analytical formulation is illustrated.

6. The theoretical studies conducted at the University of Bologna

In this chapter, the analytical formulation for the evaluation of the horizontal forces produced by grain-like material on the silo wall during earthquake proposed by Prof. Trombetti and co-workers of the University of Bologna, in 2012, is presented. First, the problem formulation and the basic assumptions are presented, then, the analytical developments considering dynamic equilibrium under accelerated conditions are reported and the so-obtained general analytical formulations are specialized for the case of constant vertical profile of the earthquake induced accelerations. The limits of validity of the present formulation are discussed and the analytical formulations for the prediction of the shear forces and the bending moments acting on the silo wall are presented. Finally, the graphic representations of (i) the horizontal pressure and overpressures exerted by the grain on the silo wall, (ii) the portions of grain interacting with the silo wall under dynamic conditions, and (iii) the wall shear, the wall bending moment and the *effective mass* are presented are compared with the Janssen (1985) formulation, the Trahair (1983) formulation and the Eurocode 8 provisions.

6.1 Problem formulation and basic assumptions

In the present section, the problem formulation and the basic assumptions considered are presented. In detail, the idealized system and the idealized conditions considered are described. In this context, a new physical model is developed consistently with the one originally identified for the static case by Janssen (1985) and modified to overcome the issues due to the lack of axial-symmetry. The main aims is to obtain an analytical formulation for the approximate evaluation of the overpressures exerted by the ensiled granular material on the silo wall under dynamic conditions.

6.1.1 Idealized system

A ground-supported circular silo with diameter d_c (radius R) and filled with grain-like material up to the height H is considered (Figure 6.1). The grain free surface is considered to be horizontal. The reference system has the vertical z axis going from the horizontal grain free surface towards the bottom of the silo.

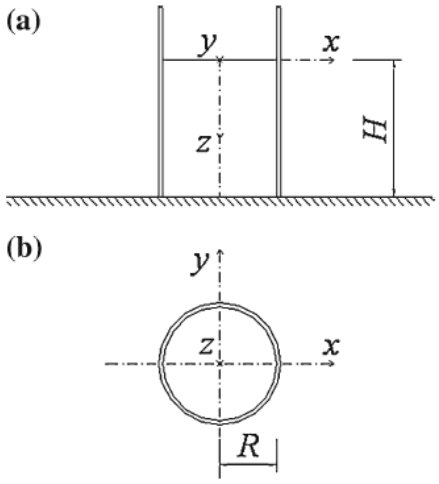

Figure 6.1 - Geometry of the flat-bottom ground-supported circular grain-silo and the reference system considered. a) Vertical view; b) Plan view

The idealized system representative of flat-bottom circular grain-silos is filled with grain-like material assumed to be incompressible and compact, without voids, as it were composed by a number of infinitely stiff and infinitely resistant spherical elements, as depicted in Figure 6.2.

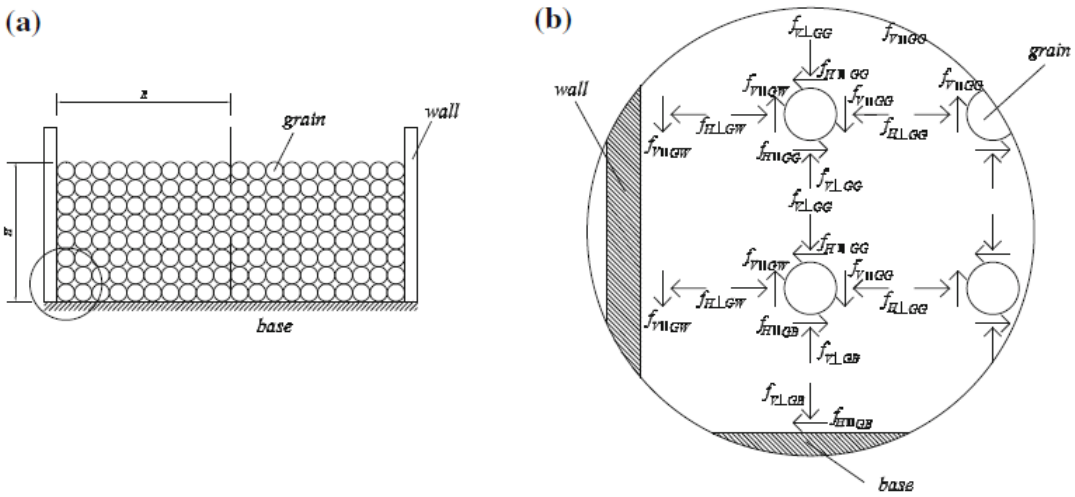

Figure 6.2 – a) Idealized system. b) Mutual forces exchanged between two adjacent grains, between the grain and the silo wall, and between the grain and the silo base

The grain-like material exerts horizontal and vertical forces on the silo wall. The mutual forces exchanged between grain and silo wall and grain and silo bottom are illustrated in Figure 6.2 with reference to the schematic idealization adopted, where:

- $f_{V,\perp,GG}$ is the vertical normal force, perpendicular to the grain surface, which is exchanged between two consecutive grains;

- $f_{H,\perp,GG}$ is the horizontal normal force, perpendicular to the grain surface, which is exchanged between two consecutive grains;
- $f_{H,\parallel,GG}$ is the horizontal tangential force, parallel to the grain surface, which is exchanged between two consecutive grains;
- $f_{V,\perp,GG}$ is the vertical tangential force, parallel to the grain surface, which is exchanged between two consecutive grains;
- $f_{H,\perp,GW}$ is the horizontal normal force, perpendicular to the grain surface, which is exchanged between the grain and the silo wall;
- $f_{V,\parallel,GW}$ is the vertical tangential force, parallel to the grain surface, which is exchanged between a single grain and the silo wall;
- $f_{H,\parallel,GB}$ is the horizontal tangential force, parallel to the grain surface, which is exchanged between the grain and the silo bottom;
- $f_{V,\perp,GB}$ is the vertical normal force, perpendicular to the grain surface, which is exchanged between the grain and the silo bottom.

It should be mentioned that horizontal shear forces which are perpendicular to the sheet plan are not reported in Figure 6.2 and either through the whole section in order to simplify the graphic representation and also notation, whilst they exist and should be considered in the analyses.

In order to perform an integral evaluation of the global forces that the grain produces on the silo wall, the grain-like material is treated as a set of overlapped layers of infinitesimal height *dz* (transition from the discrete approach to the continuous approach), where *z* represents the distance of a single horizontal grain layer from the horizontal grain free surface, consistently with approach adopted by Janssen (1895).

Within this continuous approach, the above-mentioned concentrated normal and tangential forces become distributed normal pressures p and tangential stresses τ, respectively:

- $f_{V,\perp,GG}$ becomes $p_{v,GG}(z)$;
- $f_{H,\perp,GG}$ becomes $p_{h,GG}(z)$;
- $f_{H,\parallel,GG}$ becomes $\tau_{h,GG}(z)$;

- $f_{V,\|,GG}$ becomes $\tau_{v,GG}(z)$;
- $f_{H,\perp,GW}$ becomes $p_{h,GW}(z,\theta)$;
- $f_{V,\|,GW}$ becomes $\tau_{v,GW}(z,\theta)$;
- $f_{H,\|,GB}$ becomes $\tau_{h,GB}(z,\theta)$;
- $f_{V,\perp,GB}$ becomes $p_{v,GB}(z,\theta)$.

where θ is the angle ($0° \le \theta < 360°$) measured clockwise from the negative semi-axis of *x*. Figure 6.3 illustrates the above mentioned notation, as far as normal forces are concerned.

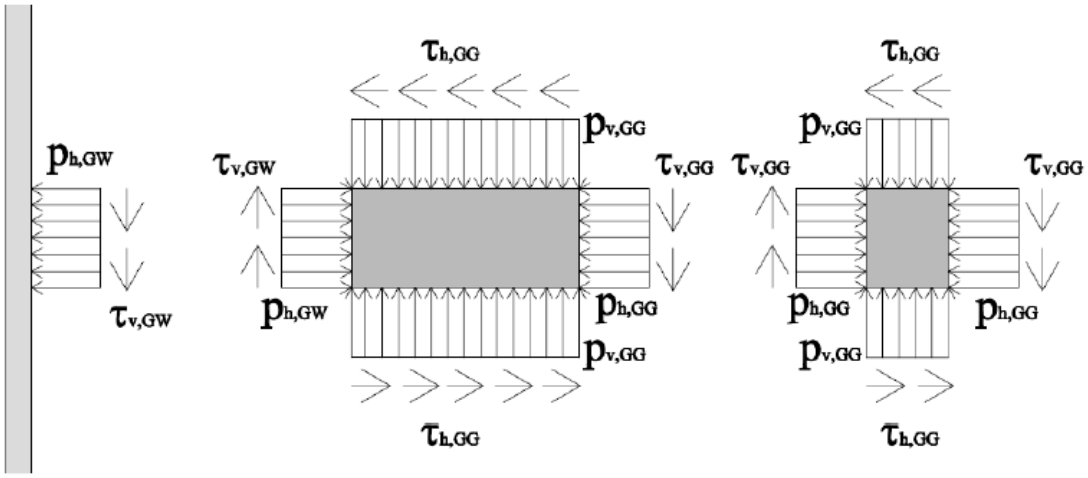

Figure 6.3 - Representation of the mutual actions exchanged between consecutive grains, between the grain and the silo wall, and between the grain and the silo bottom

It is reasonable to assume that the vertical grain-grain pressures $p_{v,GG}(z)$ tend to diminish from the core of the grain towards the silo wall, for any value of θ, where their value is equal to zero (Figure 6.4*a*).

The vertical pressures should be necessarily equal to zero next to the wall, due to the fact that some grain is sustained by the wall through friction, and not sustained by the underlying layers of grain. If it were not so, the silo wall could be designed only for their self-weight, without considering any load coming from the grain mass, in both static and seismic cases.

A first idealize model of the actual distribution of these vertical pressures was proposed by Janssen (1895). With the purpose of evaluating the *effective mass* of grain which leans against the silo wall and also providing conservative design indications under

static conditions, Janssen assumed that the vertical pressures, $p_{v,GG}(z)$, at the base of a grain portion at a generic height *z*, are equally distributed over the whole surface (Figure 6.4*b*). This model leads to a conservative estimation of the forces on the wall in that the frictional vertical stresses along the grain-wall contact surface are fully exploited, whilst the actual frictional stresses are likely to be lower.

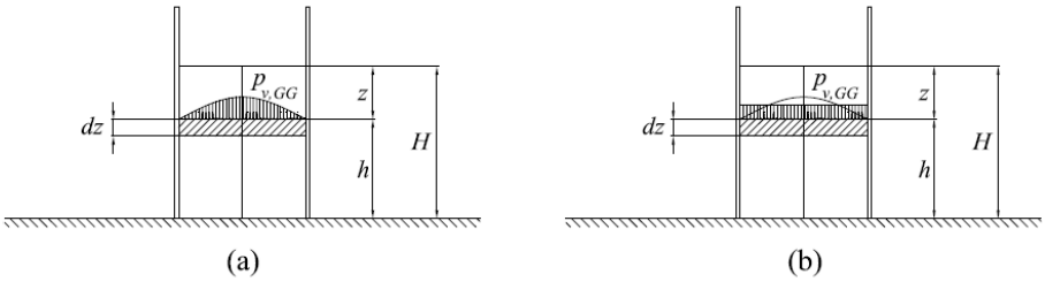

Figure 6.4 - (a) Actual distribution of $p_{v,GG}(z)$, (b) the schematization by Janssen (1895).

6.1.2 Idealized conditions

The above-described idealized system is studied in the following idealized conditions. The earthquake ground motion is simulated with vertical and horizontal accelerations, which, in general, are functions of the time *t* and the distance *z* from the free grain surface. As far as the vertical direction is concerned, the absolute acceleration experienced by the silo and its content is given by $a_v(t,z) = g + a_{ev}(t,z) \cdot g$, where *g* is the gravity acceleration and $a_{ev}(t,z) \cdot g$ is the additional vertical acceleration due to the earthquake (Figure 6.5). In this study, the term *additional* means *additional with respect to the acceleration of gravity*. As far as the horizontal direction is concerned, the absolute acceleration is given by $a_h(t,z) = a_{eh}(t,z) \cdot g$, where $a_{eh}(t,z) \cdot g$ is the horizontal acceleration due to the earthquake (Figure 6.5). Both a_{ev} and a_{eh} are expressed as fractions of *g*. For comparative purposes, Eurocode 8 Part 4 §3.3 (EN 1998-4, 2006) refers to $a_{eh}(t,z)$ as parameter $\alpha(z)$, which is defined as the ratio of the response horizontal acceleration of the silo at a vertical distance *z* from the equivalent surface of the stored contents, to the acceleration of gravity *g*.

As far as the time variation of the earthquake input is concerned, the earthquake ground motion is simulated with time constant vertical and horizontal accelerations:

$a_{ev}(t,z) = a_{ev}(z)$ and $a_{eh}(t,z) = a_{eh}(z)$. It is clear that this assumption leads to a conservative simplification, given that it is representative of a fictitious single instant of time in which both the vertical and the horizontal accelerations are supposed to reach contemporarily their peak values. The same assumption is also adopted by Eurocode 8 Part 4 §3.3 (EN 1998-4 2006) by means of parameter *α(z)*, which is not a function of time.

As far as the space variation of the earthquake input (i.e. the acceleration profile along the height of the silo) is concerned, in general, different trends, such as constant, linear, parabolic or more complex profiles, could be considered, e.g.:

- for the vertical earthquake acceleration:
  - constant: $a_{ev}(z) = a_{ev0}$;
  - linear: $a_{ev}(z) = a_{ev0} + a_{ev1} \cdot (H - z)$;
  - parabolic: $a_{ev}(z) = a_{ev0} + a_{ev1} \cdot (H - z) + a_{ev2} \cdot (H - z)^2$;
- for the horizontal earthquake acceleration:
  - constant: $a_{eh}(z) = a_{eh0}$;
  - linear: $a_{eh}(z) = a_{eh0} + a_{eh1} \cdot (H - z)$;
  - parabolic: $a_{eh}(z) = a_{eh0} + a_{eh1} \cdot (H - z) + a_{eh2} \cdot (H - z)^2$.

where a_{ev0}, a_{ev1}, a_{ev2}, a_{eh0}, a_{eh1} and a_{eh2} are constant coefficients. By introducing parameter *α(z)* as a function of the vertical distance *z*, Eurocode 8 Part 4 §3.3 (EN 1998-4 2006), accounts for but does not specify anything about the variation of the horizontal acceleration along the height of the silo. The choice of the vertical profiles of both the vertical and the horizontal earthquake accelerations is strictly related to the dynamic behavior (i.e. mass and stiffness) of the system composed by the silo wall and the grain material. If the silo is assumed to be infinitely stiff, no amplification is to be considered and thus spectral accelerations coincide with ground accelerations (i.e. the response acceleration of the silo does not vary along the height of the silo). If the silo is assumed to be flexible, variation along the height of the silo should be considered for the earthquake accelerations.

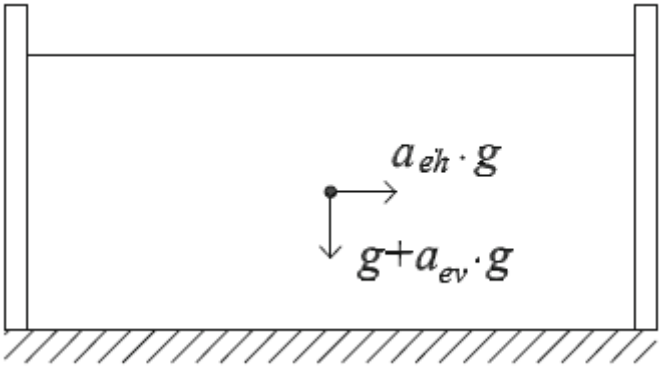

Figure 6.5 - Accelerated conditions: silo subjected to $g + a_{ev} \cdot g$ *and to* $a_{eh} \cdot g$

6.1.3 Basic assumptions

In this section, the basic assumptions formulated to perform a physical idealization of the dynamic behavior of grain-silo systems are presented. Such set of assumptions, even if resulting, generally, simple and/or strong exemplifications of the actual dynamic behavior of grain-silos under dynamic excitation, allows to analytically treat the complexity of silo phenomena (Nielsen, 2008).

The basic assumptions of the proposed analytical formulation are summarized as follows:

1. The silo wall is assumed to be axially infinitely stiff in the vertical direction as also assumed by Janssen (1895);
2. The grain-wall friction is supposed to be fully exploited, as also assumed by Janssen (1895);
3. Each grain layer is subdivided into two portions: (i) grain completely leaning against the layers below (central portion, disk *D*) and (ii) grain completely sustained by the wall through friction (external torus, element *E*);
4. Disk *D* presents equally distributed vertical pressures $p_{v,GG}(z)$, as also assumed in the Janssen (1895) idealized model;
5. On the contrary of what implicitly assumed by Eurocode 8, the horizontal grain-grain frictional stresses ($\tau_{h,GG}$) are assumed to be different from zero and thus considered in the equilibrium. They are limited by the friction law on the considered contact surface;

6. Also the $\tau_{v,GW}$, $\tau_{h,GW}$ and $\tau_{h,GB}$ frictional stresses (where v = vertical, h = radial horizontal, G = grain, W = wall and B = bottom) are considered in the equilibrium and are limited by the friction law on the contact surface;
7. No horizontal sliding of disk D occurs on the layers well below the free-surface and at the bottom of the silo;
8. Time constant vertical and horizontal accelerations $a_{ev}(z)$ and $a_{eh}(z)$ are used to simulate the earthquake ground motion investing the silo;
9. Time constant vertical and horizontal accelerations are applied simultaneously;
10. The inertial contributions of the silo wall are neglected in dynamic conditions. Furthermore, the effects of sloshing mode, horizontal sliding of the top grain layers and grain vertical settlements are not taken into account;
11. The conservative envelope of two limit conditions is taken by considering different vertical normal pressure distributions $p_{v,GG}(z)$ inside element E between consecutive layers.

Figure 6.6 shows the idealized subdivision of the ensiled grain on the vertical and horizontal sections. Figure 6.7 shows the pressures distribution acting on the grain and on the silo wall in accelerated conditions according to the physical idealized model.

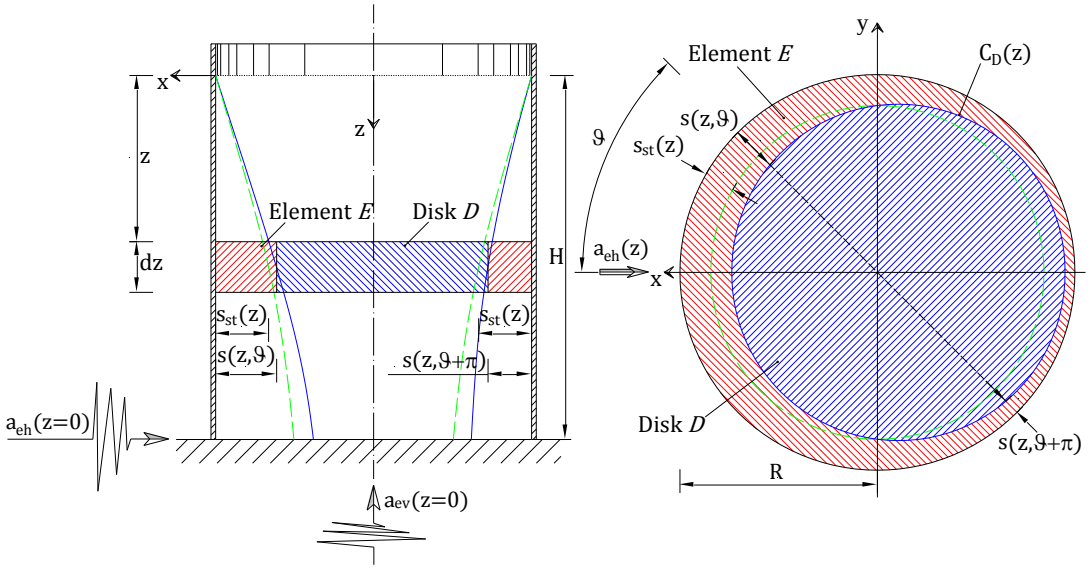

Figure 6.6 - External torus (red hatching) and internal disk (blue hatching) of the grain layer. (a) Vertical section, (b) plain view.

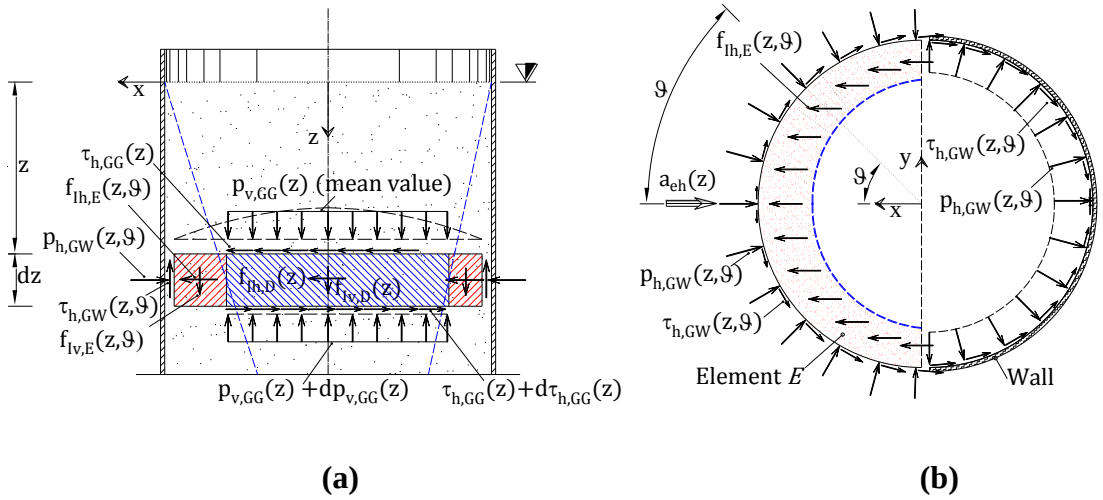

Figure 6.7 - Physical idealized model of the analytical formulation for accelerated conditions. (a) Vertical cross-section. The forces are referred to the grain. (b) Horizontal cross-section. On the left the forces are referred to the grain, on the right to the wall

Assumption 1 identifies the widespread category of silos characterized by flat vertical wall, thus excluding silos characterized by wavy wall obtained with steel corrugated sheets. Assumption 2 is consistent with the conservative idealization adopted by Janssen (1895) and is also justified by the numerical investigations conducted by Landry et al. (2003). Assumption 3 allows to overcome the issues due to the lack of axial-symmetry. Assumption 4 introduces a different distribution of the actual vertical grain-grain pressures exchanged between consecutive grain layers, by assuming that the vertical pressures should be necessarily equal to zero next to the wall, due to the fact that some grain is sustained by the wall through friction and not sustained by the underlying layers of grain. This involves a new internal schematization for each grain layer (disk *D* and element *E*), with respect to the idealized model proposed by Janssen (1895). Assumptions 3 and 4 imply the existence of a specific distance *s* from the silo wall, in correspondence of which $p_{v,GG}(z,\theta) = 0$ for all points with a distance less than *s* from the silo wall and for any value of θ (Figure 6.7*a*). Consequently, the grain portion which is completely sustained by the wall varies with the height *z* and is identified by the external torus *E* of thickness *s*. Assumptions 5 and 6 take into account the granular nature of the ensiled content. In detail, the tangential forces are limited by the Coulomb friction law of the contact surface considered, i.e.: (i) $\tau_{h,GG}(z) \le \mu_{GG} \cdot p_{v,GG}(z)$; (ii) $\tau_{h,GB} \le \mu_{GB} \cdot p_{v,GG}(z=H)$; (iii) $\tau_{v,GW}(z,\theta) \le \mu_{GW} \cdot p_{h,GW}(z,\theta)$; and (iv) $\tau_{h,GW}(z,\theta) \le \mu_{GW} \cdot p_{h,GW}(z,\theta)$, where μ_{GG}, μ_{GB}

and μ_{GW} are the friction coefficients related to the contact surfaces of grain-grain, grain-bottom and grain-wall, respectively. It has to be noted that $\tau_{h,GG}$, even if limited by the Coulomb friction criterion, is assumed different from zero. It is considered that the lateral sliding behavior of each grain layer upon the one below during an earthquake is inhibited until the friction forces are not exerted by the horizontal inertial actions. Assumption 7 excludes any horizontal sliding of disk *D* on the layers below, with exception for the grain layers close to the grain free surface. Assumption 8 is relevant to the vertical profile along *z* of both the vertical and the horizontal accelerations, which is result of the dynamic behavior (i.e. mass and stiffness) of the system composed by the silo wall and the grain material. If the silo is assumed to be infinitely stiff, no amplification occurs and it is reasonable to consider a constant vertical profile for the accelerations. On the contrary, if the silo is assumed to be flexible, amplification can occur, and it is reasonable to account for the variation along the silo height of the accelerations. In this respect, the analytical developments will be presented in the most general case of $a_{ev}(z)$ and $a_{eh}(z)$, considered as generic functions of *z*. Assumptions 8 and 9 together represent further cautionary idealized scenarios for the evaluation of the seismic actions. Assumption 10 allows to simplify the analytical treatise of the issue. As far as assumption 11 is concerned, the need of providing a robust and conservative formulation of the seismic behavior of such structures requires to consider the most pejorative scenarios, by accounting the envelope of the pressure distributions referring to different limit conditions (as typically done for conservative design in the structural engineering field). In this respect, the vertical normal pressures $p_{v,GG}(z)$ acting on element *E* play a relevant and double role. Granted that the horizontal pressures $p_{h,GW}(z,\theta)$ on the wall result as the sum of two contributions: the pressure due to the geostatic nature of the grain-like material ruled by the pressure ratio λ (Buisman 1940; Krynine 1945; Dabrowski 1957) and the dynamic overpressure due the imposed acceleration $a_{eh}(z)$, the following two limit conditions are considered:

- First, in order to maximize the dynamic overpressures $\Delta p_{h,GW}(z,\theta)$ necessary to balance the inertial horizontal forces, in the horizontal equilibrium of each elementary sector of element *E*, the contribution to horizontal pressures $p_{h,GW}(z,\theta)$ on the wall due to the geostatic nature of the grain-like material (ruled by the pressure ratio λ) is neglected by assuming the absence of $p_{v,GG}(z)$.

- Second, in order to maximize the frictional vertical stresses $\tau_{v,GW}(z,\theta)$ necessary to balance the (both self-weight and inertial) vertical forces, in the vertical equilibrium of each elementary sector of element *E*, the horizontal pressures $p_{h,GW}(z,\theta)$ on the wall are maximized (both contributions are considered) by assuming a uniform distribution of vertical pressures $p_{v,GG}(z)$.

It has to be noted that, even if from a physical point of view the assumptions on $p_{v,GG}(z)$ acting on element *E* are not consistent to each other, from a design point of view considering two limit conditions allows to obtain a conservative formulation.

Considering the envelope of the actions according to the two limit conditions leads to the most conservative evaluation of the thickness $s(z, \theta)$ and of the forces on the silo wall, which thus turn out to be the highest as possible.

6.2 Dynamic equilibrium in accelerated conditions

In this section, the dynamic equilibrium under accelerated conditions is discussed and the analytical developments are presented in the most general case of $a_{ev}(z)$ and $a_{eh}(z)$, considered as generic functions of *z*.

The objective of the analytical developments presented in the following sections is to determine the measure of the thickness of the external torus $s(z,\theta)$, under accelerated conditions, by means of plain equilibrium equations, in order to quantitatively identify the portion of the grain that leans against the layers below and the one that pushes on the silo wall. Consequently, as derivative results that are basic information regarding the pressure distributions (namely, normal pressures and tangential stresses) will be also achieved.

6.2.1 Unknown quantities and equations at disposal

The unknown quantities of the problem are represented by the pressure distributions and the thickness $s(z,\theta)$ of the external torus *E*, which are depicted in Figure 6.8 and Figure 6.9. The direction of the horizontal acceleration (towards *x*) is rotated by an angle θ on the horizontal plane compared to the direction (towards ξ) perpendicular to the external vertical surface of element *E*.

In details, the unknown quantities are:

1. $p_{v,GG}(z)$ = vertical grain-grain pressure acting on the cross-area of disk *D*;
2. $p_{h,GG}(z)$ = horizontal grain-grain pressure exchanged between disk *D* and element *E;*
3. $\tau_{h,GG}(z)$ = horizontal grain-grain tangential stresses acting on the cross-area of disk *D*;
4. $\tau_{v,GW}(z,\vartheta)$ = vertical grain-wall tangential stresses exerted by the grain on the silo wall;
5. $s(z,\vartheta)$ = thickness of element *E*;
6. $p_{h,GW}(z,\vartheta)$ = horizontal grain-wall pressure exchanged between element *E* and the silo wall
7. $\tau_{h,GW}(z,\vartheta)$ = horizontal grain-wall tangential stresses acting on the silo wall.

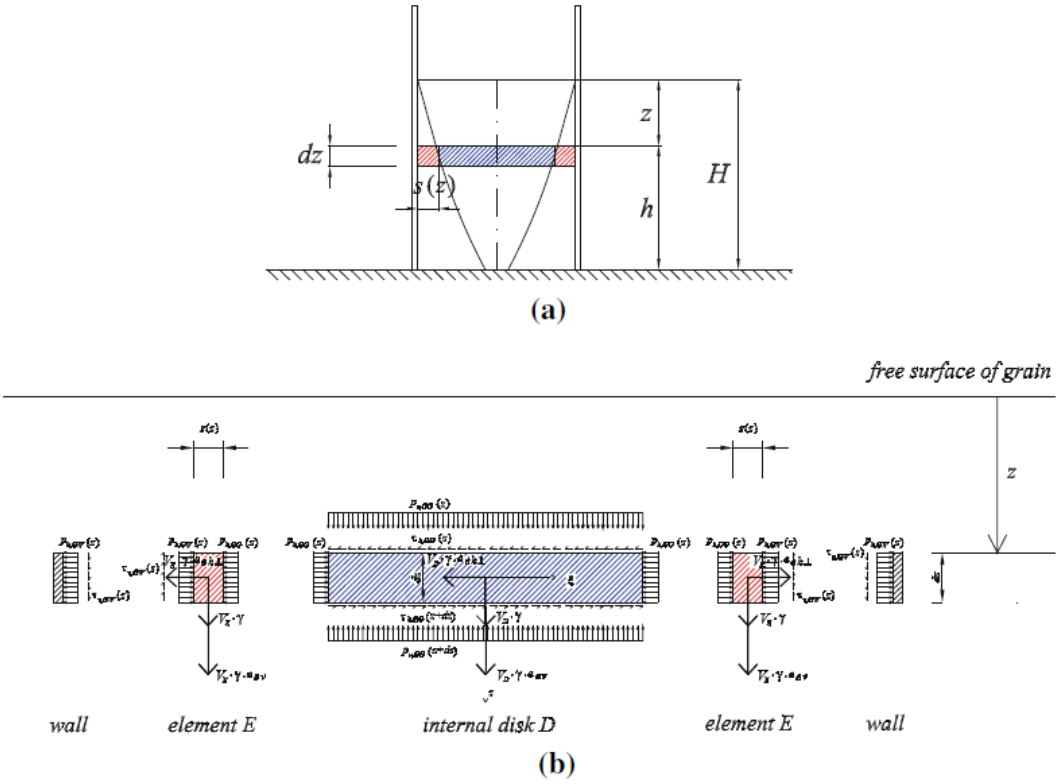

Figure 6.8 - Vertical longitudinal section: a) schematic trend of s(z,θ); b) vertical and horizontal actions operating on disk D and on the symmetrical elements E

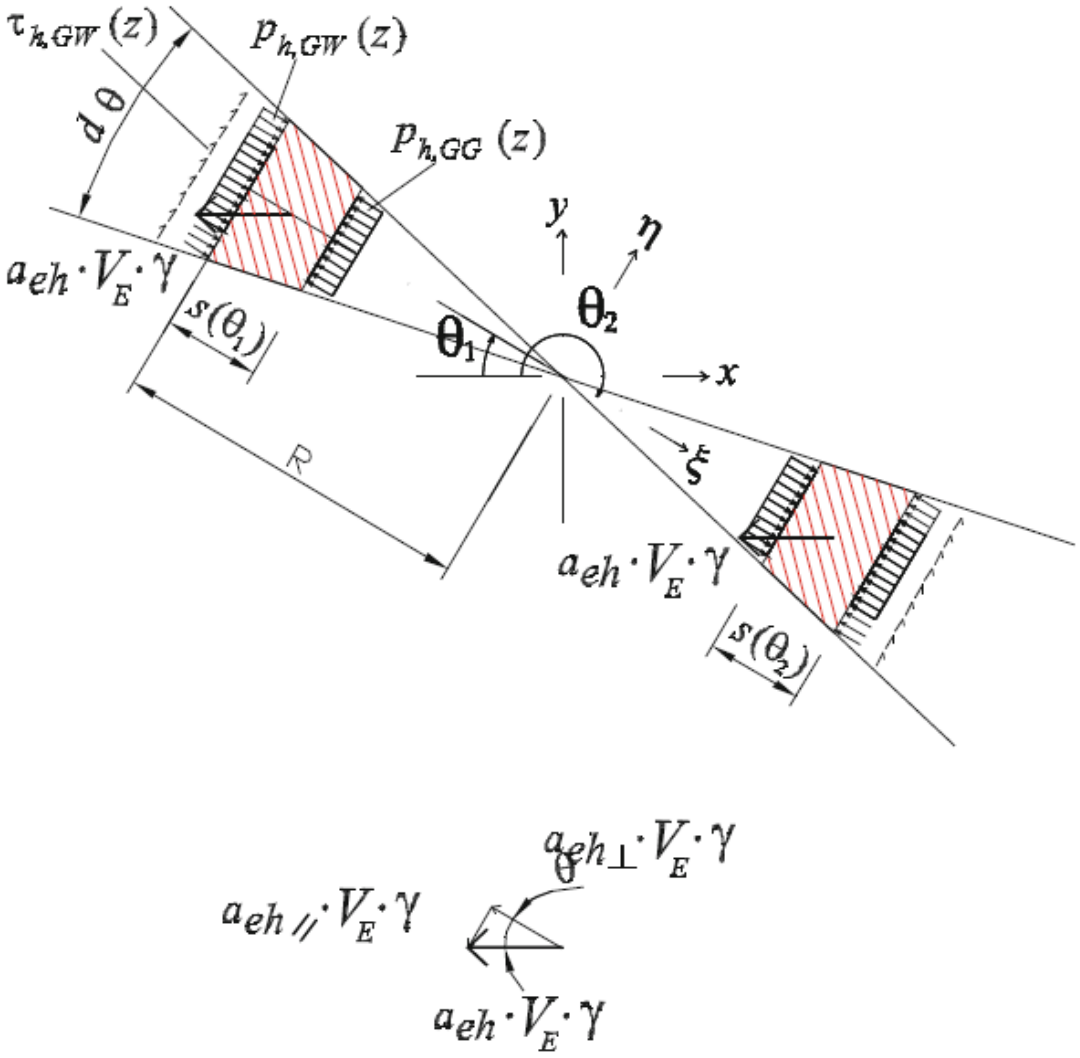

Figure 6.9 - Horizontal cross-section: horizontal actions operating on the symmetrical elements E

The mutual actions exchanged between the grain and the silo wall are assessed in this study (as it is usually done in seismic analyses where the effects of horizontal accelerations are evaluated), by the study of free-body diagrams which are representative of the dynamic equilibrium conditions.

The equations at disposal are:

1. Vertical forces equilibrium of disk *D*;
2. Pressure ratio relationship between vertical and horizontal pressures in the grain;
3. Horizontal (radial) forces equilibrium of disk *D*;
4. Friction law for the boundary between element *E* and the silo wall;
5. Vertical forces equilibrium of element *E*;

6. Horizontal (radial) forces equilibrium of element *E*;
7. Horizontal (tangential) forces equilibrium of element *E*.

Figure 6.8 and Figure 6.9 show the mutual actions that disk *D*, elements *E* and the silo wall exchange. It must be noticed that, in addition to the normal pressures and the shear stresses which are exchanged between the portions of grain and between the grain and the silo wall, there are the vertical and horizontal forces, which are detailed as follows:

- $\gamma \cdot V_D$ = self-weight of disk *D* acting towards *z* due to the effect of the gravity acceleration (γ is the unit weight of the grain-like material);
- $a_{ev}(z) \cdot \gamma \cdot V_D$ = inertial force coming from the centre of the mass of disk *D* and acting towards *z* due to the effect of the vertical acceleration $a_{ev}(z)$ (the inertial force is downward, as the acceleration a_{ev} has been assumed positive upwards);
- $a_{eh}(z) \cdot \gamma \cdot V_D$ = inertial force coming from the centre of the mass of disk *D* and acting towards *x*, due to the effect of the horizontal acceleration $a_{eh}(z)$ (inertial force towards the left as the acceleration a_{eh} has been assumed to be positive towards the right);
- $\gamma \cdot V_E$ = self-weight of element *E* acting towards *z* due to the effect of the gravity acceleration;
- $a_{ev}(z) \cdot \gamma \cdot V_E$ = inertial force coming from the centre of the mass of element *E* and acting towards *z* due to the effect of the vertical acceleration $a_{ev}(z)$ (the inertial force is downward, as the acceleration a_{ev} has been assumed positive upwards);
- $a_{eh}(z) \cdot \gamma \cdot V_E$ = inertial force coming from the centre of the mass of element *E* and acting towards *x*, due to the effect of the horizontal acceleration $a_{eh}(z)$ (the inertial force is towards the left as the acceleration a_{eh} has been assumed to be positive towards the right).

6.2.2 Vertical force equilibrium of disk *D*

Vertical forces equilibrium of disk *D* provides:

$$p_{v,GG}(z+dz)\cdot A_D = p_{v,GG}(z)\cdot A_D + \gamma\cdot V_D + a_{ev}(z)\cdot\gamma\cdot V_D \tag{1}$$

where $A_D(z)=\int_0^{2\pi}\int_0^{r(z,\vartheta)} r(z,\vartheta)\cdot dr\cdot d\vartheta$ is the surfaces of the disk, $V_D(z)=A_D(z)\cdot dz$ is the volume of the disk and clearly $p_{v,GG}(z+dz)=p_{v,GG}(z)+dp_{v,GG}(z)$. Then, Eq. (1) leads to:

$$dp_{v,GG}=\left[1+a_{ev}(z)\right]\cdot\gamma\cdot dz \tag{2}$$

Integrating Eq. (2) gives:

$$p_{v,GG}(z)=\int\left[1+a_{ev}(z)\right]\cdot\gamma\cdot dz + C_1 \tag{3}$$

where C_1 is a constant of integration that can be obtained imposing the boundary condition (on the top surface of the grain the vertical pressures are null, i.e. $p_{v,GG}(z=0)=0$).

6.2.3 Pressure ratio relationship between vertical and horizontal grain-grain pressures

If λ is the pressure ratio of the grain-like material, the following relationship holds between vertical and horizontal pressures inside the grain:

$$p_{h,GG}(z)=\lambda\cdot p_{v,GG}(z) \tag{4}$$

6.2.4 Horizontal (radial) forces equilibrium of disk *D*

Horizontal (radial) forces equilibrium of disk *D* provides:

$$\tau_{h,GG}(z+dz)\cdot A_D = a_{eh}(z)\cdot\gamma\cdot V_D + \tau_{h,GG}(z)\cdot A_D \tag{5}$$

where $\tau_{h,GG}(z+dz)=\tau_{h,GG}(z)+d\tau_{h,GG}(z)$. Thus, Eq. (5) leads to:

$$d\tau_{h,GG} = a_{eh}(z)\cdot\gamma\cdot dz \tag{6}$$

Integrating Eq. (6) gives:

$$\tau_{h,GG}(z) = \gamma\cdot\int_0^z a_{eh}(z)\cdot dz + C_2 \tag{7}$$

where C_2 is a constant of integration that can be obtained imposing the boundary condition (on the top surface of the grain the shear stress is null, i.e. $\tau_{h,GG}(z=0)=0$).

6.2.5 Friction law for the boundary between element E and the silo wall

If μ_{GW} is the friction coefficient of the grain-wall contact surface, the following relationship holds between the normal pressures and the vertical shear stresses along the contact surface between the grain of element *E* and the silo wall:

$$\tau_{v,GW}(z,\theta) = \mu_{GW}\cdot p_{h,GW}(z,\theta) \tag{8}$$

6.2.6 Vertical and horizontal (radial) forces equilibrium of element *E*

Vertical and horizontal forces equilibrium equations of element *E* are coupled in the following system of equations:

$$\begin{cases} \gamma\cdot V_E\cdot\left[1+a_{ev}(z)\right] = \tau_{v,GW}(z,\theta)\cdot A_E \\ p_{h,GW}(z,\theta)\cdot A_E = a_{eh\perp}(z,\theta)\cdot\gamma\cdot V_E + p_{h,GG}(z)\cdot A_E \end{cases} \tag{9}$$

where $A_E = R\cdot d\theta\cdot dz$ is the area of the vertical lateral surface of element *E*; $V_E = s(z,\theta)\cdot\left[R-\frac{s(z,\theta)}{2}\right]\cdot d\theta\cdot dz$ is the volume of element *E*; $a_{eh\perp}(z,\theta)$ represents the component of the horizontal acceleration $a_{eh}(z)$ perpendicular to the external vertical surface (towards ξ) of element *E* (see Figure 6.9): $a_{eh\perp}(z,\theta) = a_{eh}(z)\cdot\cos(\theta)$.

Equation (9) may be rewritten as follows:

$$\begin{cases} \gamma\cdot s(z,\theta)\cdot\left[R-\frac{s(z,\theta)}{2}\right]\cdot\left[1+a_{ev}(z)\right] = \tau_{v,GW}(z,\theta)\cdot R \\ \left[p_{h,GW}(z,\theta)-p_{h,GG}(z)\right]\cdot R = a_{eh\perp}(z,\theta)\cdot\gamma\cdot s(z,\theta)\cdot\left[R-\frac{s(z,\theta)}{2}\right] \end{cases} \tag{10}$$

Substituting Eq. (8) into the first of Eq. (10):

$$\begin{cases} \gamma \cdot s(z,\theta) \cdot \left[R - \dfrac{s(z,\theta)}{2} \right] \cdot \left[1 + a_{ev}(z) \right] = \mu_{GW} \cdot p_{h,GW}(z,\theta) \cdot R \\ \left[p_{h,GW}(z,\theta) - p_{h,GG}(z) \right] \cdot R = a_{eh\perp}(z,\theta) \cdot \gamma \cdot s(z,\theta) \cdot \left[R - \dfrac{s(z,\theta)}{2} \right] \end{cases} \tag{11}$$

After some calculations, this system of equations provides the closed-form expressions of $p_{h,GW}(z,\theta)$ and $s(z,\theta)$.

As far as the horizontal pressures exerted by the grain on the silo wall are concerned, it is possible to obtain:

$$p_{h,GW}(z,\theta) = \frac{p_{h,GG}(z)}{1 - \nu(z) \cdot a_{eh}(z) \cdot \cos(\theta) \cdot \mu_{GW}} \tag{12}$$

where $\nu(z) = \left(\dfrac{1}{1 + a_{ev}(z)} \right)$. Equation (12) gives the horizontal grain-wall pressure.

As far as the thickness of the portion of grain which is sustained entirely by the silo wall is concerned, the following quadratic equation in $s(z,\theta)$ is obtained:

$$s(z,\theta) \cdot \left[1 - \frac{s(z,\theta)}{2R} \right] = \frac{p_{h,GG}(z) \cdot \nu(z) \cdot \mu_{GW}}{\gamma \cdot \left[1 - \nu(z) \cdot a_{eh}(z) \cdot \cos(\theta) \cdot \mu_{GW} \right]} \tag{13}$$

Assuming $\beta(z,\theta) = \dfrac{2 \cdot p_{h,GG}(z) \cdot \nu(z) \cdot \mu_{GW}}{z \cdot \gamma \cdot \left[1 - \nu(z) \cdot a_{eh}(z) \cdot \cos(\theta) \cdot \mu_{GW} \right]}$, Eq. (13) can be rewritten as follows:

$$s(z,\theta)^2 - 2R \cdot s(z,\theta) + R \cdot \beta(z,\theta) \cdot z = 0 \tag{14}$$

The two solutions of the last equations are:

$$s(z,\theta) = R \pm \sqrt{\left(R^2 - R \cdot \beta(z,\theta) \cdot z \right)} \tag{15}$$

Clearly, the thickness $s(z,\theta)$ cannot be larger than the radius *R* of the silo, so that the only solution that has a physical meaning is the following (with sign -):

$$s(z,\theta) = R - \sqrt{\left(R^2 - R \cdot \beta(z,\theta) \cdot z \right)} \tag{16}$$

i.e.

$$s(z,\theta) = R - \sqrt{\left(R^2 - R \cdot \frac{2 \cdot p_{h,GG}(z) \cdot \nu(z) \cdot \mu_{GW}}{\gamma \cdot \left[1 - \nu(z) \cdot a_{eh}(z) \cdot \cos(\theta) \cdot \mu_{GW} \right]} \right)} \tag{17}$$

Eq. (17) gives the thickness $s(z,\theta)$ of the grain layer that leans against the walls.

6.2.7 Horizontal (tangential) forces equilibrium of element *E*

Horizontal (tangential) forces equilibrium of element *E* provides:

$$\tau_{h,GW}(z,\theta) \cdot A_E = a_{eh||}(z,\theta) \cdot \gamma \cdot V_E \tag{18}$$

where $a_{eh||}(z,\theta) = a_{eh}(z) \cdot \sin(\theta)$ represents the component of the horizontal acceleration $a_{eh}(z)$ parallel to the external vertical surface (towards η) of element *E* (see Figure 6.9). Thus, Eq. (18) leads to:

$$\tau_{h,GW}(z,\theta) = a_{eh}(z) \cdot \sin(\theta) \cdot \gamma \cdot s(z,\theta) \cdot \left[1 - \frac{s(z,\theta)}{2R} \right] \tag{19}$$

6.3 Specialization to the case of constant vertical profiles of both the vertical and the horizontal earthquake accelerations

In the present section, the analytical formulation describing the pressure distributions and thickness of external torus *E* are specialized for the case of constant vertical profiles of both the vertical and the horizontal accelerations. In detail, the following assumptions are made:

- constant vertical acceleration along the height of the silo, i.e. $a_{ev}(z) = a_{ev0}$;
- constant horizontal acceleration along the height of the silo, i.e. $a_{eh}(z) = a_{eh0}$.

Eq. (3) specializes as follows:

$$p_{v,GG}(z) = \left[1 + a_{ev0} \right] \cdot \gamma \cdot z \tag{20}$$

Equation (4) specializes as follows:

$$p_{h,GG}(z) = \lambda \cdot [1 + a_{ev0}] \cdot \gamma \cdot z \tag{21}$$

Equation (7) specializes as follows:

$$\tau_{h,GG}(z) = \gamma \cdot a_{eh0} \cdot z \tag{22}$$

Equation (12) specializes as follows:

$$p_{h,GW}(z,\theta) = \frac{\lambda \cdot \gamma \cdot z}{\nu_0 \cdot [1 - \nu_0 \cdot a_{eh}(z) \cdot \cos(\theta) \cdot \mu_{GW}]} \tag{23}$$

where $\nu_0 = \dfrac{1}{1 + a_{eh0}}$.

Equation (17) specializes as follows:

$$s(z,\theta) = R - \sqrt{\left(R^2 - R \cdot \frac{2 \cdot \lambda \cdot \mu_{GW} \cdot z}{1 - \nu_0 \cdot a_{eh0} \cdot \cos(\theta) \cdot \mu_{GW}} \right)} \tag{24}$$

Equation (19) specializes as follows:

$$\tau_{h,GW}(z,\theta) = \frac{a_{eh0} \cdot \sin(\theta) \cdot \gamma \cdot \lambda \cdot \mu_{GW} \cdot z}{1 - \nu_0 \cdot a_{eh0} \cdot \cos(\theta) \cdot \mu_{GW}} \tag{25}$$

6.4 Specialization to the case of null vertical and horizontal earthquake accelerations: the static case

A further formulation concerning the silo-grain interaction in static conditions is here obtained for the proposed analytical formulation. By considering null vertical and horizontal accelerations [$a_{ev}(z) = a_{ev0} = 0$ and $a_{eh}(z) = a_{eh0} = 0$] inside Eq. (12) and Eq. (13), the horizontal pressures $p_{h,GW}(z,\theta)$ on the wall and the thickness $s_{st}(z)$ result:

$$p_{h,GW,st}(z,\theta) = p_{h,GG}(z) = \lambda \cdot \gamma \cdot z \tag{26}$$

$$s_{st}(z) = R \cdot \left[1 - \sqrt{1 - \left(2 \cdot \mu_{GW} \cdot \lambda \cdot \frac{z}{R} \right)} \right] \tag{27}$$

6.5 Portions of grain relative to the behavior under accelerated conditions

Equation (24) provides the thickness $s(z,\theta)$ of the portion of grain that actually interacts and pushes on the silo wall in accelerated conditions. Therefore, two volumes arise inside the whole granular content, characterized by different dynamic behavior: $V_{E,dyn}(z)$ and $V_{D,dyn}(z)$. The former individuates the amount of grain that is completely sustained by the lateral silo wall, whilst the latter is the amount of grain leaning against the lower portion of the material up to the silo foundation without interacting with the silo wall.

From a geometrical point of view, $V_{E,dyn}(z)$ and $V_{D,dyn}(z)$ can be respectively visualized as a vertical-axis cylindrical annulus with thickness $s(z,\theta)$ and a vertical-axis truncated cone solid of radius $r(z,\vartheta)=R-s(z,\vartheta)$.

From a mathematical point of view, the volumes occupied by the disk *D* and element *E* are expressed as follows:

$$V_{D,dyn}(z)=\pi Rz^2\cdot\left[1-\frac{\lambda\cdot\mu_{GW}}{\sqrt{1-\left(a_{eh0}\cdot\nu_0\cdot\mu_{GW}\right)^2}}\right] \tag{28}$$

$$V_{E,dyn}(z)=\pi Rz^2\cdot\left[\frac{\lambda\cdot\mu_{GW}}{\sqrt{1-\left(a_{eh0}\cdot\nu_0\cdot\mu_{GW}\right)^2}}\right] \tag{29}$$

Eqs. (28) and (29) express positive values and the sum of $V_{D,dyn}(z)$ and $V_{E,dyn}(z)$ corresponds to the volume *V* of the whole ensiled content (where $V=\pi R^2H$), satisfying the mass balance.

6.6 Limits of validity of the proposed analytical formulation

In this section, the limits of validity of the proposed analytical formulation are discussed.

The proposed analytical formulation has some limitations which are related to the mathematical definition of some physical quantities related to the solution $s(z,\theta)$ and to the friction laws on the contact surfaces considered:

- it is necessary that volume $V_{D,dyn}(z)$ exists. This physical condition is rendered into the following mathematical limitation:

$$s(z=H,\theta)<R,\forall\theta \tag{30}$$

which, taking into account Eq. (16), leads to:

$$\sqrt{R^2-R\cdot\beta_0(z=H,\theta)\cdot H}>0,\forall\theta \tag{31}$$

and then to

$$R>\beta_0(z=H,\theta)\cdot H,\forall\theta \tag{32}$$

The maximum value of $\beta_0(z=H,\theta)$ occurs for θ = 0. Thus, the condition given by Eq. (32) requires that the slenderness ratio, $\Delta=H/2R$, should be:

$$\Delta<\frac{1}{2\cdot\beta_0(z=H,\theta=0)}=\frac{1-\nu_0\cdot a_{eh0}\cdot\mu_{GW}}{4\cdot\lambda\cdot\mu_{GW}} \tag{33}$$

Otherwise, the portion $V_{D,dyn}(z)$ cannot exist and the proposed analytical formulation cannot be applied;

- It is also necessary that portion $V_{E,dyn}(z)$ exists. This physical condition translates into the following mathematical limitation:

$$s(z,\theta)=R-\sqrt{R^2-R\cdot\beta_0(z,\theta)\cdot z}>0,\forall\theta,\forall z\in[0,H] \tag{34}$$

that requires:

$$R>\sqrt{R^2-R\cdot\beta_0(z,\theta)\cdot z}>0,\forall\theta \tag{35}$$

After some calculations, the conditions expressed by Eq. (35) becomes:

$$a_{eh0}<\frac{1}{\nu_0\cdot\mu_{GW}} \tag{36}$$

- It is also fundamental that the square root of Eq. (16) exists. This leads to the following condition:

$$a_{eh0}<\left(1-\frac{2\cdot\lambda\cdot\mu_{GW}\cdot H}{R}\right)\cdot\frac{1}{\nu_0\cdot\mu_{GW}}=\frac{1-4\cdot\lambda\cdot\mu_{GW}\cdot\Delta}{\nu_0\cdot\mu_{GW}} \tag{37}$$

- By referring to Eq. (23), in order to not have infinite values of the horizontal normal pressure, it is necessary that

$$1-\nu_0 \cdot a_{eh0} \cdot \cos(\theta) \cdot \mu_{GW} \neq 0, \forall \theta \tag{38}$$

which gives:

$$a_{eh0} \neq \frac{1}{1-\nu_0 \cdot \cos(\theta) \cdot \mu_{GW}}, \forall \theta \tag{39}$$

However, the condition expressed by Eq. (39) is already encompassed in the condition expressed by Eq. (36);

- Finally, in order to prevent horizontal sliding of the grain on the foundation and to guarantee that the inertial forces acting on internal disk *D* due to the horizontal acceleration are completely balanced by the resultant of the shear stresses developing at the disk foundation, it is necessary that the horizontal acceleration is lower than the following limiting value:

$$a_{eh0} \leq (1+a_{ev0}) \cdot \mu_{GB} \tag{40}$$

It should be noted that all these limitations identify a class of circular flat-bottom silos, for which the proposed analytical formulation can be applied.

6.7 The shear forces and the bending moments on the silo wall

In the present section, the wall shear and the wall bending moment acting on the shell of the silo exposed to seismic excitation are discussed.

Silos and revolution surfaces in general are structures characterized by high values of vertical and horizontal stiffness, where an eventual dynamic amplification strongly depends on the frequency features of the input provided by the earthquake ground motion at their bases.

The shear action on the silo wall is given by the integral, on the lateral surface of the silo, of the projection of the grain-wall normal pressures $p_{h,GW}(z,\theta)$ and horizontal frictional stresses $\tau_{h,GW}(z,\theta)$ towards *x* (namely, along the direction of the horizontal acceleration):

$$T_{xx}(z) = a_{eh0} \cdot \gamma \cdot \pi R z^2 \cdot \left(\frac{\lambda \cdot \mu_{GW}}{\sqrt{1 - \nu_0^{\,2} \cdot \mu_{GW}^{\,2} \cdot a_{eh0}^{\,2}}} \right) \tag{41}$$

Eq. (41) shows that the wall shear $T_{xx}(z)$ balances the horizontal inertial force of element *E* at each quote *z*, i.e. the mass of the external torus times the constant horizontal acceleration. By considering the value of the wall shear at the silo base, i.e. for *z*= *H*, the value of the wall base shear can be computed as:

$$T_{xx}(H) = a_{eh0} \cdot \gamma \cdot \pi R H^2 \cdot \left(\frac{\lambda \cdot \mu_{GW}}{\sqrt{1 - \nu_0^{\,2} \cdot \mu_{GW}^{\,2} \cdot a_{eh0}^{\,2}}} \right) \tag{42}$$

By dividing Eq. (42) for the value of the horizontal inertial action of the whole ensiled content equal to $a_{eh0} \cdot \gamma \cdot \pi H R^2$, the expression of the *effective mass* m_{eff} for the proposed analytical formulation may be computed:

$$m_{eff} = \frac{2\Delta \cdot \lambda \cdot \mu_{GW}}{\sqrt{1 - \nu_0^{\,2} \cdot \mu_{GW}^{\,2} \cdot a_{eh0}^{\,2}}} \tag{43}$$

The bending moment on the silo wall $M_{yy}(z)$ (namely, along the horizontal direction perpendicular to the earthquake) results as the integral of product between $T_{xx}(z)$ along the silo height, resulting:

$$M_{yy}(z) = \frac{1}{3} a_{eh0} \cdot \gamma \cdot \pi R z^3 \cdot \left(\frac{\lambda \cdot \mu_{GW}}{\sqrt{1 - \nu_0^{\,2} \cdot \mu_{GW}^{\,2} \cdot a_{eh0}^{\,2}}} \right) \tag{44}$$

By considering the value of the wall bending moment at the silo base, i.e. for *z*= *H*, the value of the wall base bending moment can be computed as

$$M_{yy}(H) = \frac{1}{3} a_{eh0} \cdot \gamma \cdot \pi R H^3 \cdot \left(\frac{\lambda \cdot \mu_{GW}}{\sqrt{1 - \nu_0^{\,2} \cdot \mu_{GW}^{\,2} \cdot a_{eh0}^{\,2}}} \right) \tag{45}$$

6.8 Graphic representations of the pressures, the two grain portions inside the silo and the wall actions

In the present section, graphic presentations of the pressure distributions, the two grain portions inside the silo and the wall actions are reported by means of applicative examples.

First, the profiles of the horizontal pressure exchanged between grain and silo wall under static and dynamic conditions are compared with those predicted by the Janssen (1895) formulation, the Trahair (1983) formulation (also assumed by few international standards) and the Eurocode 8 (EN 1998-4:2006) provisions. Then, graphic representations of the two grain portions (namely, disk *D* and external torus *E*) as defined by the proposed analytical formulation are shown. Finally, the vertical profiles of the wall shear and wall bending moment actions on the silo wall are presented. The applicative examples taken into considerations refer to the case of squat silo, i.e. with slenderness ratio $0.4 \le \Delta \le 1.0$ (according to EN 1991-4:2006 provisions). The physical and frictional characteristic of the grain-like material poured inside the silo and the horizontal input are selected in order to respect the limitations of the proposed analytical formulation. A constant vertical profile for both the horizontal and vertical accelerations is considered.

6.8.1 On the static pressures

In this section, the along-the-height profiles of the grain-wall pressures provided by the Janssen (1895) theory and the proposed analytical formulation are compared.

As applicative examples, three steel silos with "smooth" wall (Wall Surface Categories D2 according to Table 4.1 provisions of EN 1991-4:2006) characterized by a slenderness ratios $\Delta = \frac{H}{d_c} = 1.0$ (according to EN 1991-4:2006 provisions) containing different grain-like materials (barley, wheat and cement clinker) are considered. An horizontal free grain surface is considered, with a height above the silo base of the ensiled grain-like material $H = h_b$. The physical and frictional characteristic of the ensiled grain-like material in terms of unit weight of the bulk solid γ_b, grain-wall friction coefficient μ_{GW} and pressure ratio λ are listed in Table 6.1 and are derived from Table E.1 of EN 1991-4:2006 provisions.

Table 6.1 - Physical and frictional characteristic of the ensiled bulk solids according to Table E.1 of EN 1991-4:2006 provisions

Bulk solid	γ_b [kN/m^3]	μ_{GW} [-]	λ [-]
Barley	7.0	0.33	0.59
Wheat	9.0	0.38	0.54

Cement clinker	15.0	0.56	0.38

Figure 6.10 reports the vertical profiles of the grain-wall pressure in static conditions given by the Janssen formulation and the proposed analytical formulation (see Eq. (26)). The values are normalized with respect to the base horizontal geostatic grain-grain pressure, i.e. $\gamma \cdot \lambda \cdot h_b$.

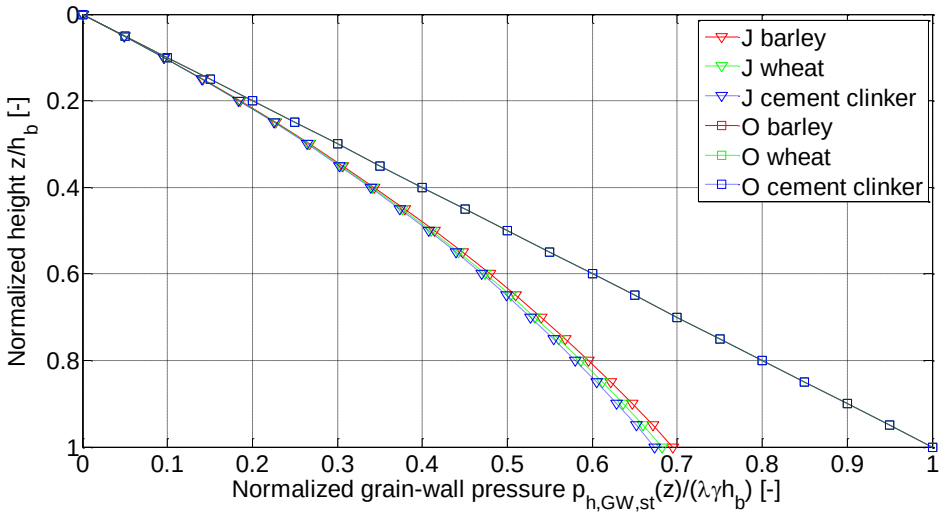

Figure 6.10 - Heightwise variation of the normalized grain-wall normal pressures for Janssen (J) and the proposed analytical formulation (O) in static conditions for squat silos containing barley, wheat and cement clinker.

The proposed analytical formulation gives a linear vertical profiles (the three plots overlap each other), whose slopes in correspondence of the grain free surface corresponds to those of the vertical profiles predicted by Janssen. Thus, the values of the grain-wall pressure are overestimated along the silo height with respect to those predicted by the Janssen formulation.

6.8.2 On the dynamic pressures

In the present section, the overpressure distributions given by the proposed analytical formulation, the Trahair (1983) formulation and the Eurocode 8 provisions are compared.

Eq. (12) represents the first fundamental result of this work and, according to the assumptions made in the previous sections, provides the horizontal grain-wall pressure under seismic conditions. Under static conditions, the grain-wall pressures are expressed

by Eq. (26). Then, the overpressure (or depression) between the grain and the silo wall due to the effects of the horizontal and vertical accelerations can be defined as follows:

$$\Delta p_{h,GW}(z,\theta) = p_{h,GW}(z,\theta) - p_{h,GW,st}(z) \tag{46}$$

Figure 6.11 reports the along-the-height profiles on the front side ($\theta = 0$) of the wall for the same grain-silos considered for the static case subjected to a dynamic input of $a_{eh0} = 0.30$, $a_{ev0} = 0.00$. The values of the grain-wall overpressures are normalized with respect to a reference value equal to $a_{eh0} \cdot \gamma \cdot A$ that represents the horizontal inertial action of the whole grain cross-section of unitary vertical thickness.

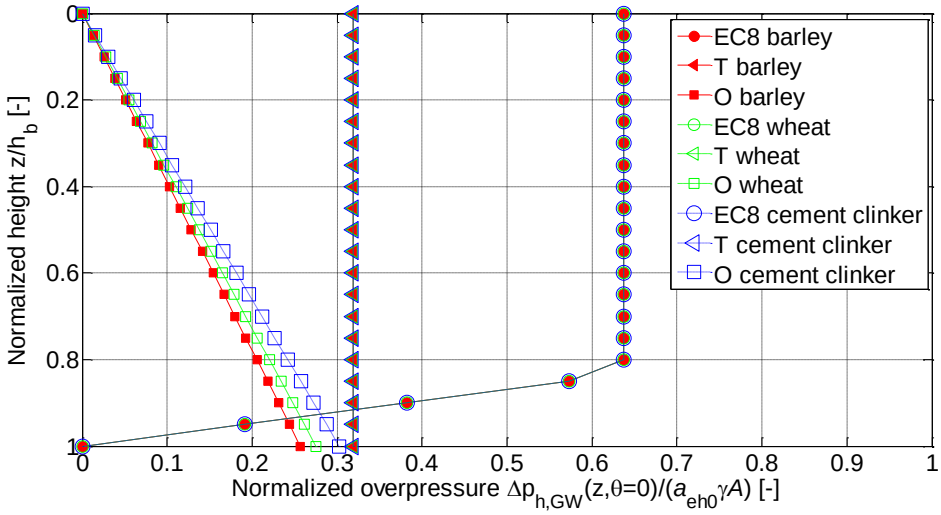

Figure 6.11 - Heightwise variation of the normalized grain-wall overpressures for Eurocode 8 (EC8), the Trahair formulation (T), the proposed analytical formulation (O) in dynamic conditions for squat silo for squat silos containing barley, wheat and cement clinker.

The vertical profiles of the horizontal grain-wall overpressure given by Eurocode 8 provisions and Trahair et al. (1983) present a similar distribution practically uniform along the whole silo height. On the contrary, the proposed analytical formulation provides similar linear distributions with null values in correspondence of the grain free surface. The discrepancy in terms of normalized values of the overpressures lay in fact that: (i) Eurocode 8 grounds on the Rotter and Hull (1989) investigation and the Younan and Veletsos (1998*a*, *b*) and considers only radial overpressure in balancing the horizontal inertia of an *effective mass* equal to roughly 0.90 (for the case in exam); (ii) the Trahair formulation considers both radial and tangential (circumferential) overpressure in balancing the horizontal inertia of an *effective mass* equal to 1.0; (iii) the proposed analytical formulation considers both radial and tangential (circumferential) overpressure

in balancing the horizontal inertia of an *effective mass* dependent on the frictional characteristic of the ensiled bulk solid.

Figure 6.12, Figure 6.13 and Figure 6.14 show the distribution along the circumference of the wall of the normalized overpressures for two salient horizontal cross-sections for the three squat silos previously considered. In the plots, the *x* and *y* coordinates are normalized with respect to the radius *R* and the black curve represents the external circumference of the silo; whilst the grey plots represent the grain-wall overpressures $\Delta p_{h,GW}(z,\theta)$ for a fixed height *z* and $0° \le \theta \le 360°$, normalized with respect to a reference value equal to $a_{eh0} \cdot \gamma \cdot h_b$. It is interesting to notice that, at any height *z*, the overpressures $\Delta p_{h,GW}(z,\theta)$ due to horizontal earthquake acceleration only are quite small, roughly the 10% ÷ 30% of $p_{h,GW,st}(z)$.

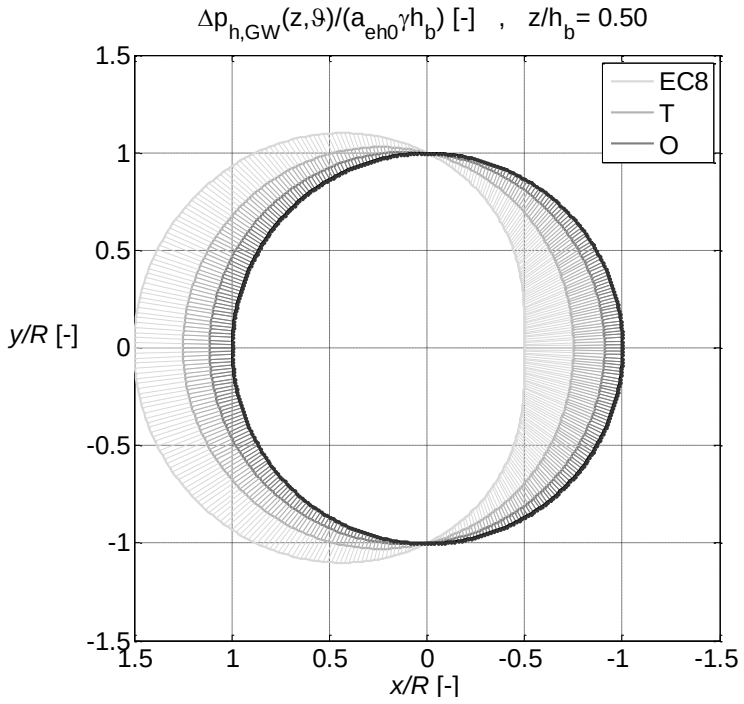

(a)

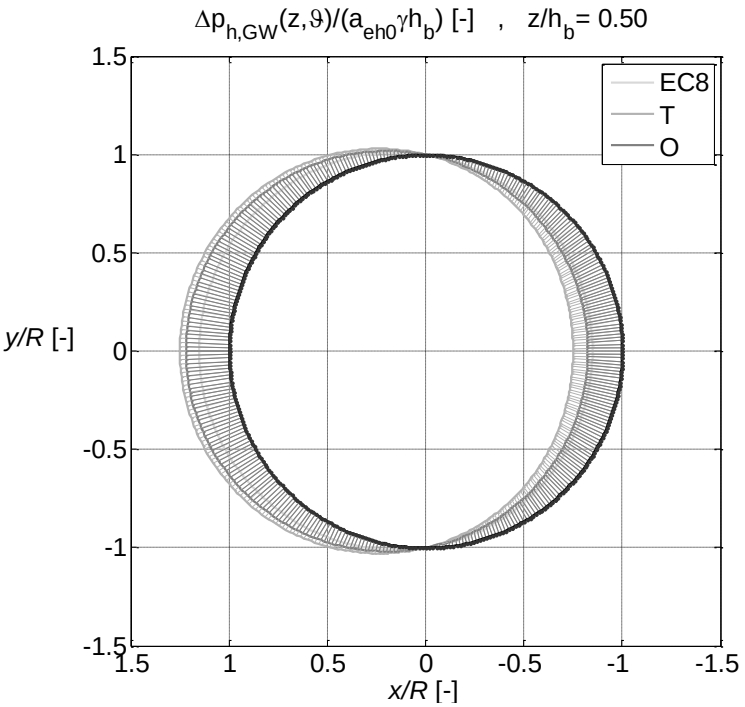

(b)

Figure 6.12 - Horizontal cross-section of the considered silo at height z = 0.50H and z = 0.95 H for the squat silo containing wheat

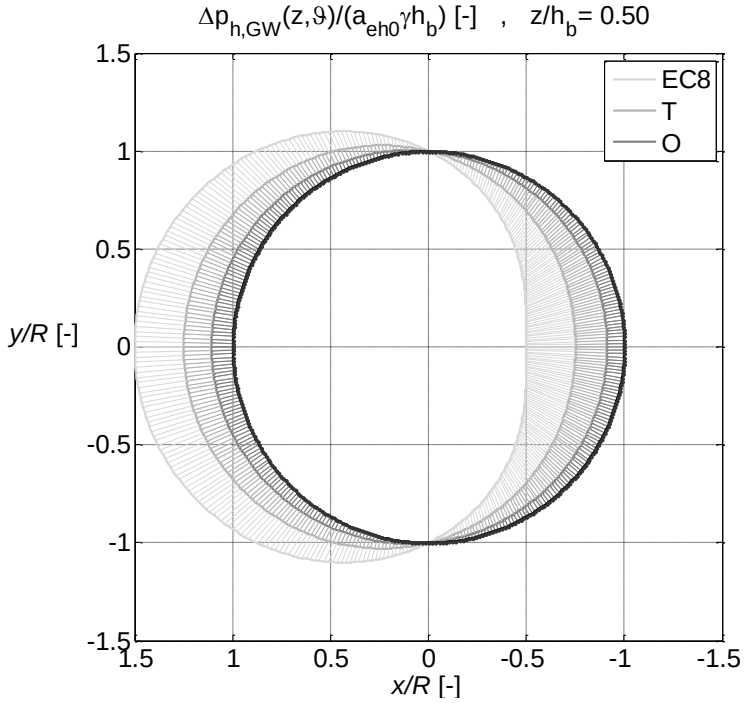

(a)

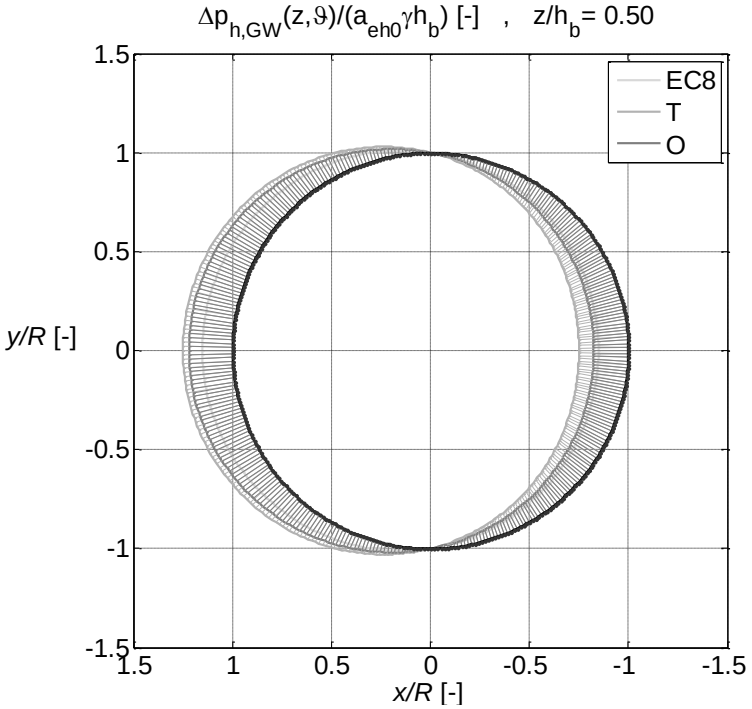

(b)

Figure 6.13 - Horizontal cross-section of the considered silo at height z = 0.50H and z = 0.95 H for the squat silo containing wheat

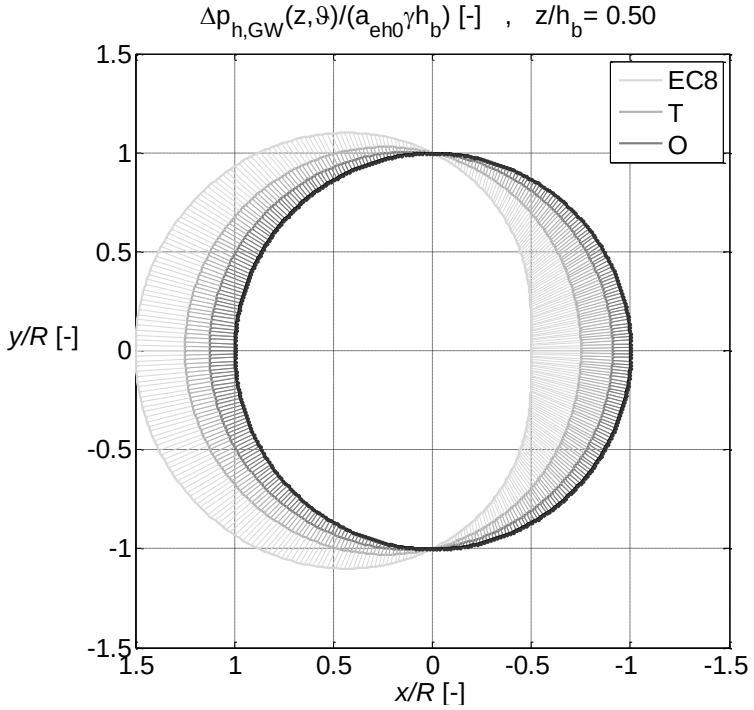

(a)

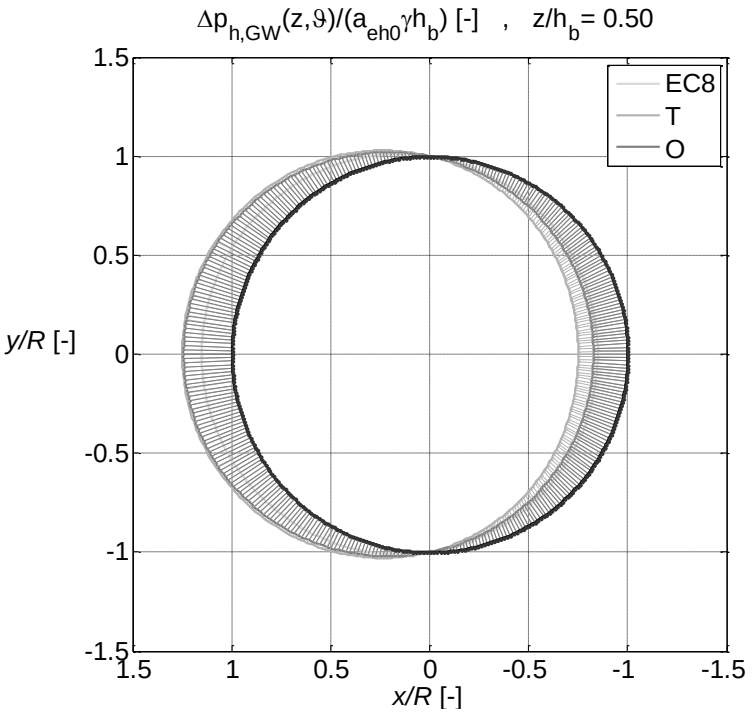

(b)

Figure 6.14 - Horizontal cross-section of the considered silo at height z = 0.50H and z = 0.95 H for the squat silo containing cement clinker

6.8.3 On the *D* and *E* volumes

In this section, the three-dimensional graphic representations of the volumes $V_{E,dyn}(z)$ and $V_{D,dyn}(z)$ are provided according to the proposed analytical formulations. As illustrative examples, the three squat silos analyzed in the previous sections are considered.

Figure 6.15, Figure 6.16 and Figure 6.17 show the two grain portions for the squat silos containing wheat, barley and cement clinker, according to the proposed analytical formulation, respectively. The red volume is the portion of grain completely sustained by the silo wall under dynamic conditions. This portion of grain interacts with the silo wall. From a geometrical point of view, it coincides with the vertical-axis cylindrical annulus with thickness $s(z,\theta)$ which is variable according to the vertical abscissa *z* and the angle θ on the horizontal plane. The blue volume is the portion of grain leaning against the lower portion of material up to the silo bottom under dynamic conditions. This portion of the grain does not interact with the silo wall. From a geometrical point of view, it overlaps with the vertical-axis truncated cone solid, in which the minor base is the one obtained drawing the curve $r(z,\theta)=R-s(z,\theta)$ for $0°\le\theta\le360°$ on the plane $z= H$ (at the silo base) and the major one is the one confine by the horizontal free grain surface $z= 0$. In general, it is shown that the volume $V_{E,dyn}(z)$ assumes a convex shape with respect to the top surface of the grain.

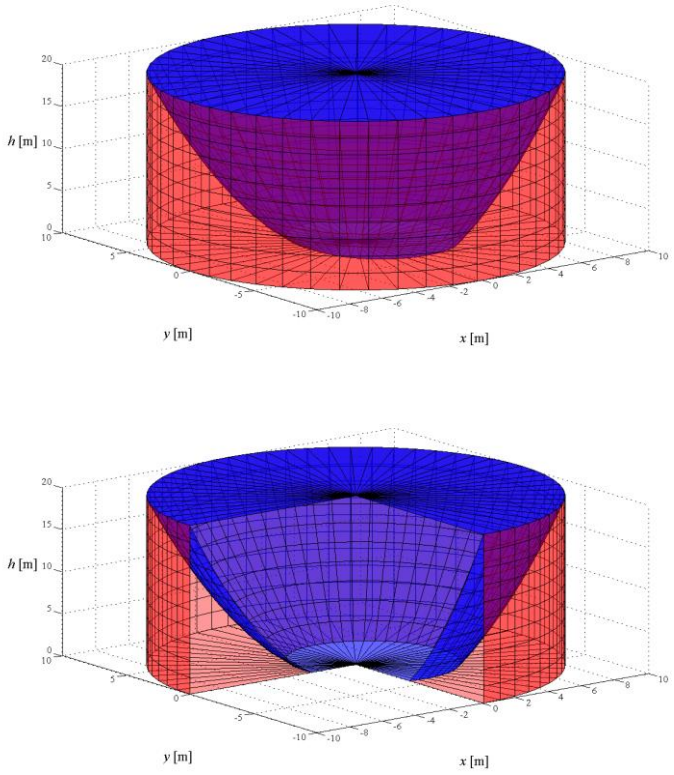

(a)

(b)

Figure 6.15 -Three-dimensional view of portion D (in blue) and of portion E (in red) of the flat-bottom squat silo containing barley for the proposed analytical formulation: (a) sectioned view and (b) overview

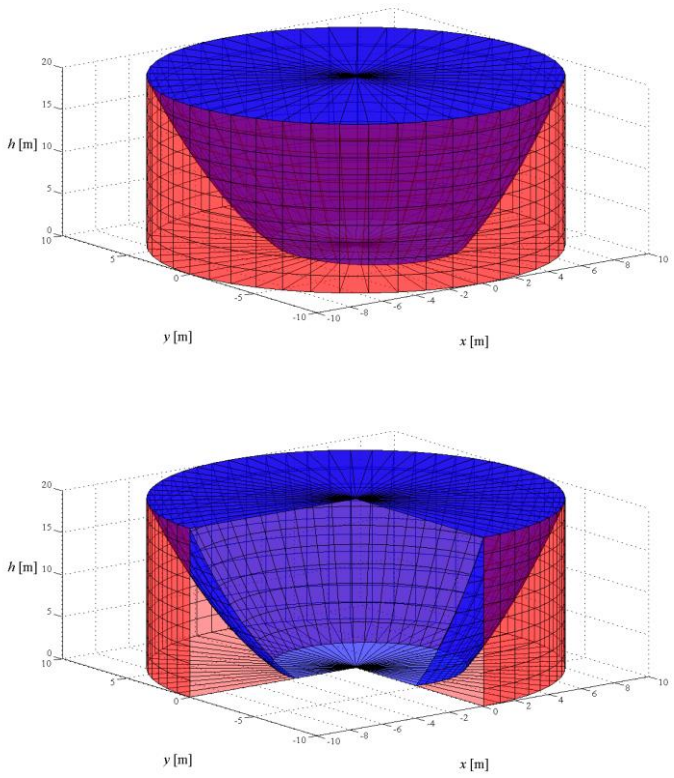

(a)

(b)

Figure 6.16 - Three-dimensional view of portion D (in blue) and of portion E (in red) of the flat-bottom squat silo containing wheat for the proposed analytical formulation: (a) sectioned view and (b) overview

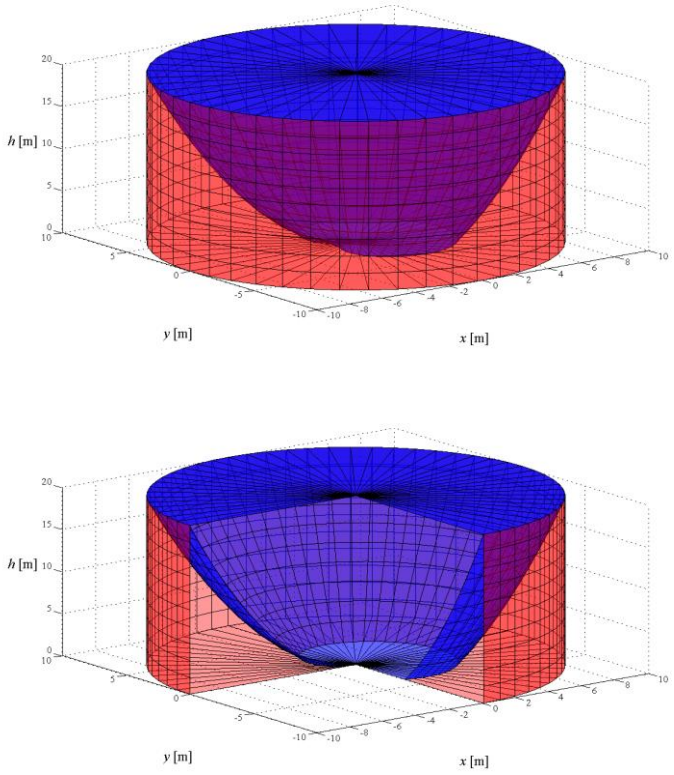

(a)

(b)

Figure 6.17 - Three-dimensional view of portion D (in blue) and of portion E (in red) of the flat-bottom squat silo containing cement clinker for the proposed analytical formulation: (a) sectioned view and (b) overview

6.8.4 On the shear

In this section, the along-the-height profiles of the wall shear provided by the proposed analytical formulation, the Trahair formulation and the Eurocode 8 provisions are compared. As illustrative examples, the three squat silos analyzed in the previous sections are considered. The wall shear is normalized with respect to the horizontal inertial force of the whole ensiled content, i.e. $a_{eh0} \cdot \gamma_b \cdot V_b$, where V_b indicates the total volume of the ensiled bulk material. The value of the nornalized wall shear at the silo bottom (for $z = h_b$) corresponds to the value of the *effective mass*.

Figure 6.18, Figure 6.19 and Figure 6.20 report the wall shear profiles $T_{xx}(z)$ according to Eurocode 8 provisions, the Trahair formulation and the propose analytical formulation for the squat silo containing barley, wheat and cement clinker, respectively. The vertical profiles given by the Eurocode 8 provisions and the Trahair formulation are practically linear and quantitatively and qualitatively similar; on the contrary, the vertical profile given by the proposed analytical formulation presents a nonlinear trend and provides, in general, lower values. In particular, for all the three squat silos, the Eurocode 8 and the Trahair formulation give a value of the normalized wall base shear, corresponding to the value of the *effective mass*, of 93% and 100%, respectively, whilst the proposed analytical formulation gives value of the *effective* mass sensibly lower, between the 40% and 45%.

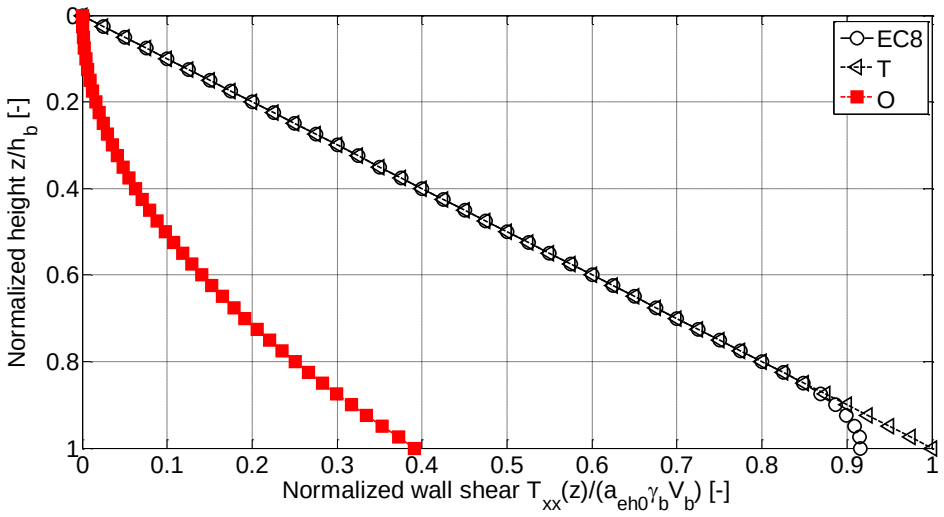

Figure 6.18 - Heightwise variation of the normalized wall shear for Eurocode 8 (EC8), the Trahair formulation (T), the proposed analytical formulation (O) in dynamic conditions for squat silo containing barley

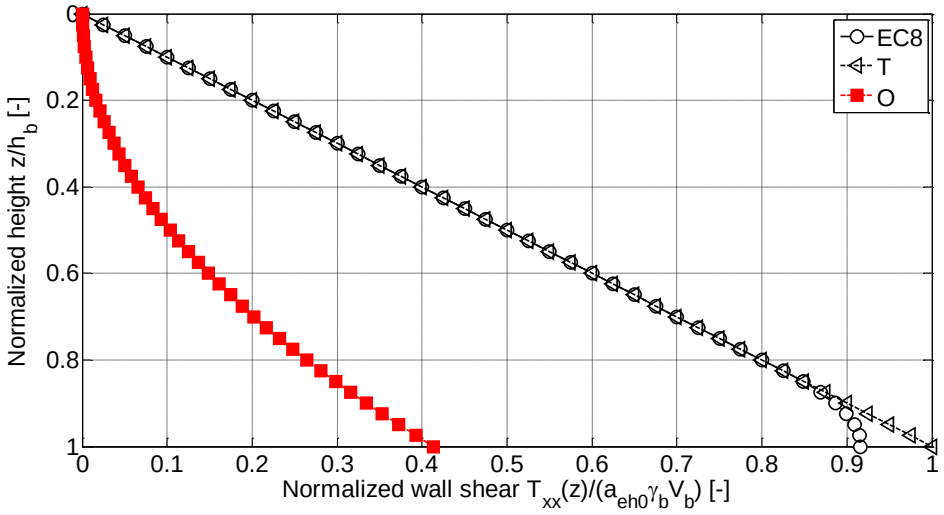

Figure 6.19 - Heightwise variation of the normalized wall shear for Eurocode 8 (EC8), the Trahair formulation (T), the proposed analytical formulation (O) in dynamic conditions for squat silo containing wheat

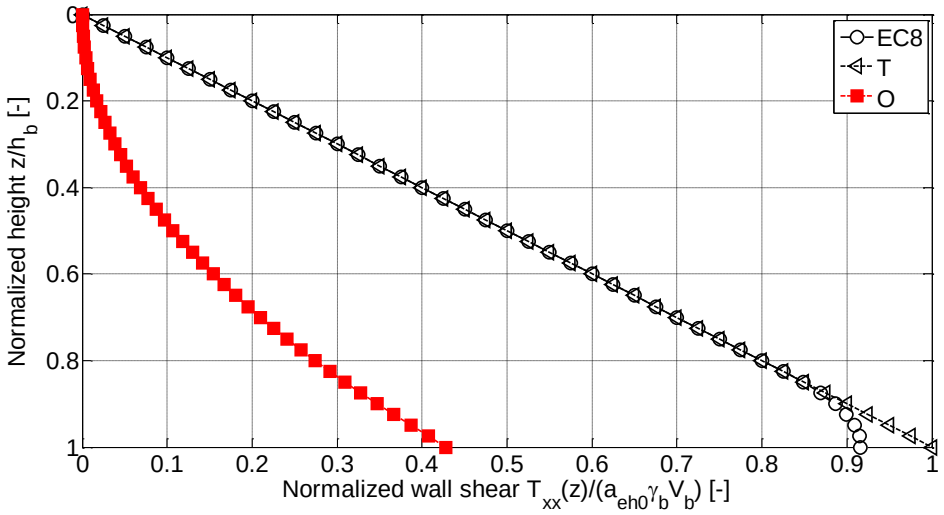

Figure 6.20 - Heightwise variation of the normalized wall shear for Eurocode 8 (EC8), the Trahair formulation (T), the proposed analytical formulation (O) in dynamic conditions for squat silo containing cement clinker

6.8.5 On the bending moment

In this section, the along-the-height profiles of the wall bending moment provided by the proposed analytical formulation, the Trahair formulation and the Eurocode 8 provisions are compared. As illustrative examples, the three squat silos analyzed in the previous sections are considered. The wall bending moment is normalized with respect to the overturning moment correspondent to the rigid rotation of the whole ensiled content with respect to the base of the silo, i.e. $a_{eh0} \cdot \gamma \cdot V_b \cdot h_b / 2$.

Figure 6.21, Figure 6.22 and Figure 6.23 report the wall bending moment profiles $M_{yy}(z)$ according to Eurocode 8 provisions, the Trahair formulation and the propose analytical formulation for the squat silo containing barley, wheat and cement clinker, respectively. The vertical profiles given by the Eurocode 8 provisions and the Trahair formulation presents a nonlinear trend and are quantitatively and qualitatively similar; the vertical profile given by the proposed analytical formulation presents a nonlinear trend and provides, in general, lower values. In particular, for all the three squat silos, the Eurocode 8 and the Trahair formulation give a value of the normalized wall base bending moment around 100%; whilst the proposed analytical formulation gives value sensibly lower, between the 25% and 30%.

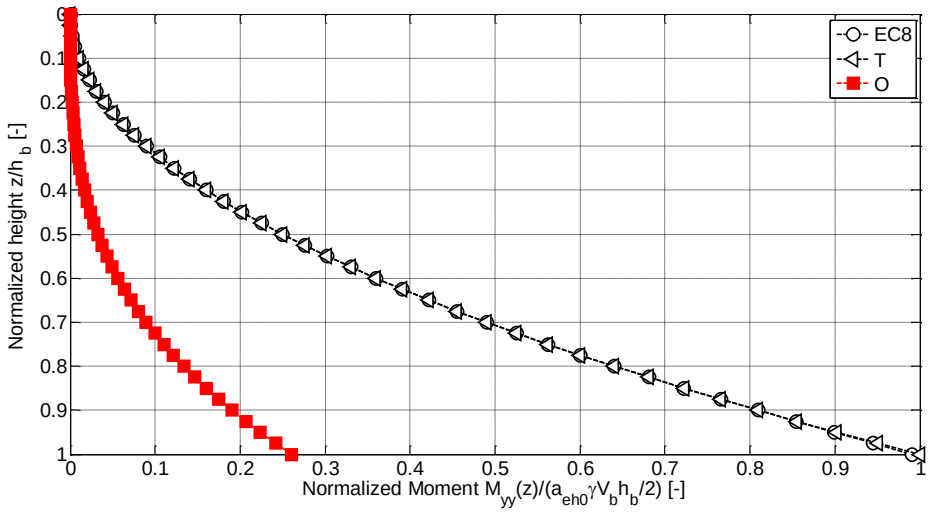

Figure 6.21 - Heightwise variation of the normalized wall bending moment for Eurocode 8 (EC8), the Trahair formulation (T), the proposed analytical formulation (O) in dynamic conditions for squat silo containing barley

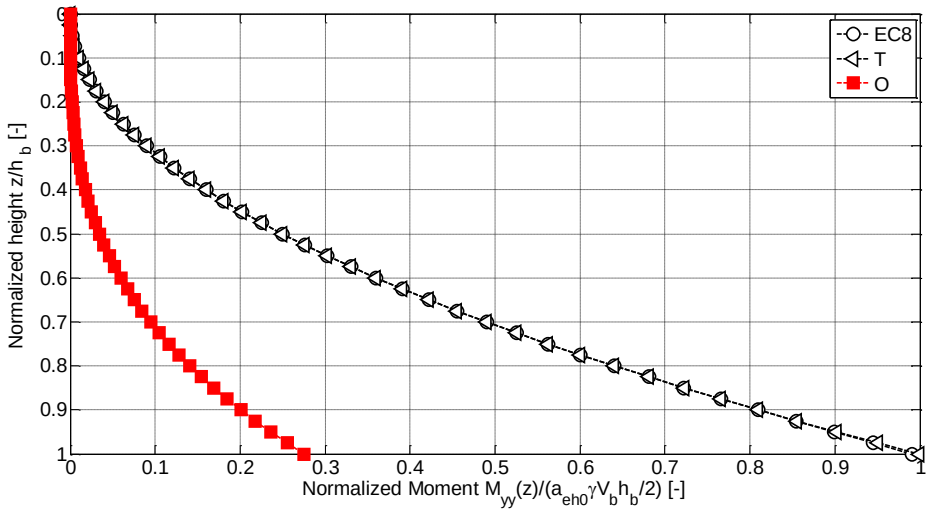

Figure 6.22 - Heightwise variation of the normalized wall bending moment for Eurocode 8 (EC8), the Trahair formulation (T), the proposed analytical formulation (O) in dynamic conditions for squat silo containing wheat

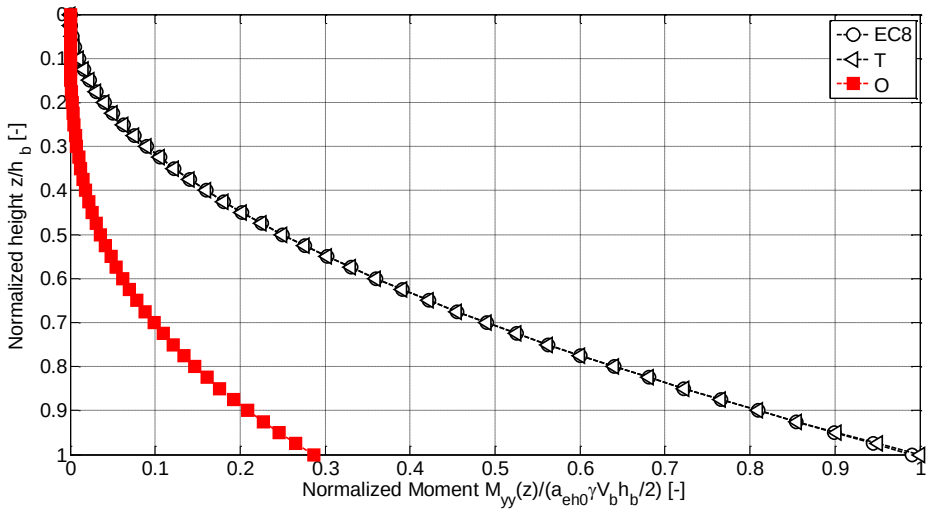

Figure 6.23 - Heightwise variation of the normalized wall bending moment for Eurocode 8 (EC8), the Trahair formulation (T), the proposed analytical formulation (O) in dynamic conditions for squat silo containing cement clinker

6.8.6 On the effective mass

In this section, the trends of the *effective mass* as function of the main geometrical and physical characteristics of grain-silos (i.e. slenderness ratio, grain-wall friction coefficient, pressure ratio and unit weight of the bulk solid) as provided by the proposed analytical formulation, the Trahair formulation and the Eurocode 8 provisions are compared.

As far as the slenderness ratio of the silo is concerned, values of Δ within the range $[0.4,1.0]$ (corresponding to the class of squat according to EN 1991-4:2006 provisions) are considered.

As far as the physical characteristics of the grain-silo system are considered, the values of grain-wall friction coefficient, pressure ratio and unit weight of the bulk solid are taken with reference to those considered previously in Table 6.1.

Figure 6.24 shows the trend of the value of the *effective mass* as function of the slenderness ratio Δ according to the proposed analytical formulation, the Trahair (1983) formulation and the Eurocode 8 provisions. In general, the values of the *effective mass* increases practically linearly within the investigated range of slenderness ratios. It can be noted that the proposed analytical formulation provides values sensibly lower to those given by Eurocode 8 provisions (discrepancies are around -50%).

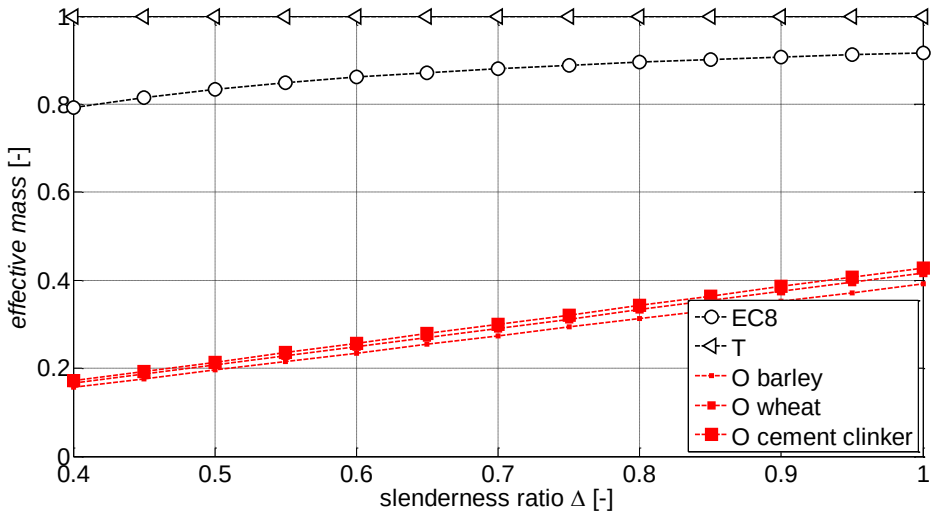

Figure 6.24 - Values of the effective mass as function of the slenderness ratio for the Eurocode 8 provisions (EC8), the Trahair formulation (T) and the proposed analytical formulation (O) for different ensiled bulk solids

6.9 Critical considerations

In this chapter, the actions exerted by the ensiled grain-like material on the wall of circular flat-bottom silos during earthquake ground motions have been studied analytically.

In this work, a new physical model is developed consistently with the one originally identified for the static case by Janssen (1985) and modified to overcome the issues due to the lack of axial-symmetry under dynamic conditions. Starting from this new

physical idealization, a set of assumptions is considered in order to simplify the complex phenomenon related to the dynamic behavior of grain-silo systems. In particular, even if from a physical point of view the assumptions on $p_{v,GG}(z)$ acting on element *E* are not consistent to each other, from a design point of view considering two limit conditions allows to obtain a conservative formulation. Even if, in general, the new physical idealization leads to a general overestimations of the horizontal grain-wall pressures under static conditions with respect to those predicted by the consolidated Janssen (1895) formulation, it allows to get a new physically-based evaluation of the *effective mass* of grain under dynamic conditions, which is proportional to the grain mass pushing on the silo wall.

The results obtained show how, even if still evaluated in a conservative way, the *effective mass* may be far less than the one given by Eurocode 8 provisions and the analytical formulation by Trahair et al. (1983). Thus the horizontal actions may be far less with respect to those that can be obtained by applying the Eurocode 8 provisions, especially for silos characterized by squat geometrical configuration. In more detail, the results indicate that, in case of squat silos characterized by low but common height-on-diameter slenderness ratios, the portion of grain mass interacting with the silo wall proves to be noticeably lower than the one obtained using Eurocode 8. Basically, for squat silos characterized by height smaller than diameter ($0.4 \le \Delta \le 1.0$), considerable reductions of the *effective mass* can be obtained, roughly around -50% (mainly depending on the slenderness ratio Δ).

The limits of validity of the analytical developments allow to identify of a class of circular flat-bottom grain-silos for which the proposed analytical formulation reported in this chapter can be applied.

Reference

Buisman ASK (1940) Grondmechanika, Waltman. EN 1998-4 (2006) Eurocode 8. Design of structures for earthquake resistance, Part 4 -Silos, tanks and pipelines. CEN, Brussels

Dabrowski, A. (1957). Parcie Materialow Sypkich w Leju (Pressures from bulk solids in hoppers). *Archiwum Inzynierii Ladowej, Warsawa*, 325-328.

EN 1991-4 (2006) Eurocode 1: Actions on structures - Part 4: Silos and tanks

EN 1998-4 (2006) Eurocode 8: Design of structures for earthquake resistance – Part 4: Silos, tanks and pipelines

Janssen, H. A. (1895). Versuche über getreidedruck in silozellen. *Zeitschr. d. Vereines deutscher Ingenieure*, *39*(35), 1045-1049.

Krynine, D. P. (1945) ‘‘Discussion of ‘Stability and stiffness of cellular cofferdams’ by Karl Terzaghi.’’ Trans. Am. Soc. Civ. Eng., 110, 1175–1178.

Landry JW, Grest GS, Silbert LE, Plimpton SJ (2003) Confined granular packings: structure, stress, and forces. Phys Rev E 67(4):041303

Nielsen, J. (2008). From silo phenomena to load models. *Structures and Granular Solids, Taylor & Francis*, 49-57

Rotter, J. M., & Hull, T. S. (1989). Wall loads in squat steel silos during earthquakes. Engineering Structures, 11(3), 139-147.

Silvestri, S., Gasparini, G., Trombetti, T., & Foti, D. (2012). On the evaluation of the horizontal forces produced by grain-like material inside silos during earthquakes. *Bulletin of Earthquake Engineering*, 1-26.

Trahair NS, Abel A, Ansourian P, Irvine HM, Rotter JM (1983) Structural design of steel bins for bulk solids. Australian Institute of Steel Construction, Sydney, Australia

Veletsos A. S., Younan A. H. (1998b). Dynamics of Solid-Containing Tanks. II: Flexible Tanks, Journal of Structural Engineering ASCE, 124(1): 62-70.

Younan A. H., Veletsos A. S. (1998a). Dynamics of Solid-Containing Tanks. I: Rigid Tanks, Journal of Structural Engineering ASCE, 124(1): 52-61.

7. The experimental campaign conducted at the EQUALS laboratory

In this chapter, the shaking-table experimental campaign carried out on silo specimens filled with Ballottini glass carried out at the EQUALS laboratory (University of Bristol) is presented. The experimental campaign is performed through a joint research work between the University of Bologna, the University of Alicante, the University of Bari and the University of Bristol (ASESGRAM project). The experimental campaign aims to experimentally verify the original analytical formulation developed at the University of Bologna and to gain a preliminary insight on the issue of the *effective mass* acting on the silo wall under dynamic and seismic conditions. First, the experimental setup, the instrumentations and the different test configurations are described. Then, the main experimental results are presented. Finally, the rupture of the silo specimen as subjected to a significant horizontal acceleration is discussed.

A full description of the experimental tests is beyond the scope of the present work and has been the objective of a previous Master thesis (Di Chiacchio 2013). Therefore, only the information necessary for a better understanding of the interpretation of the test results are recalled.

7.1 The rationale behind the experimental campaign

In this section, the main objectives and the rationale behind the experimental campaign is described.

The main objectives of the shaking-table experimental campaign are: (i) to experimentally verify the original analytical formulation and (ii) to obtain preliminary insight on the influence of the assumptions made on the base input (earthquake versus low frequency sinusoidal/constant acceleration).

Therefore, the experimental campaign has been designed both to meet the idealized conditions of the analytical formulation and to investigate the influence of the type of input on the dynamic response of grain-silos.

As far as objective (i) is concerned, the original analytical formulation (Silvestri et al. 2012) has been developed with reference to an idealized model (the grain-like material is uncompressible) in idealized conditions (the silo is subjected to a time constant

acceleration). Because the theory is exquisitely analytical and thus independent from geometrical dimensions, any cylindrical element filled with uncompressible particulate material can be consistently used to represent the idealized model. Because the analytical formulation is developed for time constant acceleration, and given that the shaking table cannot apply a time constant motion, low-frequency sinusoidal inputs have been applied at the base of the cylinder. Using low-frequency (namely, 1 and 2 *Hz*) sinusoidal input, it is possible to achieve a large duration for which the acceleration can be reasonably considered constant in time (around the peak of the sinusoid) (Figure 7.1). The comparison between the analytical formulation and the experimental results has been performed basically in terms of overturning moment at the silo base.

As far as objective 2 is concerned, time records of real strong earth motions have been utilized to investigate input motion dependence of response: in this respect, the vertical profile of the horizontal acceleration along the height of the silo has been monitored. The original analytical formulation (Silvestri et al. 2012) is capable of accounting for dynamic interaction between the ensiled grain and the silo wall, by means of general formulations, which can be specified by introducing the actual (measured) vertical profile of the horizontal acceleration along the height of the silo.

It is worth pointing out that the use of the experimental evidences of these shaking-table tests to extrapolate information on the seismic behavior of real-scale silo structures is another issue, which is beyond the objectives of the present research. In this regard, it is clear that, in the field, real-scale flat-bottom silos are characterized by a compressible grain material and can be subjected to a broadband seismic acceleration. For the sake of possible future transition from the idealized model of the theory to the actual case of real silos, Figure 7.2 provides the logical framework of the transition from the idealized conditions of the analytical model (Silvestri et al. 2012) to the tested specimen, and to the actual conditions of a real silo.

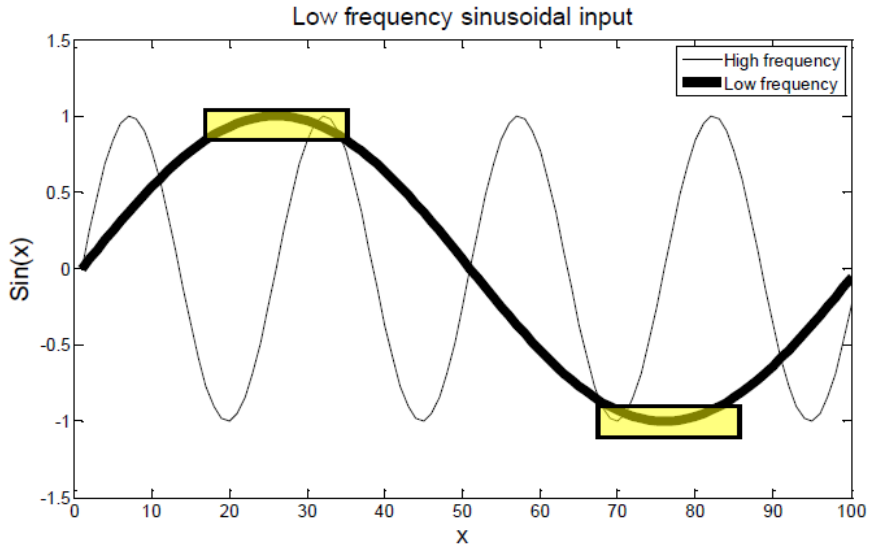

Figure 7.1 - Example of low frequency sinusoidal input

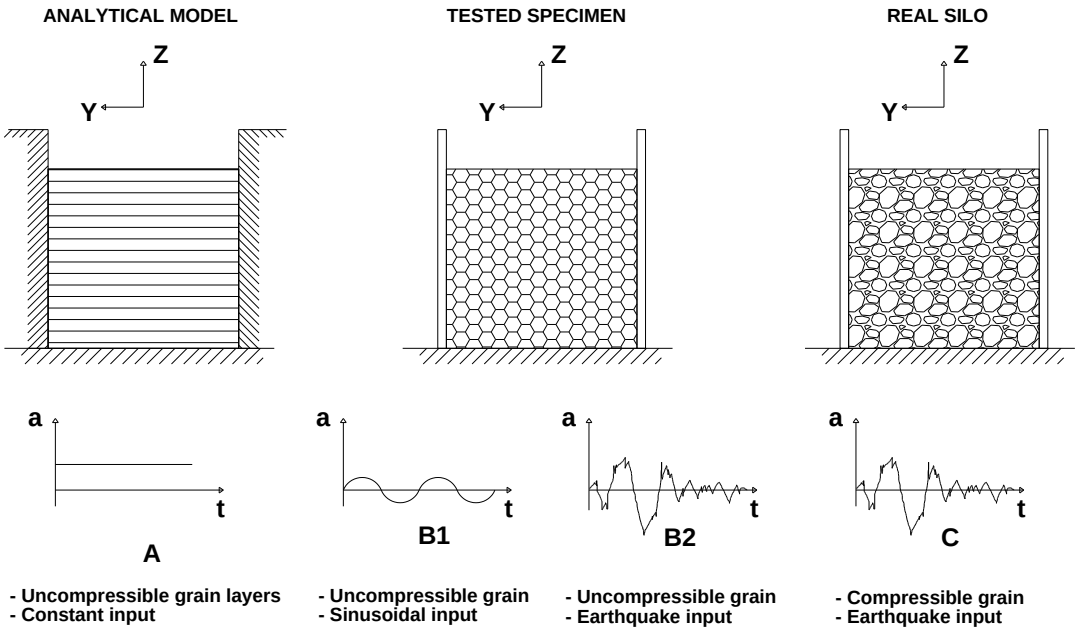

Figure 7.2 - The analytical model, the tested specimen and the real silo

7.2 The experimental campaign

In the present section, the experimental campaign is described. The experimental campaign has been carried out on two different sessions of tests (August 2012, January-February 2013). In detail, the silo specimen and its assembling process with reference to the different sessions of tests are described. The physical and frictional characteristics of

the ensiled content are investigated and presented. Then, test configurations and tests setup are described.

7.2.1 The silo specimen

A circular silo specimen has been developed and realized to meet at best the idealized conditions, upon which the original analytical formulation (Silvestri et al. 2012) to be verified is grounded. Given that the dimensions of the Earthquake and Large Structures Laboratory (EQUALS, University of Bristol) shaking table are 3 × 3 *m*, the specimen consists of a 1.2-*m*-diameter (d_c), 1.5-*m*-tall (h_w) and 3-*mm* wall thickness (t_w) polycarbonate container (Figure 7.3*a*).

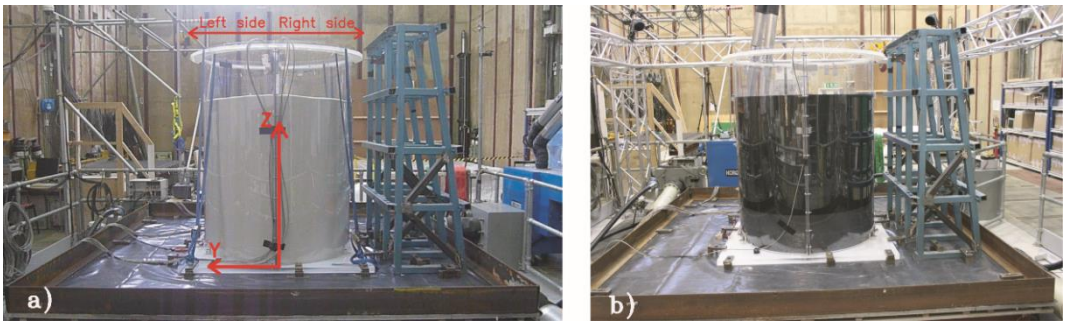

Figure 7.3 – (a) The specimen with smooth walls. (b) The specimen with roughened wall.

The circular silo was produced by bending two polycarbonate sheets to be semicircular in plan and fastening together the adjoining straight edges. Perspex rings encircle the tube at its top and bottom extremities so that it retains the intended shape. The Perspex bottom of the silo has 40 *mm* thickness.

The vertical polycarbonate sheets are connected to the bottom plate by inserting the sheets inside a 20 *mm* depth circumferential socket and by means of bolt connections through L-shaped steel profiles, as depicted in Figure 7.4 and Figure 7.5. In details, for the smooth wall specimen, two bolt connections between bottom plate and vertical polycarbonate sheets along the base of the silo have been placed on the diameter orthogonal to the base input, on the *X*-*X* direction (Figure 7.4); for the roughened wall specimen, twelve bolt connections between bottom plate and vertical polycarbonate sheets along the base of the silo have been placed along the base circumference in order to increase the fixity between the silo (Figure 7.5). The actual disposition of the bolt connections for the two different configuration is depicted in Figure 7.6.

The influence of the boundary conditions (different base connections) in terms of shell bending effects into the shell height is evaluated by means the linear cylindrical shell bending theory (Timoshenko and Woinowsky-Krieger 1959). Accordingly, the value of the linear axial bending wavelength, referred as to l_λ, results:

$$l_\lambda = \pi \cdot \sqrt{(R \cdot t_w)} \Big/ \sqrt[4]{3 \cdot (1 - \nu_w{}^2)} \tag{1}$$

where ν_w expresses the Poisson's coefficients related to the wall material and *R* is the radius of the circular cross-section of the cylinder. For values of ν_w around 0.30-0.40, $l_\lambda \cong 2.4 \cdot \sqrt{(R \cdot t_w)} \cong 100mm$, beyond which the influence of the boundary conditions (different base connections) results negligible in terms of wall deformations.

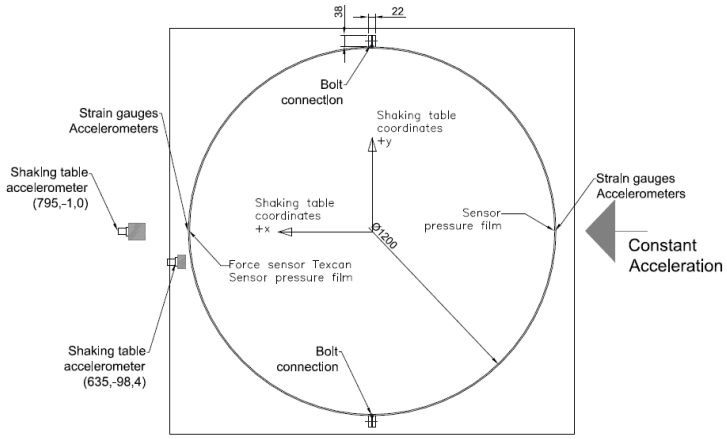

Figure 7.4 - Drawings of the positions of the bolt connections between bottom plate and vertical polycarbonate sheets along the base of the silo (XZ plan view) for the smooth wall specimen, August 2012 session (measurements are expressed in millimeters)

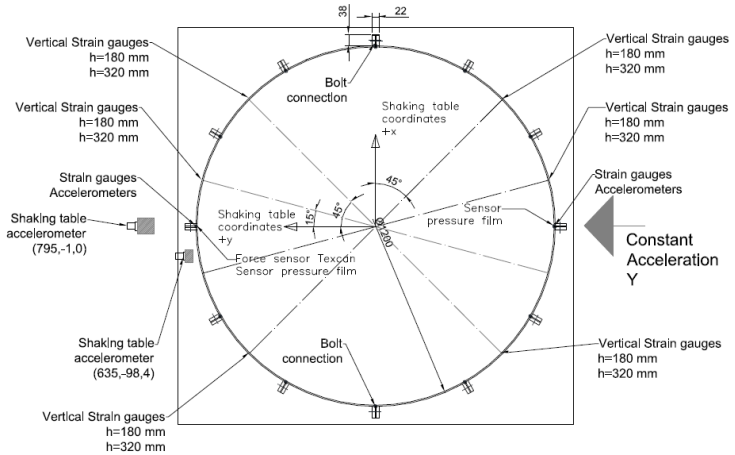

Figure 7.5 - Drawings of the positions of the bolt connections between bottom plate and vertical polycarbonate sheets along the base of the silo (XZ plan view) for the roughened wall specimen, January-February 2013 session (measurements are expressed in millimeters)

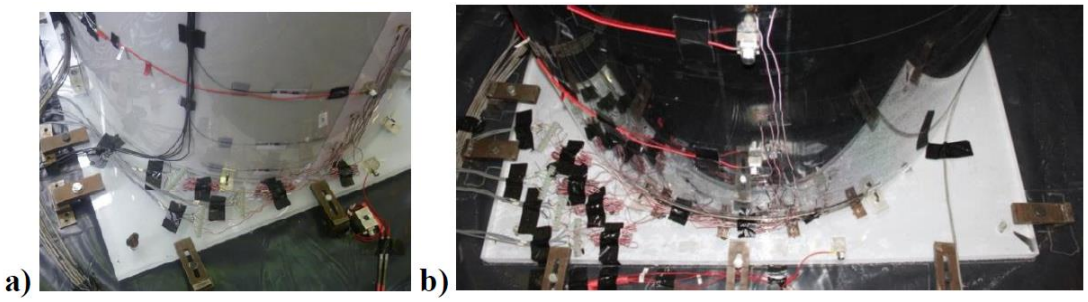

Figure 7.6 - a) Base connections of first session of tests, b) Base connections of second and third session of tests

Polycarbonate ($E_{polycarbonate}$ = 2.3 *GPa*, $\nu_{polycarbonate}$= 0.37, Figure 7.7) is selected owing to the relatively low Young modulus, which has the effect of increasing the magnitude of mobilized strain, thereby facilitating its measurement. The base of the container is covered with sandpaper to increase the grain-base friction coefficient, in order to meet the conditions related to the limits of validity of the analytical formulation (see Eq. (40) of chapter 6). Both smooth and roughened (through application of sandpaper) wall are considered in the tests (Figure 7.3*a*, *b*).

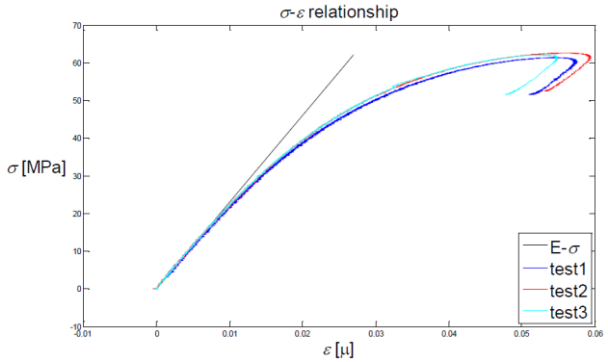

Figure 7.7 - Stress-strain relationship for the polycarbonate of the cylinder

7.2.2 The ensiled content

The silo specimen has been filled up to different heights (corresponding to different test configurations), H_i, with Ballottini glass material (Figure 7.8*a*, *b*), commonly used in granular dynamics experiments and selected for both the regularity of the particles and their density when deposited (ρ_b = 1480 kg/m^3), leading to a total weight (around 20 *kN*) compatible with the payload capacity of the shaking-table system (150 *kN*). A diameter of about 0.4-0.6 *mm* for the Ballottini glass beads has been selected. The friction coefficients of the ensiled content (grain-grain, grain-wall and grain-base friction coefficients) have

been evaluated using a modified direct shear apparatus (Lings and Dietz, 2004). Tests have been performed at appropriate densities and stress levels (5, 10, 15 and 20 *kPa*), and this may introduce some uncertainties into the results. The stress level is extremely low for the available test equipment (only a few percentage of the apparatus capacity). Also, it was difficult to prepare samples of low density consistently.

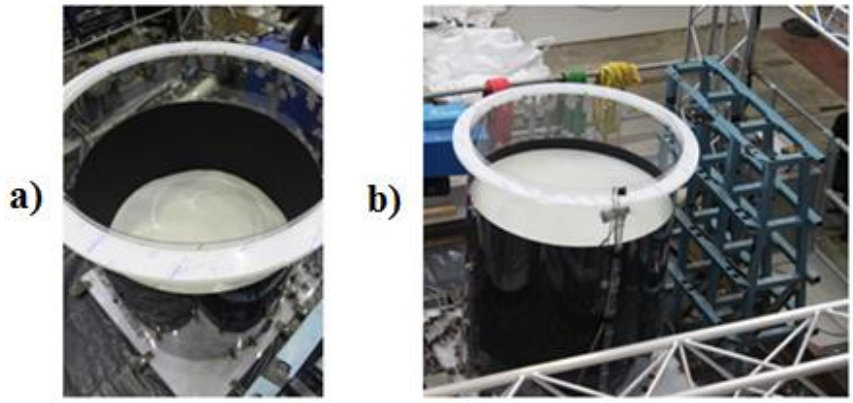

Figure 7.8 - (a) The specimen filled with Ballottini glass up to 0.6 m. (b) The specimen filled with Ballottini glass up to 1.2 m.

For the grain-grain friction coefficient (μ_{GG}), that is, the internal friction angle of the material (φ), Figure 7.9 provides the results of the shear-box tests, in terms of (a) the ratio between the shear stress (τ_{xy}) and the vertical normal stress (σ_z) as a function of the horizontal displacement (u_x), and (b) the dilatancy ($\frac{du_z}{du_x}$) as a function of the horizontal displacement (u_x). The peak direct shear angle of friction is derived from the maximum values assumed by the lines in Figure 7.9*a*, which are comprised in the range:

$$\mu_{GG} = \tan\varphi = \left.\frac{\tau_{xy}}{\sigma_z}\right|_{\max} \cong 0.45 \sim 0.50 \qquad (2)$$

Reliable values for the internal friction angle are in the range of $\varphi = 24.2° \sim 26.6°$.

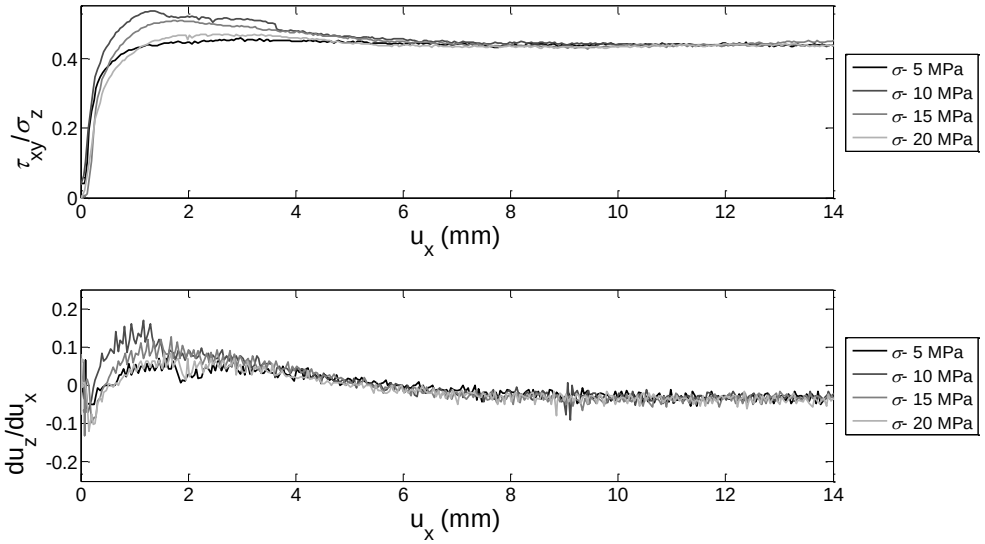

Figure 7.9 - Shear-box test results: (a) shear stress-vertical normal stress ratio versus horizontal displacement; (b) dilatancy versus horizontal displacement

For grain-wall (μ_{GW}) and grain-base (μ_{GB}) friction coefficients, Figure 7.9 provides the results of the interface tests, as conducted with the lower half of the apparatus replaced by either a polycarbonate sample (smooth interface) or a polycarbonate sample covered with sandpaper (rough interface), in terms of (a) the ratio between the shear stress (τ_{xy}) and the vertical normal stress (σ_z) as a function of the horizontal displacement (u_x), and (b) the dilatancy ($\frac{du_z}{du_x}$) as a function of the horizontal displacement (u_x). The tangent of the stress ratio gives the angle of interface friction as:

$$\mu = \tan\varphi = \left.\frac{\tau_{xy}}{\sigma_z}\right|_{\max} \tag{3}$$

The evolution of τ_{xy}/σ_z with u_x is presented for the smooth and rough interface in Figure 7.10*a* and *b*, respectively, from which values of $\mu_{GW} = 0.30$ (Figure 7.10*a*) and $\mu_{GW} = 0.45$ (Figure 7.10*b*) can be derived. Given that the base of the silo has been covered with the same sandpaper used for the roughened walls, a grain-base friction coefficient equal to $\mu_{GB} = 0.45$ is applicable.

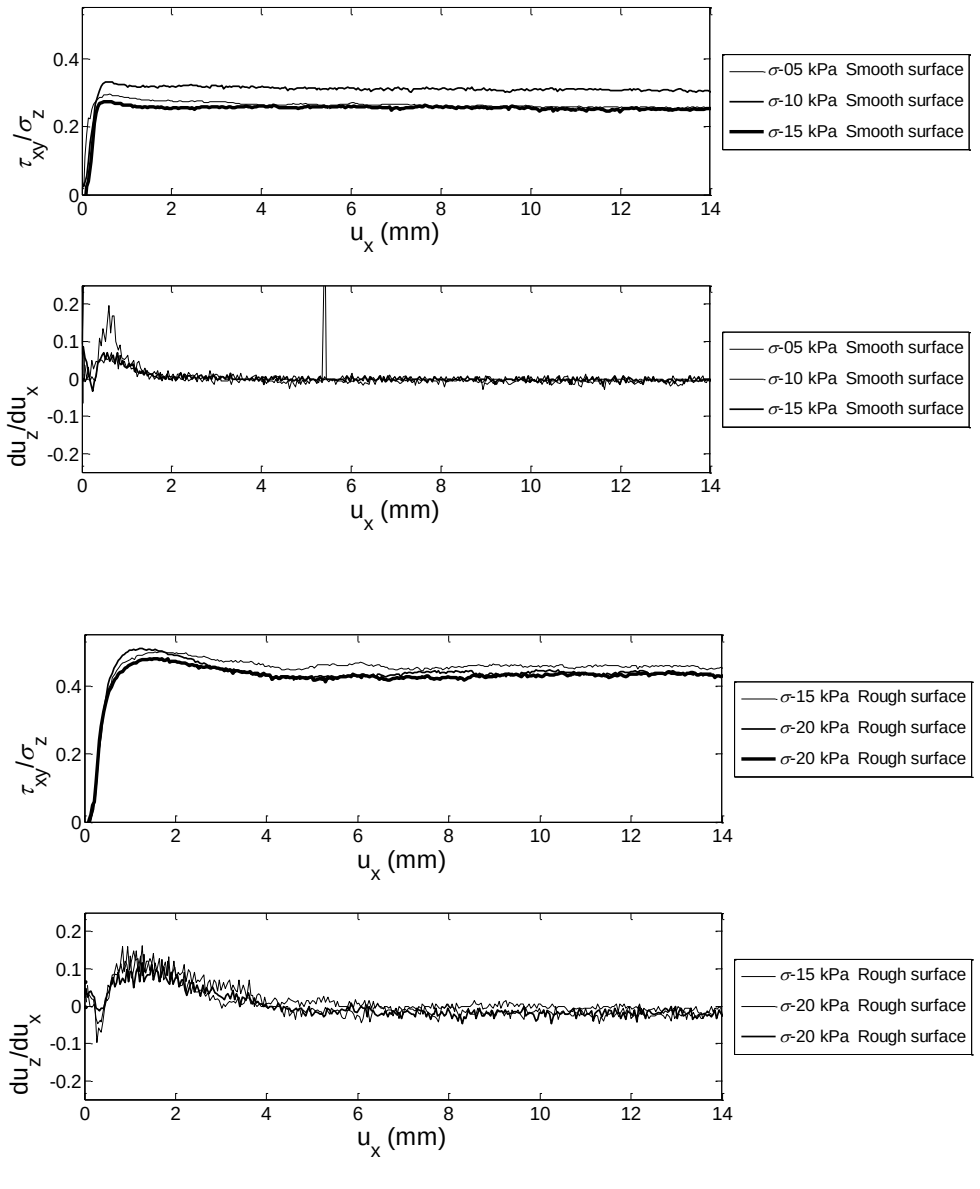

Figure 7.10 - (a) Smooth interface tests results. (b) Rough interface tests results.

The Ballottini glass pressure ratio λ has not been directly measured using the modified oedometer (so called lambameter, Kwade et al. 1994a, b). As clearly stated by (Kwade et al. 1994a, b), neither theoretical formulations nor code provisions should be adopted for the evaluation of the pressure ratio via the angle of internal friction, especially for great value of λ. As a matter of fact, the inferred values found by many researchers appear quite disperse (Vanel et al. 2000, Ovarlez et al. 2003, Arroyo-Cetto et al. 2003, Mandato et al. 2012), since, in general, they result from back analyses developed to get the best matching between theoretical formulations and experimental data. Despite the common use of glass beads for experimental tests involving bulk material Mandato et al.

(2012), no direct measurements are available in the technical and scientific literature, except from the aforementioned work by Kwade et al. (1994a, b). In this work, for a glass beads bulk solid characterized by φ =27°, ρ_b =1726 *kg/m*^{3}, and diameter of about 1 *mm*, poured in an aluminum cylinder ($\mu_{GW} = 0.31$) for a 35 *kPa* vertical stress level, the Authors experimentally found a pressure ratio λ equal to 0.65 (to be used in the Janssen formulation). Since the Ballottini glass features are similar to those of the glass beads tested by Kwade et al. (1994*a*, *b*) and since the grain-wall friction coefficient for the smooth wall configuration matches the one found by Kwade et al. (1994*a*, *b*), the same value of λ = 0.65 has been here adopted in the interpretation of the results. From an engineering point of view, this value is consistent with the one obtained with the following relationship (holding for fully mobilised friction) (Buisman, 1940; Krynine, 1945; Dabrowski 1957):

$$\lambda = \frac{1-\sin^2\varphi}{1+\sin^2\varphi} = 0.67 \div 0.71 \tag{4}$$

7.2.3 Test configurations

By varying the grain-wall interface properties and the height of the ensiled content, three different configurations have been tested:

1. First, the silo characterised by smooth walls ($\mu_{GW} = 0.30$) and filled with Ballottini glass up to a height equal to H_1 = 1.2 *m* has been tested under white noises (N), harmonic sinusoidal inputs (HS) and real earthquake records (EQK), as applied along the *Y* horizontal direction;
2. Second, the silo characterised by roughened walls ($\mu_{GW} = 0.45$) and filled with Ballottini glass up to a height equal to H_2 = 0.60 *m* has been tested under white noises, sinusoidal inputs and real earthquake records, as applied along the *Y* horizontal direction;
3. Third, the silo characterised by roughened walls ($\mu_{GW} = 0.45$) and filled with Ballottini glass up to a height equal to H_3 = 1.2 *m* has been tested under systematic sinusoidal inputs, as applied along the *Y* horizontal direction.

Table 7.1 gives details about the test sequence performed for the first configuration (conducted on August 2012), Table 7.2 gives details about the test sequence performed for the second configuration (conducted on January-February 2013) and Table 7.3 gives details about the test sequence performed for the third configuration (conducted on January-February 2013). This list is here provided in order to better contextualize the selected results which will be described in next section 7.3 (especially, the ones concerning frequency changes, grain compaction, and accelerations).

Table 7.1 - Test input for the first configuration of tests

INPUT	Tests No.	Table acceleration
White noise	N1 - N5	0.05 *g* – 0.30 *g*
1 *Hz* sinusoidal (*Y*)	S1 - S8	0.05 *g* – 0.40 *g*
White noise	N6	0.30 *g*
1 *Hz* sinusoidal (*Y*)	S9	0.03 *g*
0.5 *Hz* sinusoidal (*Y*)	S10 – S13	0.01 *g* – 0.15 *g*
White noise	N7	0.30 *g*
1 *Hz* sinusoidal (*Y*)	S14	0.50 *g*
White noise	N8	0.30 *g*
Earthquake input	E1- E18	0.04 *g* – 0.40 *g*
White noise	N9	0.30 *g*

Table 7.2 - Test input for the second configuration of tests

INPUT	Tests No.	Table acceleration
1 *Hz* sinusoidal (*Y*)	S1 – S3	0.10 *g*
White noise	N1	0.20 *g*
1 *Hz* sinusoidal (*Y*)	S4-S36	0.10 *g* – 0.58 *g*
2 *Hz* sinusoidal (*Y*)	S37-S48	0.30 *g* – 0.76 *g*
2 *Hz* sinusoidal (*Y*&*Z* in phase)	S49 – S54	0.30 *g*
2 *Hz* sinusoidal (*Y*)	S55 – S67	0.10 *g* – 0-70 *g*
1 *Hz* sinusoidal (*Y*&*Z* in and out of phase)	S68 – S75	0.10 *g* – 0.40 *g*
Earthquake input (*Y*)	E1- E3	0.30 *g* – 0.60 *g*
Earthquake input (*Y*)	E4	0.10 *g*
Earthquake input (*Y*&*Z*)	E5	0.30 *g*
2 *Hz* sinusoidal	S76-S78	0.30 *g* – 0.70 *g*
Earthquake input (*Y*&*Z*)	E6	0.60 *g*
2 *Hz* sinusoidal (*Y*)	S79-S86	0.80 *g* – 1.10 *g*
2 *Hz* sinusoidal (*X*)	S87-S89	0.30 *g* – 0.50 *g*
2 *Hz* sinusoidal (*Y*&*Z* in phase)	S90-S105	0.10 *g* – 0.85 *g*
Earthquake input (*Y*)	E7-E25	0.07 *g* – 1.2 *g*
Earthquake input (*Y*&*Z* in phase)	E26 –E44	0.08 *g* – 1.11 *g*

Table 7.3 - Test input for the third configuration of tests

INPUT	Tests No.	Table acceleration
1 *Hz* sinusoidal (*Y*)	S1	0.10 *g*
White noise	N1	0.20 *g*
1 *Hz* sinusoidal (*Y*)	S2-S8	0.10 *g* – 0-60 *g*
2 *Hz* sinusoidal (*Y*)	S9-S30	0.10 *g* – 1.2 *g*

7.2.4 Test setup

The test setup has been designed in order to provide measures of: (i) table, structure and grain accelerations at different locations, and (ii) structure deformations at different positions. The following instrumentation has been installed (Figure 7.11): (i) mono-directional accelerometers: some of them located at the shaking-table foundation, and some of them glued to the silo wall along two significant vertical generatrices (Figure 7.12); (ii) vertical and horizontal strain gauges positioned on the exterior side of the wall at four different heights along two significant generatrices, (iii) vertical strain gauges were added (at 45°) at the base circumference for the second and third test configurations (Figure 7.11*b*).

Figure 7.12*a* and *b* show three mono-directional horizontal accelerometers disposed along the height of the silo and the vertical and circumferential strain gauges mounted on of the external side of the silo wall. In detail, the mono-directional accelerometers are of the SETRA type (model 141A).

The resulting base actions (due to the pressure distribution along the height of the silo) have been monitored by means of the strain gauges placed at the base of the silo wall.

Figure 7.13 shows the final setup for the silo specimen with smooth wall (first configuration).

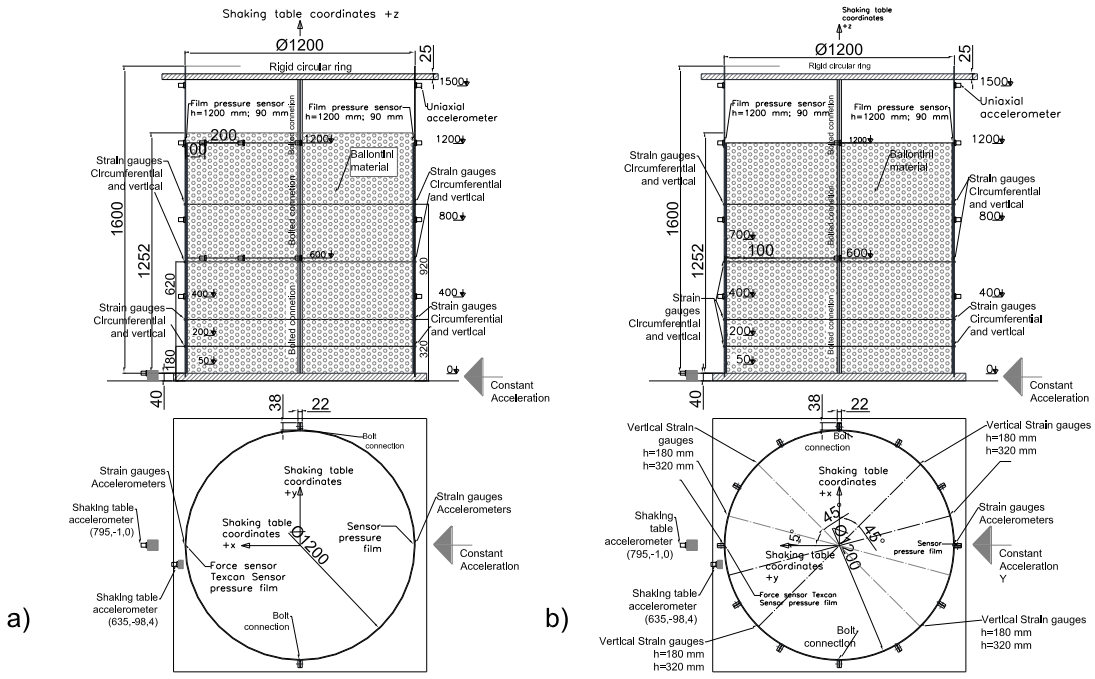

Figure 7.11 - (a) The instrumentation in the first configuration. (b) The instrumentation in the second and third configuration.

(a) **(b)**

Figure 7.12 – (a) Detail of the position of the accelerometers along the height of the silo; (b) details of the circumferential and vertical strain gauges

(a) **(b)** **(c)**

Figure 7.13 - The silo specimen; (b) the setup of the instrumentations (c) the pouring of the Ballottini glass material

7.3 Results of the experimental campaign

In the present section, the main results of the experimental shaking table tests for the different test configurations are reported. In detail, the vertical settlements experienced by the grain after progressive shaking, the frequencies of vibration of the silo specimens, the records of the accelerations and the vertical strains detected on the silo wall are presented. Finally, a comparison between sinusoidal and earthquake response of the silo specimens is discussed.

7.3.1 Vertical settlements of the ensiled material

A progressive vertical settlement was observed during the tests, probably due to specimen compliance (circumferential cross-section deformation and local adjustments at the interlocking seam between the two U sections which constitute the specimen) and reorganization of the single glass beads with voids filling resulting in a global compaction. A 3-4 *cm* settlement (roughly 3% of the initial height) was measured in 13 positions, in terms of distance between a reference ideal line at the top silo level and the compacted grain free surface of the ensiled material (Figure 7.14), according to the same approach used by Ueng et al. (2010). Figure 7.15 presents the content heights at the end of selected single tests with different 1 *Hz* sinusoidal inputs (see Table 7.1). The lines corresponding to the content grain free surface after each test indicate that a progressive settlement

occurred. Under sinusoidal input, the ensiled material assumed a convex shape with maximum height in its central portion and minimum height along the perimeter wall. On the other hand, strong earthquake input leaded to asymmetric distribution of the top layers.

From an engineering point of view, in the light of the negligible entity of the vertical settlements and of the incompressibility of the single glass beads, the assumption of uncompressible ensiled material is still reasonable.

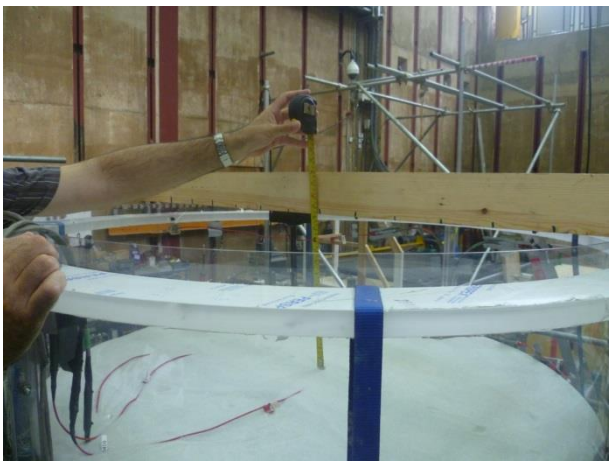

Figure 7.14 - Measurement of grain settlements

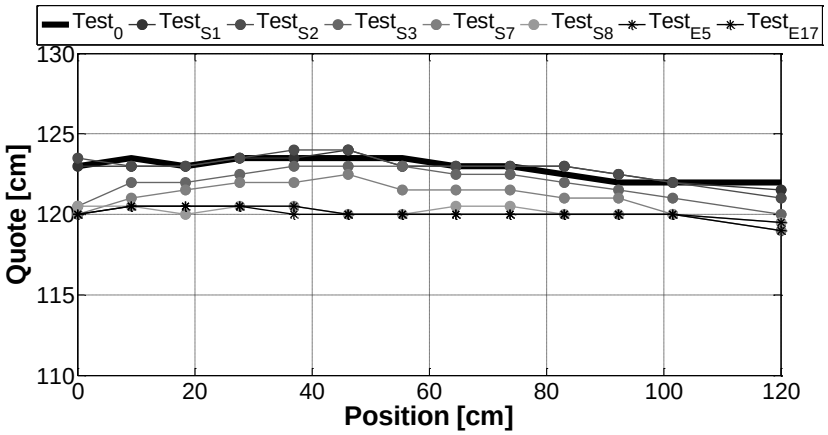

Figure 7.15 - Grain heights at the end of selected single tests.

7.3.2 Frequencies

White noise inputs were used in order to evaluate the dynamic properties of the silo for different filling configurations (empty silo equipped with top stiffening ring, half-filled

and full-filled silo) at increasing levels of peak base acceleration. The transfer function of the silo-grain system as obtained with reference to the accelerometers placed on the shaking table and at the top of the silo (Z'= 1.5 m). Results are expressed in terms of fundamental frequency of vibration and corresponding damping ratios ξ of the silo specimens.

As far as the empty configuration is concerned, four white noise inputs were applied with increasing magnitude (from 0.05 g to 0.30 g). Figure 7.16 shows the transfer functions detected for tests N1 and N3. Independently on the magnitude of the base input, the transfer functions present similar distribution. Table 7.4 presents the two frequency characterized by the highest amplitude and the corresponding damping ratios for the empty silo specimen.

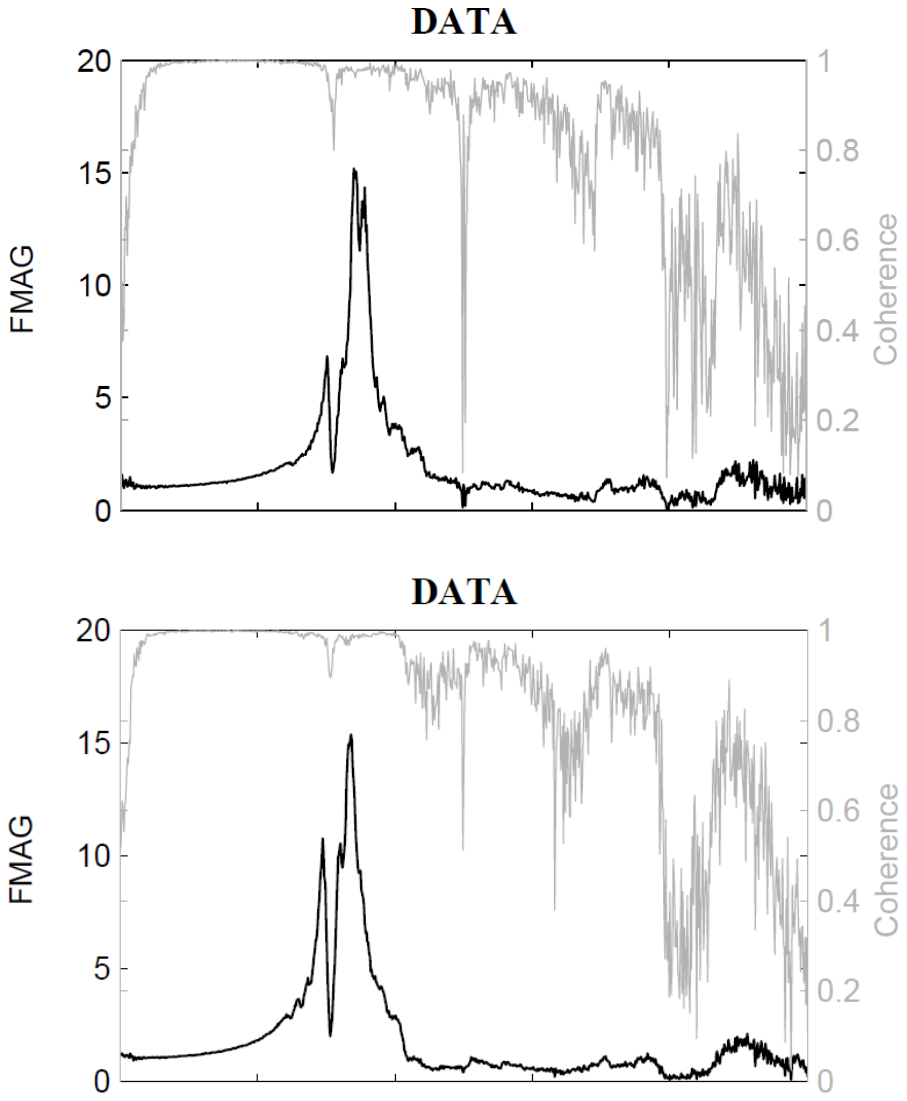

(a)

(b)

Figure 7.16 - Transfer functions for the empty silo for tests N1 and N3

Table 7.4 - First two frequencies and related damping ratios identified in the white noise tests for the empty silo (equipped with top ring)

Test No.	Peak Base Acceleration Input	Frequency 1 [*Hz*]	Frequency 2 [*Hz*]	ξ_1 [%]	ξ_2 [%]
N1	0.05 *g*	30.4	34.	0.2	3.6
N2	0.10 *g*	25.5	30.0	2.5	1.5
N3	0.20 *g*	26.0	29.9	2.7	3.8
N4	0.30 *g*	27.5	33.0	6.0	2.3

As far as the first configuration is concerned, nine white noise inputs were applied with increasing magnitude (from 0.05 *g* to 0.30 *g*). Figure 7.17 shows the transfer functions detected for tests N1 and N4. Independently on the magnitude of the base input, the transfer functions present similar distribution. Table 7.5 presents the two frequency characterized by the highest amplitude and the corresponding damping ratios for the first configuration (smooth wall and full-filled silo). The first frequency results around 14 *Hz*. Initially, a reduction of the first frequency from 14.1 to 12.7 *Hz* by increasing the peak base acceleration from 0.05 to 0.30 *g* is observed; however, in the following tests such trend is no more detected for 0.30 *g* peak base accelerations.

Table 7.5 - First two frequencies and related damping identified in the white noise tests for the first configuration (smooth wall)

Test No.	Peak Base Acceleration Input	Frequency 1 [*Hz*]	Frequency 2 [*Hz*]	ξ_1 [%]	ξ_2 [%]
N1	0.05 *g*	14.1	44.4	6.3	3.5
N2	0.05 *g*	14.1	44.9	5.7	1.9
N3	0.10 *g*	13.5	42.4	9.1	4.6
N4	0.20 *g*	12.9	42.8	13.9	7.1
N5	0.30 *g*	12.7	43.9	20.1	6.3
N6	0.30 g	14.1	46.7	16.0	3.5
N7	0.30 *g*	14.2	46.9	21.2	3.0
N8	0.30 *g*	14.2	45.5	14.7	11.0
N9	0.30 *g*	14.5	44.9	13.5	5.0

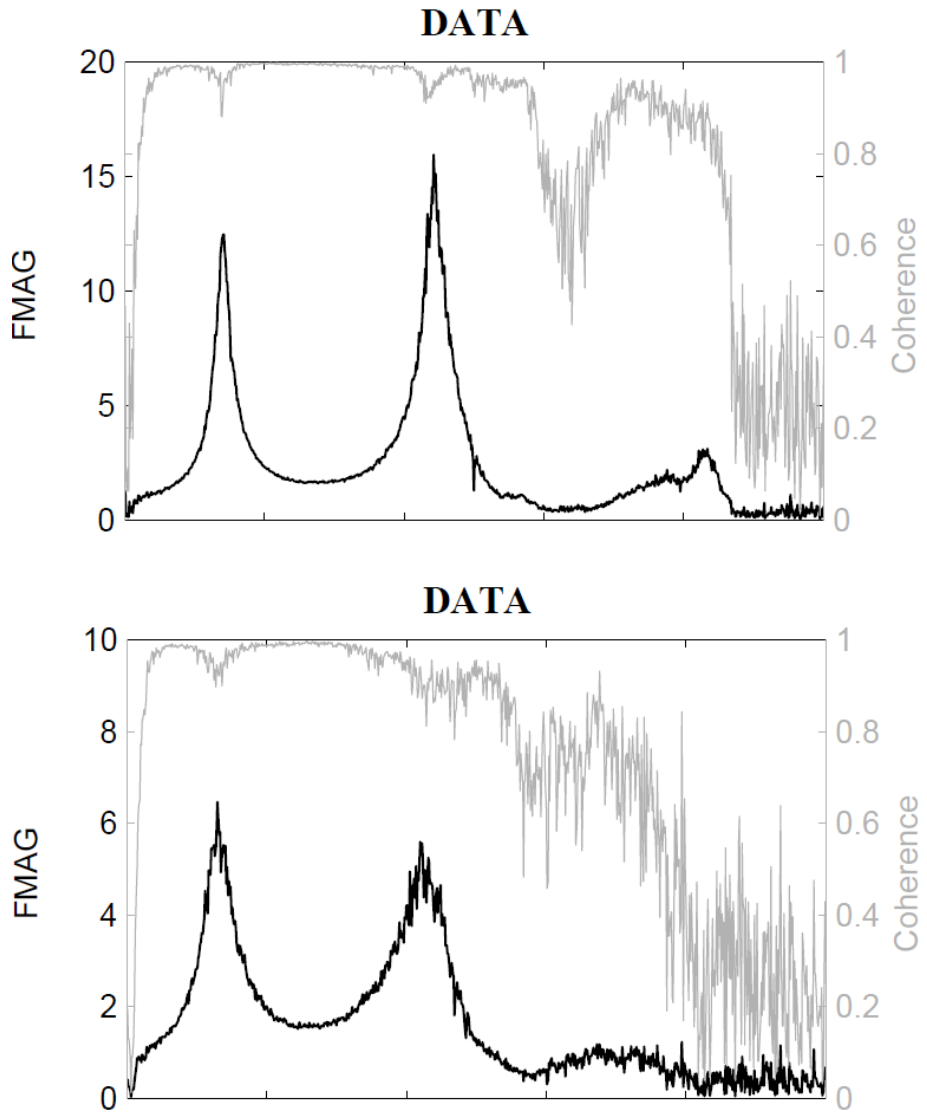

(a)

(b)

Figure 7.17 - Transfer functions for the first configuration for tests N1 and N4

As far as the second configuration is concerned, one white noise input was applied with (0.05 *g*). Figure 7.18 shows the transfer functions detected for tests N1. The two peaks related to the first and second frequencies are smoother than those observed for the full-filled silo specimen (first configuration). Table 7.6 presents the two frequency characterized by the highest amplitude and the corresponding damping ratios for the second configuration (roughened wall and half-filled silo).

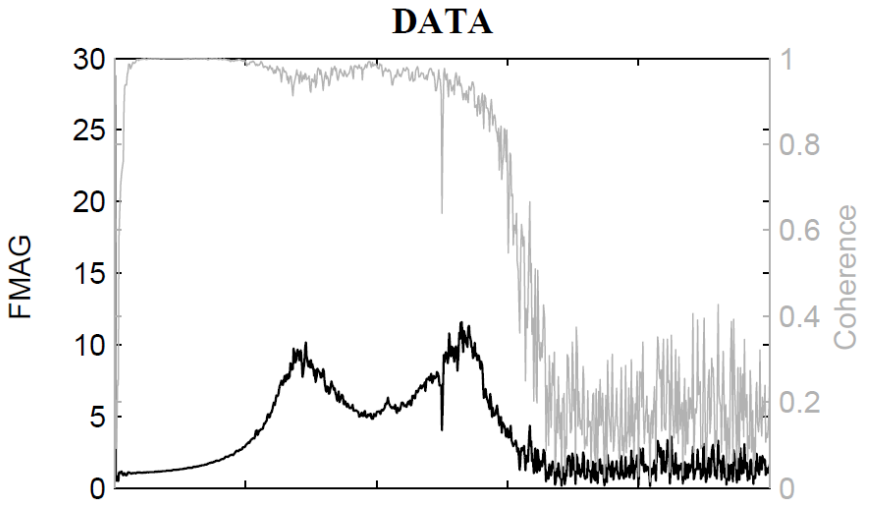

Figure 7.18 - Transfer functions for the second configuration silo for tests N1

Table 7.6 - First two frequencies and related damping identified in the white noise tests for the second configuration

Test No.	Peak Base Acceleration Input	Frequency 1 [*Hz*]	Frequency 2 [*Hz*]	ξ_1 [%]	ξ_2 [%]
N1	0.05 *g*	28.1	56.0	11.6	-

As far as the third configuration is concerned, one white noise input was applied. Figure 7.19 shows the transfer function detected for test N1. Table 7.7 presents the two frequency characterized by the highest amplitude and the corresponding damping ratios for the third configuration (roughened wall and full-filled silo).

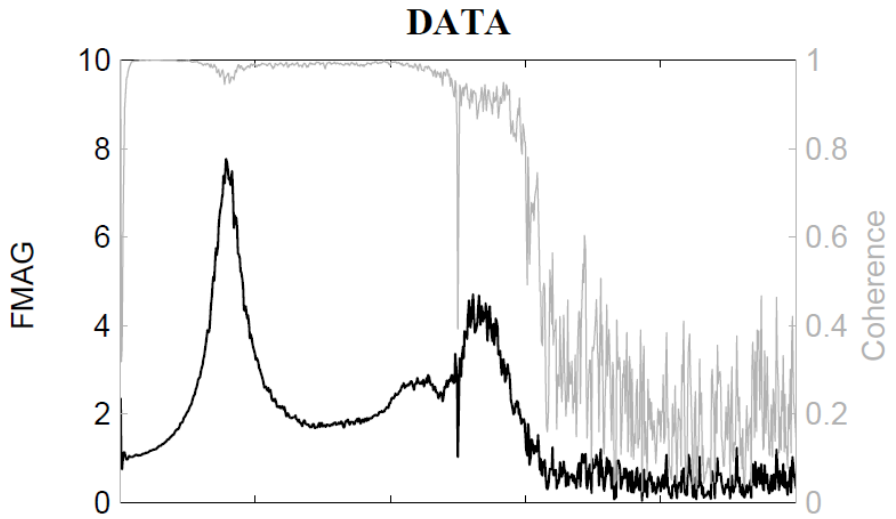

Figure 7.19 - Transfer functions for the third configuration for test N1

Table 7.7 - The first two frequencies and related damping identified in the white noise tests in the third configuration (roughened wall)

Test No.	Peak Base Acceleration Input	Frequency 1 [*Hz*]	Frequency 2 [*Hz*]	ξ_1 [%]	ξ_2 [%]
N1	0.20 *g*	15.6	43.3	10.1	5.9

In general, two peaks are apparent, indicating that the dynamic behavior of the silo-grain system is akin to a 2-degrees-of-freedom system. Also, the high values of the two frequencies suggest that a low-frequency sinusoidal input may effectively represent the constant input for the considered time ranges (around the peaks of the sinusoid), given that no dynamic interaction is expected between the input and the system frequencies. On the other hand, earthquake ground motion input characterized by frequencies comparable with the system frequency may lead to some dynamic interaction.

Table 7.8 summarizes the mean value of the first frequency of the silo-grain system as obtained for the white noise tests in the empty, first, second, third configurations. The influence of the level of filling and base connections on the fundamental system frequency is observed. By comparing the empty an the first configuration, it is observed that the filling provokes a reduction of more than the 50% of the first frequency (together with an increasing of the damping ratios). Analogously, by comparing the second and the third configurations, it is observed that the filling provokes a reduction of more than the 40% of the first frequency (together with an increasing of the damping ratios). By comparing the empty and the second configurations, it is observed that the first frequencies are similar, even if the level of filling are different, thus indicating that the base connections strongly influence the stiffness of the system and so the dynamic response of the specimens.

Table 7.8 – Summary of the mean value of the first frequency of the grain-silo system for each configuration

Test configuration	Depth of ensiled material	Typology of silo wall	Fundamental frequency [*Hz*]
Empty	0.0 *m*	Smooth	27.4
First	1.2 *m*	Smooth	12.7
Second	0.6 *m*	Rough	28.0
Third	1.2 *m*	Rough	16.0

7.3.3 Accelerations

Figure 7.20 shows the time-history of the horizontal acceleration at different heights of the silo for a 1 *Hz* sinusoidal input with peak acceleration around 0.3 *g*, for the left and right sides of the silo (Figure 7.3*a*). The response recorded on the two sides of the silo is almost identical. The uniform response of the silo at different heights indicates negligible acceleration amplification, thereby validating the assumption of uniform vertical profile of the horizontal acceleration along the height of the silo (physically related to the stiff behavior of the silo-grain system).

Figure 7.21*a* represents the peak acceleration profiles (along the height of the silo walls) as obtained under different 1 *Hz* sinusoidal inputs (Table 7.1). These profiles are almost vertical (the variation of acceleration from the silo bottom up to height 0.84 *m* is less than 12%) for table accelerations lower than 0.35 *g*: from an engineering point of view, negligible amplification occurs (no dynamic interaction). For the accelerometer placed on the top of the grain (height 1.24 *m*), the largest acceleration values that drift away from the vertical profile may be justified by the unavoidable horizontal sliding of the surface grain layers (so called “sliders”) which occur even for low values of the horizontal acceleration. On the other hand, amplifications up to 20% can be noted from the bottom to the top of the silo at accelerations above 0.35 *g*. On the basis of these results, for table accelerations lower than 0.35 *g*, the low-frequency sinusoidal input produces a near constant vertical profile of the horizontal acceleration.

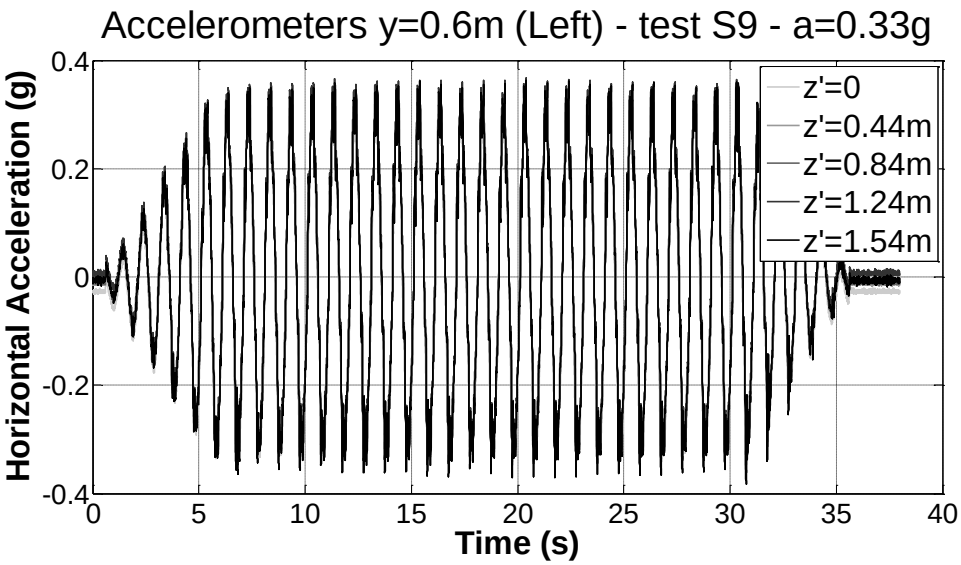

(a)

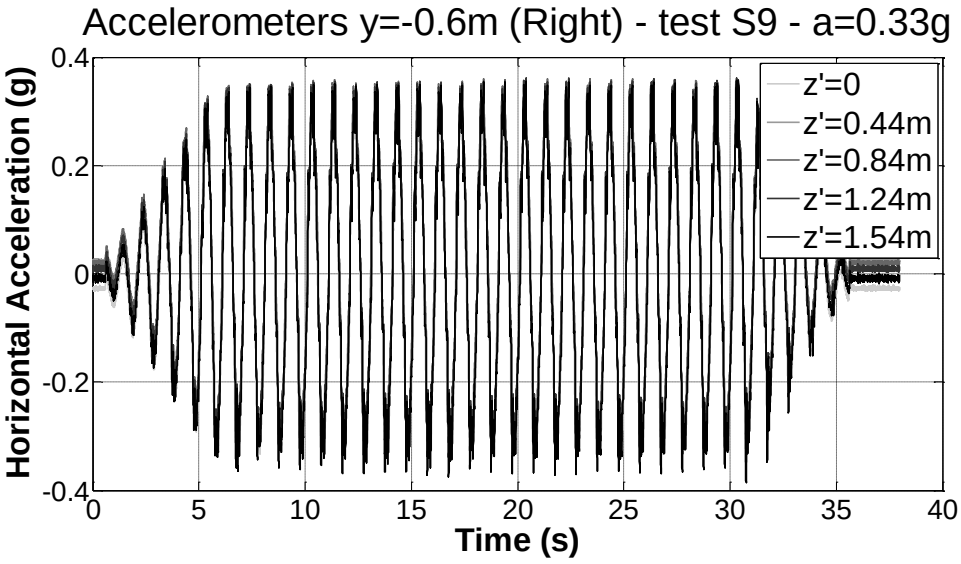

(b)

Figure 7.20 - Accelerometers on the silo wall at different heights: a) left side and b) right side for the first configuration of tests.

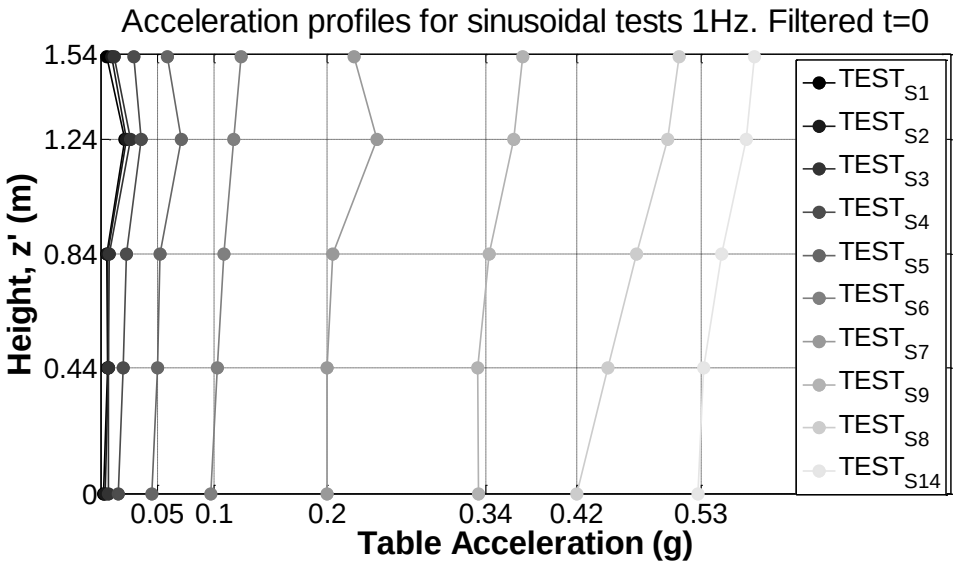

(a)

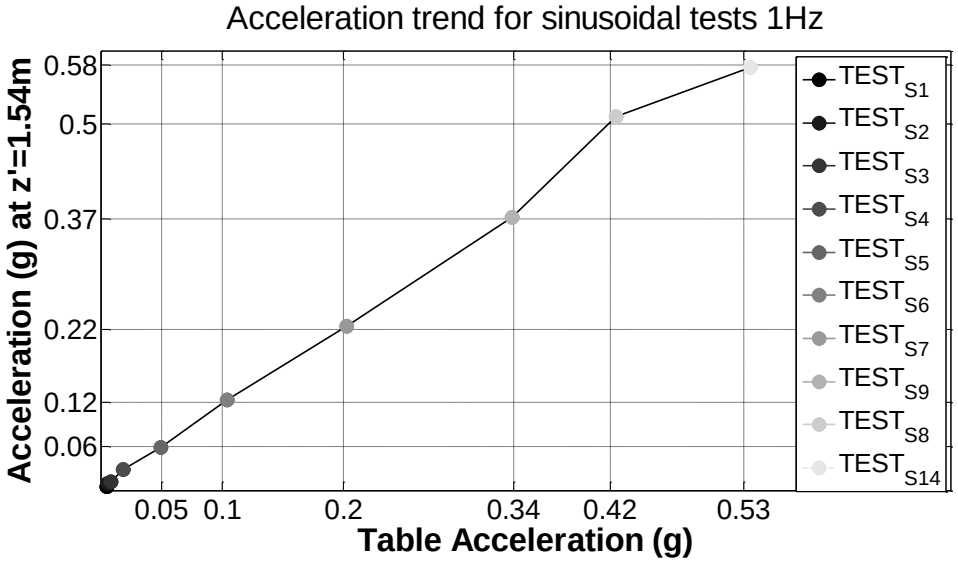

(b)

Figure 7.21 - (a) Acceleration profiles for sinusoidal tests at 1Hz. (b) Acceleration trend for sinusoidal tests at 1Hz.

Figure 7.21*b* represents the maximum acceleration at the top of the silo wall as a function of the table acceleration. A linear trend can be noted up to 0.35 *g*, where a slight slope change occurs. This is consistent with the limits of validity (see Eq. (40) of chapter 6) of the original analytical formulation (Silvestri et al. 2012), which holds only for accelerations lower than $\mu_{GB} = 0.45$.

The second and third configurations of tests present similar results for sinusoidal inputs. As illustrative examples, Figure 7.22*a* and *b* show the maximum acceleration at the top of the silo content as a function of the table acceleration for the second and third configurations, respectively. A linear trend is obtained in both cases.

These figure are representative not only for the reported tests but also for all the 149 sinusoidal tests performed. It could be concluded that the profile along the silo height of the horizontal acceleration under horizontal sinusoidal input is practically vertical. No acceleration amplification occurs for the silo-grain system under low-frequency sinusoidal input. Such evidences are in general accordance with the experimental results given by other shaking-table tests, as reported by different Authors and collected in chapter 3.

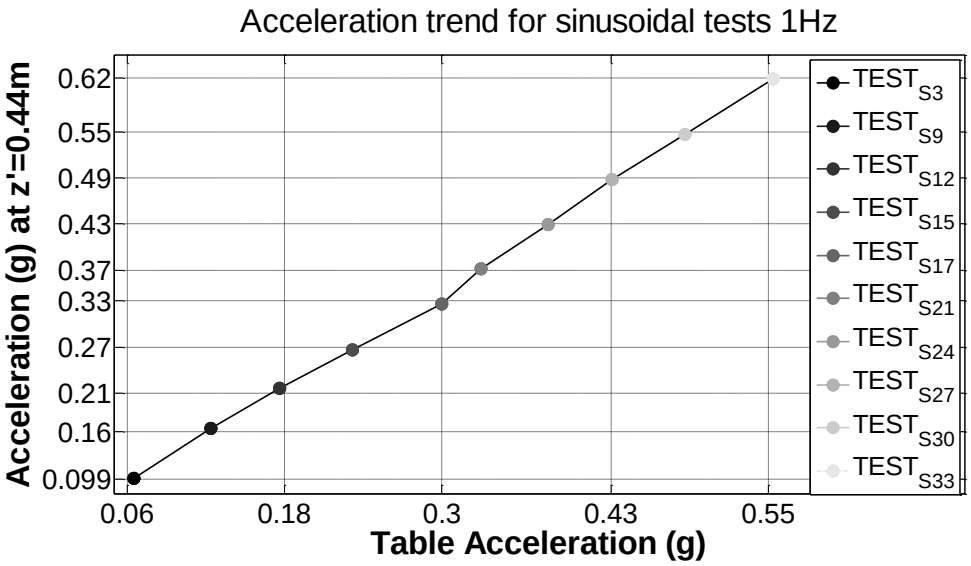

(a)

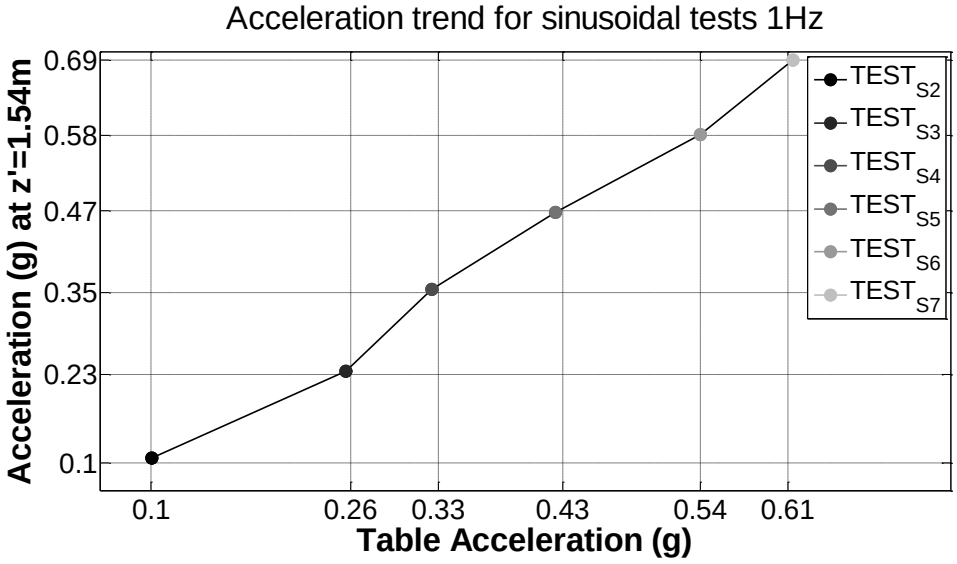

(b)

Figure 7.22 - (a) Acceleration profiles for sinusoidal tests second configuration. (b) Acceleration trend for sinusoidal test for the third configuration.

7.3.4 Vertical strains

Figure 7.23*a-c* shows the typical time-history of the vertical strains at different heights of the silo wall for a 1 *Hz* sinusoidal input with peak acceleration around 0.3 *g*, for the left side of the silo (Figure 7.3*a*) in the first, second and third configurations of test, respectively. In all cases, the response is sinusoidal like the input and symmetric with

respect the initial strain level (herein set equal to zero). All strain gauges are in phase with increasing absolute values from the top to the bottom of the silo: the maximum vertical strain is reached at the lowest strain gauge (z'= 0.18 *m*), while the minimum one is reached at the highest strain gauge (z'= 0.92 *m*). This could be expected because the bending moment increases from the top to the bottom of the silo. It is interesting to note that the increase in the grain-wall friction coefficient (Figure 7.23*c* vs. Figure 7.23*a*) leads to higher strains at all heights, thus giving a first indication that the friction coefficient modifies the response of the system. Also, the reduction of the mass (Figure 7.23*b* vs. Figure 7.23*c*) obviously leads to lower strains. The only exception is represented by the time-history of the vertical strains at different heights of the silo wall reported by Figure 7.24, where an important difference with respect to the previously reported time-histories can be detected. The maximum vertical strain is reached at z'= 0.32 *m*, instead of z'= 0.18 *m*. This may be related to the squeezing of the Ballottini glass along the vertical junction between the two polycarbonate sheets (Figure 7.25).

As an illustrative example, Figure 7.26 shows the mean of the vertical strains detected by the strain gauges symmetric with respect to the *y*-axis and measured at the base (z'= 0.14 *m*), as a function of the *y* coordinate, for the 1 *Hz* sinusoidal S4 input with peak acceleration around 0.3 *g* (third configuration of tests) for three different time instants. The general trend appears rather asymmetric with respect to the *x*-axis. However, the vertical strains do not present a linear trend along the *y*-axis. This means that cross-sections do not remain plane.

The order of magnitude of the highest vertical strains detected during the tests for the first, second and third configurations is around 550 $\mu\varepsilon$ (for 0.54 *g*), 180 $\mu\varepsilon$ (for 0.60 *g*) and 900 $\mu\varepsilon$ (for 0.75 *g*), respectively. For horizontal acceleration greater than 0.75 *g*, for the third configuration, the vertical strains detected on the right side of the silo wall do not maintain symmetric, as illustrated by Figure 7.27.

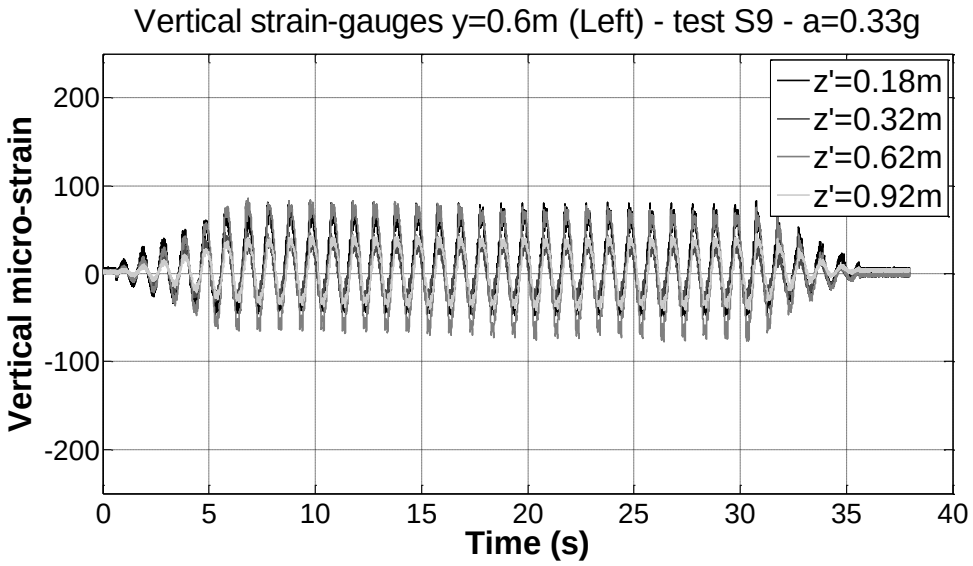
Vertical strain-gauges y=0.6m (Left) - test S9 - a=0.33g
Vertical micro-strain
Time (s)
z'=0.18m
z'=0.32m
z'=0.62m
z'=0.92m
200
100
0
-100
-200
0
5
10
15
20
25
30
35
40

(a)

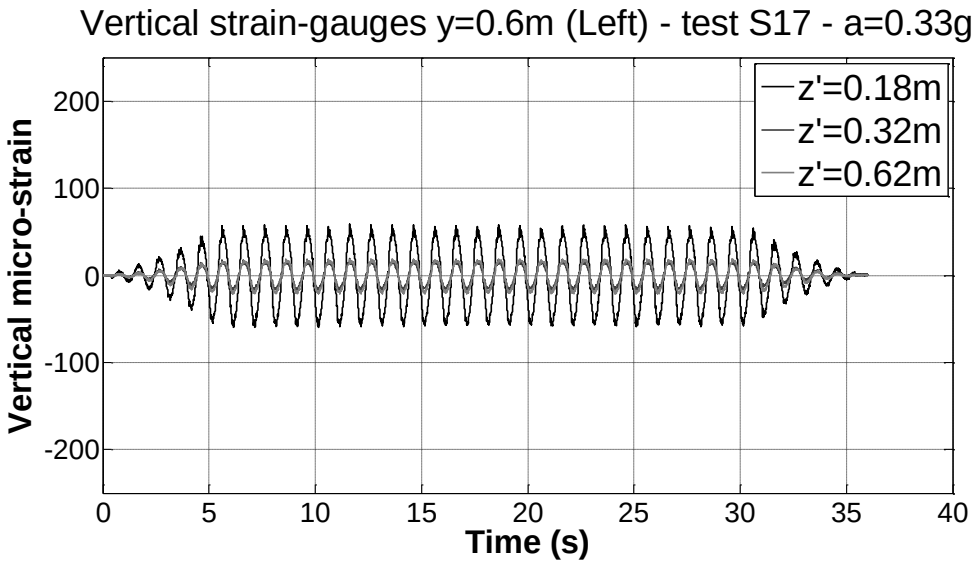
Vertical strain-gauges y=0.6m (Left) - test S17 - a=0.33g
Vertical micro-strain
Time (s)
z'=0.18m
z'=0.32m
z'=0.62m
200
100
0
-100
-200
0
5
10
15
20
25
30
35
40

(b)

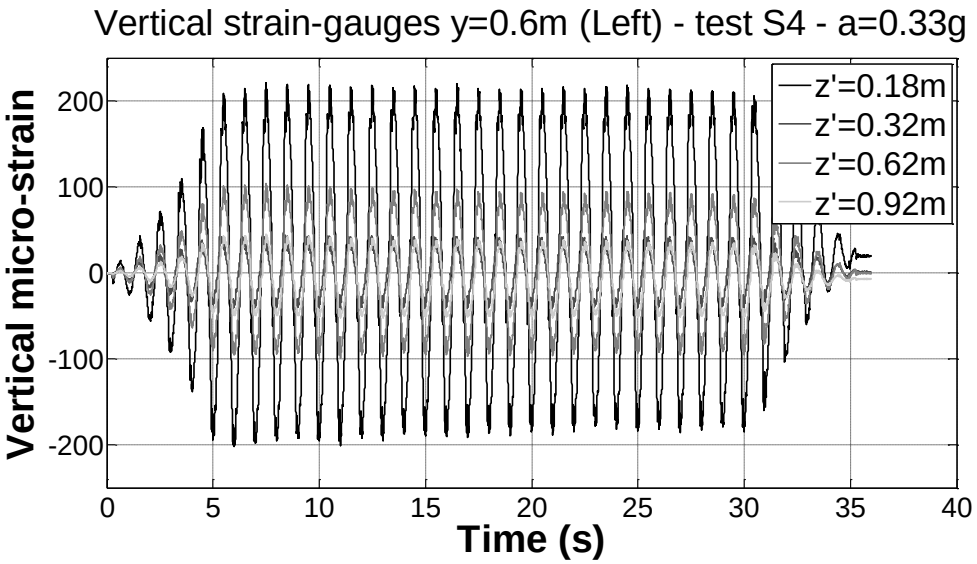

(c)

Figure 7.23 - Vertical strains at different heights for the first (a), second (b) and third (c) configurations of tests.

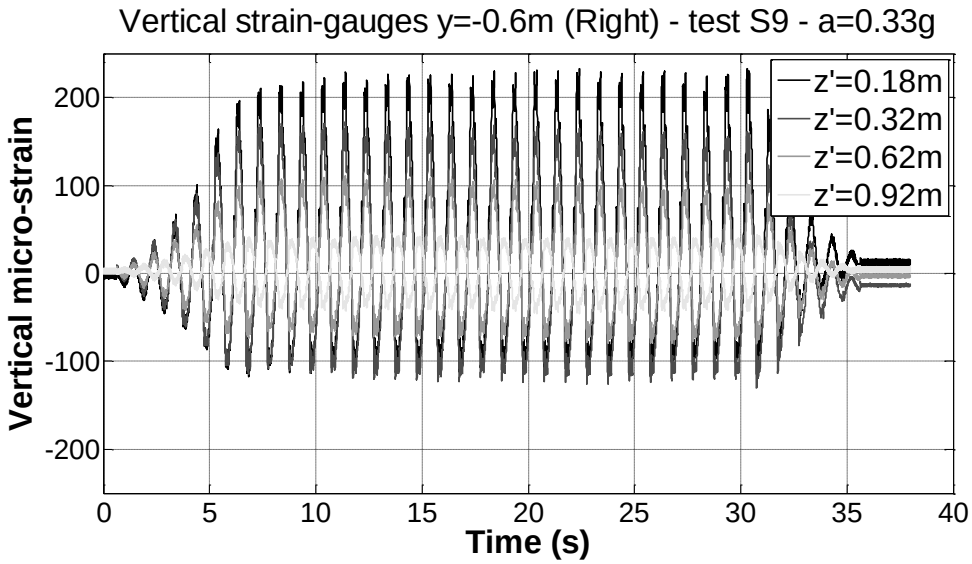

Figure 7.24 - Vertical strains at different heights for the first configuration for S9 test at the right side (y= -0.60 m).

Figure 7.25 - Infiltration of Ballottini glass along the vertical junction of the two polycarbonate sheets.

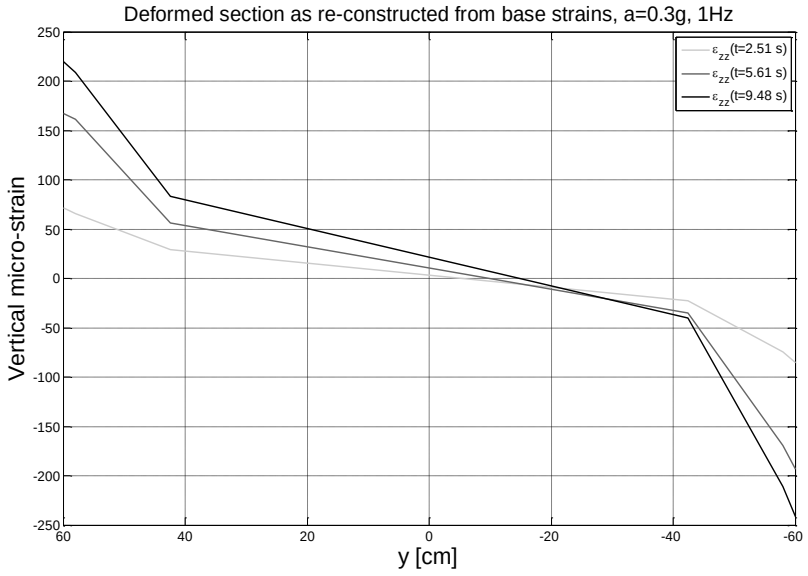

Figure 7.26 - Vertical strains at z'=0.14 m for the 1 Hz sinusoidal S4 input.

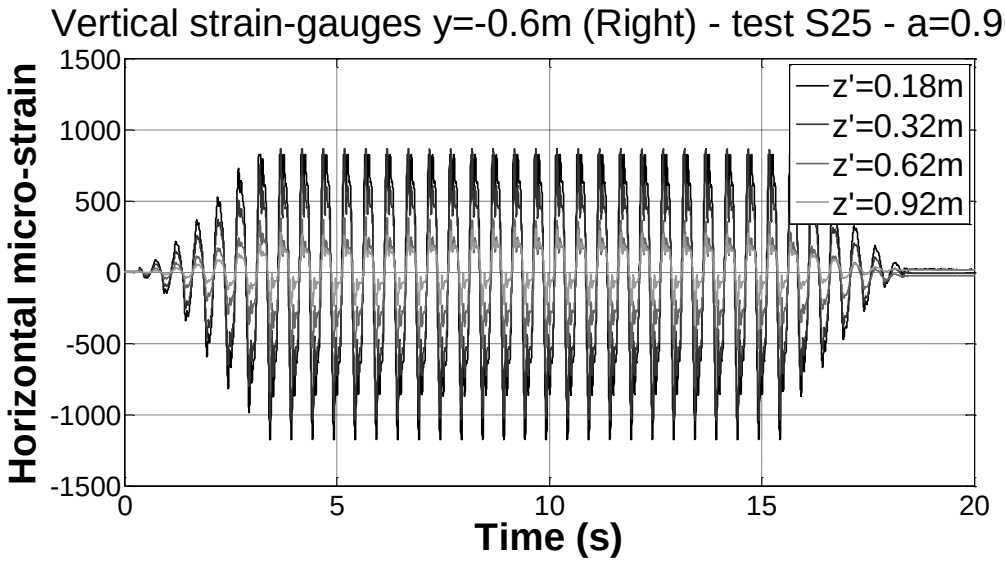

Figure 7.27 - Vertical strains at different heights for the third configuration for S25 test at the right side (y= -0.60 m).

7.3.5 Comparison between sinusoidal and earthquake response

To analyze the response of the silo specimen to a real earthquake where the excitation involves not only one frequency, several tests with different ground motion records are performed for each configuration.

In order to excite the main frequencies of the silo-grain system, the South Iceland 2000 record has been selected for its particular spectral shape (Figure 7.28). This is characterized by high values of pseudo-acceleration at high frequencies (low periods), close to the main frequencies of the system.

Figure 7.29*a* shows the peak acceleration profiles along the silo height as obtained for different levels of the table acceleration, using the South Iceland earthquake as input, for the first test configuration. The profile is not linear, thus indicating an amplification of the base acceleration due to the frequency content of the selected input. In more detail, a bilinear trend can be recognized, with maximum amplification between 2 and 2.5 at the top of the silo. The response is thus substantially different from the case of sinusoidal input, for which no amplification occurs. Such evidences are in general accordance with the experimental results given by other shaking-table tests, as reported by different Authors and collected in chapter 3. On the other hand, such results evidence that squat silos do not

respond in a quasi-static manner under seismic excitation, as considered in the numerical work by Rotter and Hull (1989).

Figure 7.29*b* shows the peak acceleration at the top of the silo versus the peak table acceleration, using the South Iceland earthquake as input, for the first test configuration. The trend is linear up to 0.3 *g*. Then, a sudden change in the slope is obtained, which is consistent both with the limit given by Eq. (41) and with the results obtained for the case of sinusoidal input depicted in Figure 7.22*b*. In this case, the slope change is more marked owing to the amplification effect.

On the basis of these results, the analytical formulation can be applied to the case of earthquake input, if an appropriate (bilinear, in the case of the South Iceland earthquake) vertical profile is adopted for the horizontal acceleration.

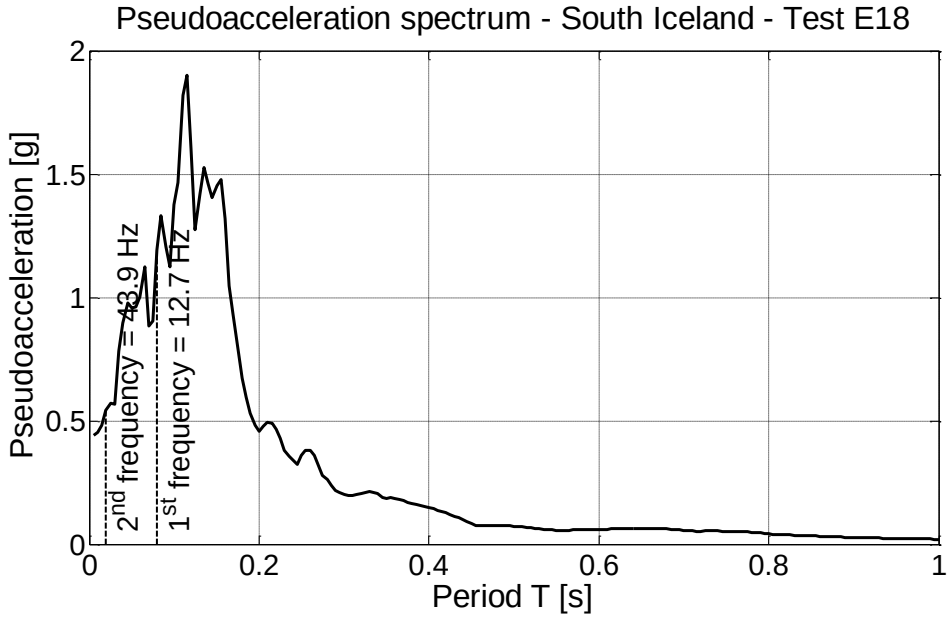

Figure 7.28 – Pseudo-acceleration spectrum of the table acceleration time-history for Test E18 (South Iceland earthquake) and fundamental frequencies of the grain-silo system.

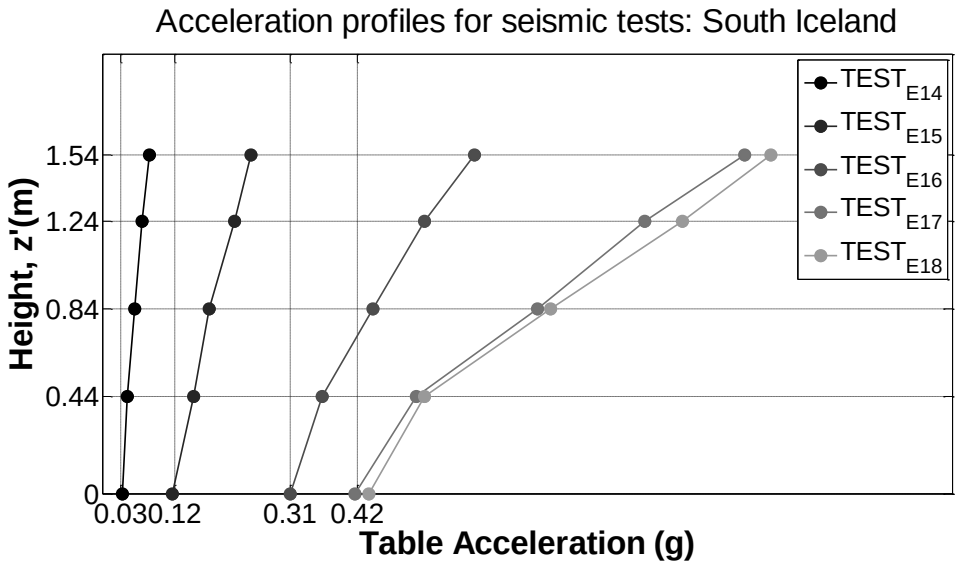

(a)

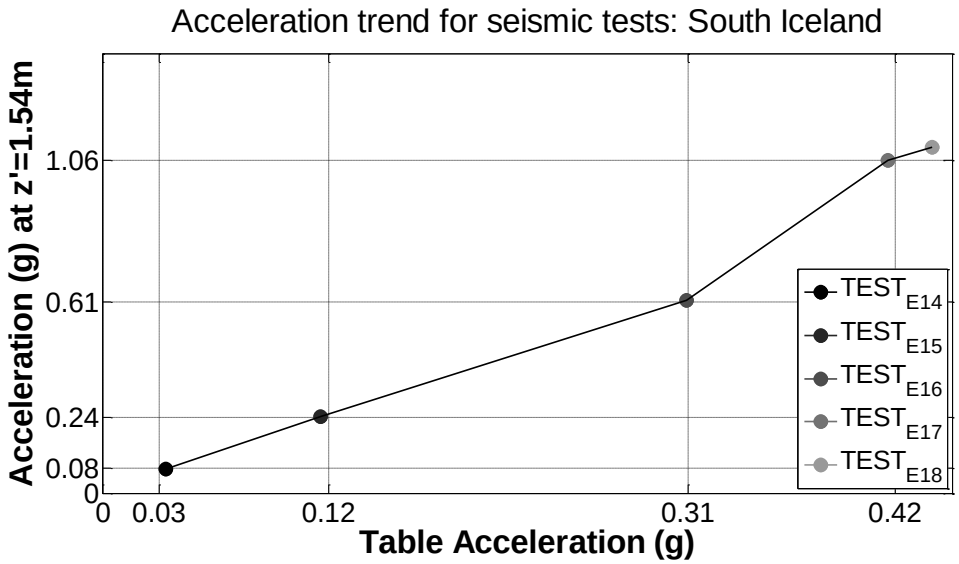

(b)

Figure 7.29 - (a) Acceleration profiles for seismic tests. (b) Acceleration trend for seismic tests.

7.4 Rupture of the silo specimen

In this section, the failure of the silo specimen is described.

In detail, the failure of the silo was triggered by the formation of a crack in the polycarbonate material under a shaking-table acceleration more than 1.0 *g* (Figure 7.30). Figure 7.31*a-d* show details about the crack shape, which originated in correspondence of the external connection bolt at the base of the specimen, on the right side. The cracking of the wall was reasonably related to reaching of the ultimate stress of the polycarbonate material in correspondence of the base bolt connections, where concentrations of stress

aroused. Then, the local rupture of the polycarbonate material evolved in the formation of the crack.

Figure 7.30 - Spilling of the Ballottini glass from the crack of the wall after the failure

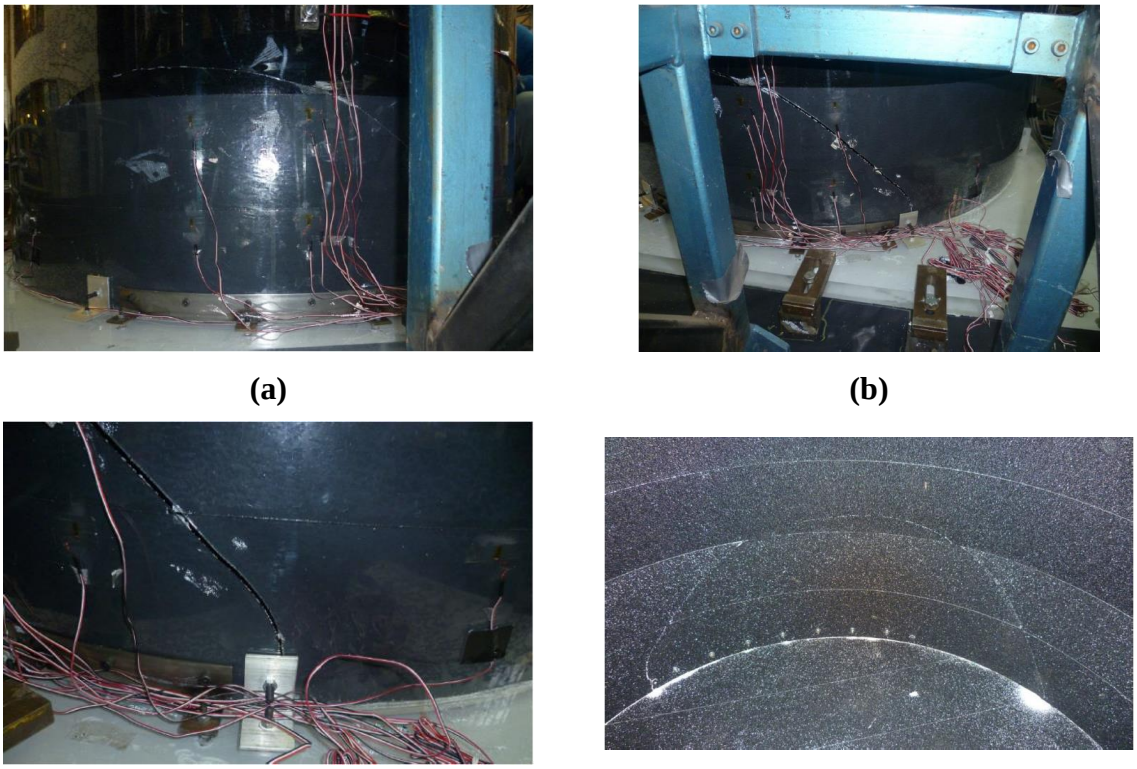

(a) **(b)**

(c) **(d)**

Figure 7.31 - (a) Frontal view of the crack shape; (b) lateral view of the crack shape; (c) Detail of the crack close to the bolted connection; (d) internal view of the crack shape

7.5 Critical considerations

In this section, the shaking-table experimental campaign carried out on silo specimens filled with Ballottini glass is presented. The experimental campaign aims to experimentally verify the original analytical formulation proposed by Silvestri et al. (2012) and gain preliminary insight on the issue of the *effective mass* acting on the silo wall under dynamic and seismic conditions. For these reasons, the experimental campaign has been designed both to meet the idealized conditions of the analytical formulation and to investigate the influence of the type of input on the dynamic response of grain-silos. Low-frequency sinusoidal input has been applied and three different configurations are considered for the silo specimen in terms of grain-wall friction coefficient and slenderness ratio. Also, real strong earth motion records have been used to further investigate the seismic response.

The following criticalities can be drawn from the experimental campaign:

1) On the first configuration (smooth wall), squeezing of the Ballottini glass between the vertical seam occurred. On the second and third configurations (roughened wall), such phenomenon was inhibited by the sand paper coverage on the internal face of the silo wall;
2) Different base connections lead to different dynamic responses of the silo specimen in terms of frequencies of vibrations;
3) Under low-frequency sinusoidal input characterized by a maximum horizontal acceleration greater than 0.70 *g*, the vertical strains detected on the right side of the silo wall do not maintain symmetric. For horizontal acceleration greater than 1.0 *g* rupture of the silo specimen occurred due to reaching of the ultimate stress of the polycarbonate material in correspondence of the base bolt connections.

The following concluding remarks containing preliminary but yet clear indications can be drawn from the experimental campaign:

4) The vertical profile of the horizontal acceleration under low-frequency sinusoidal input is almost constant, so that no acceleration amplification has to be considered for the silo-grain system;

5) The vertical profile of the horizontal acceleration under earthquake input is not linear, thus indicating a dynamic component in the system response;
6) The grain-wall friction coefficient strongly affects the response of the grain-silo system in terms of vertical strains experienced by the silo wall under low-frequency sinusoidal input;
7) Sliding of the upper grain layers appears to occur even for very low values of the horizontal accelerations (0.05 g). In such case, its effects result essentially localized at the top of the silo wall. On the contrary, for values of the horizontal accelerations around 0.30 – 0.35 g, sliding appears to become more significant and its effects start to affect the overall response of the grain-silo system.

Reference

Arroyo-Cetto D, Pulos G, Zenit R, Jimenez-Zapata MA, Wassgren CR. Compaction force in a confined granular column. Physical Review E 2003; 68(5):051301.

Buisman ASK. Grondmechanika, Waltman. 1940.

Dabrowski A. Parcie Materialow Sypkich w Leju (Pressures from bulk solids in hoppers). Archiwum Inzynierii Ladowej, Warsawa 1957; 325‑328.

Di Chiacchio, L. (2013). Interpretation of shaking-table tests of flat-bottom silos containing grain-like material. Master Thesis Dissertation, University of Bologna. http://amslaurea.unibo.it/5756/

Kwade A, Schulze D, Schwedes J. Determination of the stress ratio in uniaxial compression tests‒part 1. Powder Handling and Processing 1994a; 6(1):61‑65.

Kwade A, Schulze D, Schwedes J. Determination of the stress ratio in uniaxial compression tests‒part 2. Powder Handling & Processing 1994; 6(2):199‑203.

Lings ML, Dietz MS. (2004) An improved direct shear apparatus for sand. Geotechnique; 54(4):245‑256.

Mandato S, Cuq B, Ruiz T. Experimental study of vertical stress profiles of a confined granular bed under static and dynamic conditions. The European Physical Journal E: Soft Matter and Biological Physics 2012; 35(7):1‑8.

Ovarlez G, Fond C, Clément E. Overshoot effect in the Janssen granular column: a crucial test for granular mechanics. Physical Review E 2003; 67(6):060302.

Rotter, J. M., & Hull, T. S. (1989). Wall loads in squat steel silos during earthquakes. Engineering Structures, 11(3), 139-147.

Silvestri S, Gasparini G, Trombetti T, Foti D. On the evaluation of the horizontal forces produced by grain-like material inside silos during earthquakes. Bulletin of Earthquake Engineering 2012; 10:1535‑1560.

Timoshenko, S., & Woinowsky-Krieger, S. (1959). Theory of plates and shells.

Ueng TS, Wu CW, Cheng HW, Chen CH. Settlements of saturated clean sand deposits in shaking table tests. Soil Dynamics and Earthquake Engineering 2010; 30:50‑60

Vanel L, Claudin P, Bouchaud JP, Cates ME, Clément E, Wittmer JP. Stresses in silos: comparison between theoretical models and new experiments. Physical Review Letters 2000; 84(7):1439.

Krynine DP. Discussion of "stability and stiffness of cellular cofferdams" by Karl Terzaghi. Transactions, ASCE 1945; 110:1175‑1178.

8. Experimental-analytical correlation study

In this chapter, the main experimental results are reconstructed starting from the data acquired via shaking-table tests and compared with the predictions given by the proposed analytical formulation. The main aim is to experimentally verify the proposed analytical formulation. First, the procedure adopted for the reconstruction of the experimental base bending moments is presented. Then, the influence of the grain-wall friction coefficients on the reconstructed wall base bending moment is presented. Finally, the comparison between experimental values of the reconstructed wall bending moment and the analytical predictions given by the proposed analytical formulation is discussed.

8.1 The experimental base bending moment

In order to reconstruct the experimental bending moment at the base of the silo (z'= 0.14 *m*), because the measurements indicate that cross-sections do not remain plane (see chapter 7), a direct integration of the base vertical stresses multiplied by the corresponding lever arm over the whole circumferential cross-section has been performed.

In detail, the vertical strain, $\varepsilon_{zz,i}(t)$, as a function of time *t*, has been recorded for each *i-th* vertical strain gauge placed at z'= 0.14 *m*: channels 3 and 15 for the first configuration (Figure 8.1) and channels 42, 2, 3, 4, 44, 43, 16, 15, 14 and 41 for the second and third configurations (Figure 8.1).

Note that more precise results are obtained for the second and third configurations of the tests, given that more strain gauges were placed at the base.

The corresponding vertical stress, $\sigma_{zz,i}(t)$, has been computed assuming linear elastic behavior for the polycarbonate material of the silo:

$$\sigma_{zz,i}(t) = \frac{E_{polycarbonate}}{1-\left(\nu_{polycarbonate}\right)^2} \cdot \left[\varepsilon_{zz,i}(t) + \nu_{polycarbonate} \cdot \varepsilon_{\theta\theta,i}(t)\right] \tag{1}$$

where $\varepsilon_{\theta\theta,i}(t)$ is the circumferential strain recorded for each *i-th* horizontal strain gauge placed at z'= 0.14 *m*. Then, the experimental bending moment, $M_{\exp}(t)$, is obtained by direct integration of the base vertical stresses multiplied by their corresponding area, A_i, and lever arm, d_i, over the whole circumferential cross-section:

$$M_{\exp}(t) = \sum_i \sigma_{zz,i}(t) \cdot A_i \cdot d_i \tag{2}$$

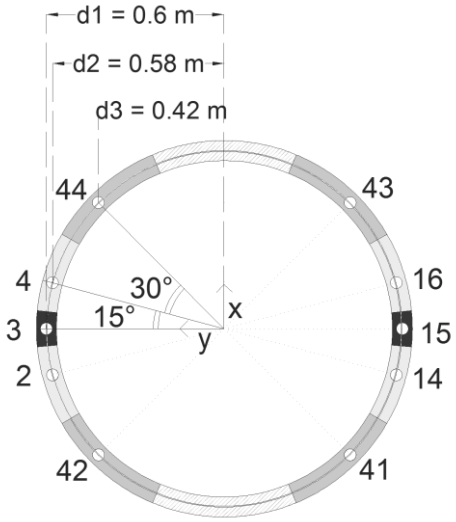

Figure 8.1 - Plan view of the strain gauges position.

8.2 The influence of the wall–grain friction coefficient

The effect of the wall-grain friction coefficient is discussed in this section. Figure 8.2 compares the experimental base bending moment as reconstructed from the base strain values, for the first (smooth wall) and third (roughened wall) test configurations. In more detail, Figure 8.2 *a* and *b* represents the moment derived from experimental measurements as a function of time, as obtained in the case of 1 *Hz* sinusoidal input with peak table acceleration equal to 0.2 and 0.3 *g*, respectively.

The results clearly indicate that the response of the silo with smooth wall is far less than the response of the silo with roughened wall. Thus, the wall-grain friction coefficient strongly affects the experimental base bending moment.

Figure 8.3 represents the reconstructed value of the base bending moment (the mean value over the maximum values obtained for each one of the 10-15 cycles of the sinusoidal input) as a function of the actual measured acceleration of the shaking table, for all the three test configurations. When comparing the first configuration with the third configuration, a significant increment of the base moment is observed because of the increase of the grain-wall friction coefficient. When comparing the third configuration with

the second configuration, an obvious decrement of the base moment is observed owing to the reduction of the grain mass.

The following conclusion can be drawn. The experimental results do not match with Eurocode 8 prescriptions, which do not take into account the wall-grain friction coefficient at all. From a qualitative point of view, according to the analytical formulation by Silvestri et al. (2012), higher wall-grain friction coefficient (roughened wall) leads to higher actions inside the wall. This is a fundamental result.

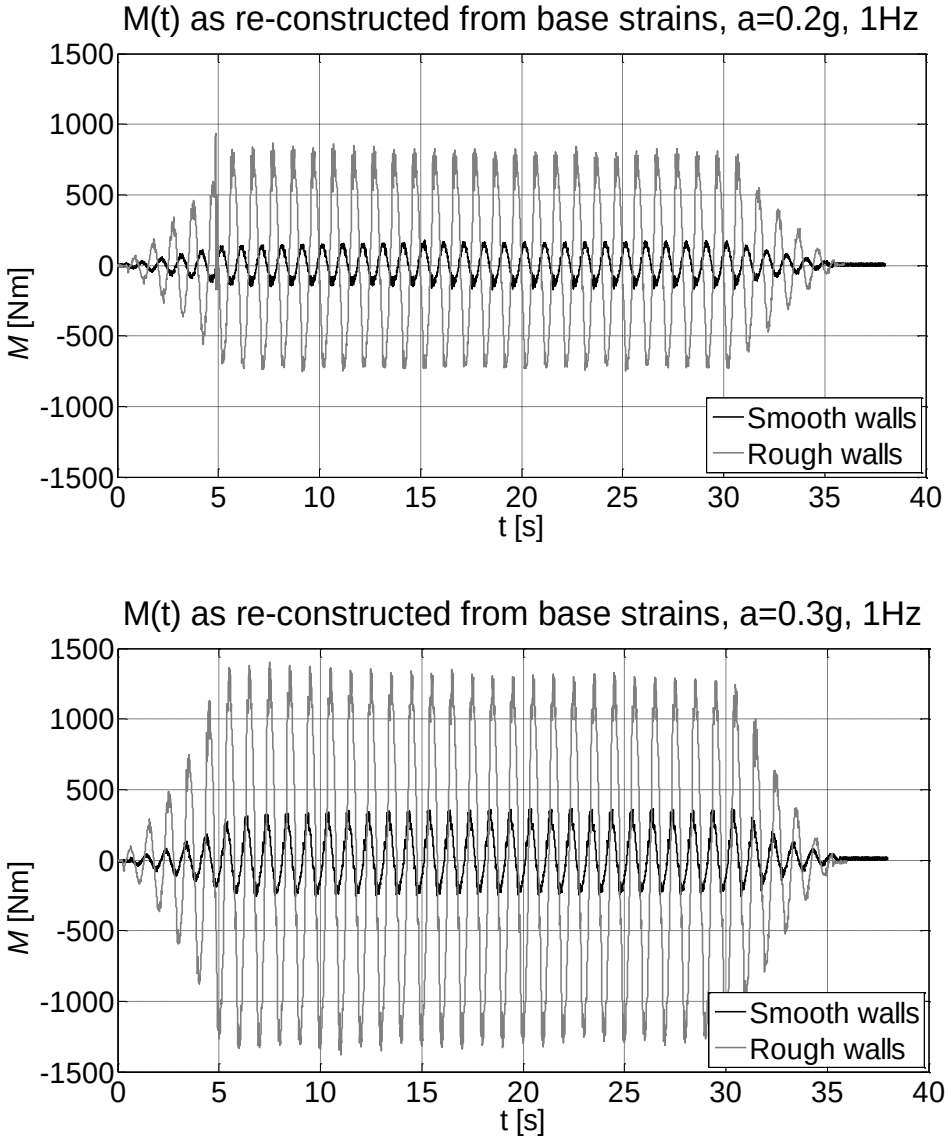

Figure 8.2 - Comparison between the first and the third configuration bending moments at (a) 0.2g and (b) 0.3g.

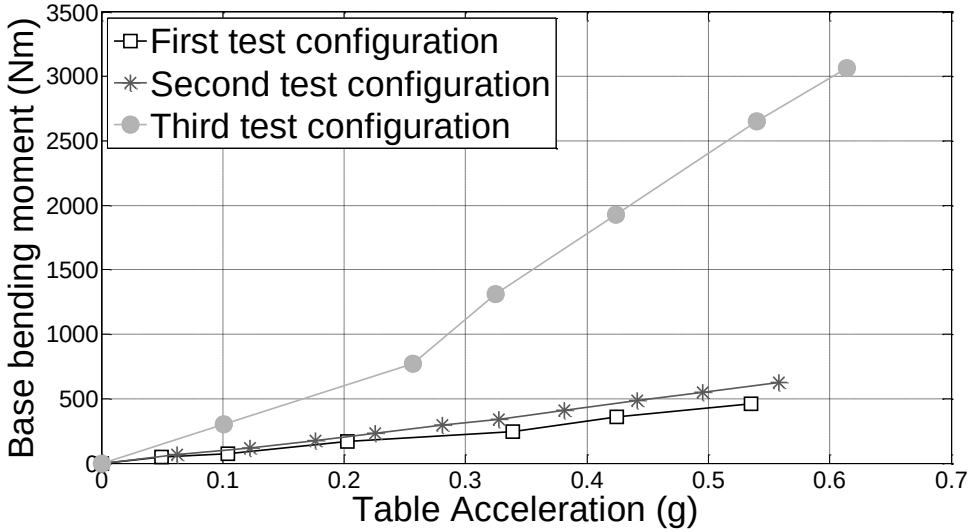

Figure 8.3 - Base bending moment vs. table acceleration for all the three test configurations.

In order to better show the effectiveness of the analytical formulation in capturing the experimental results, a further comparison of the experimental base bending moment between the first configuration and the third configuration (characterized by the same height of the silo content and different grain-wall friction coefficients) has been carried out from another point of view. The ratios between the experimental moment and the experimental moment corresponding to a selected horizontal acceleration ($\bar{a}_{eh0}$) are evaluated for both configurations:

$$\left.\frac{M_{\exp}(a_{eh0})}{M_{\exp}(\bar{a}_{eh0} \cong 0.55)}\right|_{\mu_{GW}=0.30} \quad \text{(first configuration)} \tag{3}$$

$$\left.\frac{M_{\exp}(a_{eh0})}{M_{\exp}(\bar{a}_{eh0} \cong 0.55)}\right|_{\mu_{GW}=0.45} \quad \text{(third configuration)} \tag{4}$$

and reported in Figure 8.4 as functions of the table acceleration. $\bar{a}_{eh0}$ has been chosen roughly equal to 0.55 g, because it is the maximum value reached in the first test configuration, thereby leading to a common domain for both configurations and allowing a consistent comparison.

Despite two different grain-wall friction coefficients, the two plots show the same bilinear trend, with slope change exhibited for the same value of the table acceleration (0.33 *g*) in both cases. This result can be analytically expressed by the following equality between the normalized base bending moments:

$$\left.\frac{M_{\exp}(a_{eh0})}{M_{\exp}(\bar{a}_{eh0}\cong 0.55)}\right|_{\mu_{GW}=0.30} \cong \left.\frac{M_{\exp}(a_{eh0})}{M_{\exp}(\bar{a}_{eh0}\cong 0.55)}\right|_{\mu_{GW}=0.45} \tag{5}$$

This is also confirmed by the theoretical counterpart of the experimental normalized base bending moment as evaluated using Eq. (45) of chapter 6:

$$\frac{M(a_{eh0})}{M(\bar{a}_{eh0})} = \frac{a_{eh0}}{\bar{a}_{eh0}} \cdot \frac{\sqrt{1-\nu_0{}^2 \cdot \bar{a}_{eh0}{}^2 \cdot \mu_{GW}{}^2}}{\sqrt{1-\nu_0{}^2 \cdot a_{eh0}{}^2 \cdot \mu_{GW}{}^2}} \tag{6}$$

In fact, for values of a_{eh0}, $\bar{a}_{eh0}$ and μ_{GW} lower than unity, Eq. (6) can be approximated by:

$$\frac{M(a_{eh0})}{M(\bar{a}_{eh0})} \cong \frac{a_{eh0}}{\bar{a}_{eh0}} \tag{7}$$

which indicates that the theoretical normalized base bending moment (i) does not depend on the physical parameters of the system (among which the grain-wall friction coefficient), and (ii) increases linearly with the horizontal acceleration.

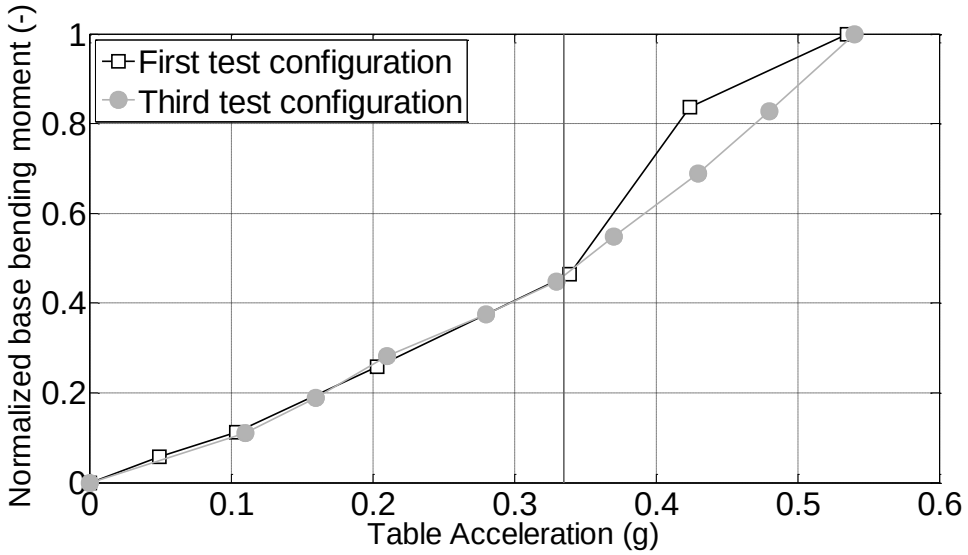

Figure 8.4 - Normalized base bending moment vs. table acceleration for the first and the third test configurations.

8.3 The comparison between the experimental and predicted values of the base bending moment

In this section, the reconstructed base bending moment (i.e. that evaluated in correspondence of the closest instrumented base section, $z' = 0.14\ m$) is compared with the prediction given by Eurocode 8 and given by the proposed analytical formulation (Silvestri et al. 2012) for both sinusoidal and earthquake inputs. A uniform vertical profile of the horizontal acceleration along the height of the silo is taken into consideration. Figure 8.5-Figure 8.7 report this comparison for the case of sinusoidal input, for all three test configurations, respectively.

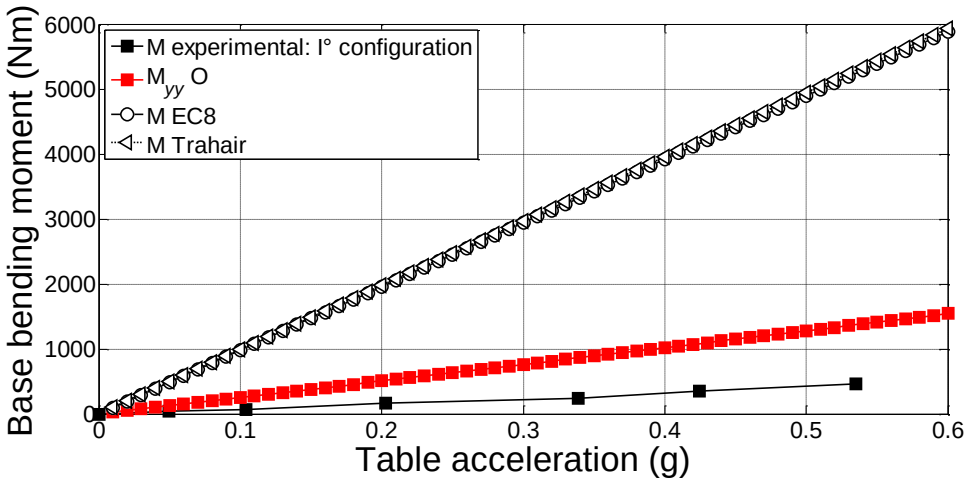

Figure 8.5 - Comparison between the reconstructed experimental bending moment as obtained in the first test configuration for the 1 Hz sinusoidal input and the predicted values by the proposed analytical formulation, the Eurocode 8 provisions and the Trahair formulation.

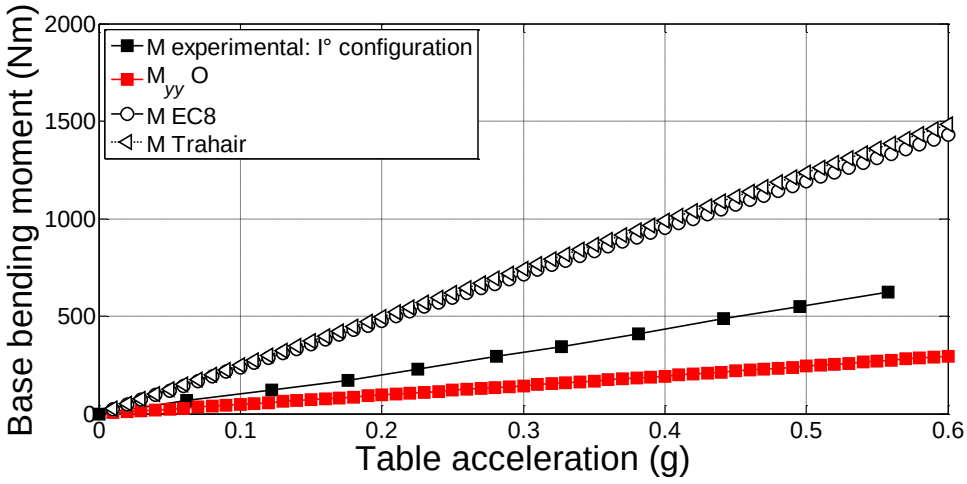

Figure 8.6 - Comparison between the experimental bending moment as obtained in the second test configuration for the 1 Hz sinusoidal input and the predicted values by the proposed analytical formulation, the Eurocode 8 provisions and the Trahair formulation.

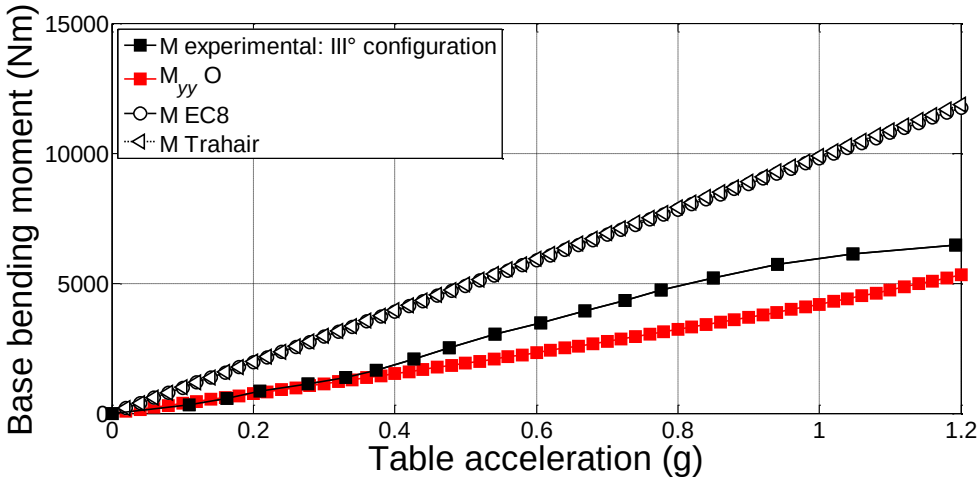

Figure 8.7 - Comparison between the experimental bending moment as obtained in the third test configuration for the 2 Hz sinusoidal input and the predicted values by the proposed analytical formulation, the Eurocode 8 provisions and the Trahair formulation.

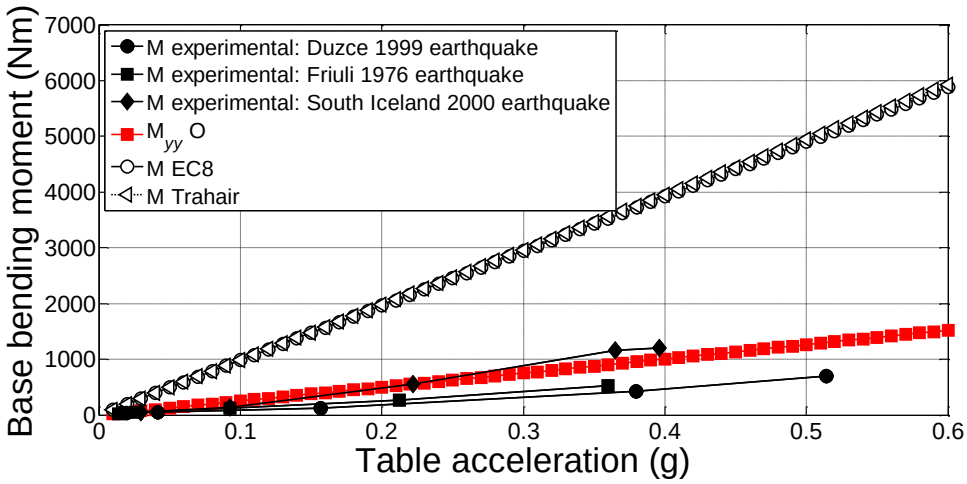

Figure 8.8 - Comparison between the experimental bending moment as obtained in the first test configuration for the three earthquakes: Duzce, Friuli, South Iceland and the predicted values by the proposed analytical formulation, the Eurocode 8 provisions and the Trahair formulation.

With reference to the first configuration (full grain mass), the values obtained by the analytical formulation represent a reasonable upper bound for the values of the experimental base bending moment. With reference to the third configuration (full grain mass), the values obtained by the analytical formulation are in good agreement with the experimental results. With reference to the second configuration (half grain mass), the values obtained by the analytical formulation are lower than the experimental results. A possible reason may lie in the disturbing effect of the mass of top ring, instrumentation and

cables on the dynamic system behavior, which becomes not negligible with respect to the half amount of grain.

The analytical formulation does not take into account the additional bending moments owing to these masses and the consequent alterations in the dynamic response.

With reference to all configurations, for different type of input (i.e. sinusoidal and real earthquake record base excitation), the analytical formulation maintains its validity in the prediction of the value of the wall base bending moment even if the value of the base horizontal acceleration exceeds the value related to the limits of validity of the analytical formulation (see Eq. (40) of chapter 6), around 0.45 g for the case in exam.

With reference to all configurations, at different input frequencies and accelerations, the values of the experimental bending moment at the base of the silo are far lower than the values obtained using the Eurocode 8 provisions. Thus, it clearly seems that these provisions are overly conservative.

To analyze the silo response to real earthquake ground motion, Figure 8.8 represents the values of the experimental bending moment at the base of the silo for three different earthquakes, together with the predicted values for the first configuration. Again, the analytical theory represents a reasonable upper bound for all values of the experimental base bending moment. It is worth noticing that this is true also for the South Iceland earthquake (whose spectrum is reported in Figure 7.28), which represents the most demanding input for the considered system.

8.4 Critical considerations

This section offers an experimental verification (via shaking-table tests) of the analytical formulation proposed in chapter 6 on the actions induced by grain-like material on the wall of flat-bottom circular grain-silos. In more detail, the objective of the shaking-table tests was to investigate the effects of the pressures exerted by the grain on the silo wall, in order to compare them with the Eurocode 8 provisions and with the analytical formulation, which was developed with reference to an idealized model (the grain-like material is uncompressible) in idealized conditions (the silo is subjected to a time constant acceleration). Low-frequency sinusoidal input has been applied to meet at best the time

constant acceleration assumption of the theory. Also, earthquake inputs have been used to further investigate the seismic response.

The following concluding remarks containing preliminary but yet clear indications can be drawn from the experimental campaign:

1) The experimental results clearly indicate that the wall-grain friction coefficient strongly affects the experimental base bending moment. This does not match with Eurocode 8 prescriptions, which disregards the wall-grain friction coefficient. From a qualitative point of view, according to the analytical formulation, higher wall-grain friction coefficient leads to higher actions inside the wall, i.e. to higher value of the *effective mass*;
2) The values of the experimental bending moment at the base of the silo are far lower than the values obtained using the Eurocode 8 provisions, for both sinusoidal and earthquake inputs. Thus, it clearly seems that these provisions are overly conservative in the prediction of the *effective mass*.
3) On the other hand, the predicted values by the analytical formulation are in good agreement (either reasonable upper bound or good approximation) with the experimental results. Thus, it appears that the analytical formulation is able to give a reliable indications on the value of *effective mass*;
4) The analytical formulation maintains its validity in the prediction of the value of the wall base bending moment even if the values of the base horizontal acceleration exceed the value related to the limits of validity of the proposed analytical formulation.

Reference

Silvestri S, Gasparini G, Trombetti T, Foti D. On the evaluation of the horizontal forces produced by grain-like material inside silos during earthquakes. Bulletin of Earthquake Engineering 2012; 10:1535‑1560.

PART C: Research developed

Part C presents some refinements of the original analytical formulation for the estimation of the maximum lateral actions developed during an earthquake as well as an analytical formulation for the estimation of the fundamental period of vibration of flat-bottom circular grain-silos. Finally, the results of a preliminary on-field experimental campaign on a real silo structure are illustrated.

9. Refinements to the original theoretical formulation

In this chapter, the refinements to the original analytical formulation proposed by Prof. Trombetti and co-workers at the University of Bologna, in 2012, are presented. The refinements are performed by means of rigorous analytical developments and following the same logic organization of the original research work (Silvestri et al. 2012). Experimental shaking-table tests were performed on silo specimens (Silvestri et al. 2016), which showed good agreement with the proposed analytical formulations, even if some theoretical limits of validity were not satisfied. This has encouraged a complete revision and refinements of the theoretical framework. In detail, the static and the dynamic actions exchanged between different grain portions and between the grain and the silo wall are idealized in a more physically consistent way. The analytical developments are carried out by means of simple free-body dynamic equilibrium equations. The refinements yield to a significant extension of the theoretical limits of validity and to a new set of analytical formulas for the wall pressures and for the wall shear and bending moment. A comparison of the analytical formulas with (i) the consolidated Janssen formulation for static design of silos, (ii) the Trahair formulation, (iii) the Eurocode 8 provisions for seismic design of silos and (iv) the experimental results is also performed in order to (i) check the refined theoretical model in static conditions and (ii) verify the reliability of the different formulations in accelerated conditions, respectively. The refined analytical formulation confirms that the portion of ensiled material that interacts with the silo wall is significantly smaller than the *effective mass* suggested by Eurocode 8 provisions.

9.1 Problem formulation and basic assumptions

In the present section, the problem formulation and the basic assumptions considered within the framework of the refined analytical formulation are presented. The same idealized system adopted in the original analytical formulation (Silvestri et al. 2012) is considered and the set of assumptions refined. Refinements to the original analytical formulation are presented with the aim of developing a more rigorous, organic and physically consistent formulation. The main aims of the refinements are extend the limits of validity and improve the accuracy in the estimation of the wall pressures and of the shear and bending moment in the silo wall.

9.1.1 Idealized system

The same idealized system adopted in the original analytical formulation, as reported in chapter 6 (Silvestri et al. 2012) is considered.

9.1.2 Idealized conditions

The same idealized conditions considered in the original analytical formulation, as reported in chapter 6 (Silvestri et al. 2012) are taken into account.

9.1.3 Basic assumptions

In the present section, the basic assumptions referring to the refined analytical formulation are presented, highlighting those which are updated and/or modified with respect to the original analytical formulation.

As highlighted in the previous chapters, the original analytical formulation does not refer to a unique configuration, but it is rather relevant to an envelope of different configurations (as per assumption 11, see chapter 6). The original aim was to obtain conservative results.

The assumptions 1-10 are kept in order to simplify the current treatise. The main refinements deal with the following assumptions:

12. The perimeter of disk *D* on the horizontal plane is assumed to be a circumference also in accelerated conditions;
13. The role played by the vertical normal pressures $p_{v,GG}(z)$ is revolutionized, leading to a more consistent evaluation of the physical interaction between disk *D* and element *E*: vertical normal pressures $p_{v,GG}(z)$ are always assumed null inside element *E*.

Assumption 12 allows simplification of the analytical resolution of the equilibrium equation without introducing significant errors, considering that the boundary of the disk *D* can be reasonably approximated by a circumference, referred to as $C_D(z)$ (Figure 9.6). Assumption 13 actually replaces the aforementioned assumption 11 related to the original analytical formulation. Therefore, no limit conditions have to be considered. The grain-

wall pressures $p_{h,GW}(z,\vartheta)$ do not derive as the sum of the two contributions described in chapter 6, but they result from the plain dynamic equilibrium equations of disk *D* and element *E* written with reference to a unique self-consistent physical idealized model.

Figure 9.1 shows the idealized subdivision of the ensiled grain on the vertical and horizontal sections for the refined analytical formulation. Figure 9.2 shows the pressures distribution acting on the grain and on the wall in accelerated conditions according to the new idealized model of the refined analytical formulation in accelerated conditions. Figure 9.3 proposes a brief overview of the models here analyzed in terms of internal subdivision of the grain and of pressures distribution.

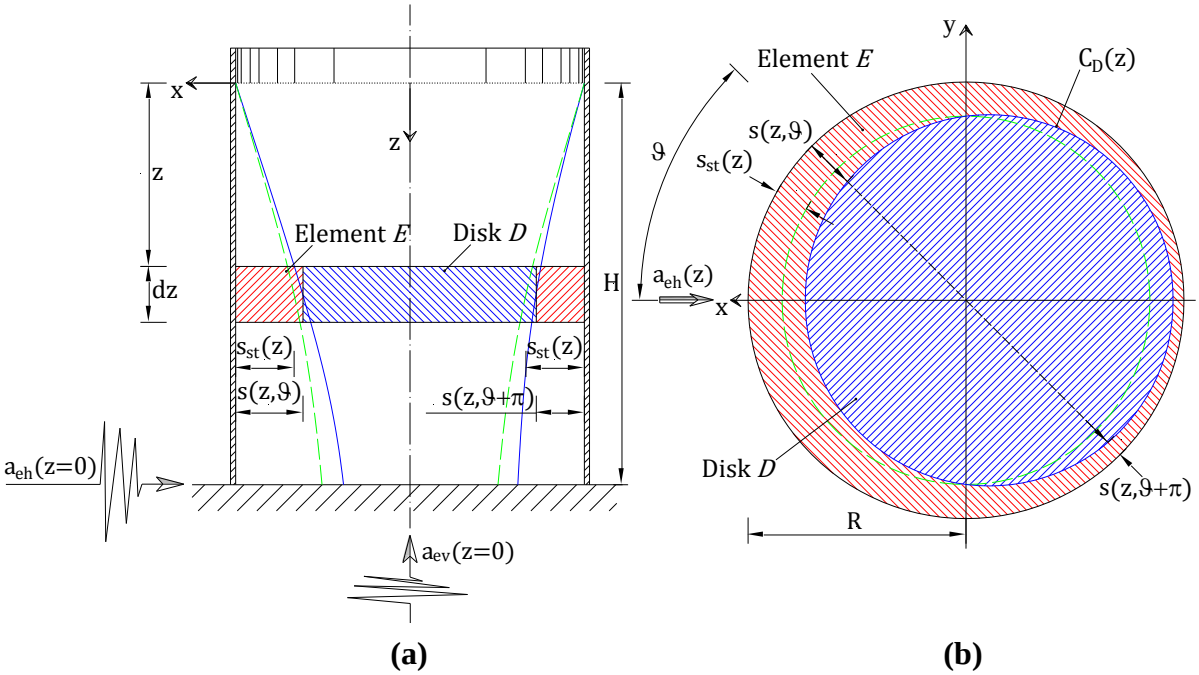

Figure 9.1 - External torus (red hatching) and internal disk (blue hatching) of the grain layer. (a) Vertical section, (b) plain view.

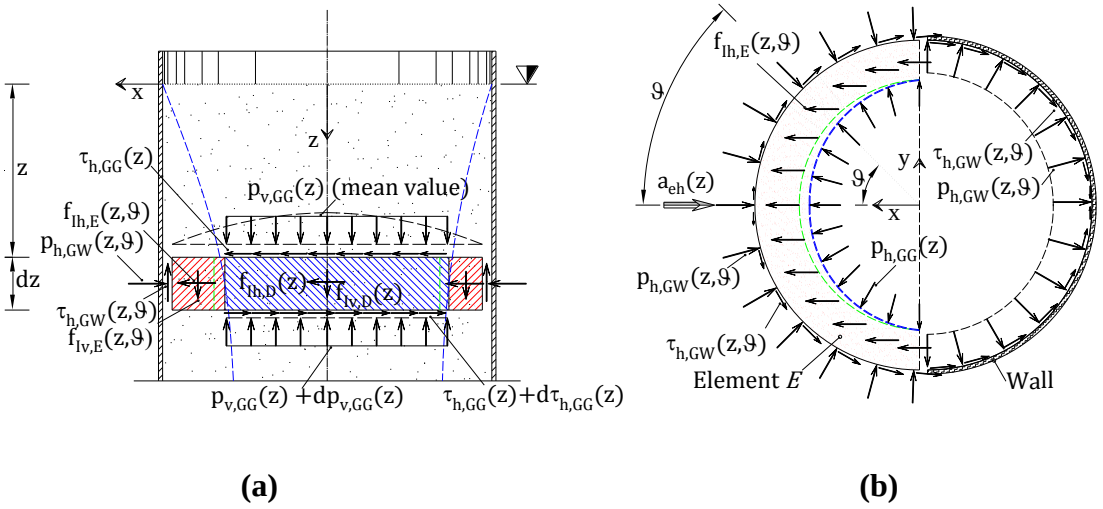

Figure 9.2 - Physical idealized model for the refined theory for accelerated conditions. (a) Vertical cross-section. The forces are referred to the grain. (b) Horizontal cross-section. On the left the forces are referred to the grain, on the right to the wall.

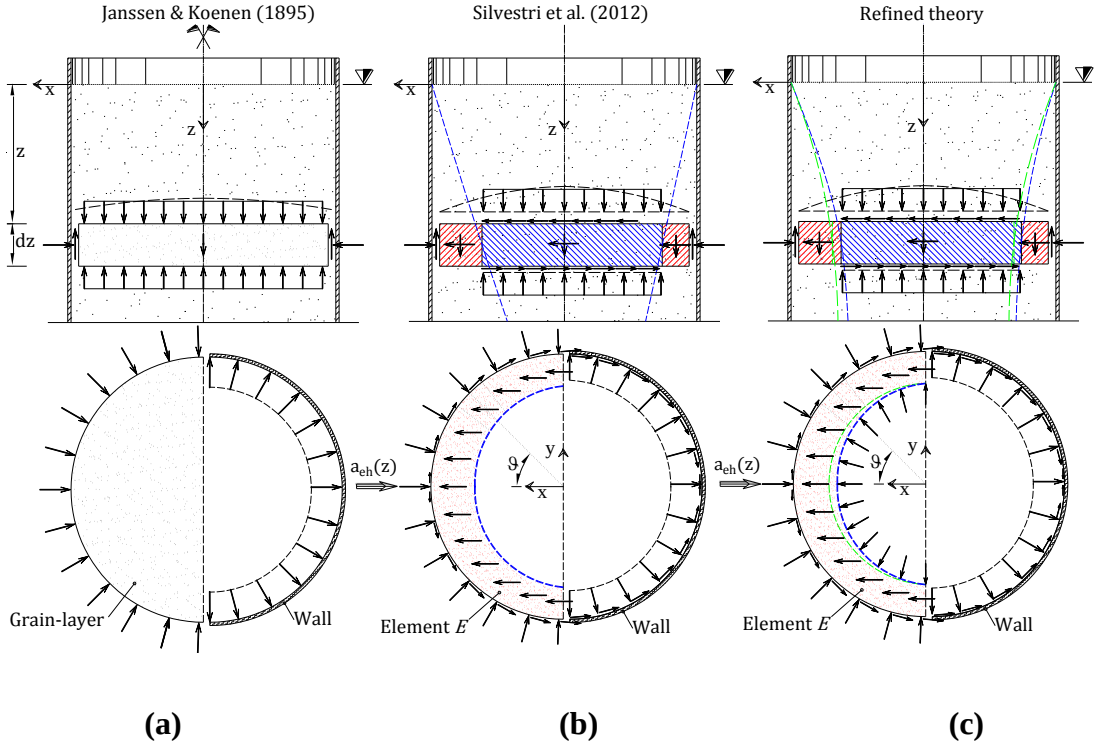

Figure 9.3 - Visual comparison of the physical idealized models. On the first line the vertical cross-section. On the second line the horizontal cross-section. (a) Janssen (1895)theory for static conditions, (b) the original analytical formulation (Silvestri et al. 2012) and (c) the refined analytical formulation under accelerated conditions.

9.2 Dynamic equilibrium in accelerated conditions

In this section, the analytical study of the dynamic behavior of silos containing grain-like material is developed according to the refined theoretical framework. As performed in the original analytical formulation, the equilibrium in accelerated conditions accounts for the additional dynamic effects generated by the two time-constant accelerations components $a_{ev}(z)$ and $a_{eh}(z)$, respectively along the horizontal and the vertical directions. Then, through simple plain dynamic equilibrium equations, pressure distributions exchanged between silo and grain are analytically defined, following the same logic organization of the original research work (Silvestri et al. 2012). Then, as derivative results, base wall shear and bending moment are calculated by means of opportune integrations.

9.2.1 Unknown quantities and equations at disposal

The unknown quantities of the problem are represented by the pressure distributions and the thickness $s(z,\vartheta)$ of the external torus *E*, as considered within the original theoretical framework. A detailed description of such quantities may be found in chapter 6. The direction of the horizontal acceleration (towards *x*) is rotated by an angle ϑ on the horizontal plane compared to the direction perpendicular to the external vertical surface of element *E*.

Figure 9.4 and Figure 9.5 show the mutual action that disk *D*, element *E* and the silo wall exchange in accelerated conditions. For sake of comparison, the same notation and the same conceptual structure followed in the original analytical formulation (Silvestri et al. 2012) is here adopted for the analytical development of the refined analytical formulation.

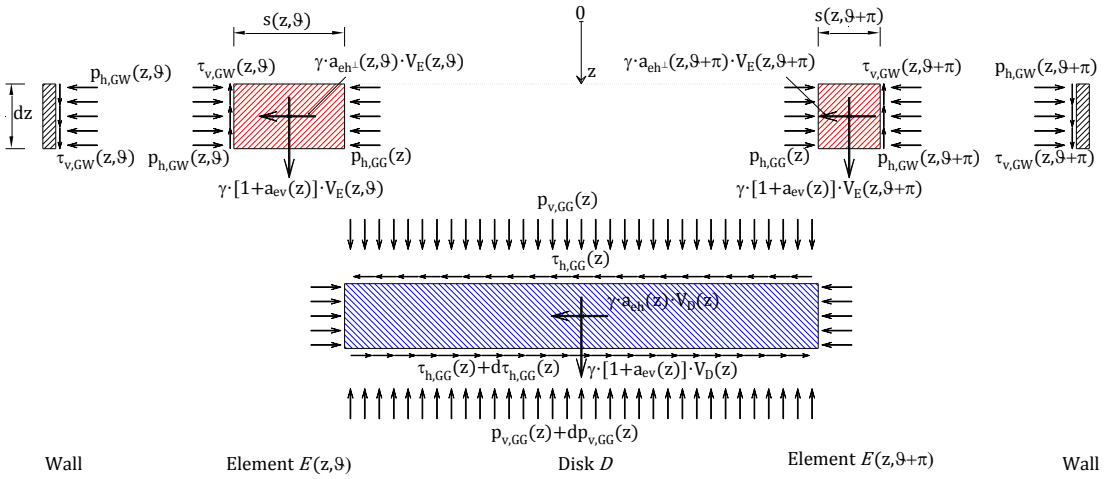

Figure 9.4 - Vertical and horizontal actions operating on disk D and element E

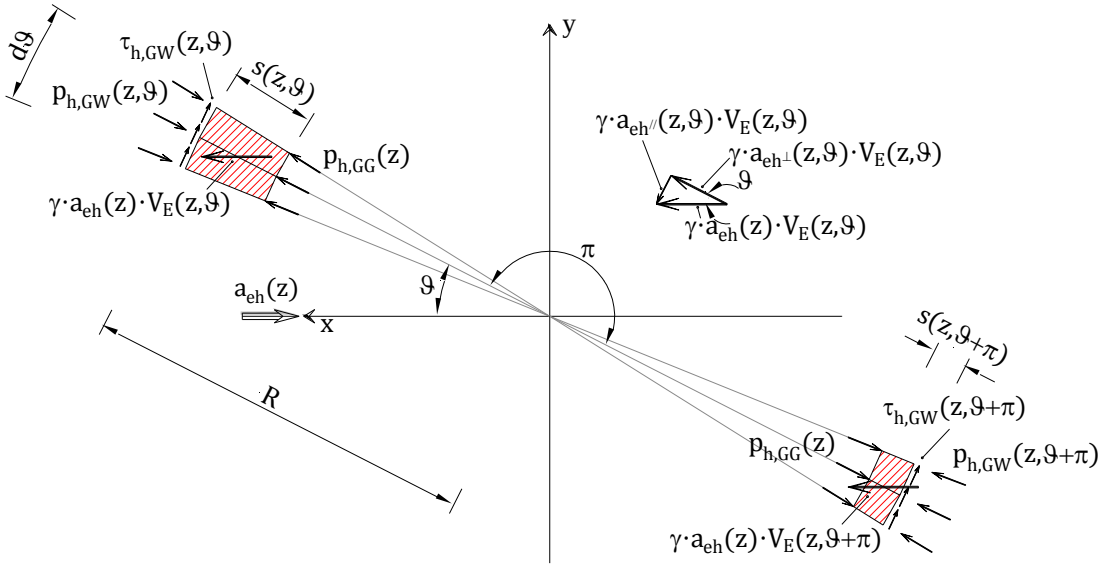

Figure 9.5 - Horizontal cross-section: horizontal actions operating on an elementary sector of the element E

9.2.2 Vertical force equilibrium of disk *D*

Vertical forces equilibrium of disk *D* in dynamic conditions provides:

$$p_{v,GG}(z)\cdot A_D(z)+f_{Iv,D}(z)-p_{v,GG}(z+dz)\cdot A_D(z)=0 \qquad (1)$$

where $A_D(z)=\int_0^{2\pi}\int_0^{r(z,\vartheta)} r(z,\vartheta)\cdot dr\cdot d\vartheta$ is the surfaces of the disk, $f_{Iv,D}(z)=\gamma\cdot\left[1+a_{ev}(z)\right]\cdot V_D(z)$ is the vertical inertial force of the disk, $V_D(z)=A_D(z)\cdot dz$ is

the volume of the disk and clearly $p_{v,GG}(z+dz) = p_{v,GG}(z) + dp_{v,GG}(z)$. Then, Eq. (1) leads to:

$$dp_{v,GG}(z) = \gamma \cdot \left[1 + a_{ev}(z)\right] \cdot dz \tag{2}$$

Integrating Eq. (2) gives:

$$p_{v,GG}(z) = \gamma \cdot \int_0^z \left[1 + a_{ev}(z)\right] \cdot dz + C_1 \tag{3}$$

where C_1 is a constant of integration that can be obtained imposing the boundary condition (on the top surface of the grain the vertical pressures are null, i.e. $p_{v,GG}(z=0) = 0$).

9.2.3 Pressure ratio relationship between vertical and horizontal grain-grain pressures

If λ is the pressure ratio of the grain-like material, the following relationship holds between vertical and horizontal pressures inside the grain:

$$p_{h,GG}(z) = \lambda \cdot p_{v,GG}(z) \tag{4}$$

9.2.4 Horizontal (radial) forces equilibrium of disk *D*

In accelerated conditions, it is supposed that disk *D* changes its shape and area, since $C_D(z)$ deforms. In this scenario, the local center of curvature of each point holding to $C_D(z)$ refers to a new pole (point O'), which differs from the center of the circular section (*O* point). Figure 9.6a and b represent and compare the disk *D* and its contour $C_D(z)$ in static and accelerated conditions, respectively. Auxiliary radius $r^*(z,\vartheta)$ and auxiliary latitude $\Omega(z,\vartheta)$ describe the position of each point holding to $C_D(z)$ with reference to the new local center of curvature O'. Due to the lack of axial-symmetry, horizontal pressures $p_{h,GG}(z)$ acting orthogonally on $A_{D,v}(z)$ produce a non-null horizontal force $R_{h,GG}(z)$.

Consequently, the horizontal forces equilibrium of disk *D* is here expressed with reference to the *x* axis, according to the ground motion direction, and leads to:

$$\tau_{h,GG}(z,\vartheta)\cdot A_D(z)+f_{Ih,D}(z)+R_{h,GG}(z)-\tau_{h,GG}(z+dz,\vartheta)\cdot A_D(z)=0 \tag{5}$$

where $f_{Ih,D}(z)=\gamma\cdot a_{eh}(z)\cdot V_D(z)$ represents the horizontal inertial force acting on disk *D*, $R_{h,GG}(z)=\int_0^{2\pi} p_{h,GG}(z)\cdot\cos\left(\Omega(z,\vartheta)\right)\cdot dA_{D,v}(z,\vartheta)$ is the resultant of the projections along the *x* axis of the horizontal grain-grain pressures acting orthogonally on contour $C_D(z)$, in which $dA_{D,v}(z,\vartheta)=r^*(z,\vartheta)\cdot d\Omega(z,\vartheta)\cdot dz$ is the infinitesimal portion of the lateral vertical surface of disk *D*, $p_{h,GG}(z)\cdot dA_{D,v}(z,\vartheta)$ is the elementary horizontal force exchanged between disk *D* and element *E* on such surface, whilst function $\cos\left(\Omega(z,\vartheta)\right)$ evaluates the projection of each mutual action on the *x* axis (Figure 9.6*b*).

By accounting assumption 12, the resultant $R_{h,GG}(z)$ can be neglected and Eq. (5) can be simplified as follows:

$$d\tau_{h,GG}(z,\vartheta)=\gamma\cdot a_{eh}(z)\cdot dz \tag{6}$$

Integrating Eq. (6) gives:

$$\tau_{h,GG}(z,\vartheta)=\tau_{h,GG}(z)=\gamma\cdot\int_0^z a_{eh}(z)\cdot dz+C_2 \tag{7}$$

where C_2 is a constant of integration that can be obtained imposing the boundary condition (on the top surface of the grain the frictional stresses are null, i.e. $\tau_{h,GG}(z=0)=0$).

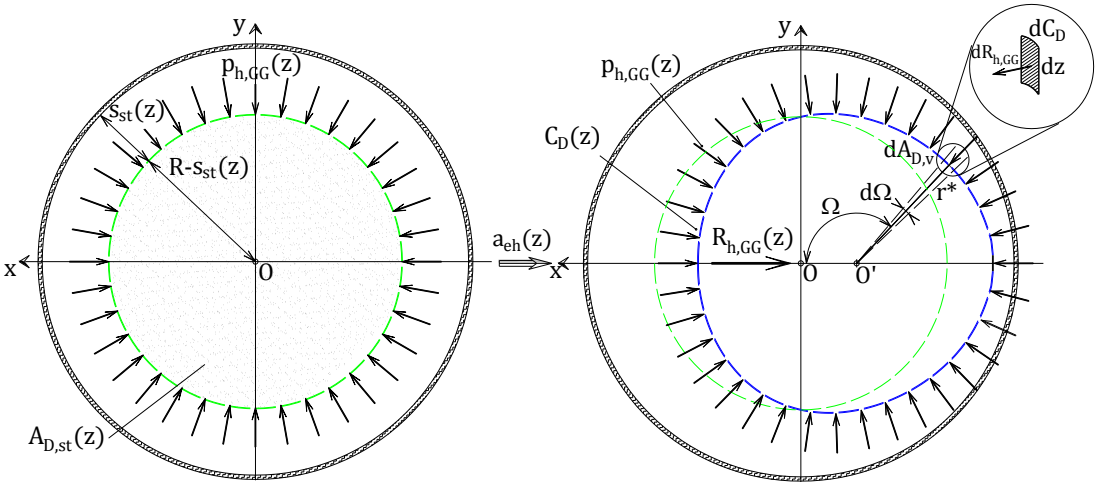

(a) **(b)**

Figure 9.6 - Thickness of the hang material on the silo wall and grain-grain pressure distribution on the lateral surface of disk D in static (a) and accelerated conditions (b).

9.2.5 Friction law for the boundary between element E and the silo wall

If μ_{GW} is the friction coefficient of the grain-wall contact surface, the following relationship holds between the normal pressures and the vertical shear stresses along the contact surface between the grain of element *E* and the silo wall:

$$\tau_{v,GW}(z,\theta) = \mu_{GW} \cdot p_{h,GW}(z,\theta) \tag{8}$$

9.2.6 Vertical and horizontal (radial) forces equilibrium of element *E*

Equilibrium of the external torus *E* refers to an elementary portion $E(z,\vartheta)$ included into an infinitesimal angle $d\vartheta$, thickness *dz*, for generic height *z* and radial direction ϑ. Vertical forces equilibrium equation means:

$$f_{Iv,E}(z,\vartheta) - \tau_{v,GW}(z,\vartheta) \cdot A_{E,Ext}(z,\vartheta) = 0 \tag{9}$$

where $f_{Iv,E}(z,\vartheta) = \gamma \cdot [1 + a_{ev}(z)] \cdot V_E(z,\vartheta)$ represents the vertical inertial force acting on $E(z,\vartheta)$, $V_E(z,\vartheta) = \left(R - \frac{s(z,\vartheta)}{2}\right) \cdot s(z,\vartheta) \cdot d\vartheta \cdot dz$ expresses the volume of $E(z,\vartheta)$ and

$A_{E,Ext}(z,\vartheta) = R \cdot d\vartheta \cdot dz$ refers to the vertical lateral surface of $E(z,\vartheta)$ in contact with the wall. Therefore, Eq. (9) provides:

$$\tau_{v,GW}(z,\vartheta) \cdot R = \gamma \cdot \left[1 + a_{ev}(z)\right] \cdot \left(R - \frac{s(z,\vartheta)}{2} \right) \cdot s(z,\vartheta) \tag{10}$$

Horizontal forces equilibrium equation of element $E(z,\vartheta)$ means:

$$p_{h,GG}(z) \cdot A_{E,Int}(z,\vartheta) + f_{Ih,E}(z,\vartheta) - p_{h,GW}(z,\vartheta) \cdot A_{E,Ext}(z,\vartheta) = 0 \tag{11}$$

where $f_{Ih,E}(z,\vartheta) = \gamma \cdot a_{eh\perp}(z,\vartheta) \cdot V_E(z,\vartheta)$ represents the horizontal inertia force acting on $E(z,\vartheta)$, $a_{eh\perp}(z,\vartheta) = a_{eh}(z) \cdot \cos\vartheta$ is the portion of horizontal acceleration on the radial direction and $A_{E,Int}(z,\vartheta) = \left[R - s(z,\vartheta)\right] \cdot d\vartheta \cdot dz$ provides the vertical lateral surface of $E(z,\vartheta)$ in contact with disk *D*. Eq. (11) leads to:

$$p_{h,GW}(z,\vartheta) \cdot R = p_{h,GG}(z) \cdot \left[R - s(z,\vartheta)\right] + \gamma \cdot a_{eh\perp}(z,\vartheta) \cdot \left(R - \frac{s(z,\vartheta)}{2} \right) \cdot s(z,\vartheta) \tag{12}$$

Coupling the Eqs. (8), (10) and (11) together, the system of Equations (13) describing the general forces equilibrium of an elementary portion $E(z,\vartheta)$ results:

$$\begin{cases} \tau_{v,GW}(z,\vartheta) = \mu_{GW} \cdot p_{h,GW}(z,\vartheta) \\ \tau_{v,GW}(z,\vartheta) \cdot R = \gamma \cdot \left[1 + a_{ev}(z)\right] \cdot \left(R - \dfrac{s(z,\vartheta)}{2} \right) \cdot s(z,\vartheta) \\ p_{h,GW}(z,\vartheta) \cdot R = p_{h,GG}(z) \cdot \left[R - s(z,\vartheta)\right] + \gamma \cdot a_{eh\perp}(z,\vartheta) \cdot \left(R - \dfrac{s(z,\vartheta)}{2} \right) \cdot s(z,\vartheta) \end{cases} \tag{13}$$

After some calculations, this system of equation provides the closed-form expressions of $p_{h,GW}(z,\vartheta)$ and $s(z,\vartheta)$.

As far as the horizontal pressures exerted by the grain on the silo wall is concerned, it is possible to obtain:

$$p_{h,GW}(z,\vartheta)=\frac{p_{h,GG}(z)}{\beta(z,\vartheta)}\cdot\frac{R-s(z,\vartheta)}{R} \tag{14}$$

where $\beta(z,\vartheta)=1-\mu_{GW}\cdot\nu(z)\cdot a_{eh}(z)\cdot\cos\vartheta$ and $\nu(z)=\frac{1}{1+a_{ev}(z)}$. Eq. (14) expresses the pressures exchanged between grain and silo wall.

As far as the thickness of the grain which is sustained by the wall is concerned, the following complete quadratic equation in $s(z,\vartheta)$ is obtained:

$$\begin{aligned}&\gamma\cdot\left(R-\frac{s(z,\vartheta)}{2}\right)\cdot s(z,\vartheta)=\\&=\mu_{GW}\cdot\nu(z)\cdot\left\{p_{h,GG}(z)\cdot\left[R-s(z,\vartheta)\right]+\gamma\cdot a_{eh\perp}(z,\vartheta)\cdot\left(R-\frac{s(z,\vartheta)}{2}\right)\cdot s(z,\vartheta)\right\}\end{aligned} \tag{15}$$

Further developments leads to the closed-form of the solution for Eq. (25). Just considering that the thickness $s(z,\vartheta)$ cannot be larger than the silo radius *R*, the solution with physical meaning is the following (with $-$ sign):

$$s(z,\vartheta)=\frac{\mu_{GW}\cdot\nu(z)\cdot p_{h,GG}(z)+\gamma\cdot R\cdot\beta(z,\vartheta)-\sqrt{\left[\mu_{GW}\cdot\nu(z)\cdot p_{h,GG}(z)\right]^2+\left[\gamma\cdot R\cdot\beta(z,\vartheta)\right]^2}}{\gamma\cdot\beta(z,\vartheta)} \tag{16}$$

Eq. (16) provides the thickness of the grain layer that leans against the silo wall.

9.2.7 Horizontal (tangential) forces equilibrium of element *E*

Horizontal (tangential) forces equilibrium of element E provides:

$$\gamma\cdot a_{eh||}(z,\vartheta)\cdot V_E(z,\vartheta)-\tau_{h,GW}(z,\vartheta)\cdot A_{E,Ext}(z,\vartheta)=0 \tag{17}$$

where $a_{eh||}(z,\vartheta)=a_{eh}(z)\cdot\sin\vartheta$ represents the component of the horizontal acceleration $a_{eh}(z)$ parallel to the external vertical surface of element $E(z,\vartheta)$. Thus Eq. (17) leads to:

$$\tau_{h,GW}(z,\vartheta)\cdot R=\gamma\cdot a_{eh}(z)\cdot\sin\vartheta\cdot\left[R-\frac{s(z,\vartheta)}{2}\right]\cdot s(z,\vartheta) \tag{18}$$

9.3 Specialization to the case of constant vertical profiles of both the vertical and the horizontal earthquake accelerations

In the present section, the refined analytical formulations describing the pressure distributions and thickness of external torus *E* are specialized for the case of constant vertical profiles of both the vertical and the horizontal accelerations. In detail, the following assumptions are made:

- constant vertical acceleration along the height of the silo, $a_{ev}(z) = a_{ev0}$;
- constant horizontal acceleration along the height of the silo, $a_{eh}(z) = a_{eh0}$.

Equation (3) specializes as follows:

$$p_{v,GG}(z) = \gamma \cdot \left[1 + a_{ev0}\right] \cdot z \tag{19}$$

Equation (4) specializes as follows:

$$p_{h,GG}(z) = \lambda \cdot \gamma \cdot \left[1 + a_{ev0}\right] \cdot z \tag{20}$$

Equation (7) specializes as follows:

$$\tau_{h,GG}(z) = \gamma \cdot z \cdot a_{eh0} \tag{21}$$

Equation (14) specializes as follows:

$$p_{h,GW}(z,\vartheta) = \frac{p_{h,GG}(z)}{\beta_0(\vartheta)} \cdot \frac{R - s(z,\vartheta)}{R} \tag{22}$$

where $\nu_0 = \dfrac{1}{1 + a_{eh0}}$.

Equation (16) specializes as follows:

$$s(z,\vartheta) = \frac{\omega(z) + R \cdot \beta_0(\vartheta) - \sqrt{\omega(z)^2 + R^2 \cdot \beta_0(\vartheta)^2}}{\beta_0(\vartheta)} \tag{23}$$

where $\omega(z) = \mu_{GW} \cdot \lambda \cdot z$ and $\beta_0(\vartheta) = 1 - \mu_{GW} \cdot \nu_0 \cdot a_{eh0} \cdot \cos\vartheta$.

Equation (18) specializes as follows:

$$\tau_{h,GW}(z,\vartheta) \cdot R = \gamma \cdot a_{eh0} \cdot \sin\vartheta \cdot \left[R - \frac{s(z,\vartheta)}{2}\right] \cdot s(z,\vartheta) \tag{24}$$

9.4 Specialization to the case of null vertical and horizontal earthquake accelerations: the static case

A further formulation concerning the silo-grain interaction in static conditions is here obtained for the refined analytical formulation. By considering null vertical and horizontal accelerations inside Eq. (22) and Eq. (23), the horizontal pressures $p_{h,GW,st}(z,\vartheta)$ on the wall and the thickness $s_{st}(z)$ result:

$$p_{h,GW,st}(z) = \lambda \cdot \gamma \cdot z \cdot \frac{\sqrt{\omega(z)^2 + R^2} - \omega(z)}{R} \tag{25}$$

$$s_{st}(z) = \omega(z) + R - \sqrt{\omega(z)^2 + R^2} \tag{26}$$

9.5 Portion of grain relative to the behavior under accelerated conditions

Equation (23) provides the thickness $s(z,\vartheta)$ of the portion of grain that actually interacts and pushes on the silo wall in accelerated conditions. Therefore, two volumes arise inside the whole granular content, characterized by different dynamic behavior: $V_{E,dyn}(z)$ and $V_{D,dyn}(z)$. The former individuates the amount of grain that is completely sustained by the lateral silo wall, whilst the latter is the amount of grain leaning against the lower portion of the material up to the silo foundation without interacting with the silo wall.

From a geometrical point of view, $V_{E,dyn}(z)$ and $V_{D,dyn}(z)$ can be respectively visualized as a vertical-axis cylindrical annulus with thickness $s(z,\vartheta)$ and a vertical-axis truncated cone solid of radius $r(z,\vartheta) = R - s(z,\vartheta)$.

From a mathematical point of view, the volumes occupied by the disk *D* and element *E* are expressed as follows:

$$V_{D,dyn}(z) = \pi R^2 H - \frac{1}{2} \cdot \int_0^z \left(\int_0^{2\pi} \left[2R \cdot s(z,\vartheta) - s(z,\vartheta)^2 \right] \cdot d\vartheta \right) \cdot dz \tag{27}$$

$$V_{E,dyn}(z) = \frac{1}{2} \cdot \int_0^z \left(\int_0^{2\pi} \left[2R \cdot s(z,\vartheta) - s(z,\vartheta)^2 \right] \cdot d\vartheta \right) \cdot dz \tag{28}$$

Mathematical integration of both Eqs. (27) and (28) involves many difficulties. Thus, a handy closed-form cannot be now provided. It has to be noted that the quantities expressed by integrals inside these equations represent positive values and the sum of $V_{D,dyn}(z)$ and $V_{E,dyn}(z)$ corresponds to the volume V of the whole ensiled content (where $V = \pi R^2 H$), satisfying the mass balance.

9.6 Limits of validity of the proposed analytical formulation

In this section a significant extension of the limits of validity of the original theory is provided. Limitations are defined by the mathematical definition of some physical quantities related to the solution $s(z,\vartheta)$ and to the friction laws on the contact surfaces considered:

- In order to avoid the loss of significance of the equilibrium equations, the vertical downward acceleration must not annihilate the gravity acceleration, so that the ensiled content is not uplifted. This leads to:

$$\nu_0 > 0 \tag{29}$$

- By referring to Eq. (23), in order to not have infinite values of the thickness $s(z,\vartheta)$, it necessary that:

$$\beta_0(\vartheta) \neq 0 \tag{30}$$

- It is necessary that portion $V_{D,dyn}(z)$ exists. This physical condition is rendered into the following mathematical limitation over all the height z:

$$s(z,\vartheta) < R, \forall \vartheta, \forall z \in [0, H] \tag{31}$$

which, taking into account Eq. (23), results in a condition on the function $\beta_0(\vartheta)$, expressed as:

$$\beta_0(\vartheta)^2 > 0 \tag{32}$$

- It is also necessary that portion $V_{E,dyn}(z)$ exists. This physical condition translates into the following mathematical limitation (with exception for $z = 0$):

$$s(z,\vartheta) > 0, \forall\, \vartheta, \forall z \in (0, H] \tag{33}$$

which, taking into account Eq. (23), results in a condition on the function $\beta_0(\vartheta)$, expressed as:

$$\beta_0(\vartheta) > 0 \tag{34}$$

The condition expressed by Eq. (33) is evaluated with reference of the latitudes on which the earthquake ground motion imposes the highest and the lowest effects (i.e. $\vartheta = 0$ and $\vartheta = \pi$), it follows that:

$$a_{eh0} < \frac{1}{\mu_{GW} \cdot \nu_0} \tag{35}$$

$$a_{eh0} > -\frac{1}{\mu_{GW} \cdot \nu_0} \tag{36}$$

Granted that the x axis is oriented in accordance with the verso of the inertial horizontal forces, a_{eh0} clearly expresses a positive value (i.e. a modulus) leading to $a_{eh0} > 0$ in accelerated conditions. Then, Eq. (35) results implicitly satisfied. In the light of above, the condition expressed by Eqs. (30) and (32) is already encompassed in the condition expressed by Eq. (33), which leads only to the condition expressed by Eq. (34).

- In order to prevent any horizontal sliding of the grain on the lower layers and on the bottom of the silo (Assumption 7), it is necessary that the horizontal acceleration is lower than the following limiting value:

$$a_{eh0} \leq \frac{\min\{\mu_{GG}, \mu_{GB}\}}{\nu_0} = \frac{\mu_{GB}}{\nu_0} \tag{37}$$

It worth noticing that, according to the physical idealization adopted by the proposed analytical formulation, horizontal sliding of the top grain layers cannot be avoided, even for low horizontal acceleration.

In the light of above, Eqs. (29), (35) and (37) represent restrictions on the vertical and horizontal accelerations acting on the silo. The most critical limitation on the slenderness ratio, which affects the original analytical formulation, is not detected in the refined analytical formulation. Eq. (35) is the same limitation obtained for the original analytical formulation, Eq. (37) represents a refinement of a precedent condition. For sake of clarity, the limitation provided by Eq. (29), implicitly required in the original analytical formulation, is taken into account.

According to Arnold et al. (1980) and Woodcock and Mason (1988), the grain-wall and the grain-bottom friction coefficients result always lower than the grain-grain friction coefficient. Therefore, the restriction provided by Eq. (37) can consider only the grain-bottom friction coefficient. The shearing failure in the particulate material (i.e. horizontal sliding on the lower layers) will potentially occur at the base, as also noted by Rotter and Hull (1989) and Veletsos and Younan (1998*a*).

By assuming similar grain-wall and grain-bottom friction coefficients and taking into account that friction coefficients are lower than unit, under equal vertical accelerations, the restriction provided by Eq. (37) results always more stringent than that provided by Eq. (35). Figure 9.7 represents the admitted horizontal acceleration as function of the vertical acceleration factor ν_0 for three different grain-wall friction coefficients μ_{GW} according to Eq. (35) and to Eq. (37).

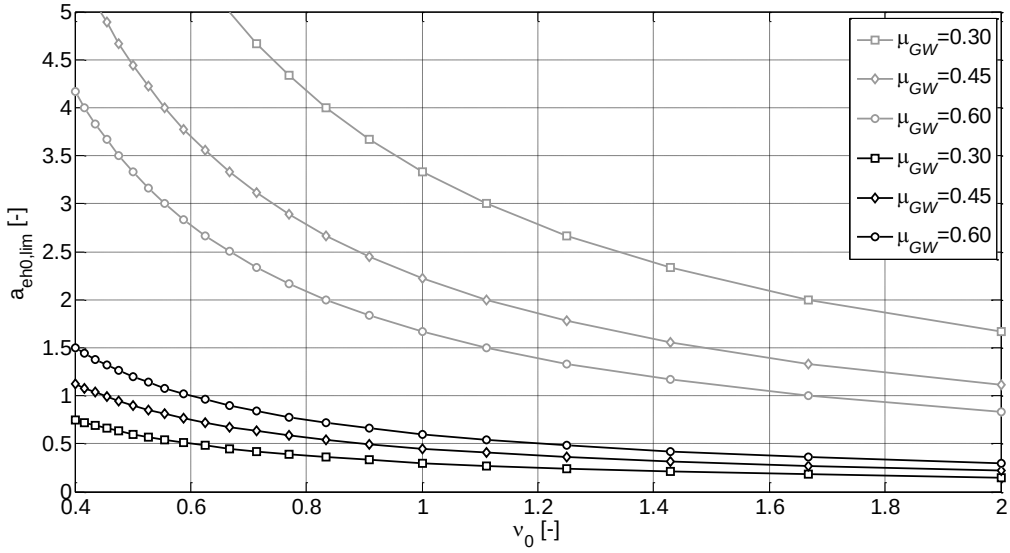

Figure 9.7 - Trend of the admitted horizontal acceleration as function of the vertical acceleration factor for three different grain-wall friction coefficients according to Eq. (35) (grey line) and to Eq. (37) (black line)

9.7 The shear forces and the bending moments on the silo wall

In the present section, the wall shear and the wall bending moment acting on the shell of the silo exposed to seismic excitation are discussed.

Silos and revolution surfaces in general are structures characterized by high values of vertical and horizontal stiffness, where an eventual dynamic amplification strongly depends on the frequency features of the input provided by the earthquake ground motion at their bases.

The shear action on the silo wall is given by the integral, on the lateral surface of the silo, of the projection of the grain-wall normal pressures $p_{h,GW}(z,\vartheta)$ and horizontal frictional stresses $\tau_{h,GW}(z,\vartheta)$ towards *x* (namely, along the direction of the horizontal acceleration):

$$T_{xx}(z)=\frac{1}{2}\gamma\cdot a_{eh0}\cdot\int_0^z\left(\int_0^{2\pi}\left[2R\cdot s(z,\vartheta)-s(z,\vartheta)^2\right]\cdot d\vartheta\right)\cdot dz \tag{38}$$

Eq. (38) shows that the wall shear $T_{xx}(z)$ balances the horizontal inertial force of element *E* at each quote *z*, i.e. the mass of the external torus times the constant horizontal acceleration, thus defining the grain corresponding to the *effective mass* for the refined analytical formulation.

By considering the value of the wall shear at the silo base, i.e. for *z*= *H* and by dividing Eq. (37) for the value of the horizontal inertial action of the whole ensiled content equal to $a_{eh0}\cdot\gamma\cdot\pi HR^2$, the expression of the *effective mass* m_{eff} for the refined analytical formulation may be computed:

$$m_{eff}=\frac{1}{2}\cdot\frac{\int_0^H\left(\int_0^{2\pi}\left[2R\cdot s(z,\vartheta)-s(z,\vartheta)^2\right]\cdot d\vartheta\right)\cdot dz}{\pi HR^2} \tag{39}$$

The bending moment on the silo wall $M_{yy}(z)$ (namely, along the horizontal direction perpendicular to the earthquake) results as the sum of the two contributions: $M_{yy,1}(z)$ and $M_{yy,2}(z)$. The former derives from the integration of the wall shear $T_{xx}(z)$ along the height of the silo; the latter derives from the integration, on the lateral surface of the wall, of the frictional vertical stresses $\tau_{v,GW}(z,\vartheta)$ multiplied by the correspondent lever

arm with respect to the horizontal direction perpendicular to the earthquake ground motion (namely along the *y*-axis).

$$\begin{aligned} M_{yy}(z) &= M_{yy,1}(z) + M_{yy,2}(z) \\ M_{yy,1}(z) &= \frac{1}{2}\gamma \cdot a_{eh0} \cdot \int_0^z \left\{ \int_0^z \left[\int_0^{2\pi} \left(2R \cdot s(z,\vartheta) - s(z,\vartheta)^2 \right) \cdot d\vartheta \right] \cdot dz \right\} \cdot dz \\ M_{yy,2}(z) &= \int_0^z \int_0^{2\pi} \tau_{v,GW}(z,\vartheta) \cdot R^2 \cdot \cos\vartheta \cdot d\vartheta \cdot dz \end{aligned} \tag{40}$$

The contribution of the frictional vertical stresses to the wall bending moment was neglected in the original analytical formulation. Similarly, it is now taken into account for the estimation of the wall base bending moment according to the original analytical formulation. For value of $\beta_0(\vartheta = 0) \le 0.50$, the expression of the wall base bending moment provided by Eq. (45) in chapter 6 can be expressed with the following formulation:

$$M_{yy,completed} = a_{eh0} \cdot \gamma \cdot \pi R H^2 \cdot \left(\frac{\lambda \cdot \mu_{GW}}{\sqrt{1 - \nu_0^{\,2} \cdot \mu_{GW}^{\,2} \cdot a_{eh0}^{\,2}}} \right) \cdot \left(\frac{H}{3} + \mu_{GW} \cdot \frac{R}{2} \right) \tag{41}$$

In contrast with the formulations by Trahair et al. (1983), Younan and Veletsos (1998), and the original analytical formulation by Silvestri et al. (2012), the refined analytical formulation leads to a *rotational effective mass* (responsible for the base bending moment) greater than the *effective mass* (responsible for the base shear). This is due to the contribution of the frictional vertical stresses and becomes clear by analyzing Eqs. (38) and (40).

9.8 Graphic representations of pressures, grain portions interacting with the silo and wall actions

In the present section a brief comparison between the Janssen (1895) theory with the original analytical formulation, the refined analytical formulation, the Trahair formulation and the Eurocode 8 (EN 1998-4:2006) provisions is presented by means of applicative examples.

The comparison is carried out in terms of grain-wall pressures, wall shear and wall bending moment in both static and accelerated conditions (assuming a constant vertical

profile for both the horizontal and vertical accelerations). It is anticipated that, in some cases, the cases analyzed may be beyond the limits of validity of the original formulation in terms of limiting slenderness ratio. Despite that, for sake of comparison with the other analytical formulations, grain-wall pressures, wall shear and wall bending moment under accelerated conditions are presented.

9.8.1 On the static pressures

In the previous sections, three different analytical formulation grounded on distinct idealized physical models and assumptions have been presented for the evaluation of the grain-wall pressures in static conditions (i.e. null value of the horizontal and vertical accelerations).

In this section, the along-the-height profiles of the grain-wall pressures provided by the Janssen (1895) theory, the original analytical formulation and the refined analytical formulation are compared. Figure 9.8 reports the pressures profiles for three steel silos with "smooth" wall (Wall Surface Categories D2 according to Table 4.1 provisions of EN 1991-4:2006) characterized by *R*= 10 *m* and different slenderness ratios $\Delta = \frac{H}{d_c}$ (squat $\Delta = 1.0$, intermediate-slender $\Delta = 2.0$ and slender $\Delta = 4.0$ in accordance EN 1991-4:2006 provisions) containing wheat characterized by the following physic and frictional parameter and by $\gamma_b = 9000\, N/m^3$, $\mu_{GW} = 0.38$, and $\lambda = 0.54$ (according to Table E.1 of EN 1991-4:2006 provisions). An horizontal free grain surface is considered, with a height above the silo base of the ensiled grain-like material $H = h_b$. The grain-wall pressures are normalized with respect to the base horizontal geostatic grain-grain pressure, i.e. $\gamma \cdot \lambda \cdot h_b$.

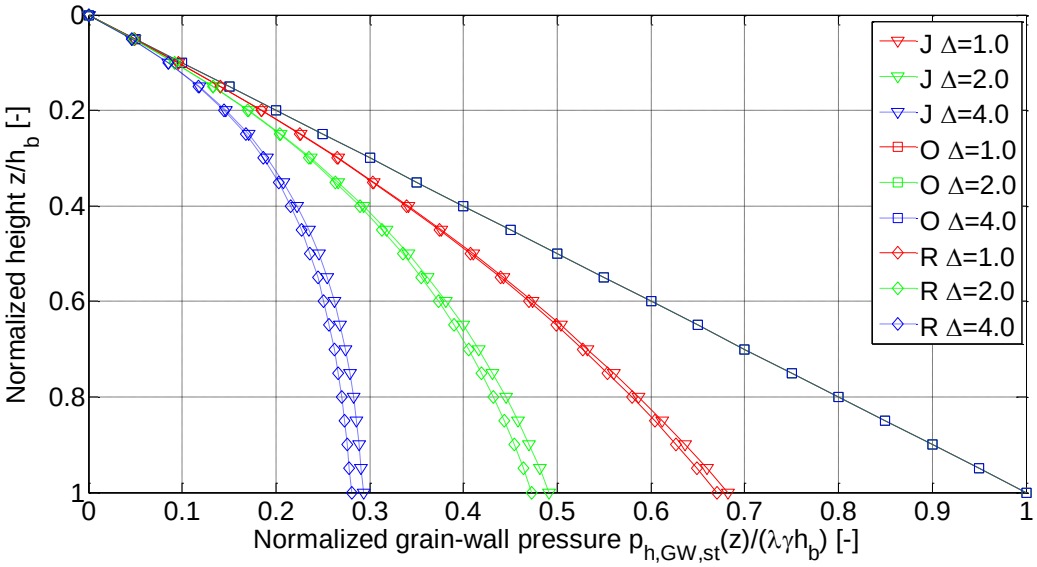

Figure 9.8 - Heightwise variation of the normalized grain-wall normal pressures for Janssen (J), the Original analytical formulation (O) and the Refined analytical formulation (R) in static conditions for squat silo (Δ=1, red color), intermediate-slender silo (Δ=2, green color) and slender silo (Δ=4, blue color)

The refined analytical formulation is able to match the consolidated Janssen formulation with good agreement (the highest relative error is less than 5%). On the other hand, it is shown that the original analytical formulation gives a linear distribution, which does not depend on the slenderness ratio Δ. The agreement of the original analytical formulation and the refined analytical formulation with the Janssen formulation, assumed as benchmark, lies in the different level of approximation of the exponential function of the grain-wall pressures, as given in Eq. (3) of chapter 2. By expressing the exponential function through the Taylor's Series as $e^{-a} = 1 - a + \frac{a^2}{2} + O(\varepsilon^3)$, where $a = \frac{2\omega(z)}{R}$, the first and the second order approximations of the Janssen (1895) formulation of the grain-wall pressure under static conditions result respectively:

$$p_{h,GW,st}(z)_{I^\circ} = \lambda \cdot \gamma \cdot z \tag{42}$$

$$p_{h,GW,st}(z)_{II^\circ} = \lambda \cdot \gamma \cdot z \cdot \left[1 - \frac{\omega(z)}{R}\right] \tag{43}$$

Eq. (42) is linear in z and exactly matches Eq. (26) of chapter 6. Granted that the original analytical formulation provides an expression of $p_{h,GW,st}(z)$ equals to $p_{h,GG}(z)$ for null vertical and horizontal accelerations, the grain-wall pressures equal the horizontal

grain-grain geostatic pressures acting on disk *D*. Such trend matches the slope of the Janssen formulation in correspondence of the grain free-surface ($z = 0$).

Eq. (41) is quadratic in *z*, as well as Eq. (25) of the present chapter. Unlike the original analytical formulation, the refined analytical formulation gives a nonlinear trend for the grain-wall pressure in static conditions. In virtue of the different physical idealizations, i.e. a unique grain layer for the Janssen theory, against two distinct portions (*D* and *E*) for the refined analytical formulation, the formulas tend to coincide when the thickness $s_{st}(z)$ results negligible with respect to the radius *R*. Then, when element *E* becomes thinner and disk *D* practically coincides with the whole cross-section *A* of the silo, the two physical models exactly match. From an analytical point of view, in case of broad and squat silos characterized by usual values of the physical parameters μ_{GW} and λ, the term $\sqrt{\omega(z)^2 + R^2}$ inside Eq. (25) results approximated with *R* and Eq. (43) can be derived. However, also for higher values of the parameters μ_{GW}, λ and Δ, the approximation appears to be negligible.

It has to be noted that, in case of null grain-wall friction coefficient, the magnitude and the along-the-height profile of the grain-wall pressures provided by the refined theory matches with the Rankine theory (1857) (where the pressure ratio λ turns to be the Rankine's coefficient of active earth pressure), as expected for the Janssen analysis (Hirshfeld and Rapaport 2001, Landry et al. 2003).

9.8.2 On the dynamic pressures

In accelerated conditions, additional pressures arise on the silo wall in order to balance the inertial forces of the grain mass interacting with the silo wall, proportional to the *effective mass*. The overpressures (or depressions) between the grain and the silo wall due to the effects of the only uniform horizontal acceleration are defined as follows:

$$\Delta p_{h,GW}(z,\vartheta) = p_{h,GW}(z,\vartheta) - p_{h,GW,st}(z) \tag{44}$$

In this section, the overpressures distribution given by the Eurocode 8 provisions, the Trahair formulation, the original analytical formulation and the refined analytical formulation are compared. Figure 9.9 reports the along-the-height profiles on the front side

($\vartheta = 0$) of the wall for the same grain-silos considered for the static case subjected to a dynamic input of $a_{eh0} = 0.30$, $a_{ev0} = 0$. The overpressures are normalized with respect to a reference value equal to $a_{eh0} \cdot \gamma \cdot A$ that represents the horizontal inertial action of the whole grain cross-section with unitary vertical thickness.

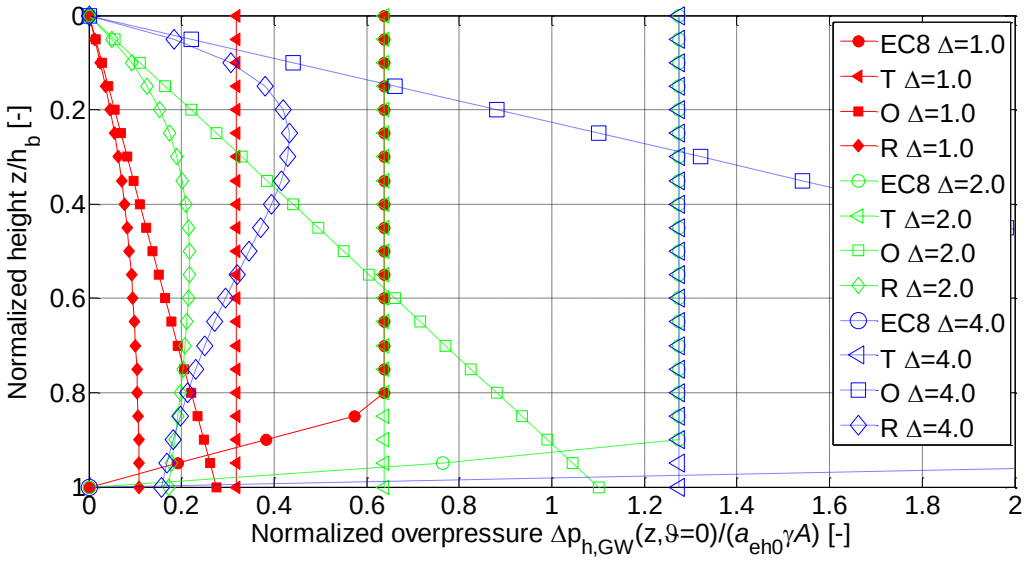

Figure 9.9 - Heightwise variation of the normalized grain-wall overpressures for Eurocode 8 (EC8), the Trahair formulation (T), the Original analytical formulation (O) and the Refined analytical formulation (R) in dynamic conditions for squat silo (Δ=1, red color), intermediate-slender silo (Δ =2) and slender silo (Δ =4)

Grounded on the Rotter and Hull (1989) investigation and the Younan and Veletsos (1998*a*, *b*) study, Eurocode 8 provides a different profile with higher magnitude of the overpressures acting on the wall if compared with the distribution proposed by the refined analytical formulation. However, both the Trahair formulation, the original and the refined analytical formulation and Eurocode 8 show that broader the silo lower the normalized overpressures along the height of the wall. For the slender silo, the highest values of the normalized overpressure given by Eurocode 8 provisions and original analytical formulation result around 2.5 and 4.5 close to the silo bottom, respectively (and thus they are not represented in Figure 9.9). The vertical profile of the normalized grain-wall overpressure given by the refined analytical formulation presents a sort of peak close to the grain free surface for the case of slender silo. The vertical profile of the grain-wall overpressure given by the refined analytical formulation for the squat silo appears qualitatively consistent with the experimental profile detected during the shaking-table tests carried out on a coal-silo with same slenderness ratio by Yokota et al. (1983).

Figure 9.10, Figure 9.11 and Figure 9.12 show the distribution of the normalized overpressures on two different horizontal cross-sections for the squat, intermediate slender and slender silo, respectively . The *x* and *y* coordinates are normalized with respect to the radius *R*, whilst the grain-wall overpressures are normalized with respect to a reference value equal to $a_{eh0} \cdot \gamma \cdot h_b$.

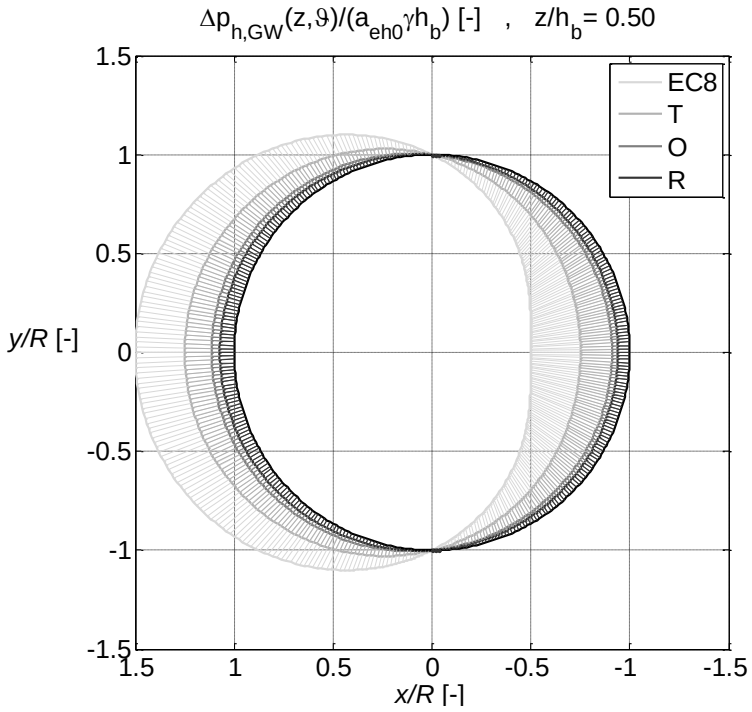

(a)

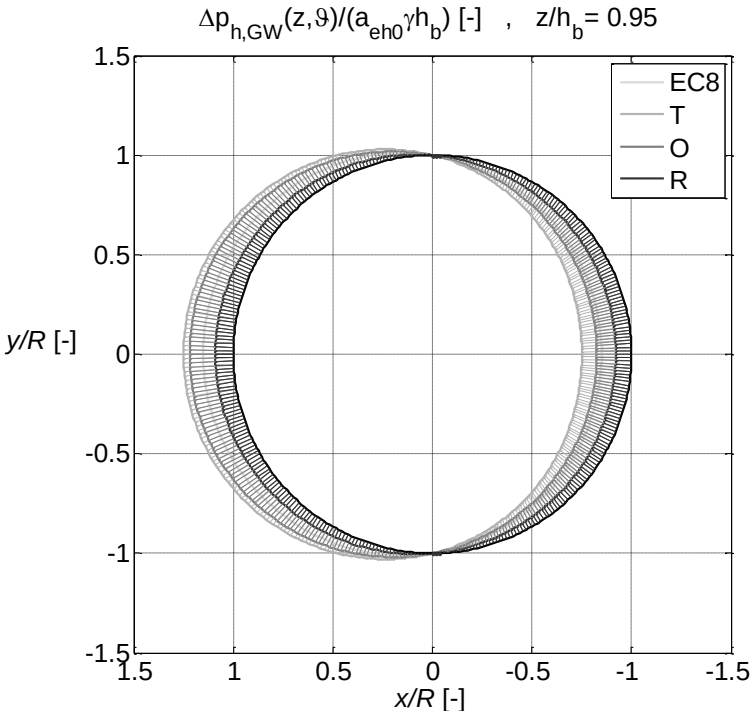

(b)

Figure 9.10 -Horizontal distribution of the normalized overpressures on the wall for the squat silo (Δ=1): (a) at z/h_b= 0.50 and (b) at z/h_b= 0.95 for Eurocode 8 (EC8), the Trahair formulation (T), the Original analytical formulation (O) and the Refined analytical formulation in accelerated conditions

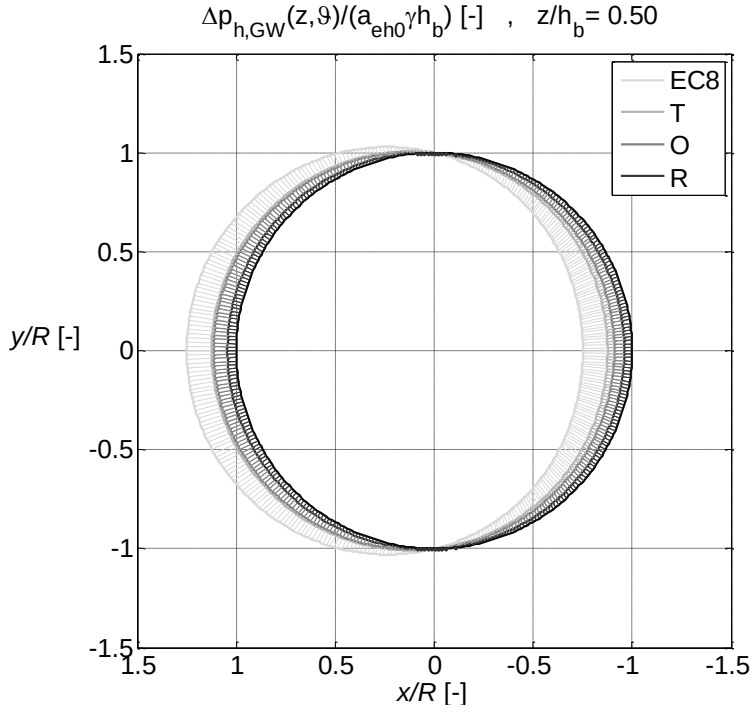

(a)

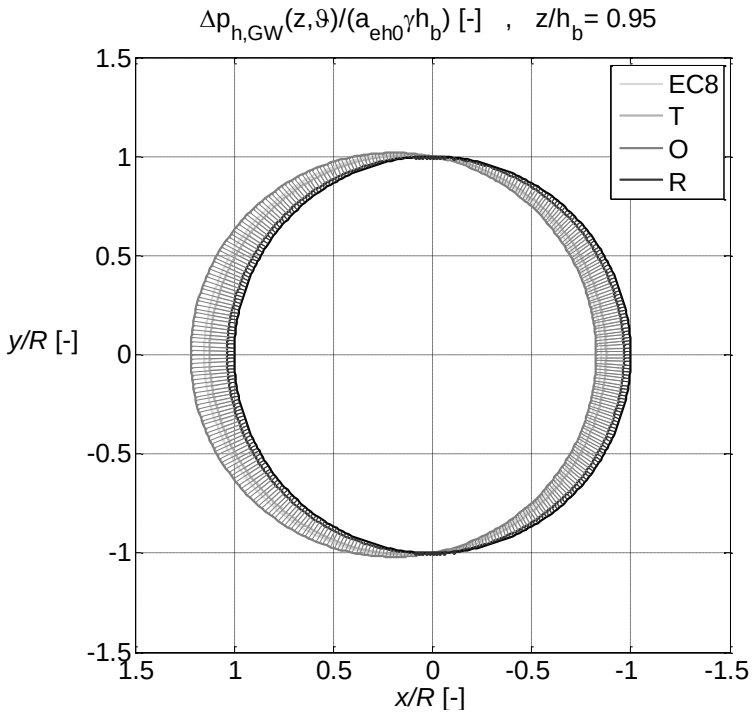

(b)

Figure 9.11 -Horizontal distribution of the normalized overpressures on the wall for the intermediate slender silo (Δ=2): (a) at z/h_b= 0.50 and (b) at z/h_b= 0.95 for Eurocode 8 (EC8), the Trahair formulation (T), the Original analytical formulation (O) and the Refined analytical formulation in accelerated conditions

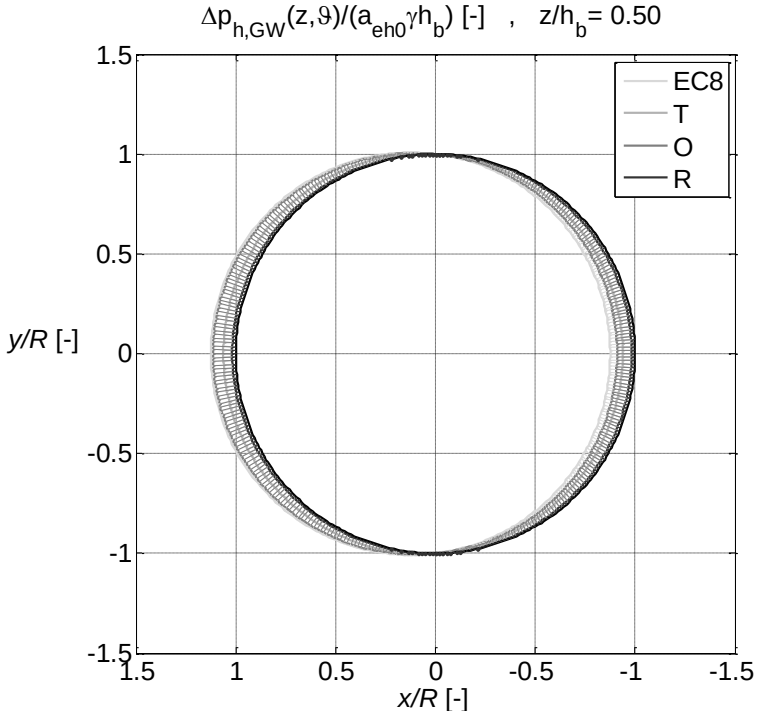

(a)

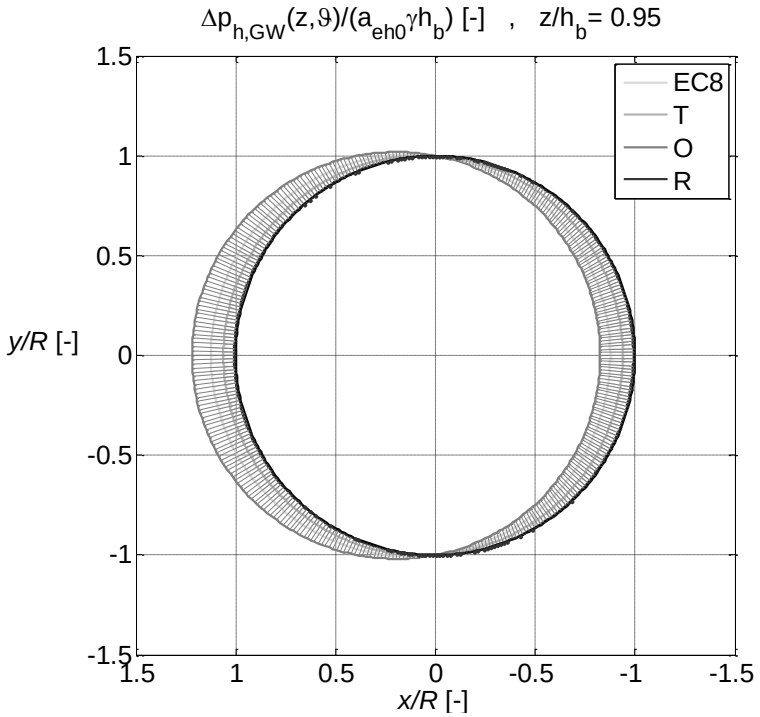

(b)

Figure 9.12 -Horizontal distribution of the normalized overpressures on the wall for the slender silo (Δ=4): (a) at z/h_b= 0.50 and (b) at z/h_b= 0.95 for Eurocode 8 (EC8), the Trahair formulation (T), the Original analytical formulation (O) and the Refined analytical formulation in accelerated conditions

9.8.3 On the *D* and *E* volumes

The original and the refined analytical formulations provide different formulations of the volumes $V_{E,dyn}(z)$ and $V_{D,dyn}(z)$ in accelerated conditions, both in terms of shape and volume.

In this section, the three-dimensional graphic representations of the volumes $V_{E,dyn}(z)$ and $V_{D,dyn}(z)$ are provided according to the original and refined analytical formulations with reference to the squat, intermediate-slender and slender silos considered in the previous sections.

Figure 9.13 and Figure 9.14 show the two grain portions for the squat silo according to the original and refined analytical formulation, respectively. Figure 9.15 shows the two grain portions for the intermediate-slender silo according to the refined analytical formulation. Figure 9.16 shows the two grain portions for the slender silo according to the refined analytical formulation. The intermediate-slender and the slender silos hold to slenderness ratios beyond the limit of validity of the original analytical formulation and thus the volumes *D* and *E* cannot be represented.

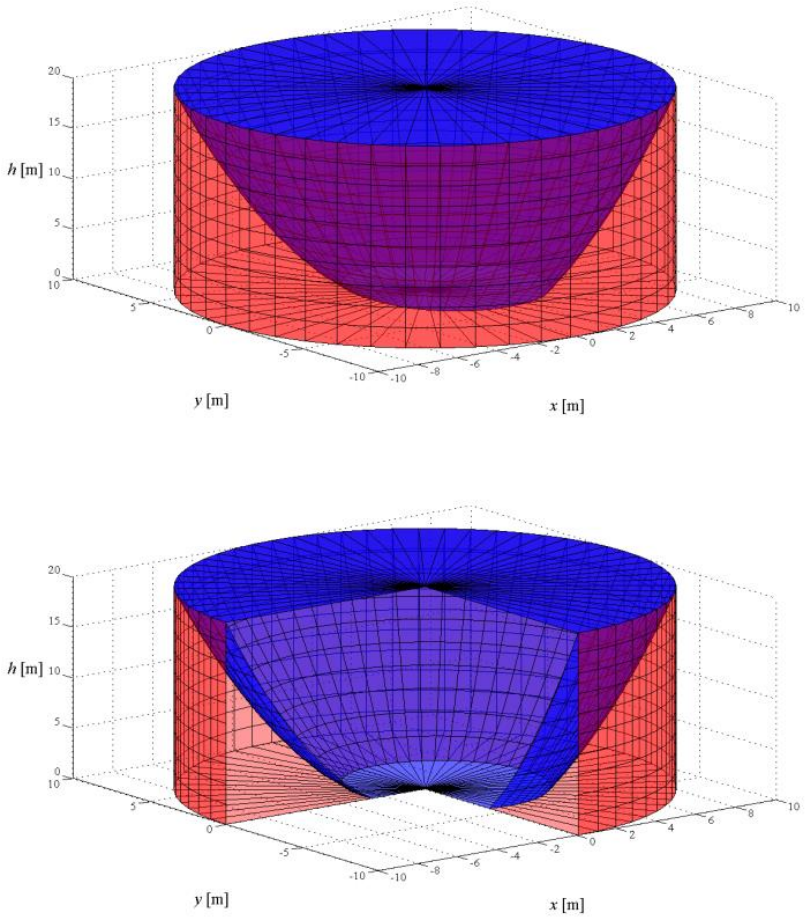

(a)

(b)

Figure 9.13 -Three-dimensional view of portion D (in blue) and of portion E (in red) of the flat-bottom squat silo for the original analytical theory: (a) sectioned view and (b) overview

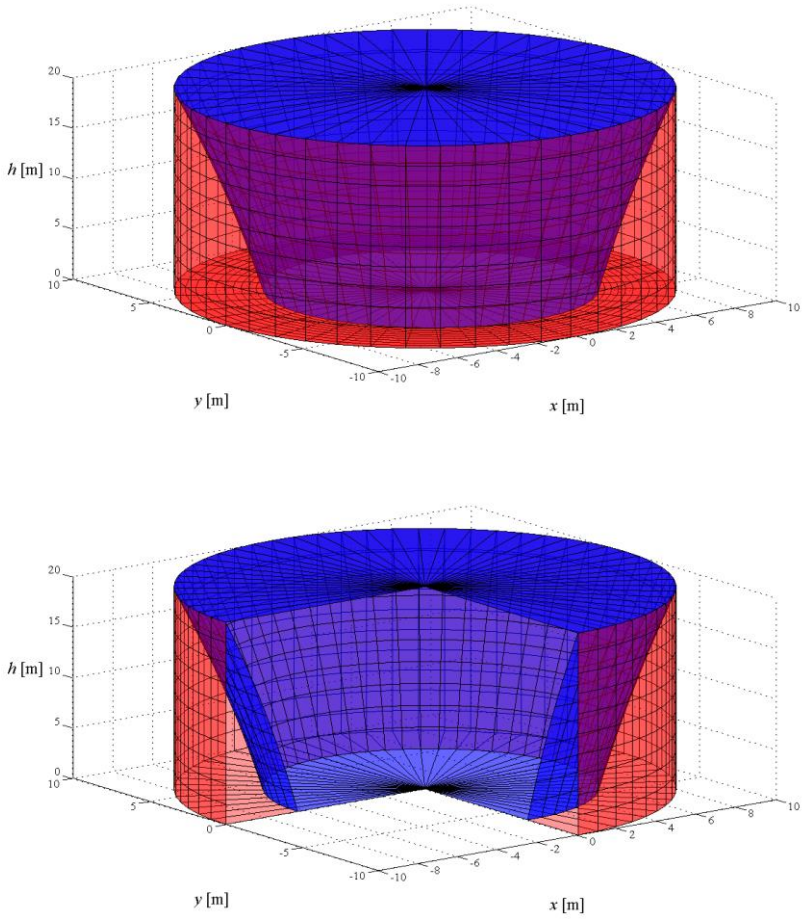

(a)

(b)

Figure 9.14 -Three-dimensional view of portion D (in blue) and of portion E (in red) of the flat-bottom squat silo for the refined analytical theory: (a) sectioned view and (b) overview

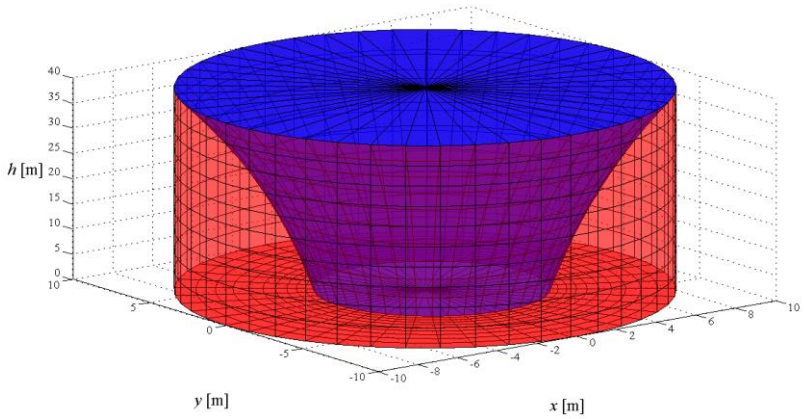

(a)

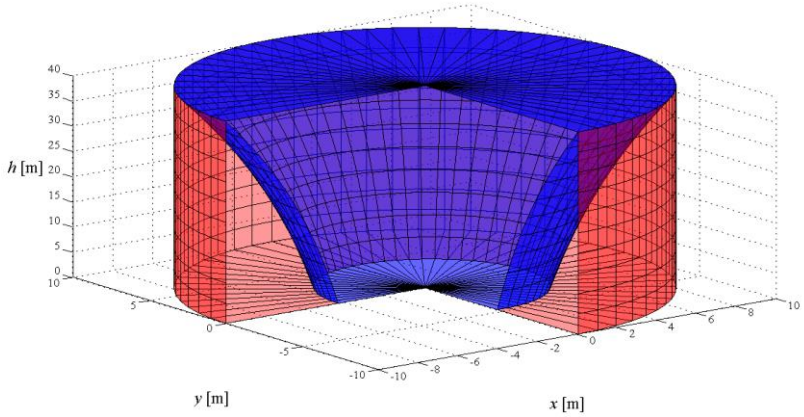

(b)

Figure 9.15 -Three-dimensional view of portion D (in blue) and of portion E (in red) of the flat-bottom intermediate-slender silo for the refined analytical theory: (a) sectioned view and (b) overview

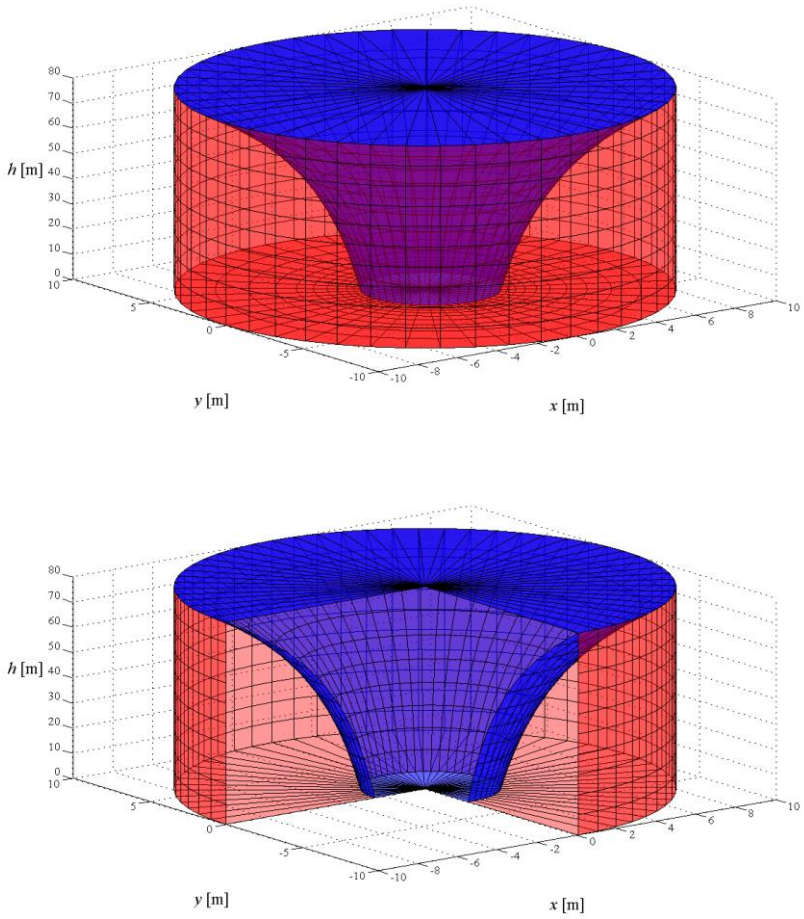

Figure 9.16 -Three-dimensional view of portion D (in blue) and of portion E (in red) of the flat-bottom slender silo for the refined analytical theory: (a) sectioned view and (b) overview

In general, it is shown that the volume $V_{E,dyn}(z)$ assumes a convex and a concave shape with respect to the top surface of the grain for the original and the refined analytical formulations, respectively.

9.8.4 On the shear

In this section, the along-the-height profiles of the wall shear provided by the Eurocode 8 provisions, the Trahair formulation, the original analytical formulation and the refined analytical formulation are compered. As illustrative examples, the squat, intermediate-slender and slender silos analyzed in the previous sections are considered. The wall shear is normalized with respect to the horizontal inertial force of the whole ensiled content, i.e. $a_{eh0} \cdot \gamma_b \cdot V_b$, where V_b indicates the total volume of the ensiled bulk

material. The value of the nornalized wall shear at the silo bottom (for $z = h_b$) corresponds to the value of the *effective mass*.

Figure 9.17 reports the wall shear profiles $T_{xx}(z)$ for the squat silo. Therefore, the ordinates represent the predicted *effective mass*, which results around the 40% and the 30% for the original and the refined analytical formulations, respectively. Such values result lower if compared with the 100% and the 93% provided by the Trahair (1983) formulation and the Eurocode 8 provisions, respectively.

Figure 9.18 reports the wall shear profiles $T_{xx}(z)$ for the intermediate-slender silo. Therefore, the ordinates represent the predicted *effective mass*, which results around the 80% and the 50% for the original and the refined analytical formulations, respectively. Such values result lower if compared with the 100% and the 93% provided by the Trahair (1983) formulation and the Eurocode 8 provisions, respectively.

Figure 9.19 reports the wall shear profiles $T_{xx}(z)$ for the slender silo. Therefore, the ordinates represent the predicted *effective mass*, which results greater than the 100% and around the 70% for the original and the refined analytical formulations, respectively. Such values result lower if compared with the 100% and the 95% provided by the Trahair (1983) formulation and the Eurocode 8 provisions, respectively.

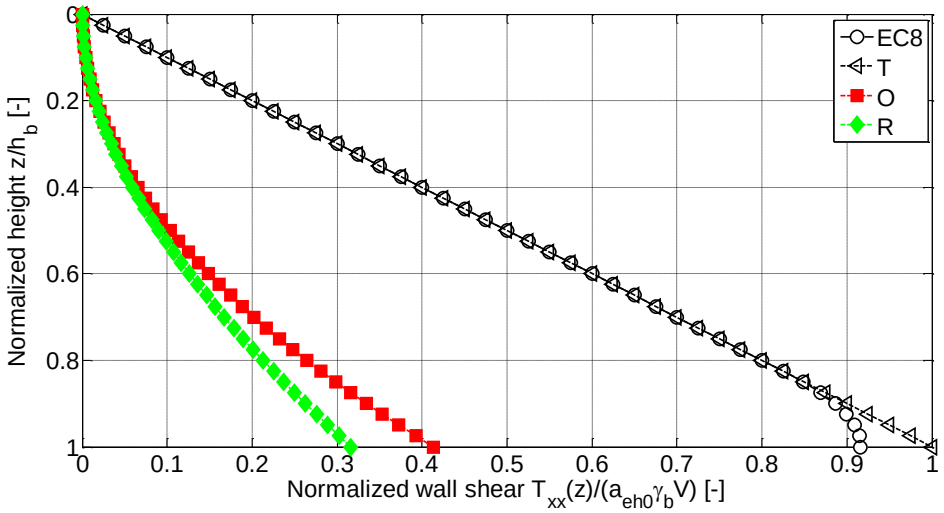

Figure 9.17 - Heightwise variation of the normalized wall shear for Eurocode 8 (EC8), the Trahair formulation (T), the Original analytical formulation (O) and the Refined analytical formulation (R) in dynamic conditions for squat silo

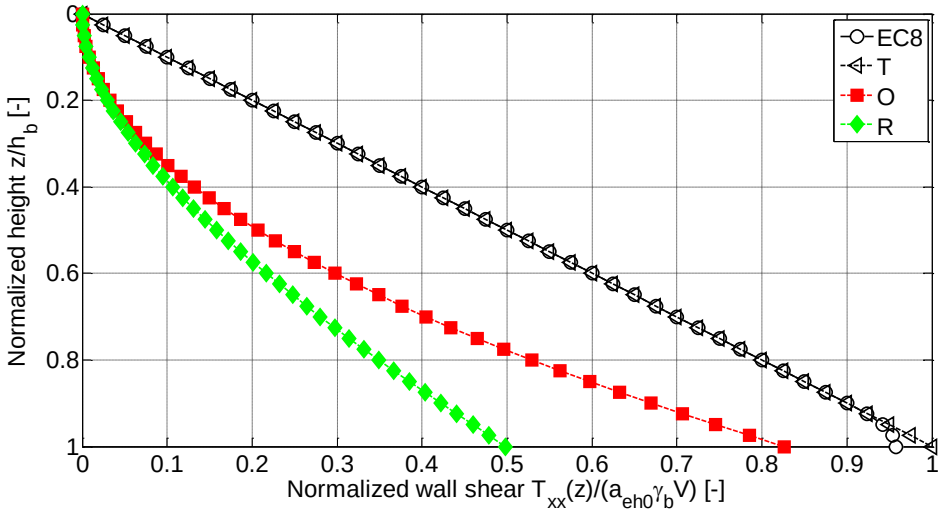

Figure 9.18 - Heightwise variation of the normalized wall shear for Eurocode 8 (EC8), the Trahair formulation (T), the Original analytical formulation (O) and the Refined analytical formulation (R) in dynamic conditions for intermediate-slender silo

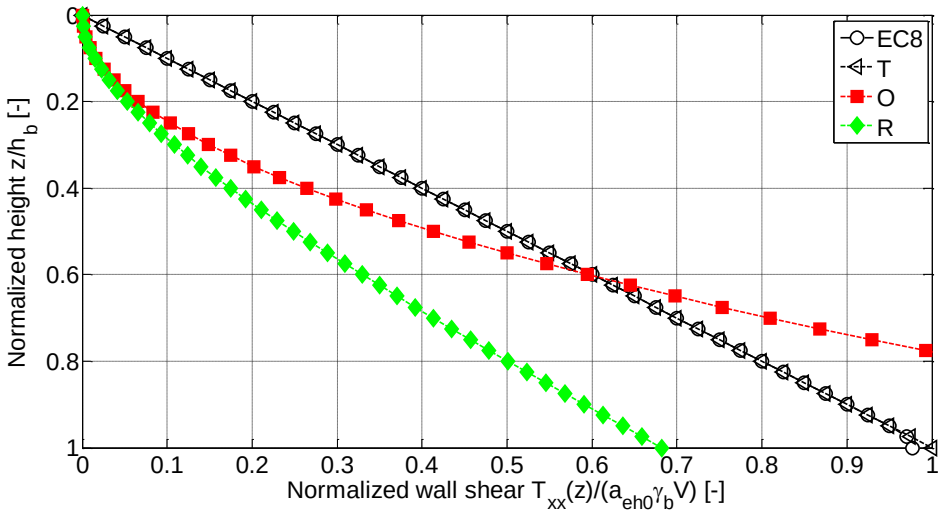

Figure 9.19 - Heightwise variation of the normalized wall shear for Eurocode 8 (EC8), the Trahair formulation (T), the Original analytical formulation (O) and the Refined analytical formulation (R) in dynamic conditions for slender silo

9.8.5 On the bending moment

In this section, the along-the-height profiles of the wall bending moment provided by the Eurocode 8 provisions, the Trahair (1983) formulation, the original analytical formulation and the refined analytical formulation are compared. As illustrative examples, the squat, intermediate-slender and slender silos analyzed in the previous sections are considered. The wall bending moment is normalized with respect to the overturning moment correspondent to the rigid rotation of the whole ensiled content with respect to the

base of the silo, i.e. $a_{eh0} \cdot \gamma \cdot V_b \cdot h_b / 2$. The along-the-height profile of the wall bending moment due to the overpressures is represented by a dashed line, whilst the actual action on the wall accounts also the contribution of the vertical frictional stresses, which is represented by a continuous line, both for the original analytical formulation (Eq. 41) and the refined analytical formulations (Eq. 40). Eurocode 8 provisions (§3.1 EN 1998-4:2006) and the Trahair (1983) formulation do not account for the latter contribution.

Figure 9.20 reports the wall bending moment profiles $M_{yy,1}(z)$ and $M_{yy}(z)$ for the squat silo. As far as the normalized wall base bending moment related to the overpressures is concerned, the original formulation, the refined formulation, the Trahair formulation and the Eurocode provisions 8 provide a value around 27, 23, 99 and 100%, respectively. As far as the normalized wall base bending moment accounting the vertical frictional stresses is concerned, the original analytical formulation and the refined analytical formulation provide a value around 35 and 28%, respectively. Therefore, the contribution of $M_{yy,2}(z)$ to the wall bending moment results around the 25% of $M_{yy,1}(z)$ for both the original and the refined analytical formulations, proofing to be not negligible.

Figure 9.21 reports the wall bending moment profiles $M_{yy,1}(z)$ and $M_{yy}(z)$ for the intermediate-slender silo. As far as the normalized wall base bending moment related to the overpressures is concerned, the original formulation, the refined formulation, the Trahair formulation and the Eurocode provisions 8 provide a value around 54, 37, 99 and 100%, respectively. As far as the normalized wall base bending moment accounting the vertical frictional stresses is concerned, the original analytical formulation and the refined analytical formulation provide a value around 62 and 40%, respectively. Therefore, the contribution of $M_{yy,2}(z)$ to the wall bending moment results around the 10% of $M_{yy,1}(z)$ for both the original and the refined analytical formulations, proofing to be still significant.

Figure 9.22 reports the wall bending moment profiles $M_{yy,1}(z)$ and $M_{yy}(z)$ for the intermediate-slender silo. As far as the normalized wall base bending moment related to the overpressures is concerned, the original formulation, the refined formulation, the Trahair formulation and the Eurocode provisions 8 provide a value around 120, 55, 99 and 100%, respectively. As far as the normalized wall base bending moment accounting the vertical frictional stresses is concerned, the original analytical formulation and the refined

analytical formulation provide a value around 120 and 54%, respectively. Therefore, the contribution of $M_{yy,2}(z)$ to the wall bending moment results far lower than the 10% of $M_{yy,1}(z)$ for both the original and the refined analytical formulations, proofing to negligible.

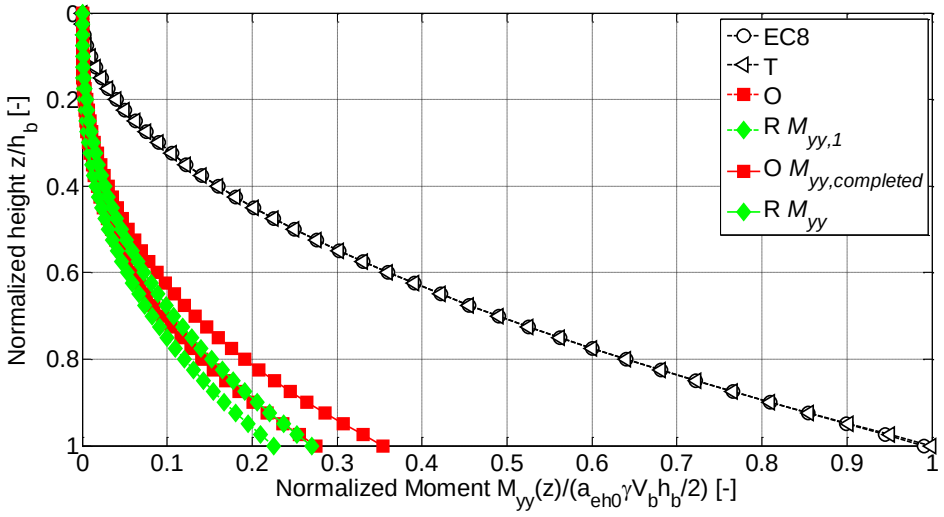

Figure 9.20 - Heightwise variation of the normalized wall bending moment for Eurocode 8 (EC8), the Trahair formulation (T), the Original analytical formulation (O) and the Refined analytical formulation (R) accounting for the frictional vertical stresses contribution (continuous line) and without (dashed line) in dynamic conditions for the squat silo

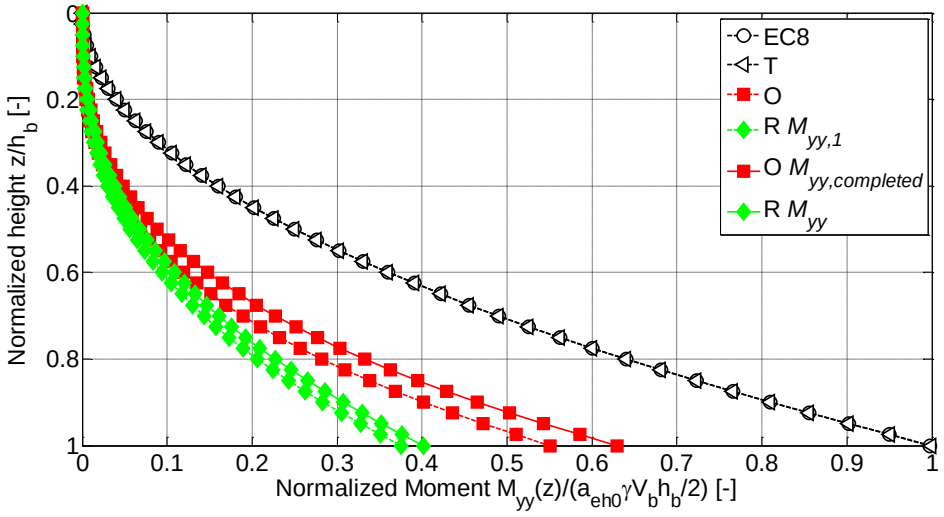

Figure 9.21 - Heightwise variation of the normalized wall bending moment for Eurocode 8 (EC8), the Trahair formulation (T), the Original analytical formulation (O) and the Refined analytical formulation (R) accounting for the frictional vertical stresses contribution (continuous line) and without (dashed line) in dynamic conditions for the intermediate-slender silo

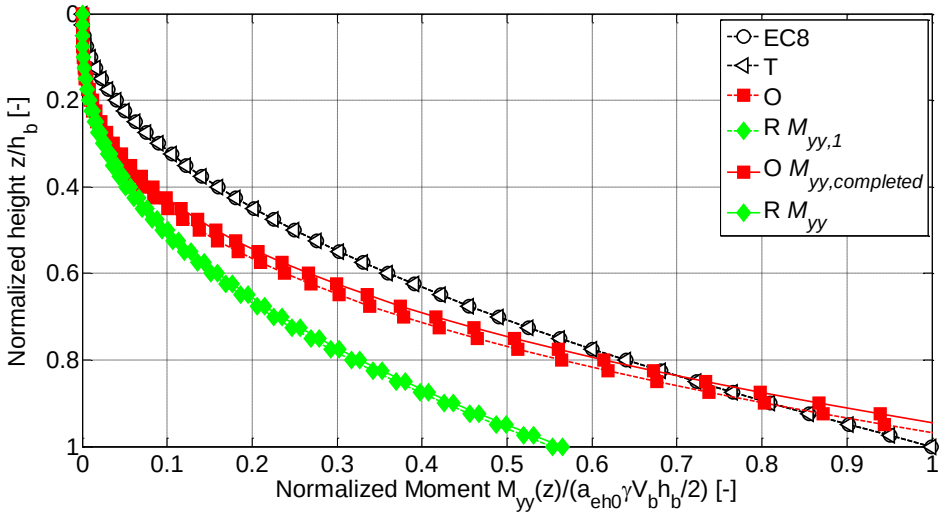

Figure 9.22 - Heightwise variation of the normalized wall bending moment for Eurocode 8 (EC8), the Trahair formulation (T), the Original analytical formulation (O) and the Refined analytical formulation (R) accounting for the frictional vertical stresses contribution (continuous line) and without (dashed line) in dynamic conditions for the slender silo

As observed, lower the slenderness ratio Δ higher the contribution of term $M_{yy,2}(z)$ in determining the wall bending moment $M_{yy}(z)$, due to the higher values of the lever arm of the frictional stresses (proportional to *R*) and the lower values of the term $M_{yy,1}(z)$ for squat silos with respect to slender silos. In general, the values of the wall bending moment as given by the refined analytical formulation (green color) result always lower than those given by the refined analytical formulation (red color), the Trahair (1983) formulation and the Eurocode 8 provisions (black color).

9.8.6 On the effective mass

In this section, the trends of the *effective mass* as provided by the refined analytical formulation, the original analytical formulation, the Trahair formulation and the Eurocode 8 provisions are compared.

As far as the slenderness ratio of the silo is concerned, values of Δ within the range $[0.4, 4.0]$ (encompassing squat and slender silos according to EN 1991-4:2006 provisions) are considered.

As far as the physical characteristics of the grain-silo system are considered, the values of grain-wall friction coefficient, pressure ratio and unit weight of the bulk solid are taken with reference to those considered in the previous examples.

Figure 9.23 shows the trend of the value of the *effective mass* as function of the slenderness ratio Δ according to the refined analytical formulation, the original analytical formulation, the Trahair formulation and the Eurocode 8 provisions. According to the refined analytical formulation, the values of the *effective mass* increases nonlinearly within the investigated range of slenderness ratios. In particular, the values of the *effective mass* are similar to those of the original analytical formulation for $\Delta \in [0.4,1.0]$ and tend to approach the value of 0.80 for high value of Δ. The values of *effective mass* given by the refined analytical formulation result sensibly lower to those given by Eurocode 8 provisions (discrepancies are around -40 and -50%).

The mathematical consistence and the physical robustness of the refined analytical formulation may be conciliated with the handy and conservative formulations of the original analytical formulation for the assessment of the *effective mass* of squat silos.

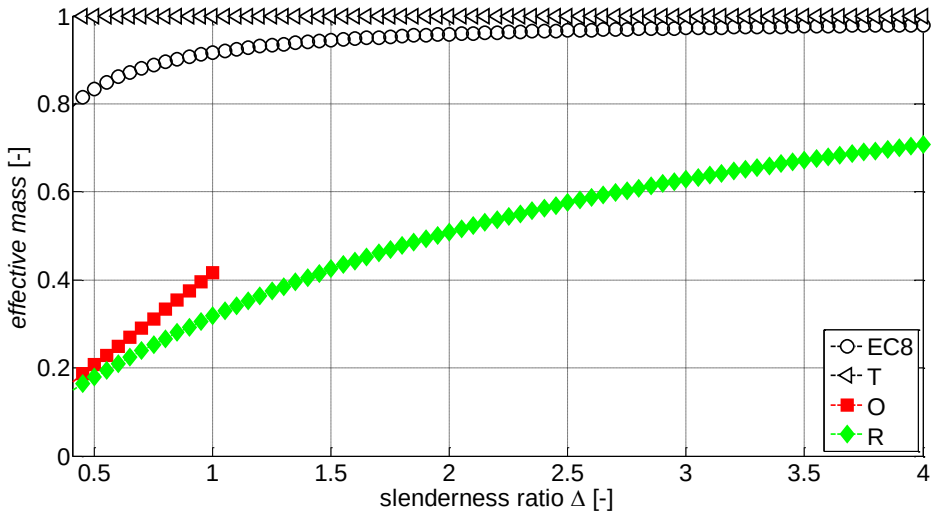

Figure 9.23 - Values of the effective mass as function of the slenderness ratio for the Eurocode 8 provisions (EC8), the Trahair formulation (T) and the proposed analytical formulation (O) for different ensiled bulk solids

9.9 On the limits of validity and the assumptions

During the shaking-table tests, the grain-silo experienced horizontal accelerations greater than the theoretical limitation provided by Eq. (37). After that a progressive

increasing gap arises between experimental data and analytical predictions. That may be explained focusing on some of the assumptions and on the related physical idealizations accounted by the analytical framework.

Assumption 7 expresses a precious physical idealization; assumption 10 essentially neglects the effects of the horizontal sliding of the top grain layers; assumption 12 allows to simplify the analytical treatise of the present issue. Both assumptions result verified until a_{eh0} and boundary $C_D(z)$ satisfied the relative conditions and horizontal sliding of the upper grain layers does not produce significant effects.

As far as assumption 7 is concerned, for horizontal accelerations greater than those expressed by Eq. (37), according to the analytical framework, disk *D* could horizontally slide on the base plane, producing additional overpressures on the silo wall (as noted by Hull and Rotter 1989). The experimental along-the-height profiles of the horizontal accelerations (see for example Figure 7.21*a* of chapter 7) does not show any evident sudden or smooth increasing along the whole vertical trend (with exception to local amplification of the horizontal accelerations at the grain free surface), but amplifications clearly occur and simultaneously theoretical prediction and experimental results drift away.

As far as assumption 10 is concerned, it should be considered that both experimental tests conducted on horizontally shaken granular media and shaking-table tests conducted on silo specimens under solely horizontal base excitation ($a_{ev}(z)=0,\forall z$, i.e. $\nu_0=1$) report that: (i) even negligible values of the horizontal acceleration trigger slight horizontal sliding of the upper grain layers (for this reasons called “sliders”); (ii) values of the horizontal acceleration close to 0.30-0.35 *g* triggers relevant horizontal grain sliding of the upper grain layers. Such evidences have been observed also in the shaking-table tests reported by Silvestri et al. (2016) (see chapter 7). Thus, assumption 10 may result, in general, consistent for values of the horizontal acceleration below 0.35 *g*. In these terms, even if the analytical limitations given by Eq. (37) refers to a different idealization of the mechanism of grain sliding, it appears able to provide a reasonable estimation of the experimentally-based range of the horizontal accelerations triggering the sliding of the upper grain layers (referred to as a_{crit} in the scientific literature).

As far as assumption 12 is concerned, for horizontal accelerations that produce considerable deformations of contour $C_D(z)$, $R_{h,GG}(z)$ may not result negligible. This action can contribute indeed to the progressive increasing of the bending moment. Therefore, the effects of the horizontal accelerations on the shape of the contour $C_D(z)$ need to be investigated in order to check the consistence of assumption 12. Figure 9.24 shows the relative contours $C_D(z)$ on the bottom (i.e. where the highest deformation occurs at the boundary) of the same silo of the so-called third configuration (see chapter 7 for further details) for two values of the horizontal acceleration (0.30 and 0.50), one below and one beyond the two aforementioned limitations related to the horizontal accelerations. The *x* and *y* coordinates are normalized with respect to the radius *R*. It can be noted that, for the considered values of horizontal acceleration, the shape of $C_D(z)$ changes due to the variation of thickness of the material which leans against the wall in accelerated conditions. However, for both values of the horizontal acceleration no appreciable variation of the boundary occurs and the deformation essentially match with the hypothesis of regularity of $C_D(z)$. Such deformations do not deal with a horizontal rigid sliding of the content on the bottom layer, since the thickness of the material does not vary with respect to the static value on the direction perpendicular to the earthquake ground motion ($\vartheta = \pm\pi/2$). Therefore, for common values of the horizontal accelerations adopted in design situations, assumption 12 results satisfied.

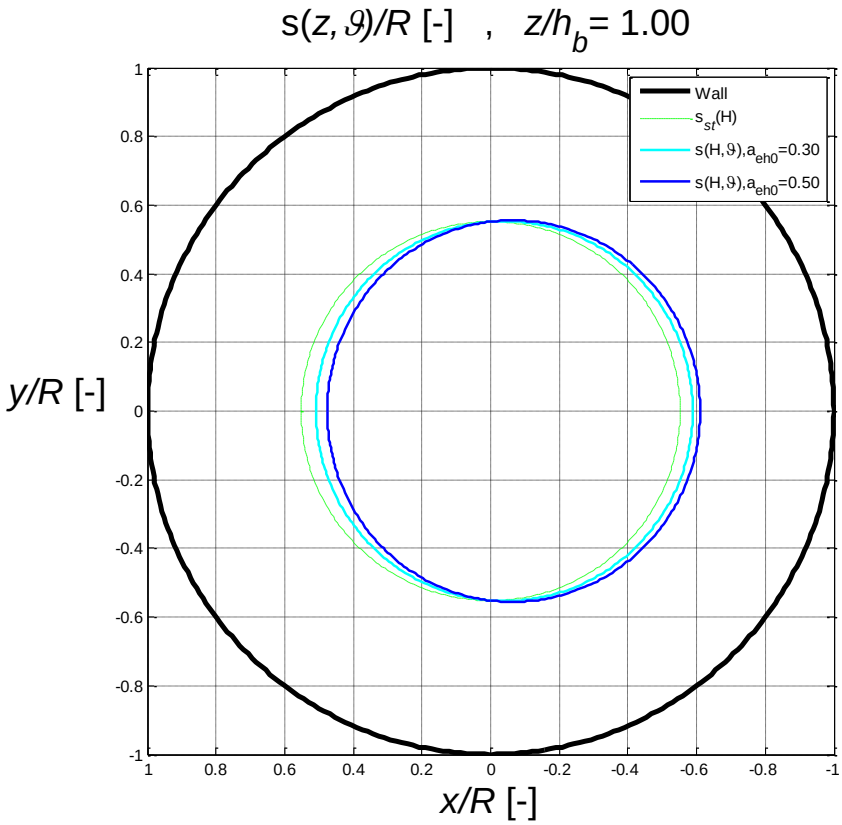

Figure 9.24 - Plot of the normalized thickness at the bottom of the silo for: static conditions (green) and accelerated conditions,0.30 (ciano), 0.45 (blue)

It appears that the most stringent limitation is referred to that related to assumption 10 that sets the maximum value of the horizontal acceleration around 0.35 *g*. However, if assumption 7, 10 12 are respected, the refined analytical formulation is able to well represent the experimental results. If not, the additional contributions in terms of wall shear and bending moment, in addition to those related to the top grain sliding, cannot be accounted. That can explain the progressive increasing gap between theoretical prediction and experimental results. However, the exceeding of both the limitations related to assumption 7 and 10 leads only to an underestimation of the wall base bending moment. Nevertheless, it appears that the refined analytical formulation keeps its consistence, since only Eq. (35) represents a mathematical limitation which must be always satisfied. According to Eq. (35), the admitted horizontal accelerations result applicable to the common civil engineering design scenarios, even in the worst conditions (high grain-wall friction coefficients with relevant negative vertical accelerations, Figure 9.7).

9.10 Comparison with the experimental evidences

In this section, the predictions of the wall base bending moment as given by the refined analytical formulation are compared with the reconstructed experimental wall base bending moment, as obtained by the shaking-table camping previously reported in chapter 8.

Figure 9.25 reports the wall base bending moment as provided by the Eurocode 8 provisions, the Trahair et al. (1983) formulation, the original analytical formulation accounting for the contribution of vertical stresses on the bending moment (Eq. 41) and the refined analytical formulation (Eq. 40) (assuming a constant vertical profile for the horizontal acceleration) with the values of the reconstructed experimental wall bending moment of the first configuration of the silo specimen. The wall base bending moment M_{yy} obtained by the refined analytical formulation (Eq. 40) and the original analytical formulation (Eq. 41) are quite similar and represents a reasonable upper bound for the values of the experimental wall base bending moment. The wall base bending moment obtained by the Eurocode 8 provisions and the Trahair formulation overestimates the experimental results, suggesting that the actual activated mass may result noticeably lower than the *effective mass* proposed by Eurocode 8.

Figure 9.26 reports the wall base bending moment as provided by the Eurocode 8 provisions, the Trahair (1983) formulation, the original analytical formulation accounting for the contribution of vertical stresses on the bending moment (Eq. 41) and the refined analytical formulation (Eq. 40) (assuming a constant vertical profile for the horizontal acceleration) with the values of the reconstructed experimental wall bending moment of the third configuration of the silo specimen. The wall base bending moment M_{yy} obtained by the refined analytical formulation (Eq. 40) is in good agreement with the experimental evidence, at least up to a horizontal acceleration around 0.30 *g*. This is consistent with the value of the critical horizontal acceleration (beyond which the effects of grain sliding on the dynamic response become relevant). The wall base bending moment $M_{yy,completed}$ obtained by the original analytical formulation (Eq. 41) represents a reasonable upper bound for the values of the experimental test. The wall base bending moment obtained by the Eurocode 8 provisions and the Trahair formulation overestimates the experimental

results, suggesting that the actual activated mass may result noticeably lower than the *effective mass* proposed by Eurocode 8.

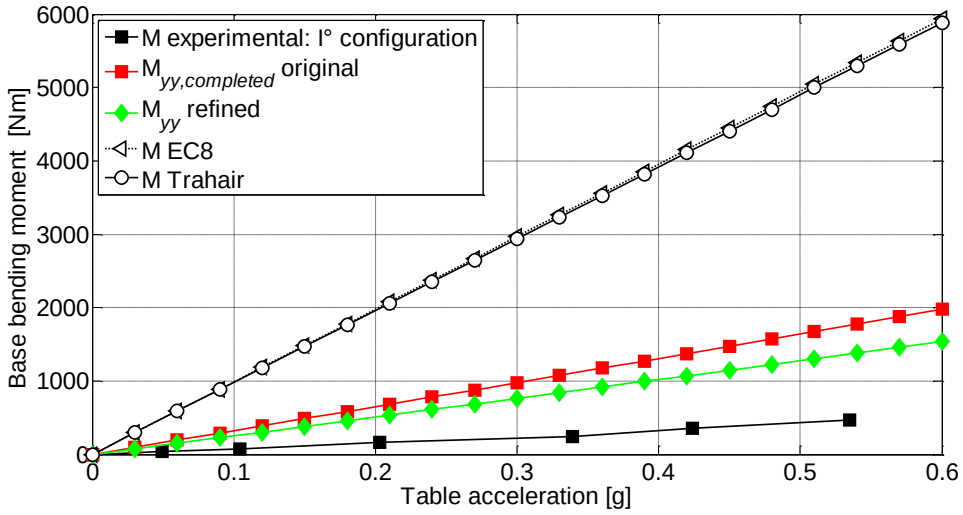

Figure 9.25 - Comparison between the reconstructed experimental bending moment and the predicted values by the original analytical formulation, the refined analytical formulation, the Eurocode 8 provisions and the Trahair formulation for the first configuration.

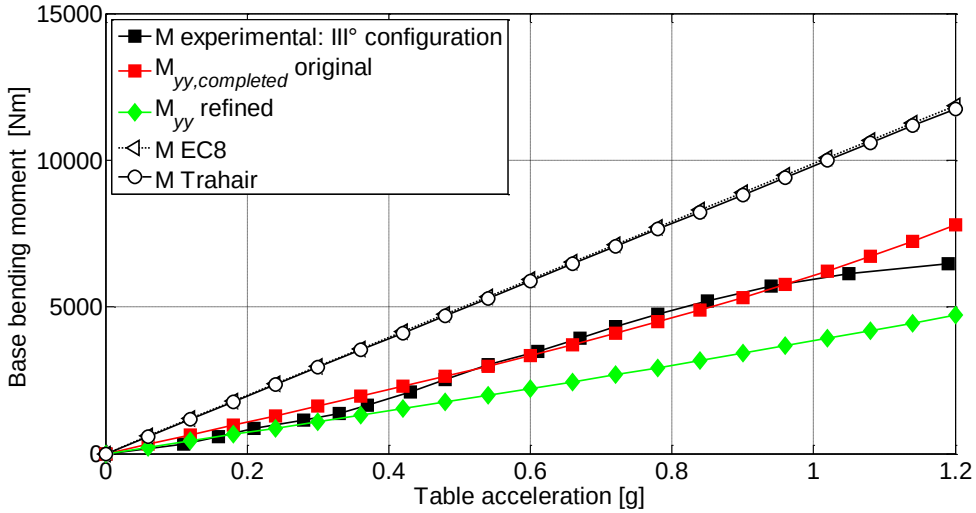

Figure 9.26 - Comparison between the reconstructed experimental bending moment and the predicted values by the original analytical formulation, the refined analytical formulation, the Eurocode 8 provisions and the Trahair formulation for the third configuration.

9.11 Critical considerations

In this section, the refinements to the original analytical formulation for the assessment of the seismic actions on the wall of flat-bottom silos containing grain-like

material are presented. This research work provides a relevant improvement of the overall original analytical formulation proposed by Silvestri et al. (2012).

Refinements to the original analytical formulation are presented by means of rigorous analytical developments and following the same logic organization of the original analytical formulation. Finally, a comparison of the refined formulation with the Janssen theory, the Trahair formulation, the original analytical formulation and the Eurocode 8 provisions is performed in both static and accelerated conditions. Also, the analytical predictions (original and refined analytical formulations, Trahair formulation and Eurocode 8) of the wall base bending moment are compared with the shaking-table test results reported in chapter 7.

A significant extension of the limits of validity of the original analytical formulation is provided. The contribution of the vertical frictional stresses in the evaluation of the wall bending moment is taken into account.

The analytical comparison of the refined analytical formulation with the consolidated Janssen theory for the static design of grain-silo shows good agreement. The experimental comparison of the refined analytical formulation with the shaking-table tests results shows good agreement as well. The experimental validation suggests that the mathematical consistence and the physical robustness of the refined analytical formulation can be conciliated with the handy and suitable formulations of the original analytical formulation for the case of squat silos.

Finally, the values of the reconstructed experimental bending moment at the base of the silo are far lower than the values obtained using the Eurocode 8 provisions, which seem to be overly conservative.

Reference

Arnold, P. C., McLean, A. G., & Roberts, A. W. (1980). Bulk solids: storage, flow and handling. TUNRA Bulk Solids Handling Research Association.

EN 1991-4 (2006) Eurocode 1: Actions on structures - Part 4: Silos and tanks

EN 1998-4 (2006) Eurocode 8: Design of structures for earthquake resistance – Part 4: Silos, tanks and pipelines

Hirshfeld D, Rapaport DC (2001) Granular flow from a silo: discrete-particle simulations in three dimensions. Eur Phys J E 4(2):193–199

Janssen H (1895) Versuche uber Getreidedruck in Silozellen. Zeitschrift des vereines deutcher Ingenieure. In: s.l.:s.n. 39:1045–1049

Landry JW, Grest GS, Silbert LE, Plimpton SJ (2003) Confined granular packings: structure, stress, and forces. Phys Rev E 67(4):041303

Rankine WM (1857) On the stability of loose earth. Philos Trans R Soc Lond 147:9–27

Rotter, J. M., & Hull, T. S. (1989). Wall loads in squat steel silos during earthquakes. Engineering Structures, 11(3), 139-147.

Silvestri, S., Gasparini, G., Trombetti, T., & Foti, D. (2012). On the evaluation of the horizontal forces produced by grain-like material inside silos during earthquakes. Bulletin of Earthquake Engineering, 1-26.

Silvestri, S., Ivorra, S., Chiacchio, L. D., Trombetti, T., Foti, D., Gasparini, G., ... & Taylor, C. (2016). Shaking-table tests of flat-bottom circular silos containing grain- like material. Earthquake Engineering & Structural Dynamics, 45(1), 69-89.

Veletsos A. S., Younan A. H. (1998b). Dynamics of Solid-Containing Tanks. II: Flexible Tanks, Journal of Structural Engineering ASCE, 124(1): 62-70.

Woodcock, C. R., Mason, J. S. (Eds.). (1988). Bulk solids handling: an introduction to the practice and technology. Springer Science & Business Media.

Younan A. H., Veletsos A. S. (1998a). Dynamics of Solid-Containing Tanks. I: Rigid Tanks, Journal of Structural Engineering ASCE, 124(1): 52-61.

10. On the fundamental period of vibration of ground-supported grain-silos

In this chapter, an analytical formulation for the estimation of the fundamental period of vibration of ground-supported grain-silo systems is discussed. The main aim is to better understand the overall response of grain-silo systems subjected to base excitation. The analytical formulation refers to the class of silo with isotropic continuous wall (such as rolled steel plate silos and, in first approximation, "lipps" silos and r.c. wall silos). Starting from the analytical framework proposed in chapters 6 and 9, the dynamic behavior of grain-silos is re-conducted to that of an equivalent linear-elastic system. In addition, a simple procedure for the numerical estimation via FE modelling of the dynamic properties of more complex typology of grain-silos, e.g. with orthotropic (corrugated) or stringer stiffened wall, composed by bolted component, is proposed. First, the theoretical framework adopted, the basic assumptions and the closed-form expressions for the analytical evaluation of the fundamental period of vibration are presented. Then, the theoretical estimation is compared with the experimental data gathered via shaking-table tests performed within the ASESGRAM project and those given by different Authors, available in the scientific literature. Finally, a simple code-like formula and a procedure for the analysis of the dynamic behavior of circular on-ground grain-silos via simplified FE model is also proposed.

10.1 Problem formulation and basic assumptions

In the present section, an analytical framework for the evaluation of the fundamental period of vibration of grain-silo systems is presented. The main aim is to better understand the overall response of grain-silo systems subjected to base excitation. The idealized system adopted by Yang (1976) is taken into consideration and specialized for the case of grain-silo systems. Starting from the experimental verification of the capability of the refined analytical formulation in predicting the value of *effective mass*, the grain mass interacting with the silo wall during dynamic excitation (for specific conditions) is provided. Then, the stiffness of general grain-silo systems is identified. Once the these two key parameters, mass and stiffness, are identified, by considering additional assumptions to those adopted within the framework of the refined analytical formulation, an theoretical formulation for the assessment of the fundamental period of vibration of grain-silo systems is established. The analytical prediction is compared with experimental

data gathered via shaking-table tests by different Authors. Finally, a modeling technique to be easily implemented in a commercial finite element software has been proposed.

10.1.1 Idealized system

The idealized system adopted by Yang (1976) for the assessment of the dynamic behavior of cylindrical shell filled with liquid is taken into consideration and then specialized for the case of grain-silo systems. Even if focused on fluid-liquid storage tanks, this research work provides an analytical framework for the evaluation of dynamic properties (such as fundamental period of vibration and modal shapes) of such cylindrical shell structures. The analytical approach by Yang (1976) consists in modeling the cylindrical shell with its content as a uniform linear-elastic shear-flexural cantilever beam.

10.1.2 Idealized conditions

The proposed analytical framework for the assessment of the fundamental period of vibration of grain-silo system refers to the same idealized conditions considered in the original and refined analytical formulation, as reported in chapters 6 and 9.

10.1.3 Basic assumptions

In the present section, the basic assumptions considered within the analytical framework proposed for the evaluation of the fundamental period of flat-bottom on-ground circular grain-silos are presented.

The proposed framework is grounded on the assumptions of the refined analytical formulation. For the sake of clearness, the fundamental assumptions of the refined analytical formulation are here summarized:

- A portion of the mass of the ensiled grain leans against the silo wall, whilst the reaming mass does not interact with the silo wall during the ground shaking;
- The grain-wall friction and the grain- grain friction are fully exploited during the ground shaking;

- No horizontal grain sliding is considered.

Further details about the assumption of the refined analytical formulation may be found in chapter 9.

The refined analytical formulation states that only the mass of the ensiled material leaning against the wall, corresponding to the *effective mass*, is activated during the horizontal shaking. The geometrical shape of the mass leaning against corresponds to the external torus of variable thickness $s(z,\vartheta)$ as represented in Figure 9.1. In principle, the thickness $s(z,\vartheta)$ varies with the assumed vertical profile of the horizontal acceleration. The mass interacting with the silo wall moves together with the silo (i.e. no relevant horizontal sliding occurs) as observed during the experiments for horizontal acceleration below a threshold value.

The set of additional assumptions considered in order to extend the Yang (1976) approach to grain-silos are reported in the following:

1. Horizontal input is applied only;
2. The *effective mass* is independent on the profile and amplitude of the horizontal accelerations;
3. In the deformed configuration, plain section remain plain, i.e. the effect of shear-lag on the behavior of the wall section is neglected and no section ovalizations occur;
4. The stiffness of the system is provided by the silo wall only;
5. The overall mass of the equivalent beam consists of two contributions: the grain mass corresponding to the *effective mass* and the mass of the silo structures, and is considered as uniformly distributed along the height;

Assumption 1 considers the scenario in which only a horizontal motion is applied. Nonetheless, even though the effects of the vertical component of the input $a_{ev}(z)$ could be included for the evaluation of the *effective mass* (following the formulation described in chapter 9), its effect would result in general negligible.

Assumption 2 states that the *effective mass* does not depend on the intensity of the shaking until no significant grain sliding occurs. This condition has been experimentally verified by many Authors (details are reported in chapter 3) for peak ground accelerations

below a certain critical horizontal acceleration (a_{crit}), around 0.30 g for the tested silo specimens. According to the refined analytical formulation the thickness $s(z,\vartheta)$ depends, in addition to the amplitude and profile of the horizontal shaking, on the grain-wall friction coefficient, μ_{GW}, the pressure ratio, λ and the slenderness ratio, Δ. Nonetheless, it can be shown that, for values of μ_{GW}, λ and Δ typical of as-built silos according to Table E.1 of EN 1991-4:2006, the variation of the volume of the external torus with respect to various acceleration profiles (uniform and linear with different dynamic amplifications at the top of the silo) and amplitudes up to the critical value $a_{,crit}$ is, for engineering purposes, negligible. For instance, Figure 10.1 displays the volume ratio (at the base of the silo) between the entire volume of the external torus under dynamic conditions, $V_{ext,dyn}(h_b)$, and the entire volume of the external torus under static conditions (i.e. for null horizontal acceleration $a_{eh}(z=h_b)=0$), $V_{ext,st}(h_b)$ versus the horizontal acceleration (normalized with respect to the critical value a_{crit}). A uniform ($\zeta=1$) and a linear vertical profile (with the amplification ζ increasing from 1 to 4) of the horizontal acceleration (symbols are explained in Figure 10.1) are considered for five different values of Δ (and for the specific values of μ_{GW} = 0.5 and λ = 0.6 , the ones leading to the largest ratios according to Table E.1 EN 1994-1:2006). It can be noted that the volume ratios are very close to unity, even with remarkable amplifications. Figure 10.2 displays the vertical profile of the volume ratio (along the height) between the volume of the external torus under dynamic conditions at the generic distance z (as measured from the free grain surface, refer also to **Errore. L'origine riferimento non è stata trovata.**), $V_{ext,dyn}(z)$, and the entire volume of the external torus $V_{ext,dyn}(h_b)$ (at the critical acceleration). The same uniform and linear ζ profiles of Figure 10.2 are considered for three different values of Δ between 0.5 and 5 (for μ_{GW} = 0.5 and λ = 0.6). It can be noted that for the same slenderness ratio the two profiles (uniform and linear) lead to almost the same *effective mass* distribution along the height.

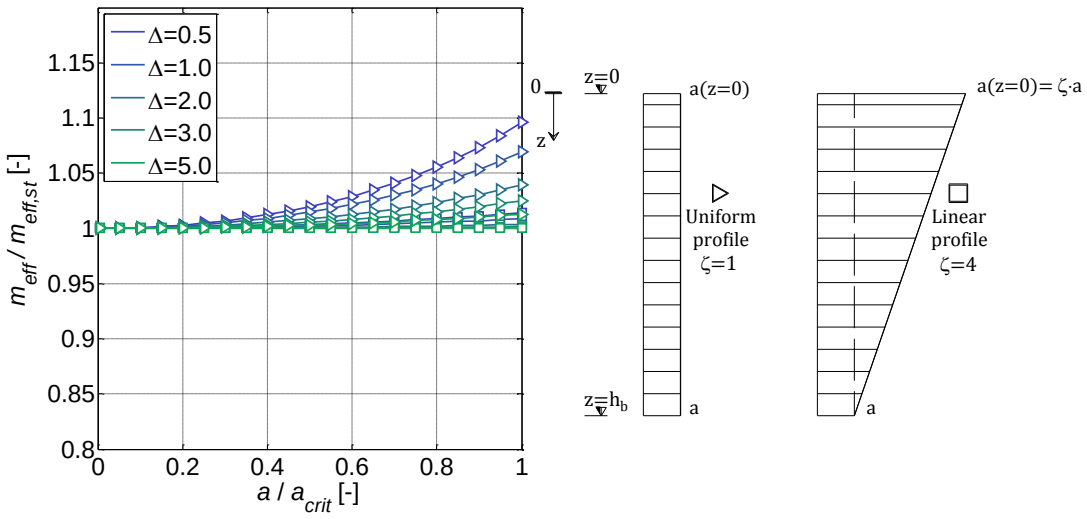

Figure 10.1 –Volume ratio of the external torus E in dynamic and static conditions considering uniform and linear vertical profile of the horizontal acceleration for different slenderness ratios

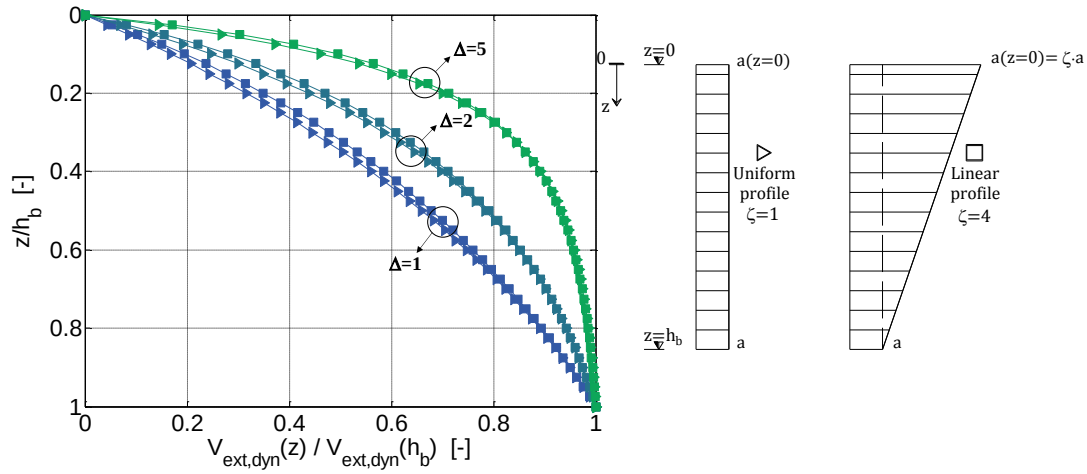

Figure 10.2 – Vertical distribution of the effective mass for uniform and linear vertical profile of the horizontal acceleration for different slenderness ratio (for a = a_{crit})

Assumption 3 states that no cross-section ovalization occurs. This happens due to the presence of the ensiled grain material that prevent for local deformations. In addition, from a theoretical point of view, it is known ("*cylindrical shell slice-beam"* theory formulated by Gould, 1988) that an almost one-harmonic circumferential distribution of the grain-wall overpressure under dynamic conditions prevents from distortions of the cross-sections (plain cross-sections remain plain) and circumferential modes are practically inhibited. Consequently, the silo shell can be treated as a vertical cantilever beam. Nonetheless, from a practical point of view, additional issues should affect the validity of such assumption: (i) the actual circumferential distribution of the grain-wall overpressure

may present local concentrations and/or no spatial smooth distribution; (ii) shells are significantly sensible to local pressure concentrations and not smoothly varying pressure distributions; (iii) the manufacturing process and structural details (as bolted connections) could detrimentally affect local sectional behavior. Despite those issues, the experimental observations by Silvestri et al. (2016) indicates that, for accelerations below the critical value, the assumption is roughly verified.

Assumption 4 states that the grain does not offer an additional contribution to the lateral stiffness of the silo wall, apart preventing from local cross deformations. In other words, the lateral stiffness of the system is coincident with the silo wall stiffness. This assumption is in agreement with experimental evidences by Chandrasekaran and Jain (1968) and numerical results as deduced by the work of Durmuş and Livaoglu (2015), reported in chapter 3.

Assumption 5 states that a uniform mass per unit length is assumed. This is necessary in order to obtain an analytical expression of the fundamental period of the silo. The value of the *effective mass* is considered for two different dynamic conditions of the grain-silo system: (i) far from resonance; (ii) close to resonance. In the former case, the *effective mass* corresponding to the closed-form as provided by the refined analytical formulation could be used; in the latter case, the *effective mass* may be estimated as roughly the 80% of the ensiled mass, independently on the slenderness ratio and the physical characteristics of the ensiled bulk content.

10.2 Analytical developments

In the present section, the analytical developments necessary for the assessment of the fundamental period of vibration of ground-supported circular grain-silos are presented.

Based on the aforementioned additional assumptions, the fundamental period of the realistic flat-bottom on-ground circular grain-silo of Figure 10.3*a* is evaluated with reference to the idealized equivalent uniform shear-flexural cantilever beam model, as represented in Figure 10.3*b*. The silo of Figure 10.3*a* has isotropic smooth wall with stepwise variable thickness $t_{w,i}$ (i is the *i-th* wall portion characterized by constant thickness $t_{w,i}$ and length Δz_i, r is the total number of wall portions). A conical roof with an

angle measured with respect to the horizontal plane equals to α_r and uniform thickness t_r covers the silo. All the other relevant geometrical properties of the silo are indicated in Figure 10.3*a*. The equivalent cantilever beam of Figure 10.3*b*, has a height H_{beam} (vertical length between the silo bottom and the highest solid-wall contact, for a full-filled silo is identified as height of overfull filling), an hollow uniform circular cross-section of diameter d_c and thickness $\bar{t}$, and is clamped at the base. The value $\bar{t}$ varies with respect to the homogenization criteria: equal mass, equal shear frequency, equal flexural frequency. The three criteria will be specified in the following sections.

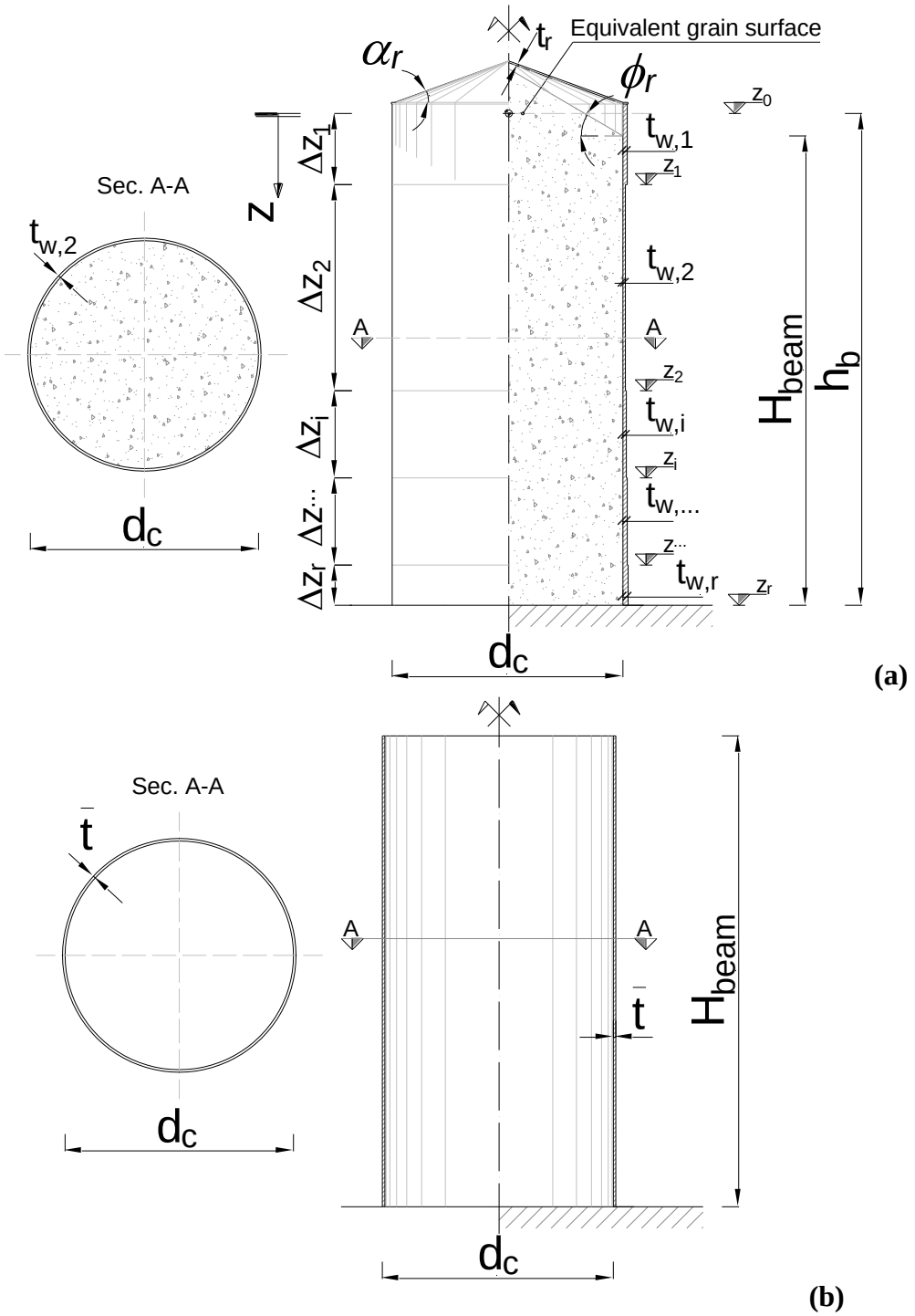

Figure 10.3 – (a) Geometry of a realistic flat-bottom ground-supported circular grain-silo;(b) Geometry of the corresponding equivalent beam

10.2.1 Evaluation of the mass

According to assumptions 1, 2, 5 and with reference to the silo configuration represented in Figure 10.3, the mass per unit length to be used for the estimation of the

fundamental period of vibration is made of the following contributions: (i) the *effective mass* of the grain; (ii) the mass of the silo wall; (iii) the mass of the silo roof.

The mass per unit length corresponding to the *effective mass* of the grain (or bulk solid) $m_b(z)$ for dynamic conditions far from the resonance is given by:

$$m_b(z) = A_{Ext}(z) \cdot \gamma_b / g \tag{5}$$

which is equivalent to:

$$m_b(z) = \frac{2\pi R}{g} \cdot p_{wf}(z) \tag{6}$$

with $A_{Ext,st}(z)$ being the surface of the external torus at a distance *z* under static conditions according to the refined analytical formulation. $p_{wf}(z)$ is the wall frictional traction at a distance *z* under static condition according to EN 1991-4:2006. For slender silos, when the grain surface may be considered almost flat, the Janssen (1895) formulation of $p_{wf}(z)$ is suitable. On the contrary, for squat silos, the contribution of the upper conical portion of the ensiled grain may become significant, and the semi-empirical Reimbert (1976) formulation of $p_{wf}(z)$ is preferable. In particular, making use of the two above mentioned formulations of $p_{wf}(z)$, the expression of $m_b(z)$ as given by Eq. (2) specifies as follows:

$$\text{Janssen (1895): } m_b(z) = \frac{2\pi R}{g} \cdot \left[\mu_{GW} \cdot p_0(z)\right] = \frac{\gamma_b}{g} \cdot \pi R^2 \cdot \left[1 - e^{-\frac{2 \cdot \mu_{GW} \cdot \lambda \cdot z}{R}}\right] \tag{7}$$

$$\text{Reimbert (1976): } m_b(z) = \frac{2\pi R}{g} \cdot \left[\mu_{GW} \cdot p_{hf}(z)\right] = \frac{\gamma_b}{g} \cdot \pi R^2 \cdot \left\{1 - \left[\left(\frac{z - h_0}{z_0 - h_0}\right) + 1\right]^N\right\} \tag{8}$$

where $p_0(z)$ is the horizontal pressure given by Janssen (1895), $p_{hf}(z)$ is the horizontal pressure given by Reimbert (1976), whilst h_0, z_0 and *N* are given by Eq. (5.77), (5.75) and (5.74) of EN 1991-4:2006, respectively.

The mass per unit length of the silo wall $m_w(z)$ can be expressed as:

$$m_w(z) = 2\pi R \cdot t_w(z) \cdot \frac{\gamma_w}{g} \tag{9}$$

where $t_w(z)$ is the thickness of the silo wall and γ_w is the unit weight of the wall material.

The mass of the conical roof M_r is equal to:

$$M_r = \pi R^2 \cdot \sqrt{1+tg(\alpha_r)^2} \cdot t_r \cdot \frac{\gamma_r}{g} \tag{10}$$

Where γ_r is the unit weight of the roof. The equivalent uniform mass per unit length $\overline{m}$ of the equivalent beam (accounting for the three contributions $m_b(z)$, $m_w(z)$ and M_r) results equal to:

$$\overline{m} = \frac{\int_0^{h_b} m_b(z) \cdot dz + \int_0^{h_w} m_w(z) \cdot dz + M_r}{H_{beam}} \tag{11}$$

Making use of Eqs. (3) and (4), $\overline{m}$ (Eq. 7) specifies as follows:

Janssen (1895): $$\overline{m} = \frac{\gamma_b}{g} \cdot \pi R^2 \cdot m_{eff} + 2\pi R \cdot \overline{t_w} \cdot \frac{\gamma_w}{g} + \frac{\pi R^2 \cdot \sqrt{1+tg(\alpha_r)^2} \cdot t_r}{H_{beam}} \cdot \frac{\gamma_r}{g} \tag{12}$$

Reimbert (1976): $$\overline{m} = \frac{\gamma_b}{g} \cdot \pi R^2 \cdot m_{eff} + 2\pi R \cdot \overline{t_w} \cdot \frac{\gamma_w}{g} + \frac{\pi R^2 \cdot \sqrt{1+tg(\alpha_r)^2} \cdot t_r}{H_{beam}} \cdot \frac{\gamma_r}{g} \tag{13}$$

Where $\overline{t_w}$ is the uniform thickness of the equivalent beam leading to the same wall mass of the silo: $\overline{t_w} = \left[\sum_{i=1}^{r} \Delta z_i \cdot t_{w,i}\right] \Big/ H_{beam}$ (equal mass criterion) and the analytical expression of the *effective mass* m_{eff} according to the Janssen (1895) and the Reimbert (1976) formulation inside Eqs. (8) and (9) results, respectively:

Janssen (1895): $$m_{eff} = 1 + \frac{1-e^{\omega}}{\omega} \tag{14}$$

Reimbert (1976): $$m_{eff} = \frac{1}{H_{beam}} \cdot \left[h_b - z_V(z = h_b)\right] \tag{15}$$

Where $\omega = -4 \cdot \mu_{GW} \cdot \lambda \cdot \Delta$, $z_V(z)$ is given by Eq. (5.80) of EN 1991-4:2006. It should be noted that the *effective mass* appears to depend on the grain-wall interaction parameters and the slenderness ratio of the silo, as qualitatively stated in the ASCE 7-10 (2010) provisions.

For dynamic conditions close to the resonance, the equivalent uniform mass per unit length $\overline{m}$ of the equivalent beam may be evaluated taking a value of the *effective mass* of the grain m_{eff} roughly around 0.80 inside Eqs. (8) and (9), regardless on the slenderness ratio of the silo and the physical characteristics of the bulk solid.

It should be recognized that, for common steel real silos, the mass contribution of the conical steel roof is negligible. As illustrative example, let us consider a steel squat silo (Sadowsky and Rotter 2011) characterized by R = 6.5 m, $h_b = 10.0m$ ($\Delta = 0.65$), $\overline{t_w} \cong 2mm$ covered by a steel conical roof of $t_r = 3mm$. The ensiled content is wheat (μ_{GW} =0.38 and λ =0.54). By making use of Eqs. (8) and (10) it turns out that the roof mass is equal to 2% of the total mass.

10.2.2 Evaluation of the elastic properties

The main elastic properties (wall cross-section shear area $A_w^{'}$ and wall cross-section moment of inertia I_w) of the equivalent beam model as represented in Figure 10.3*b*, which are necessary to evaluate the fundamental shear and flexural frequencies, can be explicated as follows:

$$A_w^{'} = \frac{2\pi R \cdot \overline{t_{w,sh}}}{\chi} \tag{16}$$

$$I_w = \pi R^3 \cdot \overline{t_{w,\,flex}} \tag{17}$$

where χ represents the shear coefficient; $\overline{t_{w,sh}}$ and $\overline{t_{w,\,flex}}$ are the thickness of the uniform shear and flexural beam satisfying the following criterion:

$$\text{Equal shear frequency } \overline{t_{w,sh}} = \frac{{H_{beam}}^2}{\sum_{i=1}^{r}\left[\frac{{z_i}^2 - {z_{i-1}}^2}{t_{w,i}}\right]} \tag{18}$$

$$\text{Equal flexural frequency } \overline{t_{w,flex}} = \frac{{H_{beam}}^4}{\sum_{i=1}^{r}\left[\frac{{z_i}^4 - {z_{i-1}}^4}{t_{w,i}}\right]} \tag{19}$$

10.2.3 Evaluation of the fundamental period of vibration

The *n-th* natural frequency of a continuous uniform linear elastic cantilever shear-beam are given by the textbook of Viola (2001):

$$f_{n,sh} = \frac{(2n-1)}{4 \cdot H_{beam}} \cdot \sqrt{\frac{G_w \cdot A_w^{'}}{\overline{m}}} \tag{20}$$

Where G_w is the shear modulus of the wall material.

The *n-th* natural frequency of a continuous uniform linear elastic cantilever flexural-beam can be expressed according to the formulation by Whitney (1999):

$$f_{n,flex} = \frac{(\phi \cdot H_{beam})_n^2}{2\pi} \cdot \sqrt{\frac{E_w \cdot I_w}{\overline{m} \cdot {H_{beam}}^4}} \tag{21}$$

Where E_w is the Young's modulus of the wall material, $(\phi \cdot H_{beam})_n^2$ is the second power of the product between the *n-th* root of the secular equation and the beam length, which can be found in Whitney (1999).

According to Dunkerley's approximation (1894) the fundamental frequency $f_{n,sh+flex}$ accounting for both shear and flexural deformations of an equivalent shear-flexural beam can be computed as follows:

$$\frac{1}{\left(f_{n,sh+flex}\right)^2} = \frac{1}{\left(f_{n,sh}\right)^2} + \frac{1}{\left(f_{n,flex}\right)^2} \tag{22}$$

Combination of Eqs. (14), (15) and Eq. (16) leads to the following expression of $f_{n,sh+flex}$:

$$f_{n,sh+flex} = f_{n,sh} \cdot \sqrt{\frac{1}{1+\left(\frac{f_{n,sh}}{f_{n,flex}}\right)^2}} = f_{n,sh} \cdot \sqrt{\frac{1}{1+\psi_n \cdot \left[\frac{\bar{\Delta}^2}{\chi \cdot (1+\upsilon_w)} \cdot r_t\right]}} \tag{23}$$

Where $\psi_n = \left[\frac{\pi \cdot (2n-1)}{(\phi \cdot H_{beam})_n^2}\right]^2$ is a function of *n*, $\bar{\Delta} = \frac{H_{beam}}{d_c}$ is the filling slenderness ratio and $r_t = \frac{\overline{t_{w,sh}}}{t_{w,flex}}$ is the ratio of the thickness of the uniform shear beam on the thickness of the uniform flexural beam.

In detail, the first frequency of vibrations (*n=1*) specifies as follows:

$$f_{1,sh+flex} \cong \sqrt{\frac{1}{\overline{m}} \cdot \frac{\pi \cdot E_w}{\chi \cdot (1+\upsilon_w)} \cdot \left(\frac{1}{32 \cdot \overline{s_w} \cdot \bar{\Delta}^2}\right)} \cdot \sqrt{\frac{1}{1+0.90 \cdot \left[\frac{\bar{\Delta}^2}{\chi \cdot (1+\upsilon_w)} \cdot r_t\right]}} \tag{24}$$

where $\overline{s_w} = d_c / \overline{t_{w,sh}}$ is the ratio of the diameter on the uniform shear thickness. The approximation is related to the value of parameter ψ_1 (approximated to 0.90). In addition, for the specific, but usual, case of a thin-walled cylindrical metal silo ($\upsilon_w = 0.30$, $\chi = 2$) Eq. (24) simplifies to:

$$f_{1,sh+flex} \cong \frac{0.2}{\bar{\Delta}} \cdot \sqrt{\frac{E_w}{\overline{m} \cdot \overline{s_w}}} \cdot \sqrt{\frac{1}{1+0.35 \cdot \bar{\Delta}^2 \cdot r_t}} \tag{25}$$

Or in terms of first natural period of vibration:

$$T_{1,sh+flex} \cong 5\bar{\Delta} \cdot \sqrt{\frac{\overline{m} \cdot \overline{s_w} \left(1+0.35 \cdot \bar{\Delta}^2 \cdot r_t\right)}{E_w}} \tag{26}$$

By making use of Eqs. (8) or (9) for $\overline{m}$ (which may depend on the slenderness of the silo and/or free grain surface configuration and on the considered dynamic conditions) a fully-analytical expression of $f_{1,sh+flex}$ (or $T_{1,sh+flex}$) could be derived. The expressions are too heavy and are here not explicitly provided. For thin-walled steel silos, a further simplification could be made by neglecting the wall and roof mass contributions, thus considering only the bulk mass inside Eqs. (8) or (9). Nevertheless, in the practice the

formulas can be easily implemented in a spreadsheet. The expression of Eq. (22) depends on: filling slenderness ratio $\overline{\Lambda}$, wall geometrical and elastic properties (E_w, r_t, $\overline{s_w}$), the ensiled material properties and *effective mass* (ρ_b, μ_{GW}, λ).

10.3 Experimental verification and numerical validation of the analytical formulation

In this section, the comparison of the proposed analytical formulation for the estimation of the fundamental period of vibration of grain-silos system with experimental results is presented. First, the experimental-analytical comparison is performed considering the data given by shaking-table tests conducted at the EQUALS laboratory (University of Bristol, ASESGRAM project). Then, the experimental-analytical comparison is performed considering the data present in the scientific literature. Finally, the numerical-analytical comparison is performed considering the data present in the scientific literature.

10.3.1 Experimental results from the ASESGRAM project

In this section, the prediction of the fundamental period (or frequency) of vibration given by the proposed analytical formulation is compared with experimental results gathered via the shaking-table tests conducted at the EQUALS laboratory (Silvestri et al. 2016).

Table 10.1 compares the values of the experimental first natural frequencies of the two silo specimens (smooth and roughened wall, as described in chapter 7) with those obtained according to Eq. (20).

Table 10.1 - Comparison of the experimental fundamental frequencies of the silo specimens filled with Ballottini glass (Silvestri et al. 2016) and the analytical prediction by Eq. (20)

Reference	Specimen			Frequencies				
	Wall material	**Δ [-]**	**Ensiled material**	**Type**	***a* [*g*]**	**Experimental [*Hz*]**	**Analytical [%]**	**Relative error [%]**
Silvestri et al. (2016)	Polycarbonate (smooth)	1.0	Ballottini Glass	WN	0.05 0.30	14.0	14.9	-19
	Polycarbonate (roughened)	1.0	Ballottini Glass	WN	0.10	15.6	14.9	+7

For the specimen with smooth wall, a relative error of -19% is detected, whilst for the specimen with roughened wall, a relative error of +7% is detected. The discrepancy in the determination of the fundamental frequency of vibration for the specimen with smooth wall and roughened wall could be mainly associated to the different rigidity of the base connections. Even if the silo specimen with roughened wall should be subjected to an higher *effective mass*, leading to a lower value of the fundamental frequency of vibration with respect to that of the silo specimen with smooth wall, the different rigidity of the base connections between the two configurations clearly affect their dynamic response. Thus, the lower relative error detected for the specimen with roughened wall may be associated to the fact that the silo base with increased rigidity better fit the theoretical case of base-clamped cantilever beam with respect to the silo specimen with smooth wall.

In addition, with the aim of verifying the effectiveness of the refined analytical formulation in the estimation of the *effective mass*, the experimental data from ASESGRAM project are compared with the ones predicted according to the refined analytical formulation. The experimental frequencies are obtained from WN tests by interpreting the Transfer functions curves (Figure 9 of Silvestri at al. 2016 and Tables 2 and 3). The effective masses can be derived from two independent measurements and tests:

- The value of the experimental first natural frequency f_1 (WN test); In detail, the *effective mass* based on f_1, m_{eff,f_1}, can be calculated by inserting the experimental frequency f_1 in Eq. (20) and using Eq. (8).

- The value of the experimental base wall bending moment M_{base} as obtained from strain measurements (HS test). In detail, the *effective mass* based on M_{base} , $m_{eff,M_{base}}$, can be obtained by mean of Eq. (40) of chpater 9.

Table 10.2 compares the two experimentally-based values of the effective mass ($m_{eff\,,f_1}$, $m_{eff,M_{base}}$) obtained from the WN test and HS test at a = 0.1 for the third configuration (silo specimen with roughened wall). It can be noted that, from an engineering point of view, the three values are equivalent.

Table 10.2 - Comparison of the fundamental period of realistic flat-bottom ground-supported circular silos filled with wheat with various slenderness ratios, according to the proposed analytical formulations and FE simulations

Analytical	Experimental WN a= 0.1	Experimental HS a= 0.1
m_{eff} Eq. (8)	$m_{eff\,,f_1}$	$m_{eff,M_{base}}$
0.43	0.38	0.42

10.3.2 Experimental results from the scientific literature

In this section, the prediction of the fundamental period (or frequency) of vibration given by the proposed analytical formulation is compared with experimental results available in the scientific literature.

Table 10.3 compares the values of the experimental first natural frequencies of grain-silos available from the scientific literature with those obtained according to Eq. (20).

Table 10.3 - Comparison of the experimental fundamental frequencies of flat-bottom ground-supported circular silo specimen filled with granular material and the analytical prediction by Eq. (20)

Reference	**Specimen**			**Frequencies**				
	Wall material	**Δ [-]**	**Ensiled material**	**Type**	***a* [*g*]**	**Experimental [*Hz*]**	**Analytical [%] (*)**	**Relative error [%]**
Lee (1981)	Lucite	4.9	Sand	FV	0.5	5.8	7.4	-25
Yokota et al. (1983)	Acrylic resin	1.0	Coal	HS	0.05	19 (*)	20.6	-8
Shimamoto et al. (1984)	PVC resin	1.0	Coal	HS	0.30	13.5 (*)	13.9	-3
	PVC resin				0.10	20.5 (*)	20.8	-1
	PVC resin				0.10	22.4 (*)	29.1	-30
	Steel				0.10	23.0 (*)	47.7	-105
Sakai et al. (1985)	Acrylic plastic	1.3	Coal	HS	0.05	28.6 (*)	37.4	-31
					0.10	31.0 (*)	37.4	-21
					0.20	33.7 (*)	37.4	-11
					0.30	28.6 (*)	37.4	-31
			Air slag		0.10	24.5 (*)	24.8	-1

(*): for the harmonic tests (HS) at resonance, m_{eff} is set equal to 0.80

Almost all the test are performed on squat and intermediate slender silos with coal as ensiled material, subjected to a harmonic input at the resonance. The only exception is represented by the FV tests of Lee (1981).

On average, excluding one of the test by Shimamoto et al. (1984) (relative error -105 %), the relative error in the prediction of the first natural frequency is of the order of 15%. For the tests of Lee (1981) the relative error is of the order of -25%; the overestimation of the fundamental frequency of vibration may be related to the underestimation of the experimental *effective mass* which may be incremented by the effect of the relevant grain sliding of the upper layers during free-vibrations (horizontal acceleration of 0.5 *g* was applied).

10.3.3 Numerical results from the scientific literature

In the present section, the prediction of the fundamental period (or frequency) of vibration given by the proposed analytical formulation is compared with numerical results available in the scientific literature.

Table 10.4 reports the data reported by Hardin et al. (1996), regarding the numerical estimation of the first natural frequency of vibration of a squat steel silo filled with hard wheat ($\Delta = 0.9$). The grain-silo in analyzed by means of a composite shear-beam model (see chapter 2 for further details). For the case in exam, the value of the fundamental frequency of vibration as given by the numerical analysis by Hardin et al. (1996) and that given by the analytical prediction of Eq. (20) are quite similar and result 4 and 3.9 *Hz*, respectively.

Table 10.4 - Comparison of the numerical fundamental frequencies of flat-bottom ground-supported circular silo specimen filled with granular material and the analytical prediction by Eq. (20)

Reference	Specimen			Frequencies				
	Wall material	**Δ [-]**	**Ensiled material**	**Type**	***a* [*g*]**	**Numerical [*Hz*]**	**Analytical [%] (*)**	**Relative error [%]**
Hardin et al. (1996)	Steel	0.9	Hard wheat	EQK	0.1	4.0	3.9	2.5

10.4 A simple code like-formula steel silos

For steel silos containing common grain-like materials and designed according to EC1 ($\overline{s_w}$ = 5000, 2000 and 1000 for squat, intermediate slender and slender silos, respectively) a simple code-like formula for the first natural period is calibrated starting from the proposed analytical formulation. A dynamic conditions far from resonance is considered.

As ensiled bulk solid, wheat is considered suitable to be representative of different granular bulk solids (Sondej et al. 2015). The physical and frictional characteristics of wheat result $\gamma_b = 9000\ N/m^3$, $\mu_{GW} = 0.38$ and $\lambda = 0.54$ for wall type D2 (as per Table E.1 EN 1991-4).

The code-like formula for the first natural period results:

$$T_{1,sh+flex} \cong \left[0.0035 \cdot \bar{\Delta}^2 + 0.015 \cdot \bar{\Delta}\right] \cdot d_c\,(m) \tag{27}$$

Eq. (23) has been calibrated through least square fit technique (R^2 = 0.98). Figure 10.4 displays the fundamental period of vibration $T_{1,sh+flex}$ has predicted by Eqs. (20) and (23) vs the slenderness filling ratio $\bar{\Delta}$ for various silo's diameters d_c (expressed in *m*). It can be noted for the range of common steel grain silos the fundamental periods cover a quite broad range (from 0.1 *s* for very small and squat silos, to 3 *s* for very slender and large silos).

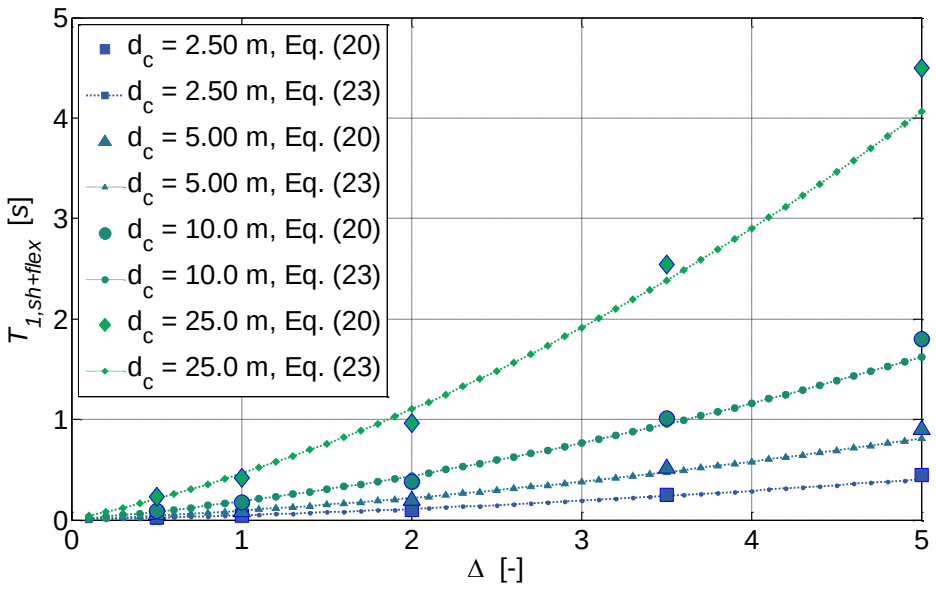

Figure 10.4 - Comparison of the values of the first fundamental period given by the fully analytical formula of Eq. (20) (solid markers) and the code-like formula of Eq. (23) (dotted line) for silos with various diameter and filled with aggregate

10.5 A modeling technique based on the analytical formulation

In this section, a modeling technique for the evaluation of the fundamental period of vibration of grain-silos trough numerical Finite Element (FE) modelling is proposed. The modeling technique implements the analytical formulation introduced in section 10.2 and is consistent with the equivalent silo wall model approach as introduced in chapter 2. Clearly, with respect to the proposed analytical formulation, it allows to encompass more

complex structural configuration, such as horizontally-corrugated silos with vertical stiffeners, typically used for agricultural silos (e.g. silos containing maize, grain, soya beans). The modeling technique here proposed is based on the following steps:

1. Development of the actual FE model of the silo structure including: the shell (smooth or corrugated, with the actual stepwise variations of the thickness), horizontal stringer, vertical stiffeners, the roof. A regular mesh of quad elements is suggested for the walls. In case of smooth wall, all elements are modeled with their own elastic properties (elastic modulus and Poisson's coefficient). In case of corrugated wall, the orthotropic behavior should be considered.

2. Application of rigid horizontal diaphragms at each vertical shell mesh level in order to prevent from section ovalizations (no local modes arises).

3. Assignment of an equivalent material density:

Uniform:

$$\overline{\rho_{eq}} = \frac{\gamma_w}{g} \cdot \left\{ 1 + \frac{\gamma_b}{\gamma_w} \cdot \frac{R}{2 \cdot \overline{t_w}} \cdot \left(\frac{1}{1 - \frac{tg(\phi_r)}{6\overline{\Delta}}} \right) \cdot m_{eff} + \frac{\gamma_r}{\gamma_w} \cdot \sqrt{1 + tg(\alpha_r)^2} \cdot \frac{t_r}{2 \cdot \overline{t_w} \cdot H_{beam}} \right\} \tag{28}$$

Stepwise:

$$\rho_{eq,i} = \frac{\gamma_w}{g} \cdot \left\{ 1 + \frac{1}{\gamma_w} \cdot \frac{n_{zSk}(z = z_i) - n_{zSk}(z = z_{i-1})}{t_{w,i} \cdot \Delta z_i} + \frac{\gamma_r}{\gamma_w} \cdot \sqrt{1 + tg(\alpha_r)^2} \cdot \frac{t_r}{2 \cdot \overline{t_w} \cdot H_{beam}} \right\} \tag{29}$$

where $n_{zSk}(z)$ represents the resulting characteristic value per unit length of perimeter of the vertical compressive force (due to friction) acting on the silo wall after filling. According to the Janssen (1895) and the Reimbert (1976) formulations, the analytical expression of $n_{zSk}(z)$ is defined by Eq. (5.7) and (5.81) by EN 1991-4:2006, respectively.

10.5.1 The fundamental period of vibration of realistic grain-silos

The silos already analyzed by Sadowski and Rotter (2011) are here considered in order to compare the analytical and numerical estimations of the fundamental period of vibration for realistic cases. Five cases are analyzed. All the studies refer to circular flat-bottom silos filled with wheat. The slenderness ratios Δ varies between 0.65 and 5.2, while the silo diameter varies between 5 *m* and 10 *m*. The silos have stepwise wall thickness variation (increasing from the top to the bottom). For each specimen two FE models (uniform and stepwise equivalent wall density) have been developed following the modeling technique previously described, for a total amount of 10 numerical models. Table 10.5 summarizes the values of the first period of vibration according to the analytical Eq. (20), the code-like Eq. (24) and the FE models (with uniform and stepwise distribution of equivalent wall density).

Table 10.5 - Comparison of the fundamental period of realistic flat-bottom ground-supported circular silos filled with wheat with various slenderness ratios, according to the proposed analytical formulation, the code-like formula and FE simulations

Geometrical properties			**First natural period**			
Δ	$\overline{\Delta}$	d_c	Code-like formula Eq. (23)	Rigorous formula Eq. (20)	FE model (*uniform*)	FE model (*stepwise*)
[-]	[-]	[*m*]	[*s*]	[*s*]	[*s*]	[*s*]
0.65	0.55	10.0	0.10	0.06	0.06	0.04
1.47	1.37	7.6	0.19	0.12	0.14	0.11
2.06	1.94	6.8	0.24	0.16	0.15	0.14
3.00	2.88	6.0	0.32	0.27	0.23	0.21
5.20	5.08	5.0	0.47	0.60	0.46	0.45

The level of accuracy decrease going from the FE model (*stepwise*), to FE model (*uniform*), to the rigorous formula Eq. (20), and finally to the simple code-like Eq. (23). It can be noted that: (i) going from the refined FE model (*stepwise*) to the simpler FE model (*uniform*) only a minor variation in the fundamental period is detected (order of few percent); (ii) going from the simple FE model (*uniform*) to the rigorous analytical estimation of Eq. (20) differences are appreciated especially for larger slenderness ratios (order of 30%); (iii) going from the rigorous analytical estimation of Eq. (20) to the simple code-like formula more significant discrepancies appear (except for the very slender silo). Nonetheless, the simple equation seems adequate to capture the essence of the response and thus a potential code-like candidate.

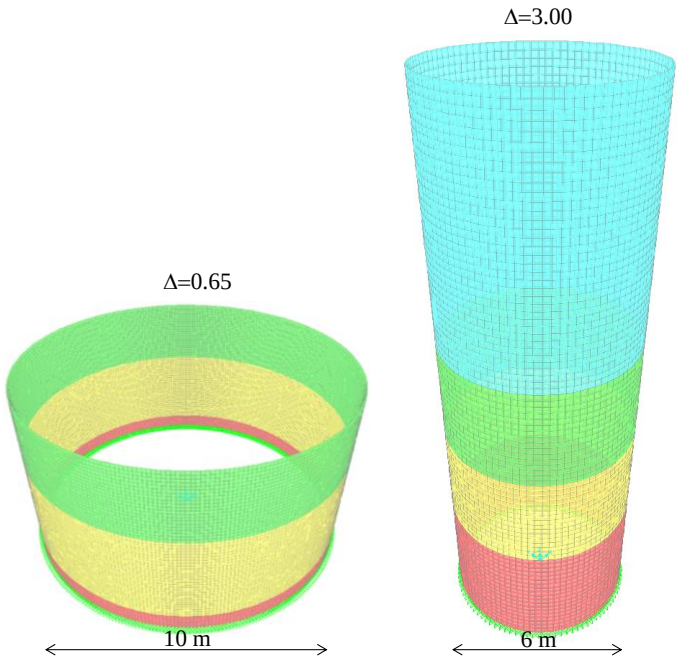

Figure 10.5 - FE models for the squat silo (Δ=0.65) and the slender silo (Δ =3.00) with stepwise variation of the wall thickness and uniform equivalent wall density

10.6 Critical consideration

In the present section, an analytical formulation for the estimation of the fundamental period of vibration of grain-silos is proposed. The formula is grounded on the refined analytical formulation. The silo is modelled as an equivalent shear-flexural cantilever beam with an applied mass equal to the mass of the silo structure plus the mass corresponding to the portion of the ensiled mass which is activated during the earthquake ground motion. Doing so, a fully analytical formula has been derived. The fully analytical expression is verified by comparing the predictions of the fundamental period of vibration with that experimentally gathered by the shaking-table tests conducted within the ASESGRAM project and given by different Authors in the scientific literature. The agreement with the experimental data is quite satisfactory and an average relative error around 15% is detected between experimentally-based values and those predicted by the analytical formula. In addition to the fully analytical formulation, an approximate code-like formula for cylindrical steel silos containing common grain-like materials has been finally derived. Finally, a modeling technique to be easily implemented in a commercial finite element software has been proposed.

Reference

ASCE-7 (2010) - Chapter 15. Seismic Design Requirements for Nonbuilding Structures

Chandrasekaran, A. R., & Jain, P. C. (1968). Effective live load of storage materials under dynamic conditions. Indian Concrete Journal, 42(9), 364-365.

Dunkerley, S. (1894). On the whirling and vibration of shafts. Philosophical Transactions of the Royal Society of London. A, 279-360.

Durmuş, A., & Livaoglu, R. (2015). A simplified 3 DOF model of A FEM model for seismic analysis of a silo containing elastic material accounting for soil–structure interaction. Soil Dynamics and Earthquake Engineering, 77, 1-14.

EN 1991-4 (2006) Eurocode 1. Actions on structures, Part 4 -Silos, tanks and pipelines, CEN, Brussels.

Gould, P. L. (1988). Cylindrical shell slice-beam. Journal of engineering mechanics, 114(5), 905-911.

Janssen, H. A. (1895). Versuche über getreidedruck in silozellen. *Zeitschr. d. Vereines deutscher Ingenieure*, *39*(35), 1045-1049.

Hardin, B. O., Bucklin, R. A., & Ross, I. J. (1996). Shear-beam analysis for seismic response of metal wheat bins. Transactions of the ASAE, 39(2), 677-687.

Lee, S. J. (1981). Experimental study of cylindrical silos subject to seismic excitation (Doctoral dissertation, The Ohio State University).

Reimbert, M. and A. Reimbert. 1976. Silos—Theories and Practice. Clausthal, Germany, Trans Tech Publishers. 250p.

Sadowski, A. J., & Rotter, J. M. (2011). Steel silos with different aspect ratios: I—Behaviour under concentric discharge. Journal of Constructional Steel Research, 67(10), 1537-1544.

Silvestri, S., Ivorra, S., Chiacchio, L. D., Trombetti, T., Foti, D., Gasparini, G., ... & Taylor, C. (2016). Shaking-table tests of flat-bottom circular silos containing grain-like material. *Earthquake Engineering & Structural Dynamics*, *45*(1), 69-89.

Sondej, M., Iwicki, P., Tejchman, J., & Wójcik, M. (2015). Critical assessment of Eurocode approach to stability of metal cylindrical silos with corrugated walls and vertical stiffeners. Thin-Walled Structures, 95, 335-346.

Viola, E. (2001). Fondamenti di dinamica e vibrazione delle strutture. Pitagora.

Whitney, S. (1999). Vibrations of Cantilever Beams: Deflection, Frequency, and Research Uses. Website: Apr, 23, 10.

11. An experimental campaign on a real steel silo containing maize grain

In this chapter, the main results of an on-field experimental campaign carried out on a real operational, horizontally corrugated, vertically stiffened steel silo under progressive symmetric filling are reported. Although it is beyond the scope of the present work, the main aim of such experimental activity is to investigate the structural behavior under static loading of such typology of complex silo structures, which is still not fully understood. This represents a preliminary, first, essential step to be performed in order to gain confidence on the peculiar structural response of horizontally corrugated vertically stiffened silos and to develop future experimental investigations focused on the dynamic behavior. Dynamic tests will be developed to assess the actual dynamic response of such real silo structures exposed to base excitation and to verify if the theoretical predictions given by the proposed analytical formulations (developed for idealized silo models) are able to capture the response of more complex real structures. The analysis of the experimental results will provide further insight into the peculiar structural behavior of horizontally corrugated vertically stiffener grain-silos and it will give some indications for the future developments of specific Finite Element models for the numerical analysis of the dynamic response of such complex structures and the preparation of on-field dynamic tests.

First, the on-field experimental campaign and details about the real silo structure, the ensiled content, the filling procedure, the instrumentation and the test setup are described. Then, the main experimental results as given by the measurements performed on the structure are analyzed and the stresses and the internal actions on the silo structure are reconstructed. Finally, a comparison between the reconstructed values of the internal actions on the structure and those predicted by making use of classical theories for the static conditions is performed.

11.1 Objectives

The on-field experimental campaign reported has been developed as joint research work by the University of Bologna and *Mulmix S.p.a.*, one of the leading Italian manufacturers in the field of steel grain-silo structures. The main aim of such experimental activity is to investigate the structural behavior under static loading of such typology of complex silo structures, which is still not fully understood (Ayuga et al. 2001, 2005; Rotter

2009). This represents a preliminary, first, essential step towards a wider experimental campaign that aims to assess the actual dynamic response of complex real silo structures and to verify if the theoretical predictions given by the proposed analytical formulations (developed for idealized silo models under idealized conditions) are able to capture the actual structural response of real grain-silos subjected to dynamic excitations.

Up until this time, only few experimental investigations have been carried out on real horizontally corrugated vertically stiffened steel silo structures and they exclusively refer to static conditions (Thompson and Prather 1984; Thompson et al. 1997, Németh and Brodniansky 2013). As matter of fact, the economic impact and the practical difficulties of performing on-field experimental tests on such real silo structures make it difficult to perform extensive experimental investigations. Dynamic investigations on real scale industrial facilities have been conducted by Arze (1992). However, such investigations have been mainly focused on the dynamic response of r.c. frame structures, elevated water tanks, chimney stack, without investigating grain-silo structures. In addition, the most of the numerical simulations and experimental works conducted in the last forty years have been focused on the dynamics of simpler silo models with isotropic wall. Thus, progress in the assessment of the actual dynamic response of real silo structures is required.

The experimental results of this campaign will provide a further, preliminary, insight on the structural behavior of such complex real silo structure and will give some indications for the future developments of specific Finite Element models for the numerical analysis of the dynamic response of such complex structures under dynamic base excitation and the preparation of dynamic tests on real scale silo structures.

11.2 The experimental campaign

In the present section, the on-filed experimental campaign conducted on a horizontally corrugated, vertically stiffened real silo structure is described. The experimental campaign has been carried out on two different sessions of tests (conducted on October and November 2014). First, the full operational real silo structure, the ensiled granular content and the filling procedure are described. Then, the instrumentation phases, the test setup and the organization of the in-situ measurements are described.

11.2.1 The silo structure

The silo structure in exam is a horizontally corrugated vertically stiffened circular steel silo grounded on a flat r.c. foundation slab, covered by a conical steel roof, located in the North Italy (Figure 11.1). The vertical cylinder composing the silo wall has 14.8 *m* diameter (d_c) and 14.1 *m* height (h_w), for roughly 2500 m^3 volume. The silo walls are composed by horizontal strips of horizontally corrugated steel plates (each strip is 0.80 *m* height) bolted with thin cold-formed hat-shaped vertical stiffeners (Class 4 cross-section). The vertical stiffeners are composed by joining together, along the vertical axis, different elements by means of ad-hoc shaped elements (Figure 11.2*a*, *b*). In some cases, the hat-shaped vertical stiffeners are composed by more than one superposed steel profiles which are closely bolted together (Figure 11.2*a*). In total, 48 vertical stiffeners are equally spaced along the external circular perimeter of the silo. The general arrangement of the bolted connections allows to avoid continuous lines of connections, both in the horizontal plane and along the vertical direction, as shown in Figure 11.2*c*, *d*. In order to do this, along the circumference of the silo wall, two different vertical alignments of vertical stiffeners are considered (referred to as line A and line B). In total, the vertical cylinder composing the silo wall is made up by superposing 17 horizontal levels of corrugated curved strips (Figure 11.3).

Table 11.1 reports the vertical distribution of the horizontally corrugated curved strips, their thickness variation along the height of the silo wall (t_w), and the cross-section type of the hat-shaped vertical stiffeners in correspondence of the discrete *i-th* level (taking with reference the lower edge of each strip), with reference to the vertical abscissa *z'*, going from the upper edge of the silo wall towards the silo bottom. Table 11.2 reports the main geometrical characteristics of the cross-sections of the vertical stiffeners, such as the gross cross-section area of the stiffeners (A_s) and the corresponding principal moment of inertia evaluated with respect to the *x-x* axis (parallel to the web of the profile) (I_{xx}). In case of cross-sections composed by more than one profile, such values are computed neglecting any shear/sliding deformation (plane cross-sections remain plane), with reference to the total gross-section. Figure 11.4 shows an example of the local reference system considered for the stiffener cross-sections.

Figure 11.1 - Horizontally corrugated vertically stiffened flat-bottomed silo in exam

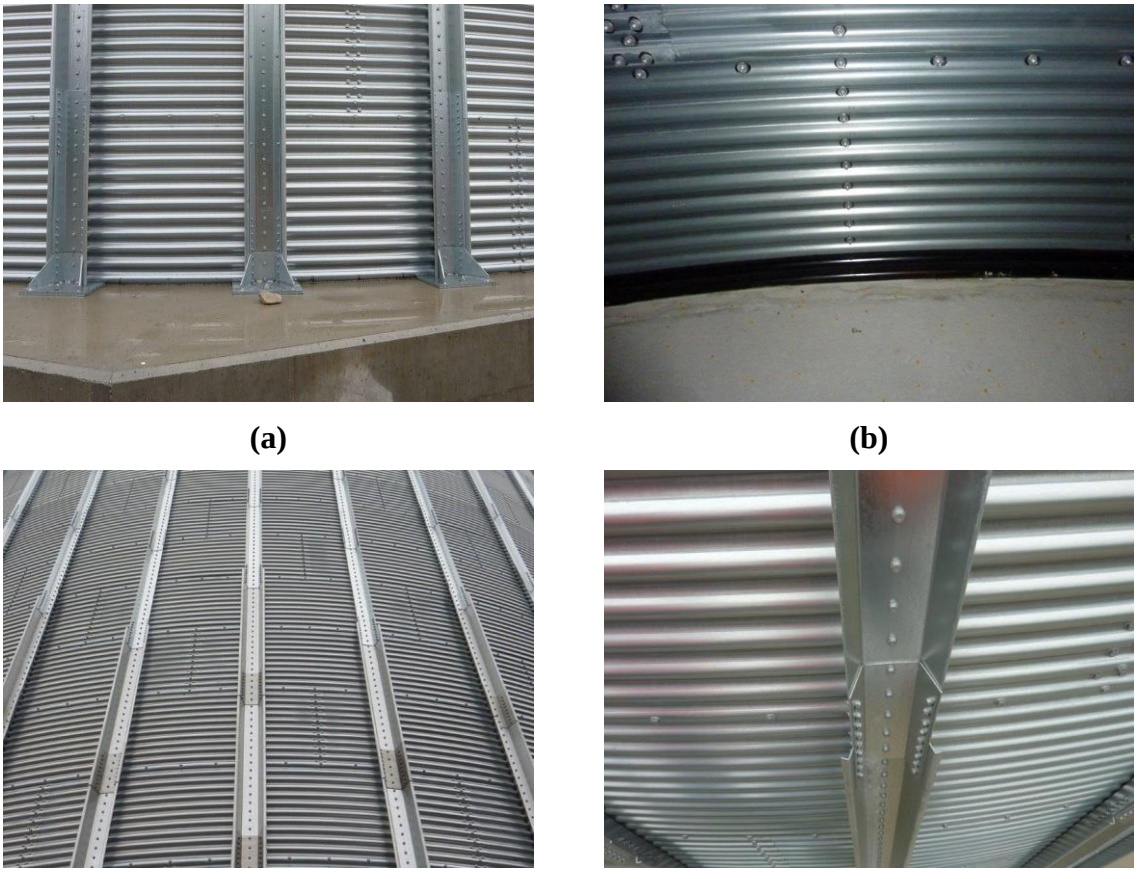

(a) **(b)**

(c) **(d)**

Figure 11.2 - a) External view of the horizontally corrugated vertically stiffened silo wall; b) internal view of the silo wall; c) general external view of the silo wall and arrangement of the bolted connections; d) view of the joint between two consecutive vertical stiffeners

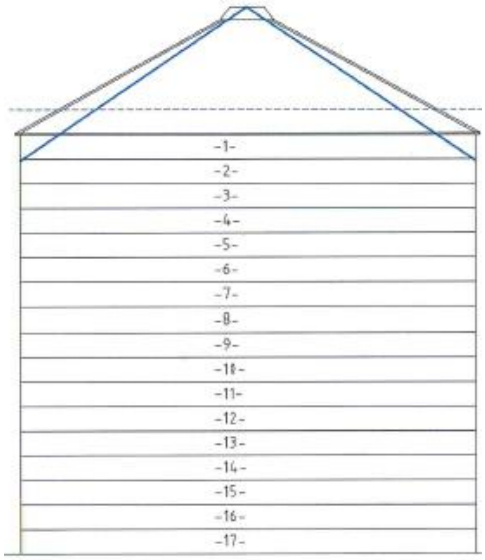

Figure 11.3 - Horizontal levels composed by consecutive horizontally corrugated wall strips

Table 11.1 - Vertical distribution of the horizontally corrugated plates, the thickness variation along the height of the silo wall (t_w), and the cross-section type of the hat-shaped vertical stiffeners in correspondence of the discrete i-th level, with reference to the vertical abscissa z'

Level	t_w	z'_i	Line A	Line B
[-]	[mm]	[m]	[Initial]	[Initial]
1	1.5	0.8	L2PS	L2PS
2	0.8	1.6	L2PS	L2PS
3	0.8	2.4	L2PS	L2PS
4	1.0	3.2	L2PS	L2PS
5	1.0	4.0	L2PS	L2PS
6	1.25	4.9	L2PS	L3PS
7	1.25	5.7	L3PS	L3PS
8	1.5	6.5	L3PS	L3PS
9	1.5	7.4	L3NS	L3PS
10	1.5	8.2	L3NS	L3NS
11	1.5	9.1	L3NS	L3NS
12	1.5	9.9	L3NS	L3NS
13	1.5	10.7	L4NS	L3NS
14	1.5	11.6	L4NS	L4NS
15	1.5	12.4	L4NS	L4NS
16	1.5	13.2	L4NS	L7PD
17	1.75	14.1	L7PD	L7PD

Table 11.2 – Values of the gross cross-section area and gross cross-section moment of inertia along the x-x axis

Initial	A_s [cm^2]	I_{xx} [cm^4]
L2PS	5.0	25.7
L3PS	7.5	38.2
L3NS	10.0	118.1
L4NS	13.5	155.4
L7PD	20.8	196.5

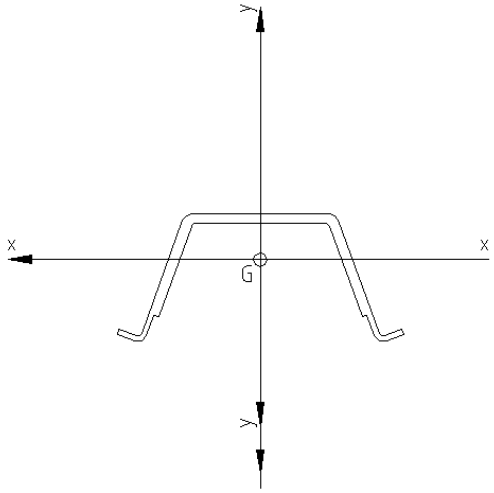

Figure 11.4 - Example of the reference system for L7PD cross-section composed by two superposed steel profiles.

11.2.2 The ensiled content

The silo structure has been specifically designed for storing maize grain. The physical characteristic of the maize grain have not been investigated by means of direct measurements or tests. The only exceptions regard the estimation of the unit weight of the maize grain γ_b and its mean moisture content *w*, which have been measured directly in-situ before filling the silo. The physical characteristics of the bulk solid taken into account are those considered during design, referred to those reported in Table E.1 EN 1991-4:2006 and summarized in Table 11.3. It should be noted that the measured unit weight of the maize grain is around 7 kN/m^3, resulting lower to that indicated by Table E.1 of EN 1991-4:2006.

Table 11.3 - Physical characteristic of the maize grain according to Table E.1 EN 1991-4:2006

Bulk solid	Maize
Unit weight γ_b [kN/m^3]	7
Angle of repose ϕ_r [°]	35
Mean angle of internal friction ϕ_{im} [°]	31
a_ϕ [-]	1.14
Mean lateral pressure ratio K_m [-]	0.53
a_K [-]	1.14
Wall friction coefficient wall type D1 μ [-]	0.22
Wall friction coefficient wall type D2 μ [-]	0.36
Wall friction coefficient wall type D3 μ [-]	0.53
a_μ [-]	1.24
w [%]	14

11.2.3 The filling procedure and the filling height

The maize grain is delivered in situ by trucks and its volume and weight are measured before being poured in the storage area (Figure 11.5). Then, the maize is raised up from the storage area and the silo is centrally filled from an outlet disposed on the top of the silo roof, by pouring approximately 360 *kN/h* of maize inside the silo, according to the availability of the product. The total grain mass poured inside the silo M_b after each filling step is registered.

The equivalent filling height reached by the product poured inside the silo h_b is estimated equaling the total grain mass poured inside the silo M_b with that corresponding to a cylinder with same horizontal cross-section of the silo and height h_b. The height above the silo bottom of the highest grain-wall contact h_c is computed by considering the formation of a granular upper conical pile:

$$h_b = \frac{4 \cdot M_b}{(\gamma_b / g) \cdot \pi \cdot d_c^2} \tag{30}$$

$$h_c = h_b - \frac{d_c}{6} \cdot tg(\phi_r) \tag{31}$$

The maximum value of the equivalent filling height (i.e. after full filling of the silo) is computed considering that at the end of the filling process around 1700 *tons* of maize grain were poured inside the silo (a total amount of around 50 *h* of filling process were necessary). According to Eqs. (1) and (2), the maximum equivalent filling height of the grain-wall contact with respect to the silo base h_b (at the end of the filling) resulted around

14.7 *m*, while the corresponding height above the bottom of the highest grain-wall contact h_c resulted 12.9 *m* (below the maximum allowable value of 13.7 *m*).

It is worth mentioning that the filling process under exam resulted the first one for the silo in exam.

Figure 11.5 - Maize delivered by truck

11.2.4 Instrumentation and test setup

The instrumentation adopted to carry out the present experimental campaign consisted in:

- One digital invar micrometer "DEMEC" (measuring base 250 *mm*) (referred to as M250), Figure 11.6*a*;
- One analogic metal micrometer "RNU" (measuring base 300 *mm*) (referred to as M300), Figure 11.6*b*;
- Reference bases of length 250 *mm* and 300 *mm* (male and female), Figure 11.7*a*, *b*;
- Temperature detector, Figure 11.8;
- Strain gauges of 8 *mm* length (referred to as *E*), Figure 11.9.

Micrometers and strain gauges will provide two different, but correlated, pieces of information regarding the vertical deformations occurring on the corrugated wall and the vertical stiffener. The former will provide "average" measurements of deformation, while the latter will provide "local" measurements of deformation. The comparison between the so-called average and local measurements could give preliminary information regarding

the effect of eventual stress concentrations (related to the presence of bolted connections) on the strain field experienced by the structural members.

The typology of instrumentation adopted has been selected in order to provide preliminary, economic, non-invasive, but realistic measurements of the deformations experienced by selected portions of the wall and stiffeners during progressive filling. Thus, only a limited number of measuring points have been considered and only a limited number of repetitions have been carried out. In general, the repetitions have been carried out every 1-2 hours in order to trace a reliable time-evolution of the deformations.

In order to perform the measurements of the vertical deformations on the structural members by using the micrometers, ad-hoc metal disks were glued and spaced at a specified vertical distance (referred to as l_h) with the help of the male reference bases, both on the wall and the hat-shaped stiffeners. This operation allows to materialize the vertical measuring bases on the wall and on the stiffener, which represents the measuring points (Figure 11.10*a*, *b*). The measuring points are located on one vertical strip of the silo wall (corresponding to the portion of wall enclosed between two consecutive vertical stiffeners) and on one vertical stiffener. The measuring points are located on silo wall and stiffeners avoiding, as possible, highly bolted zones (connections between consecutive stiffeners and consecutive wall portions). In addition, due to the geometrical configuration of the wave of corrugation of the silo wall, only measuring bases of length l_b = 300 *mm* have been mounted on the wall; while on the vertical stiffener measuring bases of length l_b = 250 *mm* have been placed.

(a) **(b)**

Figure 11.6 - a) Digital invar micrometer "DEMEC" 250; b) Analogic invar micrometer "DEMEC" 300

(a) **(b)**

Figure 11.7 – a) Male reference base of length 250 mm for the positioning of the metal-disks on the structural members; b) female invar reference base for the assessment of the thermal deformation of the instrument

Figure 11.8 - Instrumentation to measure the temperature of the air and the temperature of the structural members

Figure 11.9 – Typology of 8 mm long strain gauges mounted on the silo wall and vertical stiffeners

As far as the corrugated wall are concerned, measuring bases are instrumented along two reference vertical lines: one along the vertical axis of symmetry of the wall portion enclosed between two consecutive stiffeners (Figure 11.11*a*) and one 10 *cm* far from the vertical stiffener under exam (Figure 11.11*b*), in order to appreciate eventual difference on the vertical deformations detected on the two alignments. As far as the hat-shaped vertical stiffeners are concerned, measuring bases are instrumented along three vertical lines: one on the front face of the stiffener's web, along the middle vertical axis (Figure 11.12*a*), two along the middle vertical axis of the inclined flange, in detail, one on the internal face (Figure 11.12*a*) and one on the external face (Figure 11.12*b*), in order to appreciate eventual difference on the vertical deformations detected on the web and the flanges and on the internal face and the external face of the vertical portion of the stiffener composed by more than one profiles. For vertical portion of the stiffener composed by only one steel profile, the measuring base on the flange reduces to that one applied on the internal face only.

The thermal deformation investing the micrometers is detected by performing measurements of the length of the invar female reference base (Figure 11.7*b*).

The vertical measuring bases are disposed on discrete levels along the height of the vertical cylinder composing the silo wall. In detail, 10 measuring bases are disposed on the corrugated silo wall, while 11 measuring bases are mounted on the vertical stiffener, for a total of 21 measuring bases. Table 11.4 reports the general nomenclature of the measuring bases, their vertical distance z^* from the flat-bottom of the silo (taken with reference to their centroid) and the number of their level of application. On the corrugated wall, the measuring bases along the middle vertical axis have initial *M*, while those at 10 *cm* from the vertical stiffeners have initial *V*. On the vertical stiffener, the measuring bases along the middle vertical axis of the web have initial *A*, while those placed on the internal face (inside) and the external face (outside) have initials *I* and *O*, respectively. The consecutive number individuates the corresponding level of the corrugated wall on which the measuring bases are applied.

Table 11.5 reports the distance of the measuring basis, measured along the *y*-*y* axis, with respect to the centroid of the gross cross-section of each profile.

Table 11.4 - General nomenclature of the measuring bases placed on the wall (M, V) and the vertical stiffener (A, I, O), their distance z from the flat-bottom of the silo (taken with reference to their centroid) and the level of application.*

Wall	Stiffener	z^* [m]	Level
M16, V16	A16, I16, O16	1.40	16
M13, V13	A13, I13	3.80	13
M9, V9	A9, I9	7.95	9
M3, V3	A3, I3	11.30	3
M1, V1	A1, I1	12.95	1

Table 11.5 - Distance of the measuring bases along the y-y axis with respect to the centroid of the gross cross-section

Initial	y_A [cm]	y_I [cm]	y_O [cm]
L2PS	-1.8	1.2	-
L3PS	-1.7	1.2	-
L3NS	-3.4	1.2	-
L4NS	-	-	-
L7PD	-2.4	2.4	2.4

In correspondence of the measuring bases located in proximity of the silo bottom (i.e. only for $z^* = 1.40\ m$), three strain gauges are applied on the corrugated wall and the vertical stiffener. In detail, a strain gauge is mounted on the apex of a wave of the corrugated wall along the horizontal direction (E_M), in correspondence of the middle point of the wall portion, on the centroid of the measuring base M16 (Figure 11.13), while two vertical strain gauges are mounted on the internal and external faces of the flange (on the centroid the corresponding measuring bases), on the centroid of the measuring bases O16 (E_O) (Figure 11.14*a*) and I16 (E_I) (Figure 11.14*b*). Table 11.6 summarizes the details about the three strain gauges. The strain measurements gathered via strain gauges allow to: (i) detected the strains experience by the silo wall and the stiffener during progressive filling; (ii) compare the values with those given by the micrometers.

Table 11.6 - General nomenclature of the strain gauges placed on the middle of the wall and the vertical stiffener at z=1.40 m from the flat-bottom of the silo and level of application.*

Location	Initial	z^* [m]	Level
Wall	E_M	1.40	16
Stiffener (inside)	E_I	1.40	16
Stiffener (outside)	E_O	1.40	16

(a) **(b)**

Figure 11.10 – a) Metal disks glued on the wall and the hat-shaped stiffeners in order to materialize vertical measuring bases; b) example of application of the metal disks on the silo wall

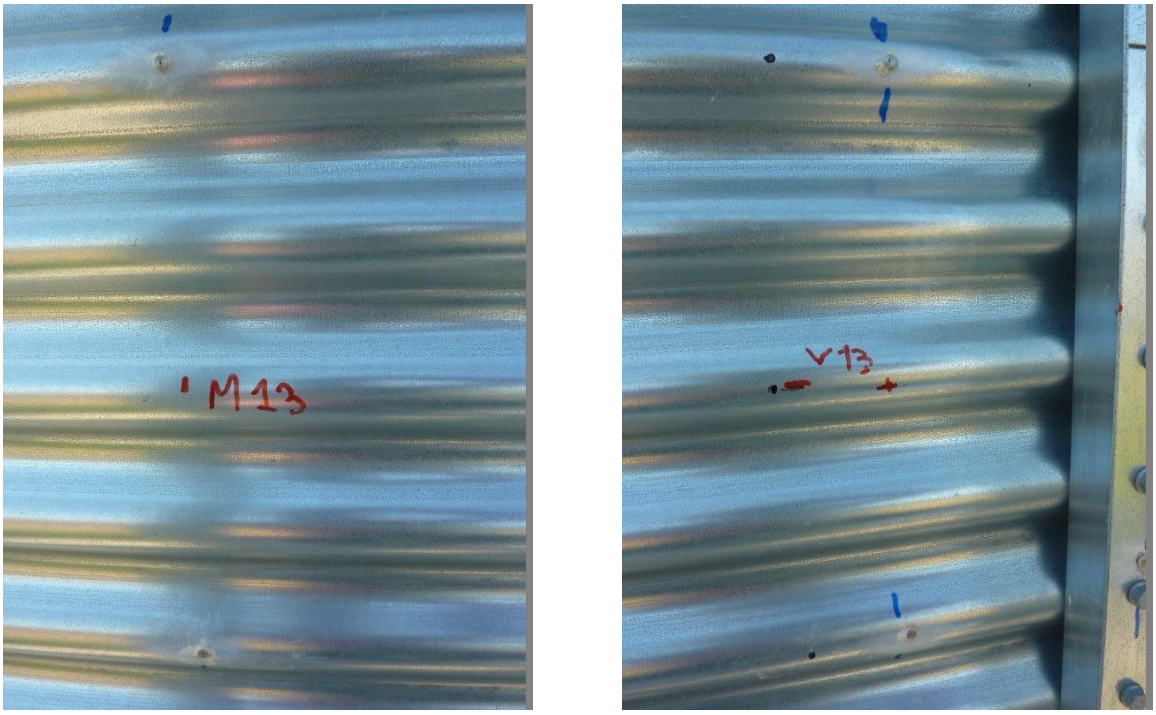

(a) **(b)**

Figure 11.11 – a) Measuring base along the vertical axis of symmetry of the wall portion enclosed between two consecutive stiffeners; b) measuring base close to vertical stiffeners.

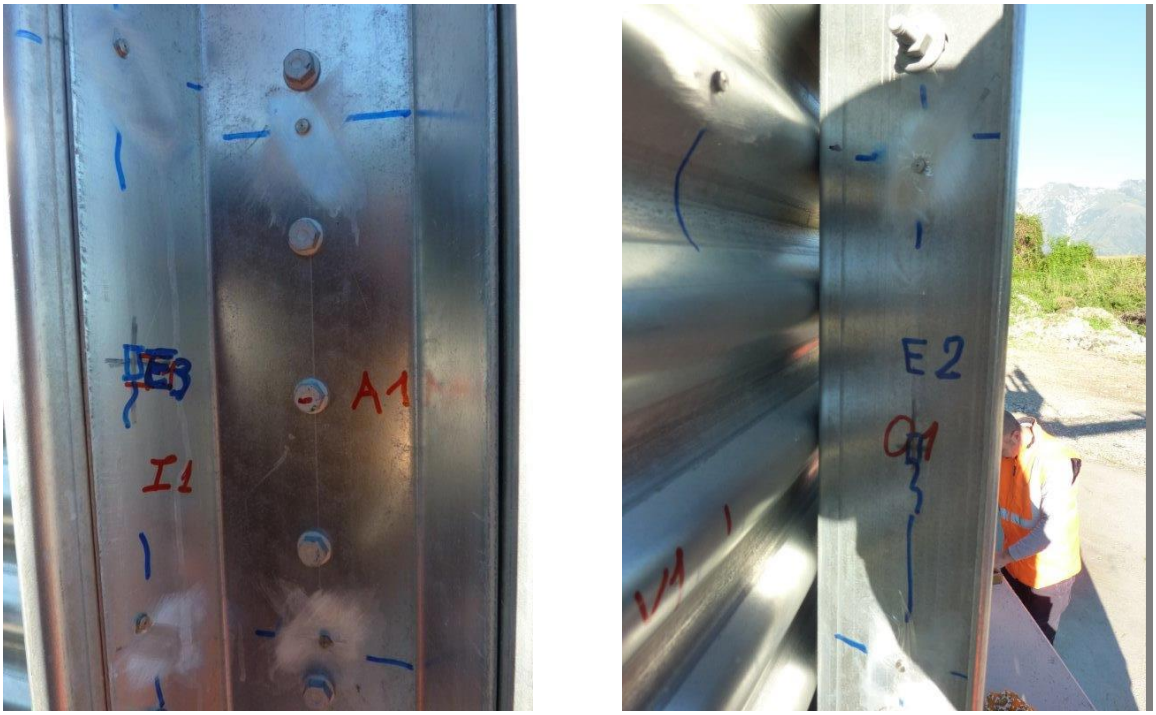

(a) (b)

Figure 11.12 – a) Measuring bases along the front face of the stiffener's web along the middle vertical axis and along the middle vertical axis of the inclined flange, on the internal face; b) measuring base along the middle vertical axis of the inclined flange, on the external face.

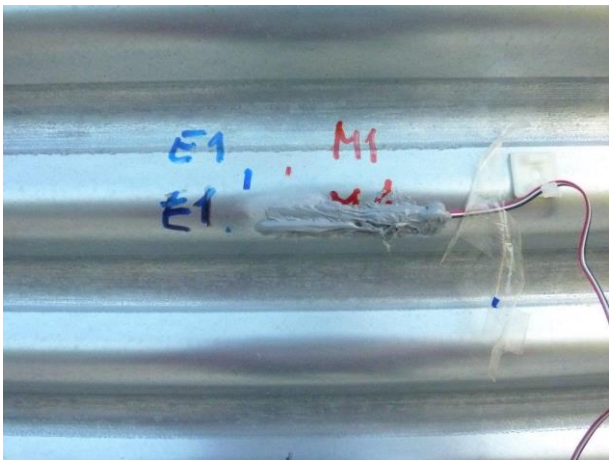

Figure 11.13 – Horizontal strain gauge on the apex of a wave on the corrugated wall in correspondence of the measuring base M1 at z = 1,40 m*

(a) **(b)**

Figure 11.14 – a) Vertical strain gauge placed on the external face of the external profile composing the hat-shaped stiffeners in correspondence of the measuring base O1 at z= 1,40 m; b) Vertical strain gauge placed on the internal face of the internal profile composing the hat-shaped stiffeners in correspondence of the measuring base I1 z*= 1,40 m.*

Micrometer M250 has been adopted to measure the vertical deformation occurring on the vertical stiffeners, while the micrometer M300 has been adopted to measure the vertical deformation occurring on the corrugated wall.

11.2.5 Phases of measurement

The measurements have been conducted by following two distinct phases:

1. Phase 1: identification of the reference values of the measuring bases and strain gauges placed on the corrugated wall and the vertical stiffener for the empty silo, performed on October 2014;
2. Phase 2: measurement of the deformation on the corrugated wall and the vertical stiffener for the silo under progressive filling, performed on October and November 2014.

On each phase, several repetitions of the measurements are performed on the measuring bases and the strain gauges, starting from the silo base towards the silo roof

with the help of an elevator. For each repetition, on each measuring base and strain gauge, three readings are performed (namely, 1st, 2nd and 3rd reading). As far as the readings on the measuring bases are concerned, the measurements have been performed by detecting the length of the measuring base, included between two metal disks. As far as the readings on the strain gauge are concerned, the readings have been taken by simply recording the deformation level given by the control unit.

The phase 1 consisted in measuring the deformations induced by thermal actions on the structural members (wall and stiffener). Such phase lasted one day (from early morning to late afternoon) and consisted of 3 repetitions, in total (roughly, one every 4 hours), on all the measuring bases, in order to observe the structural deformations induced for different levels of temperature (due to different solar irradiation of the silo structure).

The main aims of this phases are to:

- Identify the reference values of the measuring bases and strain gauges placed on the corrugated wall and the vertical stiffener for the empty silo;
- Take confidence with the modality of measurements (performed on the elevator);
- Establish the order of magnitude of eventual deformation induced by the thermal variations on the structural members.

The phase 2 consisted in measuring the deformations induced by the action of the ensiled grain on the structural members (wall and stiffener). This phase lasted three days in total (two consecutive days in October, one in November) and consisted of 8 repetitions in total, in order to observe the structural deformations for different levels of filling. The filling levels have been reconstructed, as described in the previous sections. As additional data, the vertical level of the filling and its uniformity around the circumference were confirmed by the output given by the measurements of the grain temperature sensors placed inside the silo at various vertical levels and by simply knocking on the silo wall. The main aim of this phase was to detect the deformations occurring on the corrugated wall and the vertical stiffener for increasing levels of filling.

11.3 Experimental result of the measurements

In the present section, the main experimental results of the measurements carried out on phase 1 and phase 2 are reported. In detail, the vertical deformations detected on the wall and on the stiffener are reported and discussed.

11.3.1 Phases 1: reference values for the empty silo and deformations induced by thermal variations

The protocol adopted for the identification of the reference values of the measuring bases and strain gauges placed on the corrugated wall and the vertical stiffener for the empty silo, conducted on phase 1, and the corresponding processing are described.

For the *j-th* repetition of the measurements, first the temperature readings are performed on the steel in correspondence of the measuring base at the *i-th* level and the values of temperature (referred to as $T_j^{(i)}$) are measured by means of the temperature detector (Figure 11.15*a*, *b*). Then, three readings of the length of the invar female reference bases are performed and contextually three readings on each measuring bases and strain gauges are performed (Figure 11.16). The mean of the three readings performed on the invar female reference bases is referred to as $\rho_{u,j}^{(i)}$, while the three readings performed on the structural members are referred to as $r_{u,j}^{(i)}$ (where *u* results *A*, *I*, *O* for the different measuring bases of the stiffener, *M*, *V* for the different measuring bases of the wall). The values of $\rho_{u,j}^{(i)}$ and $r_{u,j}^{(i)}$ are correlated with the detected values of temperature $T_j^{(i)}$.

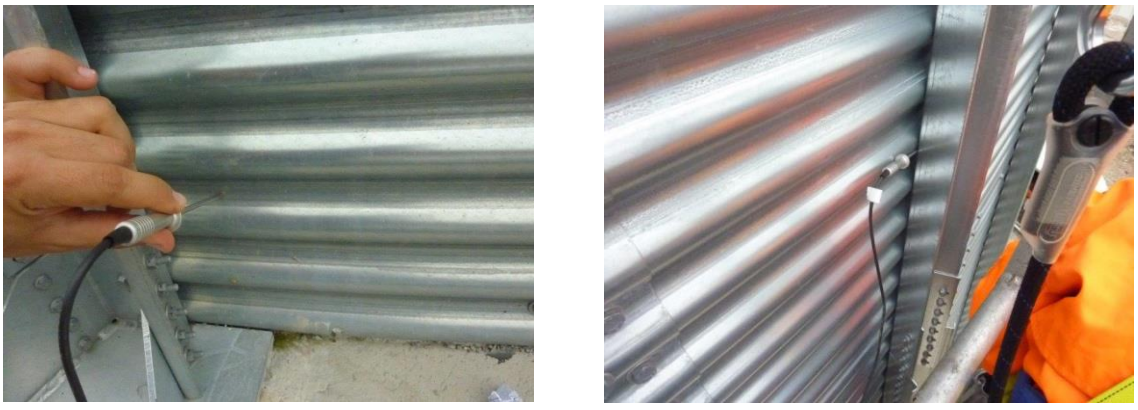

(a) **(b)**

Figure 11.15 - a) Example of measurement of the temperature on the wall; b) on the stiffener.

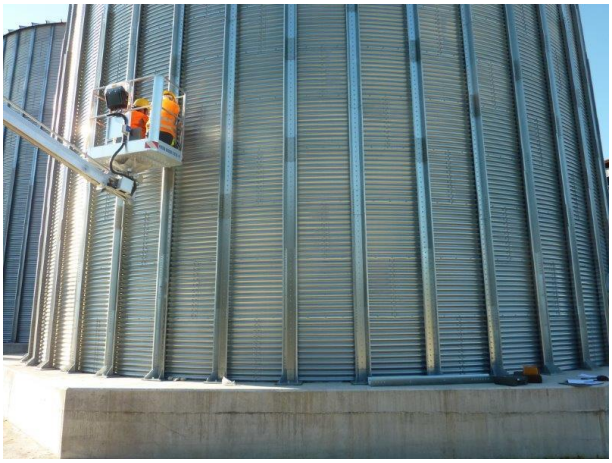

Figure 11.16 - Measurements on the measuring bases on the elevator

For phase 1, three repetitions were performed in total. Thus, for the generic *i-th* level, three variation of the temperature between the generic *j-th* repetition and the *k-th* repetition (where $k \neq j$) $\Delta T_{jk}^{(i)}$ is computed:

$$\Delta T_{jk}^{(i)} = T_j^{(i)} - T_k^{(i)} \tag{32}$$

where j = 1, 2, 3.

The value of the length of the measuring base (placed on the empty structure) for the *j-th* repetition $R_{u,j}^{(i)}$ may be computed as follows:

$$R_{u,j}^{(i)} = r_{u,j}^{(i)} - \rho_{u,j}^{(i)} \tag{33}$$

The variation of length corresponding to the difference between the mean value of readings of the *j-th* repetition and the *k-th* repetition performed on the structural members $\Delta r_{u,jk}^{(i)}$ could be computed:

$$\Delta r_{u,jk}^{(i)} = r_{u,j}^{(i)} - r_{u,k}^{(i)} \tag{34}$$

The thermal deformation investing the micrometers is taken into account by computing the variation of readings corresponding to the difference between the mean value of readings of the *j-th* repetition and the *k-th* repetition performed on the invar female reference bases $\Delta\rho_{u,jk}^{(i)}$ could be computed:

$$\Delta\rho_{u,jk}^{(i)} = \rho_{u,j}^{(i)} - \rho_{u,k}^{(i)} \tag{35}$$

Then, the corrected value of the variation of length $\Delta R_{u,jk}^{(i)}$ is obtained by subtracting the quantity $\Delta\rho_{u,jk}^{(i)}$ to the value of $\Delta r_{u,jk}^{(i)}$, i.e.:

$$\Delta R_{u,jk}^{(i)} = \Delta r_{u,jk}^{(i)} - \Delta\rho_{u,jk}^{(i)} \tag{36}$$

The vertical strain induced by the thermal variation corresponding to the corrected value of the variation of length $\Delta R_{u,jk}^{(i)}$, referred to as $\varepsilon_{u,jk}^{(i)}$ may be computed as follows:

$$\varepsilon_{u,jk}^{(i)} = k_h \cdot \frac{\Delta R_{u,jk}^{(i)}}{l_h} \tag{37}$$

where l_h is the length of the measuring base, k_h is the conversion factor equal to 0.81 and 1.00 for M250 and M300, respectively.

The value of $R_{u,j}^{(i)}$ and $\varepsilon_{u,jk}^{(i)}$ represent the first fundamental results of phase 1 and provides the reference values of the measuring bases placed on the corrugated wall and the vertical stiffener for the empty silo and the magnitude of the vertical strains induced by thermal variations.

In order to check the reliability of the of the measurements of the vertical deformations experienced by the structural members, starting from the vertical strains induced by the thermal variation $\varepsilon_{u,jk}^{(i)}$, the value of the coefficients of linear thermal expansion of the material composing the structure (α_T) is determined and checked as follows:

$$\alpha_T = \frac{\varepsilon_{u,jk}^{(i)}}{\Delta T_{jk}^{(i)}} \tag{38}$$

The mean value of the reading provided by the strain gauges (placed on the empty structure) for the *j-th* repetition $\varepsilon_{l,j}$ (where the subscript *l* may result equal to E_M, E_I, E_O) corresponds to the reference values of the measuring bases placed on the corrugated wall and the vertical stiffener for the empty silo.

The values of the variations of strain induced by the thermal variations detected by the strain gauges, referred to as $\Delta\varepsilon_{l,jk}$ may be computed as follows:

$$\Delta\varepsilon_{l,jk} = \varepsilon_{l,j} - \varepsilon_{l,k} \tag{39}$$

As illustrative example, the experimental readings and the relevant reconstructed values of the vertical strains for the measuring base placed on the web of the stiffeners (*A*) at the level 16 (z^* = 1.40 *m*) are reported. Table 11.7 reports the values of the three readings performed for all the three repetitions performed on phase 1 at the level 16 (z^* = 1.40 *m*) on the measuring base placed on the web of the stiffeners (*A*) and the corresponding temperature measured are reported. Table 11.8 reports the values of the three readings performed for all the three repetitions performed at the level 16 (z^* = 1.40 *m*) on the female reference base for the micrometers of length 250 *mm*. Table 11.9 reports the values of the length of the measuring base (placed on the empty structure) for the *j-th* repetition $R_{u,j}^{(i)}$.

Table 11.7 - Values of the readings performed on the measuring base V16 for phase 1

A16	1st reading [*mm*]	2nd reading [*mm*]	3rd reading [*mm*]	$r_{A,j}^{(16)}$ [*mm*]	$T_j^{(16)}$ [*C°*]
1st repetition (*j*= 1)	-0.021	-0.019	-0.020	-0.020	21.45
2nd repetition (*j*= 2)	-0.005	-0.006	-0.006	-0.006	24.80
3rd repetition (*j*= 3)	-0.015	-0.015	-0.014	-0.015	22.34

Table 11.8 - Values of the readings performed on the female reference base at level 16 for the micrometer 250 for phase 1

250	1st reading [*mm*]	2nd reading [*mm*]	3rd reading [*mm*]	$\rho_{A,j}^{(16)}$ [*mm*]	$T_{S,j}^{(16)}$ [*C°*]
1st repetition (*j*= 1)	-0.008	-0.008	-0.008	-0.008	21.45
2nd repetition (*j*= 2)	-0.003	-0.003	-0.003	-0.003	24.80
3rd repetition (*j*= 3)	-0.007	-0.006	-0.006	-0.006	22.34

Table 11.9 - Values of the length of the measuring base A (placed on the empty structure) at level 16 for the micrometer 250 for phase 1

A16	$R_{A,j}^{(16)}$ $[mm]$
1st repetition (j= 1)	-0.012
2nd repetition (j= 2)	-0.003
3rd repetition (j= 3)	-0.009

According to Eqs. (3)-(8), the variation of the temperature between different repetitions, the corresponding difference between the mean value of readings of the *j-th* repetition and the *k-th* repetition $\Delta R_{u,jk}^{(i)}$ and the vertical strain $\varepsilon_{u,jk}^{(i)}$ experienced by the measuring base placed *A* on level 16 are reported in Table 11.10.

Table 11.10 - Values of the variations of length, thermal variations of the instruments, corrected variations of length for the measuring base V16 for phase 1

A16 *(j-k)*	$\Delta T_{jk}^{(16)}$ $[C°]$	$\Delta r_{A,jk}^{(16)}$ $[mm]$	$\Delta \rho_{250,jk}^{(i)}$ $[mm]$	$\Delta R_{A,jk}^{(16)}$ $[mm]$	$\varepsilon_{A,jk}^{(16)}$ $[10^{-6}]$
2-1	3.35	0.014	-0.005	0.090	30.3
2-3	2.46	0.009	-0.003	0.006	18.4
3-1	0.89	0.005	-0.002	0.003	11.9

According to Eq. (9), the reconstructed values of the coefficient of linear thermal expansion of the steel material α_T are summarized in Table 11.11.

Table 11.11 - Values of the reconstructed coefficient of thermal variation of the material composing the stiffeners for phase 1

A16	α_T $[10^{-6}C°^{-1}]$
2-1	9.0
2-3	7.5
3-1	13.4
mean	10.0

Table 11.12 summarizes the mean values of the reconstructed vertical deformations detected on the measuring bases on the stiffener under investigation for the correspondent values of the variation of temperature.

Table 11.12 - Mean values of the reconstructed vertical deformations detected on the measuring bases on the stiffeners corresponding to the mean values of the variation of temperature

Level	**Stiffener**			
	A [10^6]	**I** [10^6]	**O** [10^6]	ΔT [$C°$]
16	24	32	28	3.0
13	29	49	-	4.4
9	32	35	-	3.0
3	30	40	-	2.5
1	29	28		4.0

It can be noted that:

- The mean values of the reconstructed vertical deformations induced by thermal variations around 3 $C°$ are around 25 and 50 $\mu\varepsilon$, and thus may result significant for the data processing of phase 2;
- The values of the reconstructed vertical deformations experienced by the internal flange of the cross-section of the stiffener are always higher than those experienced by the web of the cross-section of the stiffener;
- The measurements performed on the stiffener during the phase 1 allow an estimate of mean values of the coefficient of linear thermal expansion of the material composing the silo α_T, expressed as the mean value of reconstructed vertical deformation over the difference of temperature ΔT, roughly around 10.1×10^6 (against a value of 12.0×10^6).

As far as the reconstructed vertical deformation induced by thermal variations on the wall are concerned, it is found that the measurements conducted on the measuring bases are strongly affected by the thermal deformation of the micrometer (M300), built in common metal steel. Thus, a stable and reliable identification of the corresponding reference length and thermal induced deformations was not possible.

As far as the variation of the strain detected by the strain gauges are concerned, low values (around 7 $\mu\varepsilon$) are measured for a variation of temperature of the order of 3 $C°$.

11.3.2 Phases 2: deformations induced by grain actions

The protocol adopted for the identification of the variation of the length of measuring bases and variation of strain detected by the strain gauges placed on the corrugated wall and the vertical stiffener for the filled silo, conducted on phase 2, and the corresponding processing of the data are described.

On phase 2, for the *f-th* repetition of the measurements during filling, first the temperature readings are performed, similar to with those performed on phase 1. Then, three readings of the length of the invar female reference bases are performed and contextually three readings on each measuring bases and strain gauges corresponding at the same level are performed (Figure 11.16). The mean of the three readings on the female reference bases $\rho_{u,f}^{(i)}$ and the three readings on the structural members $r_{u,f}^{(i)}$ are evaluated and their values are correlated with the detected temperature.

The value of the length detected on the measuring base corrected by the possible thermal effects on the instrumentation, for the *f-th* repetition during filling, $R_{u,f}^{(i)}$ results:

$$R_{u,f}^{(i)} = r_{u,f}^{(i)} - \rho_{u,f}^{(i)} \tag{40}$$

In order to identify the shortening of the length of the measuring base occurred between the *f-th* repetition during filling and *j-th* repetition performed during the empty conditions, referred to as $s_{u,fj}^{(i)}$, the values of length of the measuring bases reconstructed for the phase 1 $R_{u,j}^{(i)}$, as given by using Eq. (4), are considered. Thus:

$$s_{u,fj}^{(i)} = R_{u,f}^{(i)} - R_{u,j}^{(i)} \tag{41}$$

The value of $s_{u,fj}^{(i)}$ is corrected in order to account for the effects related to the different values of the temperature detected on the structural member between the *f-th* repetition performed during filling and the *j-th* repetition performed during empty condition, leading to the value of $S_{u,fj}^{(i)}$:

$$S_{u,fj}^{(i)} = k_h \frac{s_{u,fj}^{(i)}}{l_b} - \Delta T_{u,fj}^{(i)} \cdot \alpha_T \tag{42}$$

The value of $S_{u,fj}^{(i)}$ averaged over the three repetition performed during empty condition (j = 1, 2, 3), referred to as $\overline{S}_{u,f}^{(i)}$, results:

$$\overline{S}_{u,f}^{(i)} = \frac{\Sigma_{j=1}^{n=3} S_{u,fj}^{(i)}}{3} \tag{43}$$

The values of the variation of strain induced by the filling during the *f-th* repetition detected by the strain gauges, with respect to the mean values detected on the phase 1 ($\overline{\varepsilon}_{l,j}$), referred to as $\Delta\varepsilon_{l,fj}$ may be computed as follows:

$$\Delta\varepsilon_{l,fj} = \varepsilon_{l,f} - \overline{\varepsilon}_{l,j} \tag{44}$$

where the subscript l may result equal to E_M, E_I, E_O.

During the filling process, the repetitions have been conducted for different values of total grain mass of the poured inside the silo M_b. Table 11.13 reports the correspondence between the values of the total ensiled mass poured inside the silo M_b, the equivalent height of grain above the bottom h_b, the height of the highest grain-wall contact h_c.

Table 11.13 - Values of the total ensiled mass, equivalent heights of the grain above the bottom, highest grain-wall contact height

Repetition	Date	Hour	M_b [*tons*]	h_c [*m*]	h_b [*m*]
1	16/10/2014	12:30	400	1.8	3.6
2	16/10/2014	15:45	500	2.6	4.2
3	16/10/2014	17:00	565	3.2	4.6
4	17/10/2014	8:00	780	5.1	5.8
5	17/10/2014	9:30	835	5.5	6.6
6	17/10/2014	11:30	880	5.9	7.0
7	17/10/2014	13:30	940	6.5	7.5
8	22/11/2014	11:00	1685	14.7	12.9

As illustrative example, Table 11.14 and Table 11.15 report the values of $\overline{S}_{u,f}^{(i)}$ reconstructed at level 16 (z^* = 1.40 *m*) and level 13 (z^* = 3.80 *m*) on the vertical stiffener under exam for the measuring base *A*, *I*, *O*, respectively. Table 11.16 reports thee values of the variation of strain induced by the filling detected by the strain gauges on the corrugated wall and the stiffener, at z^* = 1.40 *m* (level 16).

Table 11.14 - Values of the vertical deformation (expressed in $\mu\varepsilon$) as detected on the measuring base A, I, O on level 16 of the stiffener in exam during the process of filling of phase 2

	f	u		
		A [$\mu\varepsilon$]	**I** [$\mu\varepsilon$]	**O** [$\mu\varepsilon$]
$\overline{S}_{u,f}^{(16)}$	1	5.5	-34.5	-3.1
	2	-11.4	-62.7	-22.7
	3	-44.7	-63.6	-25.8
	4	-56.4	-111.1	-
	5	-68.8	-125.7	-72.3
	6	-81.9	-139.1	-84.0
	7	-75.9	-147.1	-83.4
	8	-134.5	-426.2	-78.4

Table 11.15 - Values of the vertical deformation (expressed in $\mu\varepsilon$) as detected on the measuring base A, I on level 13 of the stiffener in exam during the process of filling of phase 2

	f	u	
		A [$\mu\varepsilon$]	***I*** [$\mu\varepsilon$]
$\overline{S}_{u,f}^{(13)}$	1	5.9	17.9
	3	12.5	-16.3
	5	-38.8	-41.1
	7	-63.7	-81.6
	8	-230.1	-344.6

Table 11.16 - Values of the variation of strain induced by the filling detected by the strain gauges on the corrugated wall and the stiffener at z = 1.40 m*

	f	E_M	E_I	E_O
$\Delta\varepsilon_{l,fj}$ [$\mu\varepsilon$]	1	178	-15	-10
	2	204	-26	-19
	3	222	-35	-30
	4	228	-40	-35
	5	297	-82	-75
	6	312	-90	-80
	7	326	-92	-83
	8	347	-92	-80

It can be observed that, in general, for increasing filling level (h_b) the modulus of the reconstructed deformations and strains tend to increase.

It should be reported that for the measuring bases at higher levels than 13, during the filling procedure, only a limited number of repetitions could be performed on such

measuring bases as effectively subjected to the actions of the ensiled grain. Thus, in the next sections, attention will be focused on the processing of the data acquired for levels 16 and 13 only.

11.4 Reconstruction of the internal actions in the structural members

In the present section, the internal actions in the structural members (wall and stiffener) are reconstructed. In detail, the internal action on the wall is represented by the hoop tension $\sigma_{\theta\theta}$ induced by the horizontal grain-wall pressure; while, for the stiffener the internal actions are represented by the axial force N_{zz} and the eventual internal bending moment along the *x*-*x* axis M_{xx}. First, the methodology for the reconstruction of the stresses starting from the values of the reconstructed strains and the reconstruction of the internal actions is described. Then, the methodology is applied to the wall and the stiffener under investigation in order to reconstructed the internal actions.

11.4.1 Reconstruction of the internal actions

The values of the internal actions exerted in the vertical stiffener and the wall portion under exam are reconstructed starting from the data acquired by the measurements. Then, the values of the internal actions exerted in the vertical stiffener and the wall portion under exam are reconstructed starting from the pressure distributions for the load case of symmetrical filling.

As far as the reconstruction of the internal actions starting from the data acquired by the measurements is concerned, first the values of the stresses are reconstructed by starting from the values of the reconstructed strains detected on the measuring bases placed on the wall and the stiffener under exam. The stresses are considered proportional to the strains trough the modulus of elasticity *E* (equal to 200000 *MPa*), neglecting the effect of the transversal deformations (which were not measured):

$$\sigma = E \cdot \varepsilon \tag{45}$$

As far as the reconstructed internal actions acting on the stiffener are concerned, it is assumed that plane cross-sections remain plane (even in the case of sections composed

by two or more superposed steel profiles bolted together) and the formula of Euler-Bernoulli is taken into account:

$$\sigma_{zz}(y) = \frac{N_{zz}}{A_s} \pm \frac{N_{zz} \cdot e_y}{I_{xx}} \cdot y \tag{46}$$

where $\sigma_{zz}(y)$ is the vertical stress along the vertical *z* axis, acting on the fiber of coordinate *y*, i.e. the distance of the generic fiber with respect to the centroid of the gross cross-section, e_y is the eccentricity of the axial internal action N_{zz} with respect to the *x*-*x* axis. By considering the values of $\sigma_{zz}(y)$ referred to two different measuring bases placed on the web (*A*) and the internal flange (*I*) with different coordinates y_A and y_I, respectively, it results:

$$\begin{cases} \sigma_{zz}(y_A) = \dfrac{N_{zz}}{A_s} \pm \dfrac{N_{zz} \cdot e_y}{I_{xx}} \cdot y_A \\ \sigma_{zz}(y_I) = \dfrac{N_{zz}}{A_s} \pm \dfrac{N_{zz} \cdot e_y}{I_{xx}} \cdot y_I \end{cases} \tag{47}$$

By subtracting and summing together the equations inside the system of Eq. (18), the values of the two unknown quantities, i.e. the axial force N_{zz} and the eccentricity along the *y*-*y* axis e_y, can be calculated as follows:

$$N_{zz} = \frac{A}{2} \cdot \left[\Delta\sigma_+ - \Delta\sigma_- \cdot \left(\frac{\Delta y_-}{\Delta y_+} \right) \right] \tag{48}$$

$$e_y = \frac{\Delta\sigma_- \cdot I_{xx}}{N_{zz} \cdot \Delta y_+} \tag{49}$$

where $\Delta\sigma_\pm = \sigma_{zz}(y_A) \pm \sigma_{zz}(y_I)$ and $\Delta y_\pm = y_A \pm y_I$.

As far as the reconstructed internal hoop action $n_{\theta\theta}$ acting in the wall is concerned, the resultant of the hoop tension $\sigma_{\theta\theta}$ over the unit of vertical length results:

$$n_{\theta\theta} = \sigma_{\theta\theta} \cdot t_w \tag{50}$$

As far as the reconstruction of the internal actions starting from the pressure distributions for the load case of symmetrical filling is concerned, the provisions of EN 1991-4:2006 are taken into account for the assessment of the vertical grain-wall frictional stresses and the horizontal grain-wall pressures. The indications given by EN 1993-4-

1:2007 for the case of horizontally corrugated, vertically stiffened steel silos are considered as well. In detail, for the case in exam, the Reimbert and Reimbert (1976) formulation is taken into account, since the slenderness ratio of the silo (under progressive filling) results always lower than unity. According to EN 1991-4:2006, the values of the values of horizontal pressure p_{hf} and wall frictional traction p_{wf} at any depth z after symmetrical filling may be computed according to Eqs. (5.71) and (5.72) (see §5.3.1.1 of EN 1991-4:2006). Thus, the value of the resulting characteristic value of the vertical force (compressive) in the wall n_{zSk} per unit length of perimeter at any depth z may be determined according to Eq. (5.81) of EN 1991-4:2006.

Such values depend on the bulk solid's parameters under consideration. In this regard, the estimation of the horizontal pressure p_{hf} and wall frictional traction p_{wf} in symmetric filling conditions is carried out by considering, for each pressure pattern, two different scenarios, in order to provide a reliable range of the quantities under investigation (as also suggested by EN 1991-4:2006). In detail, each scenario consists of a specific combination of the parameters (i) effective grain-wall friction coefficient μ_{eff} and (ii) lateral pressure ratio K. The so-called upper characteristic value and lower characteristic value of the parameters μ_{eff} and K are considered according to the indications given by Table 11.17, which summarizes the combination of the two parameters for the different scenarios.

Table 11.17 - Combination of the parameters for different scenarios for stiffener and wall

Purpose	μ_{eff}	K
Maximum value of the axial force on stiffeners	Upper characteristic value	Upper characteristic value
Minimum value of the axial force on stiffeners	Lower characteristic value	Lower characteristic value
Maximum value of the hoop action	Lower characteristic value	Upper characteristic value
Minimum value of the hoop action	Upper characteristic value	Lower characteristic value

The upper and lower characteristic values of the lateral pressure ratio K are evaluated by multiplying and dividing the value of K by the factor a_K (see Table 11.3), as suggested by EN 1991-4:2006 (see §4.2.3), resulting:

- Upper characteristic value, $K^{(upper)} = 0.60$;
- Lower characteristic value, $K^{(lower)} = 0.47$;

The value of the effective grain-wall friction coefficient μ_{eff} to be used in presence of horizontally corrugated wall results as combination of grain-grain and grain-on-metal friction coefficient (Moore et al. 1984) and it is computed according to the procedure given by Annex D of EN 1991-4:2006 (see Eq. D.1) for wall surface category D4. In detail, it results:

$$\mu_{eff} = (1 - a_w) \cdot tg(\phi_i) + a_w \cdot \mu_w \tag{51}$$

where μ_w is the wall friction coefficient (against a flat wall surface) and a_w is the wall contact factor.

By takin into account the values of $a_w = 0.20$ and $\mu_w = \mu = 0.36$ (mean value corresponding to wall surface category D2, "moderate friction classed as smooth", smooth mild carbon steel [welded or bolted construction], see Table 4.1. of EN 1991-4:2006), Eq. (22) provides a value of $\mu_{eff} = 0.5$.

The upper and lower characteristic values of the effective grain-wall friction coefficient μ_{eff} are respectively evaluated by multiplying and dividing the value of μ_{eff} by the factor a_μ (see Table 11.3), resulting:

- Upper characteristic value, $\mu_{eff}^{(upper)} = 0.69$;
- Lower characteristic value, $\mu_{eff}^{(lower)} = 0.47$.

The values of effective grain-wall friction coefficient and lateral pressure ratio (nominal, upper characteristic, lower characteristic) obtained above are compared with those given in the scientific literature for real scale horizontally corrugated steel silos filled with maize grain, which are reported in Table 11.18.

Table 11.18 - Values of the effective grain-wall friction coefficient and lateral pressure ratio available in literature

Reference	μ_{eff} [-]	K [-]	w [%]
Thompson and Prather (1984)	0.42	0.44	12
Thompson et al. (1996)	0.60	0.52	-
	0.55	0.52	-

It can be noted that the values of effective grain-wall friction coefficient and lateral pressure ratio calculated by means of the data and the procedure given by EN 1991-4:2006, even if slightly greater, are consistent with those reported in literature.

As far as the assessment of the predicted internal actions on wall and stiffener under symmetric filling conditions is concerned, the indications given by EN 1993-4-1:2007 for the case of horizontally corrugated, vertically stiffened steel silos for the estimation of the internal axial force and internal hoop action are considered. In details, according to the indications given by §5.3.4 of EN 1993-4-1 (2007), where the cylindrical wall is fabricated from corrugated sheeting with the corrugations running horizontal1y and vertical stiffeners are attached to the wall, the corrugated wall should be assumed to carry no vertical forces (unless the wall is treated as an orthotropic shell), thus the internal axial force on the stiffener is calculated by multiplying the resulting characteristic value of the vertical force (compressive) in the wall n_{zSk} per unit length of perimeter, at any depth z, for the circumferential length $l_{\inf} = \pi \cdot d_c / n_s$ corresponding to each equally spaced stiffener (where n_s is the total number of vertical stiffener). It results:

$$N_{zz}(z) = n_{zSK}(z) \cdot l_{\inf} \tag{52}$$

The estimation of the internal bending moment may be performed by means of cylindrical shell bending theory for shells under general axisymmetric pressure distributions. However, unless the wall is treated as an orthotropic shell, the vertical stiffeners are simply considered uniformly compressed. Thus, the internal bending moment and the corresponding eccentricity e_y are considered null.

As far as the assessment of the predicted internal hoop action in the wall, for a generic abscissa z, $n_{\theta\theta}(z)$ is concerned, the membrane shell theory is considered, so that:

$$n_{\theta\theta}(z) = p_{hf}(z) \cdot \frac{d_c}{2} \tag{53}$$

11.4.2 The reconstructed stresses in the stiffener

On the basis of the reconstructed values of the strains detected on the stiffener under investigation, the stresses on such members are reconstructed by making use of Eq. (16).

Figure 11.17 reports the trends of the reconstructed vertical stresses acting on different points of the stiffeners at level 16 as a function of the equivalent filling height h_b, for the measuring bases. Figure 11.18 reports the trends of the reconstructed vertical stresses acting on the stiffeners at level 16 as a function of the equivalent filling height h_b, for the strain gauges. Figure 11.19 provides a comparison of the trends of the reconstructed vertical stresses of the stiffener at level 16 given by the measuring bases and the strain gauges as a function of the equivalent filling height h_b for the external face and the internal face of the stiffener.

In general, an increasing trend can be observed. In particular, a significant increase in the slope of the general trend may be observed on the last portion of the graph, referred to the last repetition performed on 22th November, for the completely filled condition. In addition, it can be noted that the trends given by the measuring bases and strain gauges are quite similar; the only exception is represented by the values reconstructed on the external face, for the completely filled condition. The values given by the strain gauges are generally higher than those given by the measuring base.

Figure 11.20 reports the trends of the reconstructed vertical stresses acting on different points of the stiffeners at level 13 as a function of the equivalent filling height h_b, for the measuring bases. The increasing trend is still visible, as already observed for level 16.

In general, an increasing trend of the reconstructed stresses appears for increasing values of the equivalent filling height. It can be observed that the reconstructed vertical stresses on the web portion of the stiffener's profile result always greater than those reconstructed for the flanges; thus, during progressive filling the arising of a positive bending moment acting along the *x*-*x* axis seems to take place, especially on the lower level 16. It should be noted that, for the stiffener with cross-section composed by bolting together two superposed steel profiles (level 16), under increasing vertical stresses, discrepancy between the values of stresses reconstructed on the external face of the flange

and the internal face of the flange arises. This could be related to a progressive mutual sliding between the two profiles, leading to an increasing in the stresses exerted on the internal profile.

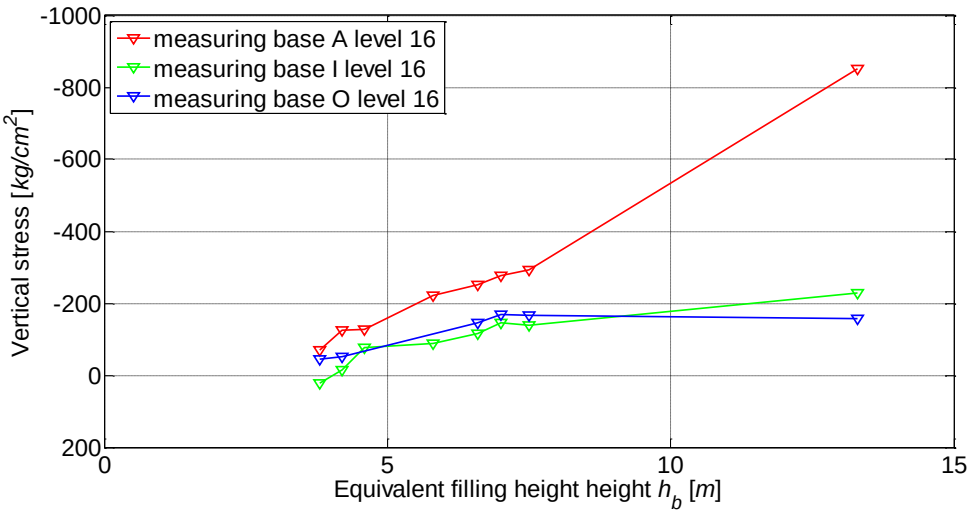

Figure 11.17 - Trends of the reconstructed vertical stresses of the stiffener at level 16 as given by the measuring bases as a function of the equivalent filling height h_b

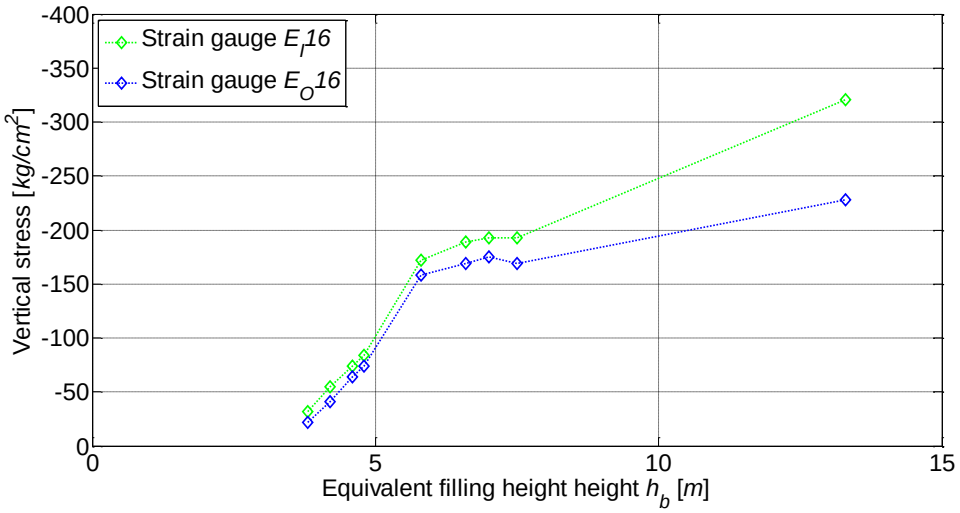

Figure 11.18 - Trends of the reconstructed vertical stresses of the stiffener at level 16 as given by the strain gauges as a function of the equivalent filling height h_b

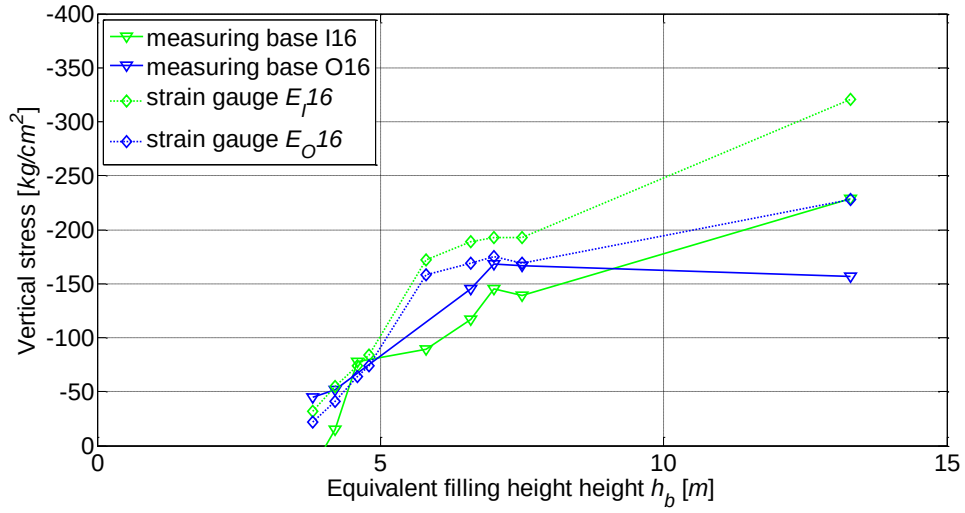

Figure 11.19 - Comparison of the trends of the reconstructed vertical stresses of the stiffener at level 16 given by the measuring bases and the strain gauges as a function of the equivalent filling height h_b for: a) the external face and b) the internal face of the stiffener.

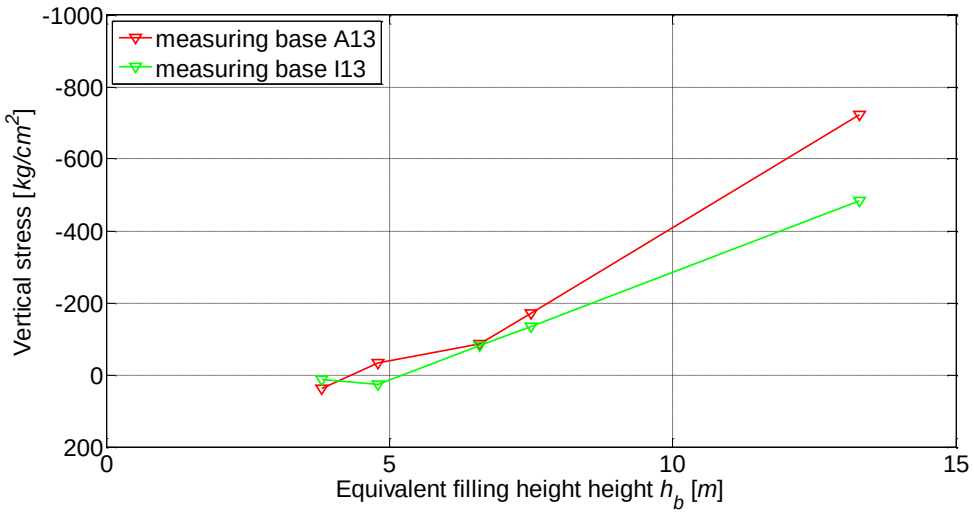

Figure 11.20 - Trends of the reconstructed vertical stresses of the stiffener at level 13 given by the measuring bases as a function of the equivalent filling height h_b

11.4.3 The reconstructed stresses in the wall

On the basis of the acquired values of the strains detected on the wall portion under investigation, the stresses on such members are reconstructed by making use of Eq. (16).

Figure 11.21 shows the trend of the reconstructed hoop stress of the wall portion at level 16, as given by the strain gauge, as a function of the equivalent filling height h_b. It can be observed a general increasing asymptotic trend of the value of the hoop tension as a function of the equivalent filling height.

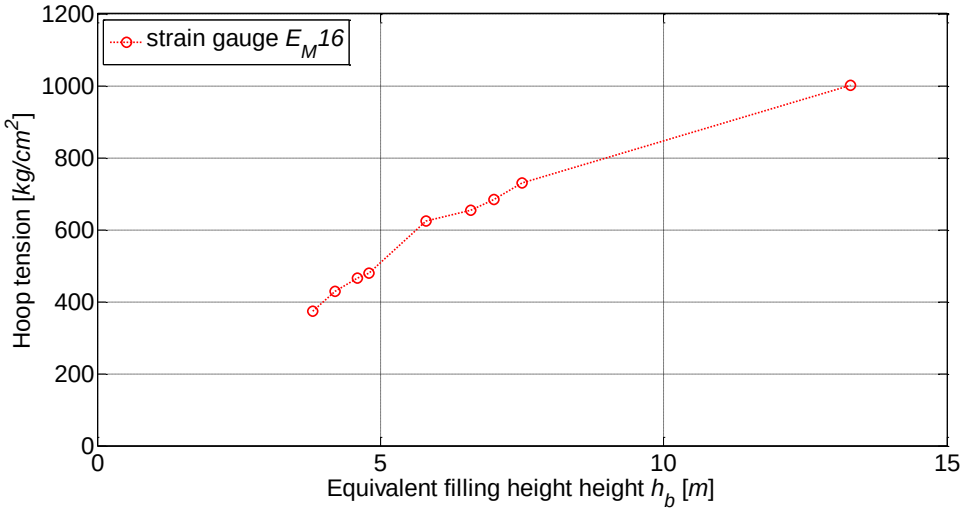

Figure 11.21 - Trends of the reconstructed hoop tension of the wall at level 16 as given by the strain gauge as a function of the equivalent filling height h_b

11.4.4 The reconstructed internal axial force and the internal bending moment acting on the stiffener

On the basis of the reconstructed values of the vertical stresses detected on the stiffener under investigation and by making use of Eqs. (17)-(20), the values of the internal axial force N_{zz} and the internal bending moment M_{xx} (expressed by the related eccentric e_y) are reconstructed. It is pointed out that the reconstruction of the internal axial force in the stiffener is carried out by means of the Euler-Bernoulli model even in occurrence of mutual sliding between the superposed steel profiles composing the stiffener's cross-section, which may affect the estimation of the axial force acting on the stiffener at level 16 in the full filled condition.

Figure 11.22 and Figure 11.23 show the trends of the reconstructed values of the internal axial forces exerted on the stiffener and the corresponding eccentricity along the *y-y* axis for level 16, as a function of the equivalent filling height h_b, respectively.

Figure 11.24 and Figure 11.25 show the trends of the reconstructed values of the internal axial forces exerted on the stiffener and the corresponding eccentricity along the *y-y* axis for level 13, as a function of the equivalent filling height h_b, respectively.

Obviously, increasing trends of the internal axial forces appear. The maximum internal axial forces reached at level 16 and 13 result around 13 and 6 *tons*, respectively.

The trends of the eccentricities along the *y-y* axis e_y present a less smooth profile. In detail, high module values appear on the first part of the loading process, then the values tend to progressively reduce. At level 16, negative values appear, while at level 13 positive values appears, thus indicating the presence of internal bending moment acting along the *x-x* axis with opposite versus. The magnitude of the eccentricities results, in both levels, at the end of the filling of the order of 1-2 *cm*, thus leading to values of the internal bending moment around 0.3 and 0.1 *tons×m*.

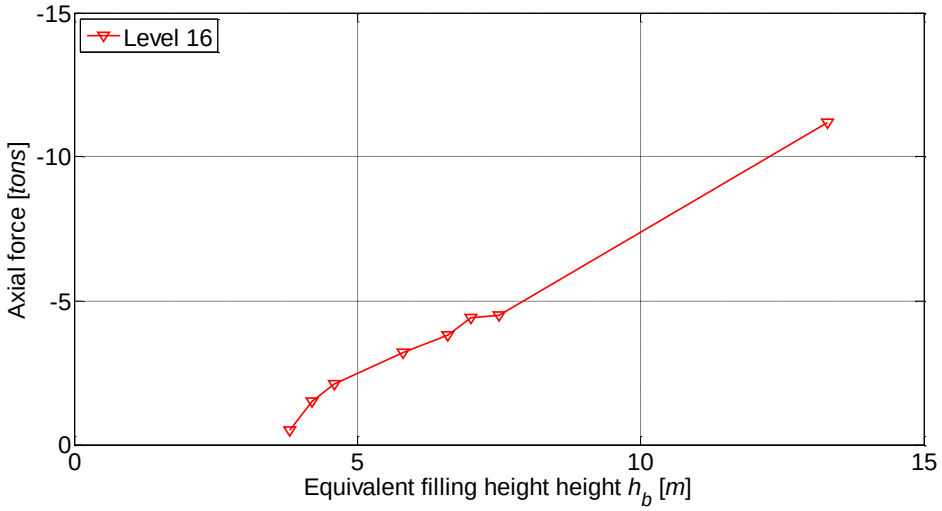

Figure 11.22 - Trend of the reconstructed values of the internal axial forces exerted on the stiffener at level 16 as a function of the equivalent filling height h_b

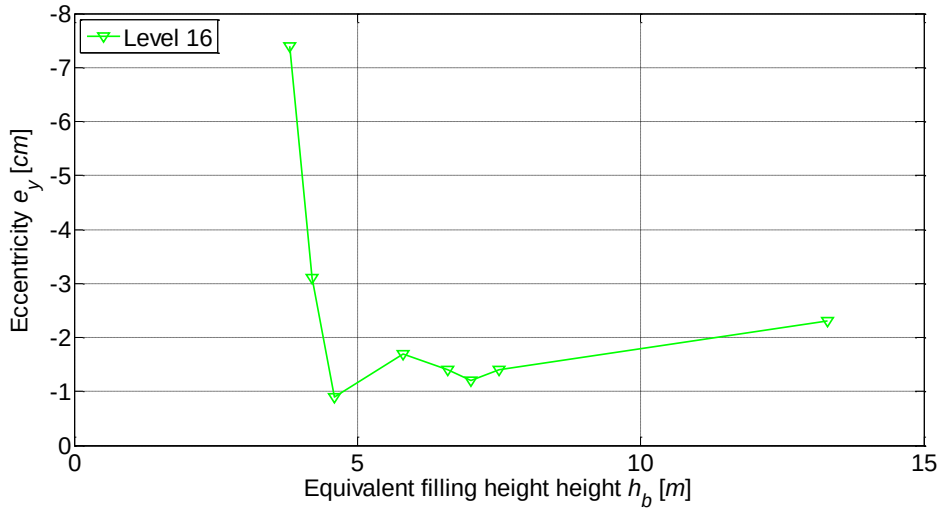

Figure 11.23 - Trend of the reconstructed values of the eccentric of the axial force on the stiffener at level 16 as a function of the equivalent filling height h_b

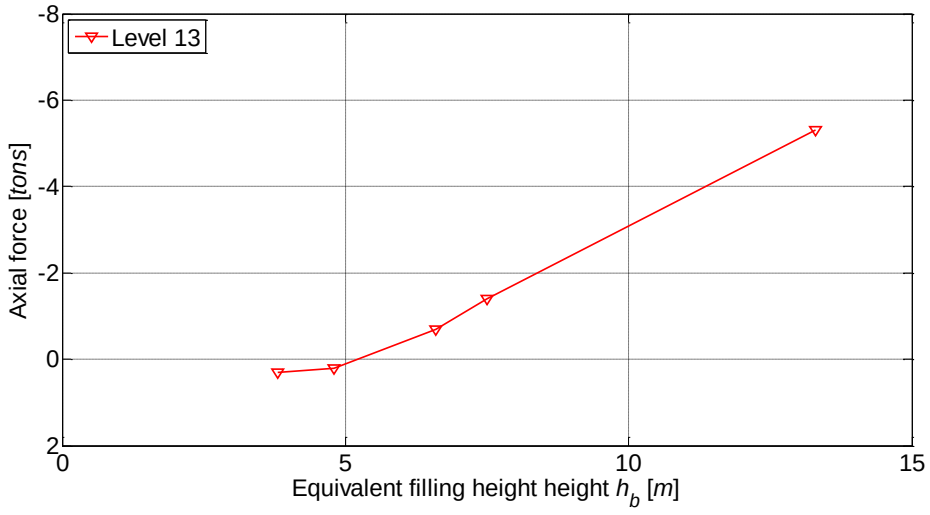

Figure 11.24 - Trend of the reconstructed values of the internal axial forces exerted on the stiffener at level 13 as a function of the equivalent filling height h_b

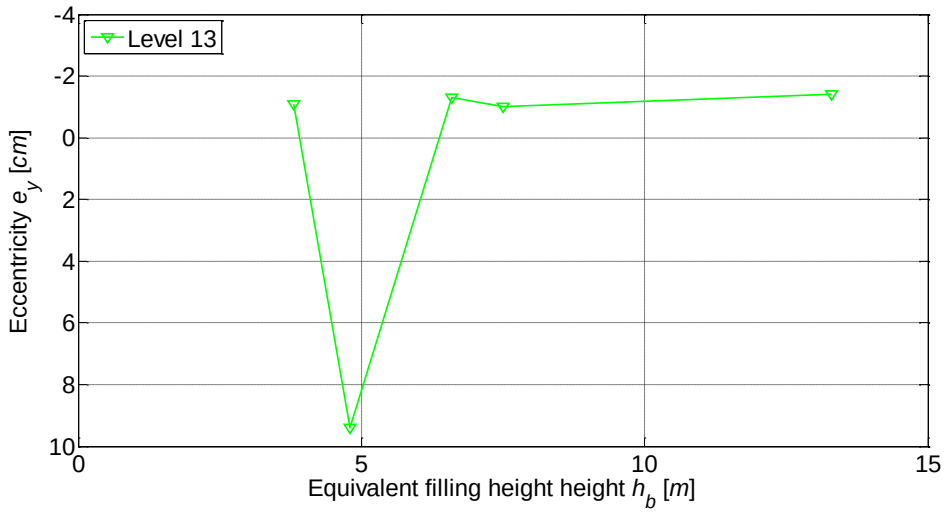

Figure 11.25 - Trend of the reconstructed values of the eccentric of the axial force on the stiffener at level 13 as a function of the equivalent filling height h_b

11.4.5 The reconstructed internal hoop action on the wall

On the basis of the reconstructed values of the hoop tension detected on the wall under investigation and by making use of Eq. (21), the values of the internal hoop action $n_{\theta\theta}$ are reconstructed.

Figure 11.26 shows the trends of the reconstructed values of the internal hoop action of the wall for level 16, as a function of the equivalent filling height h_b.

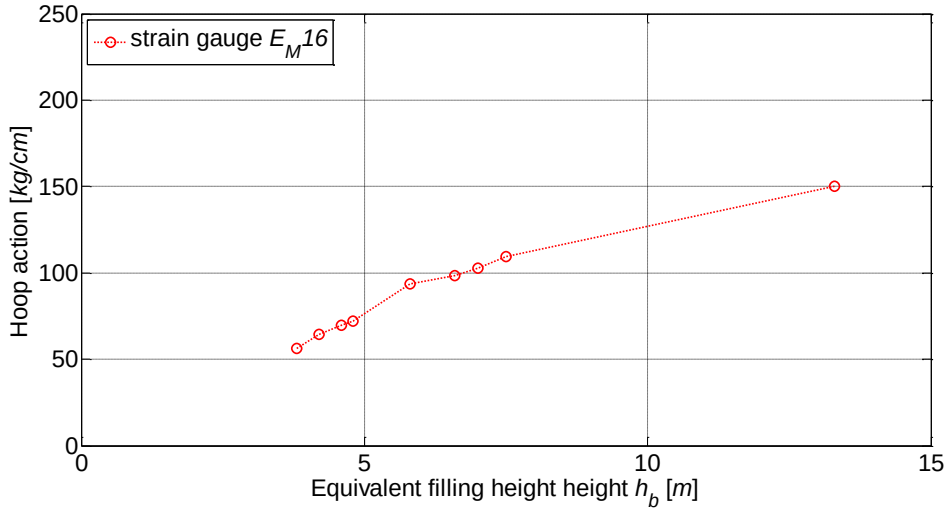

Figure 11.26 - Trend of the reconstructed values of the internal hoop action on the wall at level 16 as a function of the equivalent filling height h_b

11.5 Comparison between reconstructed actions and predicted actions

In the present section, the comparisons between the values of the reconstructed internal actions with the values predicted making use of the EN 1991-4:2006 provisions are presented. First, the comparison between the reconstructed values of the internal axial action and the ones predicted is presented; then, the comparison between the reconstructed values of the internal hoop action with the ones predicted is presented.

11.5.1 Comparison of the internal axial forces on the stiffener: reconstructed vs predicted

Figure 11.27 and Figure 11.28 report the comparison of the reconstructed values of the internal axial forces with the predicted (maximum and minimum) values of the internal axial forces for level 16 and 13, respectively, as a function of the equivalent filling height h_b. On level 16, the reconstructed values first appears to slightly exceed the predicted ones, while for the full filled condition, the reconstructed value appears centered between the minimum and maximum predicted values. On level 13, the reconstructed values present a smoother trend with respect to that observed on level 16 and for the full filled condition, the reconstructed value tends to approach the minimum predicted value.

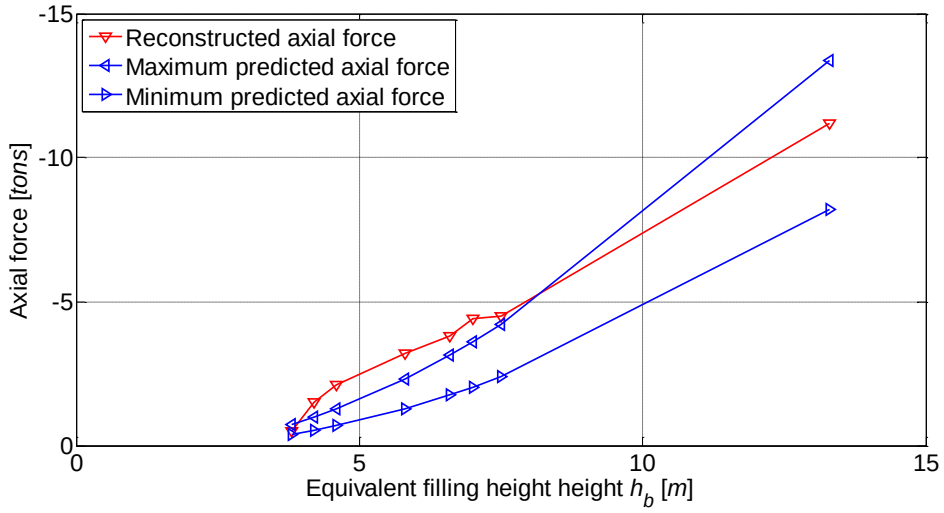

Figure 11.27 - Comparison of the reconstructed values of the axial forces and the minimum and maximum predicted values for level 16 as a function of the equivalent filling height

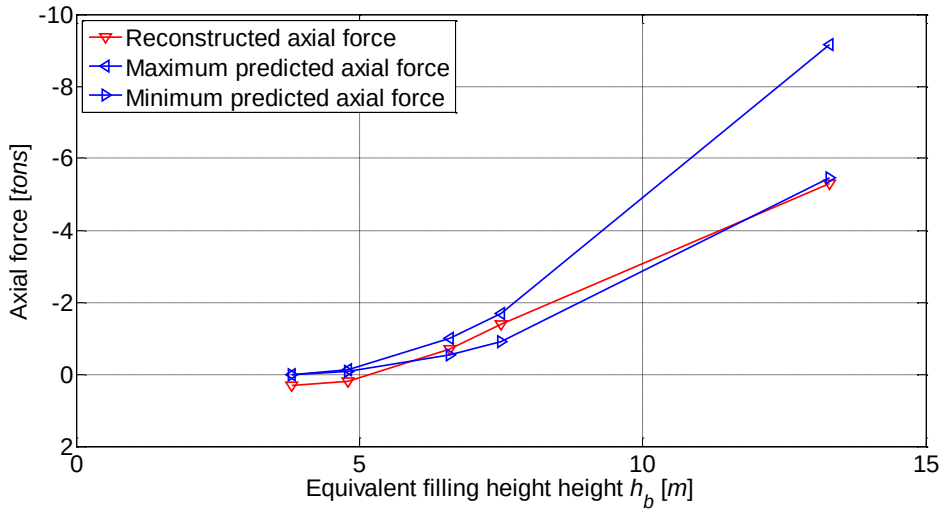

Figure 11.28 - Comparison of the reconstructed values of the axial forces and the minimum and maximum predicted values for level 13 as a function of the equivalent filling height

11.5.2 Comparison of the internal hoop action on the wall: reconstructed vs predicted

Figure 11.29 reports the comparison of the reconstructed values of the internal hoop action with the predicted (maximum and minimum) values of the internal hoop action for level 16, as a function of the equivalent filling height h_b. It can be observed that for filling heights lower than 8 *m*, the reconstructed values tend to approach the minimum predicted

values of the hoop action, while for greater filling heights the reconstructed values result lower.

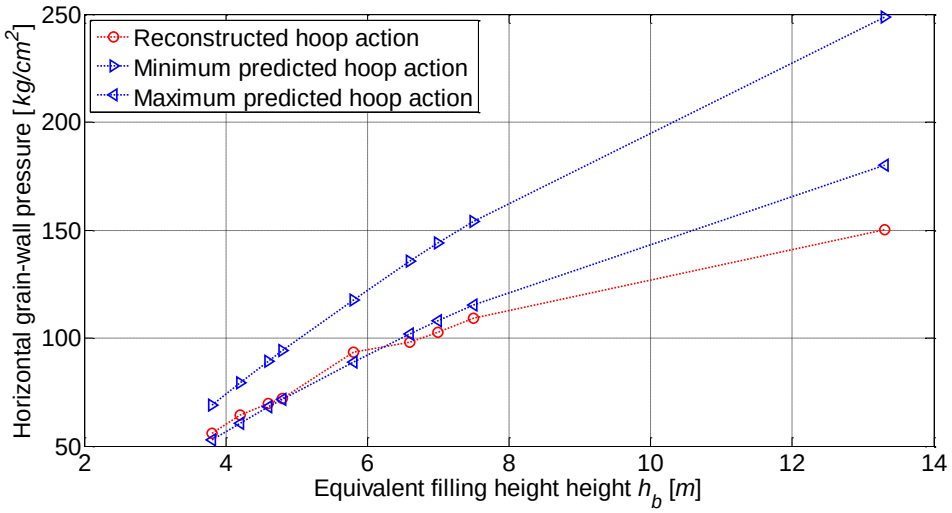

Figure 11.29 - Comparison of the reconstructed values of the internal hoop action of the wall with minimum and maximum predicted value for level 16 as a function of the equivalent filling height

11.6 Critical considerations

In this section, the main results of an on-field experimental campaign carried out on a real operational, horizontally corrugated, vertically stiffened steel silo under progressive symmetric filling have been reported, with the main aim of investigating the structural behavior under static loading of such typology of complex silo structures. Such experimental activity represents a preliminary, first, essential step to be performed in order to develop further experimental investigations for the assessment of the response of such real silo structures exposed to base excitation and the comparison with the predictions given by the proposed analytical formulations (developed for idealized silo models).

The on-field experimental campaign consisted in detecting the deformations and the strains experienced by wall and stiffener. The measurements quantified the values of the deformations induced by thermal variations and progressive filling of the silo. The detected deformations are translated into strains and then into internal axial actions and internal bending moments on the stiffener and internal hoop action on the wall. The reconstructed values of the internal actions are compared to those predicted by applying the EN 1991-4:2006 and EN 1993-4-1:2007 provisions for steel silos.

It is observed that:

- The effects induced by thermal variations may result significant in the study of real structures exposed to outdoor ambient conditions. Thus, such effects should be evaluated and taken into account in the processing of the acquired data. The instrumentation and the experimental procedures should be designed in order to limiting the influence of the thermal variations;
- The values of the strains reconstructed by using micrometers and the values of the strains given directly by strain gauges are essentially in agreement, even if the latter results generally higher than the former;
- Stiffeners with cross-section composed of two (or more) superposed steel profiles bolted together may be affected by mutual sliding between the profiles for relevant stress levels, with consequent increasing of the stress demand on a portion of the cross-section. Thus, the structural response may be strongly affected by such structural details.
- The reconstructed values of internal axial forces in the stiffener and the internal hoop action in the wall for progressive symmetric filling appear in line with those predicted by considering the amount of grain portion leaning against the wall due to vertical friction under static conditions (proportional to the *effective mass*) according to the classical theories.

Reference

Arze L., (1992). Seismic design practices of industries, Tenth World Conference on Earthquake Engineering, 19-24 July, Madrid, Spain.

Ayuga, F., Guaita, M., & Aguado, P. (2001). SE—Structures and Environment: Static and Dynamic Silo Loads using Finite Element Models. Journal of Agricultural Engineering Research, 78(3), 299-308.

Ayuga, F., Aguado, P., Gallego, E., & Ramirez, A. (2005). New steps towards the knowledge of silos behaviour. International Agrophysics, 19(1), 7-17.

EN 1991-4 (2006) Eurocode 1. Actions on structures, Part 4 -Silos, tanks and pipelines, CEN, Brussels.

EN 1993-4-1 (2007) Eurocode 3. Design of steel structures - Part 4-1: Silos, CEN, Brussels.

Janssen, H. A. (1895). Versuche über getreidedruck in silozellen. Zeitschr. d. Vereines deutscher Ingenieure, 39(35), 1045-1049.

Moore, D. W., White, G. M., & Ross, I. J. (1984). Friction of wheat on corrugated metal surfaces. Transactions of the ASAE, 27(6), 1842-1847.

Németh, C., & Brodniansky, J. (2013). Silo with a Corrugated Sheet Wall. Slovak Journal of Civil Engineering, 21(3), 19-30.

Reimbert, M. and A. Reimbert. 1976. Silos—Theories and Practice. Clausthal, Germany, Trans Tech Publishers. 250p.

ROTTER, J. M. (2009, November). Silos and tanks in research and practice: state of the art and current challenges. In Symposium of the International Association for Shell and Spatial Structures (50th. 2009. Valencia). Evolution and Trends in Design, Analysis and Construction of Shell and Spatial Structures: Proceedings. Editorial Universitat Politècnica de València.

Thompson, S. A., Galili, N., & Williams, R. A. (1997). Lateral and vertical pressures in two different full-scale grain bins during loading Presiones laterales y verticales durante el llenado de diferentes silos para granos. Food science and technology international, 3(5), 371-379.

Thompson, S. A., & Prather, T. G. (1984). Dynamic wall loads in a corrugated walled model grain bin. Transactions of the ASAE, 27(3), 875-878.

12. Conclusions and future developments

The study presented in this dissertation is focused on the analysis of the seismic response of flat-bottom cylindrical grain-silos. Part A constitutes an updated state-of-the-art on the structural seismic design of flat-bottom cylindrical grain-silos. Part B critically analysis the theoretical framework developed in the last decade at the University of Bologna by the research work coordinated by Prof. Trombetti and the experimental tests conducted in 2012-2013 for its experimental verification. Part C provides some refinement on the theoretical framework and some further insight into the dynamic behavior of flat-bottom cylindrical grain-silos representing the main scientific contribution of the work. Thesis. Summary and detailed discussions on all above cited issues have been taken up at the end of the relevant chapters. The purpose of this chapter is to summarize the main findings and to suggest some further research directions.

12.1 Main conclusions of part A

Part A begins with a comprehensive review of the main analytical, numerical and experimental researches devoted to the study of the static and dynamic behavior of flat-bottom cylindrical grain-silos, together with a review of the current design code provisions for the seismic design of grain-silo structures. A comparison between the current code provisions and the actual scientific knowledge on the seismic behavior of flat-bottom grain-silo structures is provided. In summary, the following conclusions are drawn:

- Computational models (both continuum finite element and discrete element) appear not able to capture the complex grain-silo interaction, thus sound and reliable design cannot disregard from the application of analytical treatment of the silo problems;
- A remarkable gap appears between the actual dynamic behavior of grain-silos, the body of knowledge and the current code provisions dealing with seismic design of silo structures. Thus, further investigations in such direction is needed;
- Despite more than one century of research, many uncertainties still exist in various areas of silo structural behavior, especially for the case of horizontally corrugated vertically stiffened steel silos, making such complex

silo typology more prone to structural failures induced by discharging and seismic loading.

12.2 Main conclusions of part B

Part B is focused on the previous research works conducted by Prof. Trombetti and co-workers in the year 2012-2013. First, the theoretical study on the horizontal forces produced by grain-like material inside silos during earthquakes has been presented. Then, the experimental investigation conducted via shaking-table tests at the EQUALS laboratory of the University of Bristol (ASESGRAM project) has been reported. Finally, the analytical-experimental correlation study for the verification of the original analytical formulation has been illustrated. In summary, the following conclusions are drawn:

- The reconstructed values of the *effective mass* are far lower than the values obtained using the Eurocode 8 provisions, for both sinusoidal and earthquake inputs. Thus, it clearly seems that these provisions are overly conservative in the prediction of the *effective mass*;
- The experimental results clearly indicate that the wall-grain friction coefficient strongly affects the experimental base bending moment. This does not match with Eurocode 8 prescriptions, which disregards the wall-grain friction coefficient. From a qualitative point of view, according to the analytical formulation, higher wall-grain friction coefficient leads to higher actions inside the wall, i.e. to higher value of the *effective mass*;
- Acceleration amplifications of the horizontal acceleration over the height and the effect of the sliding of the upper grain layers on the silo wall should be taken into account in the seismic design of silo-grain system;

12.3 Main conclusions of part C

Part C presents some refinements of the original analytical formulation for the estimation of the maximum lateral actions developed during an earthquake as well as an analytical formulation for the estimation of the fundamental period of vibration of flat-bottom circular grain-silos. Finally, the results of a preliminary on-field experimental

campaign on a real silo structure have been illustrated. In summary, the following conclusions are drawn:

- The refined analytical formulation provides a significant extension of the limits of validity of the original analytical formulation and takes into account the contribution of the vertical frictional stresses in the evaluation of the wall bending moment. Furthermore, it is able to capture both the static and the dynamic response of flat-bottom circular grain-silos in terms of pressures distributions and the comparison with the shaking-table tests results shows good agreement as well. The experimental verification suggests that the mathematical consistence and the physical robustness of the refined analytical formulation can be conciliated with the handy and suitable formulations of the original analytical formulation for the case of squat silos;
- A fully analytical formula for the estimation of the fundamental period of vibration of flat-bottom circular grain-silo system is derived and compared with experimental data available in the scientific literature showing quite satisfactory agreement. For common flat-bottom cylindrical steel silos containing common grain-like materials (designed according to EC1) the value of the fundamental period of vibration could range roughly from 0.1 *s* to more than 1.0 *s*;
- The structural response of the real silo structures could be influenced by the structural details when stiffeners with cross-section composed by two or more superposed steel profiles bolted together are adopted, since mutual sliding between the profiles for relevant stress level could appear. This phenomenon could affect both the static and the dynamic structural response and it should be taken into account;
- The reconstructed values of internal axial forces on the stiffener and the internal hoop action on the wall under progressive symmetric filling appear in line with those predictable by considering the amount of grain portion leaning against the wall due to vertical friction under static conditions (proportional to the effective mass) according to classical theories.

12.4 Future developments

A list of future developments related to the research works presented in this thesis are here summarized.

As far as Part A of the thesis, presenting an updated state-of-the-art of the structural seismic design of flat-bottom cylindrical grain-silos, is concerned, the following issue is still to be addressed:

- A continuous updating of the scientific literature of the analytical, numerical and experimental studies should be carried in order to account for past and new researches performed worldwide by different research teams.

As far as Part B of the thesis, dealing with the previous analytical and experimental works conducted by Prof. Trombetti and co-workers in the years 2012-2013, is concerned, the following issue is still to be addressed:

- Deep analyses of the dynamic response of the silo specimens under low-frequency sinusoidal inputs, white noise inputs of increasing magnitude, real strong earth motion records (characterized by different magnitude and frequency content) in terms of amplification of the horizontal acceleration on the wall and the ensiled content;

As far as Part C of the thesis, dealing with the main original contributions of this Ph.D. Thesis, is concerned, a number of issues are still to be addressed:

- Development of the analytical formulation for the assessment of the grain-wall pressures distributions and wall actions for more general vertical profile of the horizontal acceleration (linear, parabolic) in order to take into account the effect of the amplification of the horizontal base acceleration on the seismic response of grain-silo systems;
- Identify the eventual correlation between magnitude and frequency content of the base excitation (one harmonic inputs, multi-harmonic inputs, real strong earth motion records) and the dynamic structural response of grain-

silos (such as amplification of the horizontal acceleration on the wall and the ensiled content);

- Investigate the combined effect of the application of simultaneous horizontal and vertical base excitations on the dynamic response of grain-silo systems;
- Develop on-field campaigns for the assessment of the structural response of real grain-silo structures under dynamic excitation. This phase should be of fundamental importance to get a first insight into the actual dynamic response of real grain-silo structures.